VOLUME 27 (1961) No. 1

NUCLEAR PHYSICS

JOURNAL DEVOTED TO THE EXPERIMENTAL AND THEORETICAL STUDY OF THE FUNDAMENTAL CONSTITUENTS OF MATTER AND THEIR INTERACTIONS

EDITOR: L. ROSENFELD - COPENHAGEN

K. MATSUDA, Y. NAGAHARA, Y. ODA, N. YAMAMURO and S. KOBAYASHI, The elastic and inelastic scattering of protons by magnesium in the energy range from 7.3 MeV to 15.9 MeV 1
O. BORELLO, S. COSTA and F. FERRERO, The E. C./β^+ ratio in Pr^{139} 25
B. N. SUBBA RAO, Angular correlation studies of the 358 keV → 81 keV cascade in Cs^{133} 28
V. K. KEMBHAVI, Reduced matrix elements in nuclear shell theory . . . 38
J. E. EVANS, Polarization in C^{12}(p, p) scattering from 5 to 10.5 MeV 41
TH. A. J. MARIS, An interpretation of the isobaric spin space 46
V. AMAR and M. PAURI, On the $K^+ + n \rightarrow K^0 + p$ scattering amplitude poles 52
M. L. RUSTGI, Alpha-deuteron model of the Li^6 nucleus and the $Be^9(Li^6, \alpha)B^{11}$ reaction 58
W. D. HAMILTON and B. S. SOOD, The resonant scattering of gamma rays in ^{177}Hf 66
J. P. HURLEY and J. M. FERGUSON, Measurement of K conversion coefficient of 279 keV gamma radiation in Tl^{203} 75
J. R. ROOK and L. J. B. GOLDFARB, The use of polarised deuterons to study the D+D reactions 79
H. SOKOLIK, Interpretation of isobaric multiplets in terms of the space-time reflection group 94
O. DIETZSCH, Y. HAMA, E. W. HAMBURGER and F. C. ZAWISLAK, Study of the O^{16}(d, n)F^{17} reaction 103
ROLF NORDHAGEN, The spin and parity of the 648 keV resonance in $Mg^{26}(p, \gamma)Al^{27}$ 112
A. S. REINER, Electric monopole transitions in collective nuclei 115
A. S. DAVYDOV, V. S. ROSTOVSKY and A. A. CHABAN, The shape of the atomic nucleus and zero spin excited states 134
K. D. TOLSTOV, On the mechanism of interaction of fast protons with nuclei 144
P. S. ISAEV and M. V. SEWERYNSKI, Scattering of π-mesons on K-mesons at low energies 148
J. G. CUNINGHAME, G. P. KITT and E. R. RAE, The ratio of asymmetric to symmetric fission in p-wave neutron fission of U^{235} 154
E. KONDAIAH, M. L. JHINGAN and C. BADRINATHAN, Surface direct interaction of 14 MeV neutrons with fluorine 166

September 1961

NORTH-HOLLAND PUBLISHING COMPANY-AMSTERDAM

EDITORIAL BOARD

AUSTRALIA & NEW ZEALAND:	H. Messel (Sydney), M. L. Oliphant (Canberra)
AUSTRIA:	B. Karlik (Vienna), H. Thirring (Vienna)
BELGIUM:	M. de Hemptinne (Louvain), J. Verhaeghe (Ghent)
CANADA:	G. Volkoff (Vancouver)
DENMARK:	C. Møller (Copenhagen), S. Rozental (Copenhagen), G. E. Brown (Copenhagen)
FINLAND:	L. Simons (Helsinki)
FRANCE:	A. Berthelot (Saclay), S. Gorodetzky (Strasbourg)
GERMANY (DEM. REP.):	G. Hertz (Leipzig)
GERMANY (FED. REP.):	W. Gentner (Freiburg i. B.), J. H. D. Jensen (Heidelberg)
GREAT BRITAIN:	W. E. Burcham (Birmingham)
HUNGARY:	L. Janossy (Budapest)
INDIA:	H. Bhabha (Bombay), R. Ramanna (Trombay)
IRISH REPUBLIC:	J. McConnell (Maynooth)
ISRAEL:	G. Racah (Jerusalem)
ITALY:	E. Amaldi (Rome)
JAPAN:	S. Kikuchi (Tokay), S. Tomonaga (Tokyo)
MEXICO:	M. Moshinsky (Mexico)
NETHERLANDS:	H. Brinkman (Groningen), S. R. de Groot (Leiden)
NORWAY:	E. Hylleraas (Oslo), A. Lundby (Oslo), H. Wergeland (Trondheim)
POLAND:	L. Infeld (Warsaw), J. Werle (Warsaw)
PORTUGAL:	J. M. Araújo (Porto), J. R. de Almeida Santos (Coimbra)
SOUTH AMERICA:	G. Beck (Rio de Janeiro), J. Leite Lopes (Rio de Janeiro)
SPAIN:	J. M. Otero (Madrid), C. Sanchez del Rio (Madrid)
SWEDEN:	O. Klein (Stockholm), K. Siegbahn (Uppsala), I. Waller (Uppsala)
SWITZERLAND:	P. Huber (Basel), P. Scherrer (Zürich)
U.A.R. & ARAB COUNTRIES:	F. El Bedewi (Cairo), M. G. Nooh (Cairo)
U.S.A.:	H. H. Barschall (Madison, Wisconsin), S. Devons (New York)
U.S.S.R.:	M. A. Markov (Moscow), I. S. Shapiro (Moscow), D. V. Skobeltzyn (Moscow)
YUGOSLAVIA:	I. Supek (Zagreb)

CONTRIBUTIONS may be sent to the Editor, Professor L. Rosenfeld, NORDITA, Blegdamsvej 17, Copenhagen Ø, either directly, or preferably through the intermediary of one of the members of the Editorial Board of the country or region in which the author is working. They may be written in English, French or German.

NUCLEAR PHYSICS is published in fortnightly issues. The subscription price per volume of 700 pages is fl 57.00; 114s; $ 15.00. Post-free.

SUBSCRIPTIONS should be sent to the publishers, NORTH-HOLLAND PUBLISHING COMPANY P.O. Box 103, Amsterdam or to any subscription-agent.

BOOKS FOR REVIEW should be sent to Professor Rosenfeld.

No part of this issue may be reproduced in any form, by print, photoprint, microfilm or any other means without permission from the publisher.

Printed in the Netherlands

2.L

Nuclear Physics **27** (1961) 1—24; © *North-Holland Publishing Co., Amsterdam*

Not to be reproduced by photoprint or microfilm without written permission from the publisher

THE ELASTIC AND INELASTIC SCATTERING OF PROTONS BY MAGNESIUM IN THE ENERGY RANGE FROM 7.3 MeV TO 15.9 MeV

K. MATSUDA, Y. NAGAHARA †, Y. ODA ††, N. YAMAMURO †† and S. KOBAYASHI †††

Institute for Nuclear Study, University of Tokyo, Tanashi-machi, Tokyo

Received 17 March 1961

Abstract: Twenty seven proton angular distributions for the elastic scattering from magnesium and for the inelastic scattering from Mg^{24}, leading to the first excited state at 1.37 MeV, are presented in the energy range from 7.32 MeV to 15.85 MeV. The elastic angular distribution shows generally maxima and minima of the diffraction type. The absolute cross sections at fixed angles, however, vary appreciably from energy to energy, particularly at backward angles. The angular distribution for inelastic scattering varies remarkably with the incident energy, especially in the energy range less than 12 MeV. The integrated cross section for the inelastic scattering also shows variations with energy.

The results are compared with those which have been obtained in other laboratories and with those for other target nuclei obtained in our laboratory. The emitted spectrum of inelastic protons is also presented in connection with the study of angular distribution. The conlcusion is that neither the simple theory of direct process and/or optical model, nor that of compound process explains the results completely.

1. Introduction

The angular distribution for elastic and inelastic scattering of nucleons from nuclei is one of the basic techniques for the investigation of reaction mechanisms and nuclear structure. Many experiments have been made in this field, but the energy domains explored were generally limited by the range of existing accelerators. Angular distributions for the elastic and the inelastic scattering of protons from magnesium have been reported by many authors [1–11]) Some authors have reported [2, 11, 12]) their investigations on the angular correlation of Mg^{24} (p, p′γ). Others have reported their studies on the scattering angular distribution for other projectiles incident on magnesium [13–15]).

As pointed out by Greenless *et al.* [5]), the angular distribution for elastic and inelastic scattering of protons from magnesium changes remarkably with incident energy in the region around 10 MeV. Oda *et al.* [9]) revealed that this situation is generally true when the mass number of the target nucleus is less than 40. On the other hand, Hu *et al.* [16]) showed that it is rather different

† Present address: Yokohama National University, Yokohama
†† Present address: Tokyo Institute of Technology, Tokyo
††† Present address: Institute for Solid State Physics, University of Tokyo, Tokyo

for nuclei whose mass numbers are larger than 40. The energy dependence of angular distribution is not so remarkable for these nuclei ($A > 40$) as for light nuclei.

We must note that the above mentioned experiments in our laboratory are mainly concerned with even nuclei, and that the results might be somewhat different for the other types of nuclei. As the INS (Tokyo) variable energy cyclotron gives us a proton beam of any desired energy between 7.5 MeV and 16 MeV, the experiments on the angular distribution of protons from light even nuclei were tried over a wide range of bombarding energy. In previous papers, Kobayashi [17]) reported results for oxygen and neon and Nagahara reported results for carbon [18]). This paper mainly concerns the results for magnesium. Magnesium is interesting because it is considered to be a strongly deformed nucleus [19, 20]). Yoshida pointed out that in the scattering of nucleons from such a nucleus the coupling between the elastic and the inelastic channel by collective interactions plays an important role [21]). He also investigated the nucleon scattering from Mg^{24} taking into account both surface interaction and single particle interactions [22]).

The aim of this paper is to survey the general trend of the proton scattering from magnesium over a wide energy range. We have tried to obtain as accurate results as possible, but increase in precision was not the main purpose of this experiment.

2. Experimental Details

2.1. THE CYCLOTRON BEAM

The performance of the cyclotron has been reported in an earlier paper [23]). As stated there, the beam energy can be changed easily. Energy changes less than 1.0 MeV require only a few minutes adjustment of dial settings at the console. We can also change the beam energy slightly by inserting absorber foils of aluminium just in front of the collimator of scattering chamber. When an energy change of more than 1.5 MeV is required, exchange of the coupling condensers of the oscillator system becomes necessary. Even in this case, it requires only about ten minutes. No trouble has been experienced in changing the beam energy to any desired value within a short period.

Whenever the conditions of the cyclotron were changed, the beam energy was measured by the absorption method, which has been described elsewhere [24]). The relative accuracy of the noted value of the energy may be ± 50 keV and the error in the absolute value is estimated as ± 100 keV. The correspondence between the cyclotron frequency and the measured beam energy is shown approximately in fig. 1. The spread of incident beam energy is an important factor to be considered for experiments such as described here, but it is difficult to measure. The energy spectrum of the cyclotron beam, which did not pass

through the collimator system, was measured by a beam analyzing system with energy resolution of 0.05 %. The results revealed the following two points:

(i) The energy spread depends largely on the cyclotron conditions and varies from 0.5 % to 1.5 % with a change in cyclotron parameters. The spectrum is also changeable.

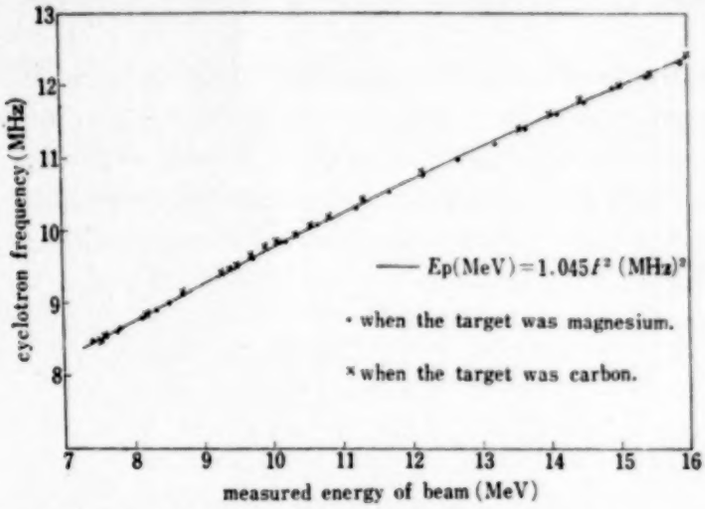
cyclotron frequency (MHz)
measured energy of beam (MeV)
Ep(MeV)=1.045f² (MHz)²
· when the target was magnesium.
× when the target was carbon.

Fig. 1. The correspondence between the cyclotron frequency and the measured energy of beam. The carbon points are taken from ref. [18]).

(ii) When we carefully keep the cyclotron conditions constant, the energy value and the spectrum remain constant within ± 0.1 % for more than an hour. Even under usual operation without any drastic drift of the parameters, the beam energy does not change by more than 0.5 %.

2.2 THE DETECTOR SYSTEM

For the measurement of angular distributions, we used the multi-counter system described elsewhere [17–19, 25]). We installed 15 scintillation counters on the side window of the scattering chamber at the laboratory angles 20°, (25°), 30°, 40°, 50°, 60°, 70°, 80°, 90°, (95°), 115°, 125°, 135°, 145°, 155° and 165°. High tension was fed to each multiplier and signals from it were sent to the counting room through a cathode follower and a coaxial cable. We had only five sets of electronics to analyse the pulse height, each of which consists of an Al amplifier and a multi-channel pulse-height analyser (10 channels or 20 channels). After measuring the yields from detectors at five detection angles, we changed the input connections and measured the yields from the next five detectors and so on. Only four sets of such measurements provided complete data for the angular distribution at a given energy. As the energy sensitivity of each counter is, of course, different, the gains of the amplifiers were adjusted before each set of measurements, so that the elastic peaks might appear at nearly the same voltages. This procedure was not troublesome. The strong points of the method are as follows:

(i) The required machine time was made very short.

(ii) The angular distribution thus obtained was more reliable.

(iii) The energy spectrum at forward angles became very clear. The reason for the last fact is that the solid angles at forward angles were made small and the counters always received nearly constant counting rates, which is important because photomultipliers are sensitive to excess and abrupt changes of counting rate.

One counter telescope was installed on the turn table in the scattering chamber. It consisted of proportional counters and a scintillation counter. In the angular distribution measurement, it served as an auxiliary detector. It was also used for the measurement of the emitted spectrum. In this case, the proportional counter served as a gamma and alpha supressing counter.

2.3. ERRORS

As to the relative errors of differential cross section, detailed discussions were given in previous papers [17, 18]). Some errors mentioned there, which arose mainly from the gas target system, were neglected in this paper. For the angular distribution study, the counts from the 90° detector were always recorded at each set of measurements for monitoring. The yield of this monitor and the reading of the current integrator were in agreement within the error of 3 %, and errors due to the counting statistics were less than ± 3 % in most cases, Thus, considering the various sources of errors, we can say that the relative errors in the cross sections were within ± 5 %. There were, however, the following exceptions for the case of inelastic scattering:

(1) at the extreme forward angles, i.e. at 20° and 25°, errors arising from the background subtraction were so large that relative errors of ± 10 % were involved in the cross section.

(2) We tried to discriminate against the contributions from Mg^{25} and Mg^{26} but the discrimination was considered to be insufficient and the contribution from Mg^{24} is probably over-estimated. The latter errors were large when 10 channel pulse-height analysers were used. In this case we modified the estimate of errors, i.e. $+5$ % and -8 % at angles from 90° to 165°. Absolute errors of the cross section arising from the non-uniform thickness of the target are serious for the experiment with a foil target. We made the targets by evaporation of magnesium ribbon and the contamination of oxygen or hydrogen was negligibly small; this fact was demonstrated by the energy spectrum of inelastic protons. The absolute error of the cross section was estimated to be ± 10 %, which was determined from the results of the check measurement described in sect. 2.4.

2.4. PROCEDURE

The emitted spectrum of inelastic protons was measured at 9.5, 12.6 and 15.7 MeV. The whole spectrum at 90° was obtained with the counter telescope.

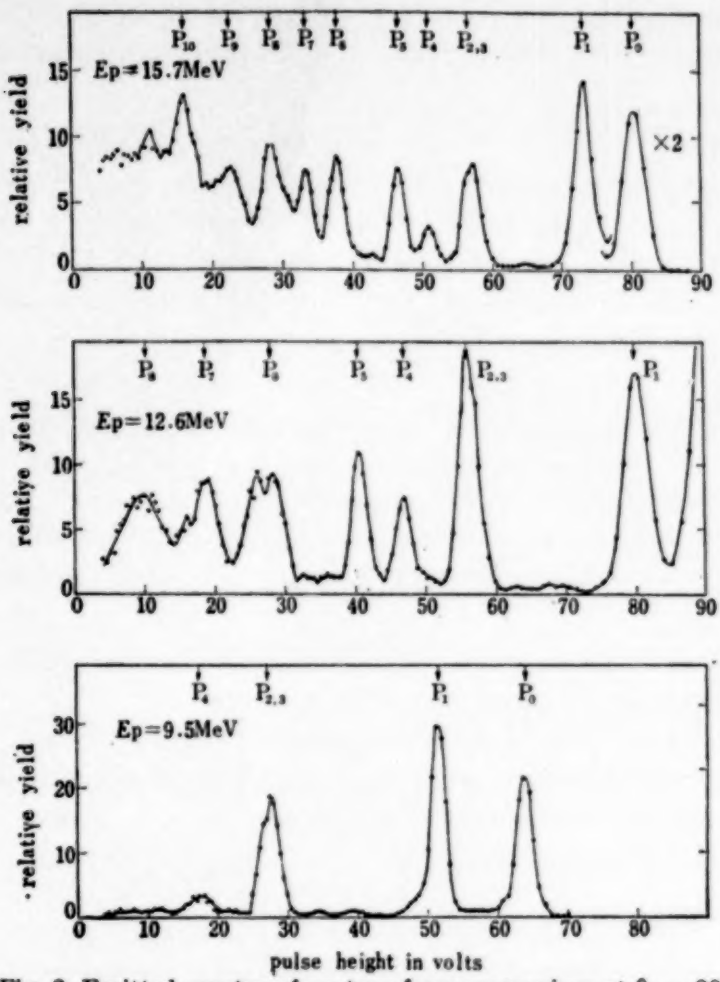

Fig. 2. Emitted spectra of protons from magnesium at $\theta_L = 90$.

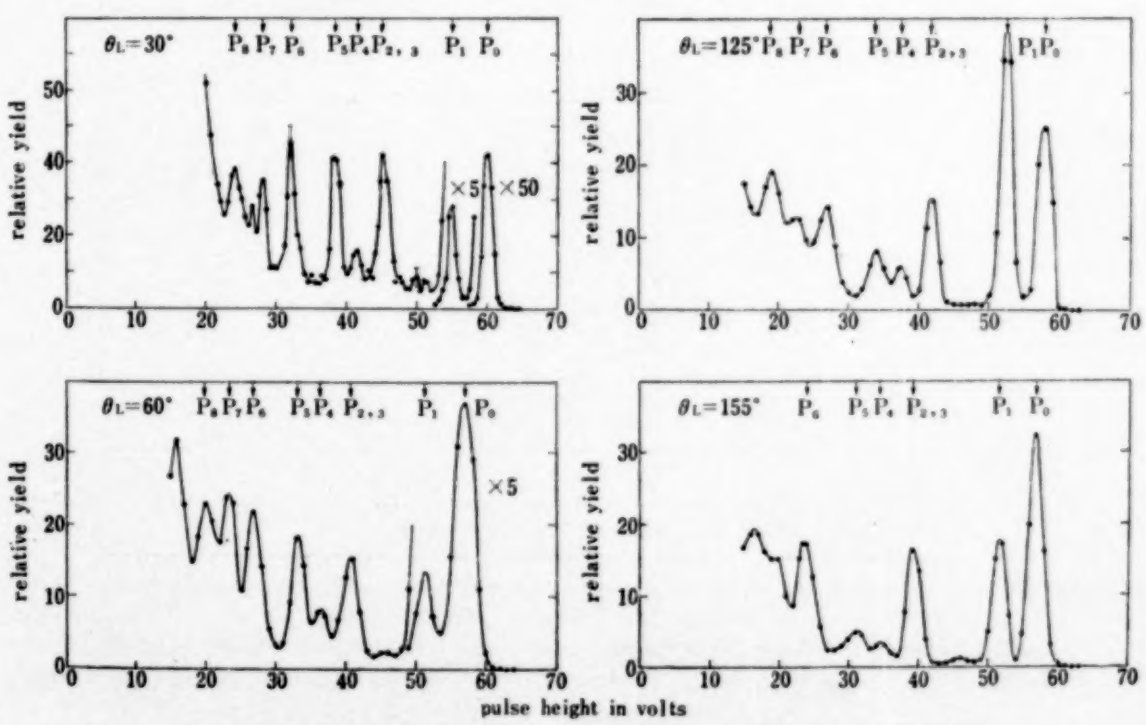

Fig. 3. Emitted spectra of protons from magnesium at $E_p = 15.7$ MeV.

Spectra at 30°, 60°, 125° and 150° were also obtained by scintillation counters at the same time. These four spectra were not free from the gamma-ray background.

The angular distribution study is devided into four groups, i.e. from 7.32 to 7.79 MeV, from 8.30 to 10.20 MeV, from 10.64 to 14.06 MeV and from 14.45 to 15.85 MeV. Each group was measured at a different time with a different target. Absolute values of the cross section were checked at several energies with a carefully prepared uniform target. Considering the result of the check measurement, we normalised the absolute values of the cross sections for the four groups. Considering the fact that corrections of about 10 % were needed for the data obtained at different times, we estimated errors of ± 10 % for the absolute values of the corrected cross sections. The beam energy was changed by changing the cyclotron parameters, with the exception of the second group, where the energy was changed by inserting aluminium foils.

3. Results

3.1. EMITTED SPECTRUM

Fig. 2 shows the emitted spectra, measured by the scintillation counter, of the inelastic proton groups from magnesium at 90°. Fig. 3 shows the same at 30°, 60°, 125° and 155°, all at an energy of 15.7 MeV. The energies, and the

TABLE 1

Absolute cross section from emitted spectrum

E_p (MeV)		15.7	12.6	9.6
group	level energy (MeV)	Cross section at 90° (mb/sr)		
p_0	0	12.2		
p_1	1.37	7.4	12.2	24.8
$p_{2,3}$	4.2	4.5	10.2	18.4
p_4	5.3	1.4	3.1	4.0
p_5	6.0	2.8	4.3	
p_6	7.4	4.1	8.3	
p_7	8.5	3.4	6.2	
p_8	9.5	5.4	8.2	
total $\sigma_t(90°)$		56.1	58.0	52.5
$4\pi\sigma_t$		710	750	670
σ_{ist}/σ_t		13 %	21 %	47 %

These values are obtained with the assumption that all the inelastic proton comes from Mg^{24}, so that the total cross sections must be overestimated. From this point of view, the total cross section will be 600 ± 100 mb over the energy range, which corresponds to $\pi r^2 = \pi(A^{\frac{1}{3}} r_0)^2$, for $r_0 = 1.52$ fm.

differential cross sections at 90° for these levels obtained from the data † in fig. 3 are listed in table 1. We tentatively assumed that the yields are due to only Mg^{24}, and assumed moreover that the 4π times of the differential cross section at 90° gives a rough estimate of the integrated cross section. The results in fig. 3 suggest that the anisotropy of the angular distribution is not so remarkable and the latter assumption gives us a fairly good approximation. These values are also shown on table 1 and the total inelastic cross section is estimated to be 600 ± 100 mb for the incident energies from 9.5 MeV to 15.7 MeV. This value is of the order of the geometrical cross section. For Mg^{24}, the main isotope of magnesium (78.6 %), the Q values of proton induced reactions are highly negative in general. The exceptions are the (p, α) ($Q = -6.87$ MeV) the (p, pα) ($Q = -9.03$), the (p, p2α) ($Q = -13.78$) and the (p, γ) ($Q = 2.26$ MeV) reactions which are considered to be less probable than the inelastic events. The other reactions arising from Mg^{24} +p are forbidden in the whole energy range investigated. This fact suggests that the total inelastic scattering cross section is roughly equal to the total reaction cross section in these energy ranges ††. In the energy region less than 10 MeV, the reaction occurs mainly through the four channels of Mg^{24}, i.e. p_0, p_1 and $p_{2,3}$. The total reaction cross section does not seem to change considerably with energy, while the contribution of p_1 varies appreciably with energy. Unfortunately, the energy points where the spectra were investigated are limited to the above-mentioned three and the target is not made of the pure isotope, so we cannot say anything in detail regarding the total reaction cross section.

3.2. ELATIC SCATTERING

Results of the elastic angular distribution are shown in fig. 4. The numerical values have been reported ††† elsewhere [26]). The distribution shape shows maxima and minima of the diffraction type. In the energy range from 7.7 MeV to 9.0 MeV, the diffraction pattern disappears. Fig. 5 shows the positions of the first and the second minima and the first maximum in the angular distribution. In fig. 5, the breadth of lines indicates the angular range where the cross section lies within 5 % of the value at the maximum and the minimum, so that it expresses something about the sharpness of the diffraction pattern. Fig. 6 shows the dependence of the differential cross section on energy. The variation with energy is appreciable even when the positions of the minimum and the maximum remain almost unchanged. The fluctuation with energy is large at

† Recently, such spectra have been measured with a magnetic analyser in our laboratory [36]). The results are more complicated than those obtained by the scintillation. For example, the 7.4 MeV level probably consists of four levels at 7.35, 7.55, 7.62 and 7.75 MeV and the 8.5 MeV level of three levels at 8.37, 8.43 and 8.65 MeV. Other levels are found at 8.91, 9.14, 9.28, 9.53 and 10.15 MeV.

†† This result agrees roughly with that of recent total reaction cross section measurements and that of the optical model analysis for near-by nuclei.

††† The report is available upon request.

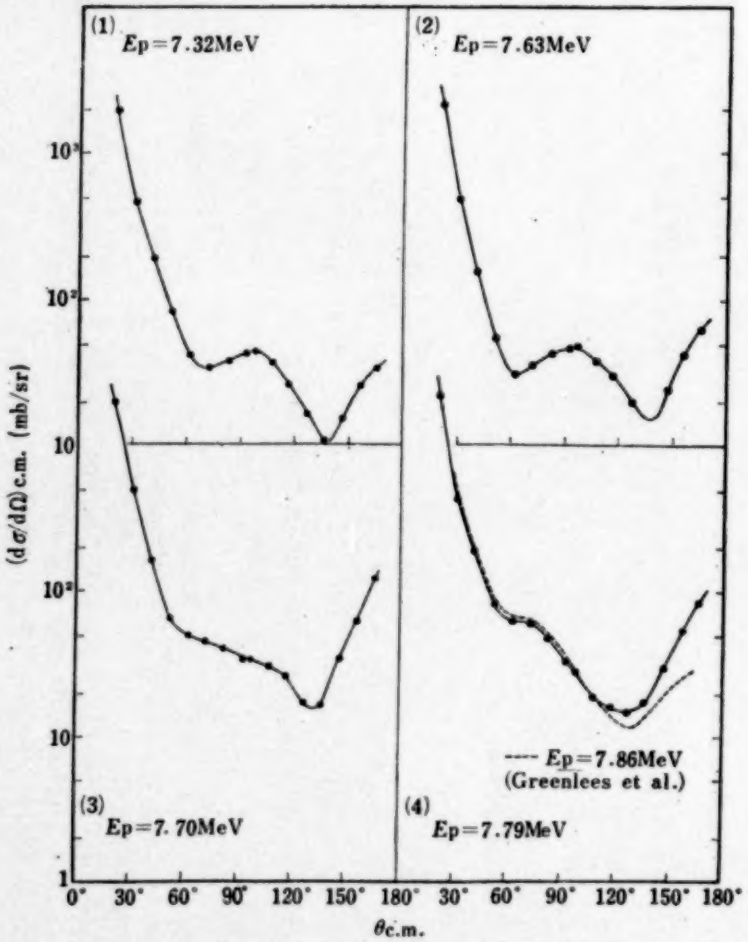

Fig. 4. (1) Angular distributions of elastic protons from magnesium.

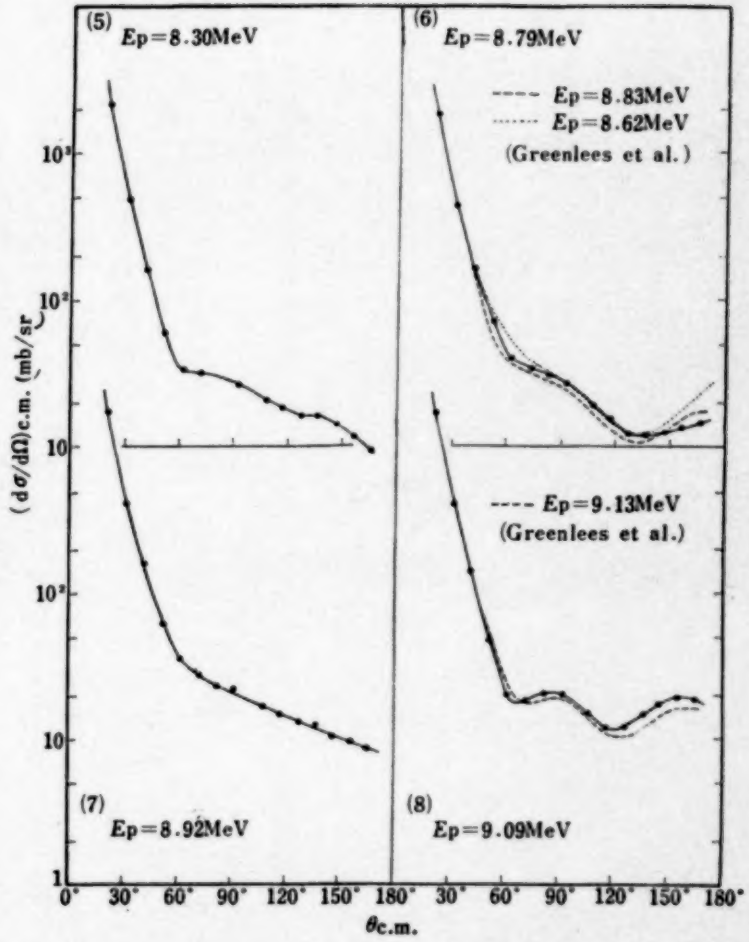

Fig. 4. (2) Angular distributions of elastic protons from magnesium.

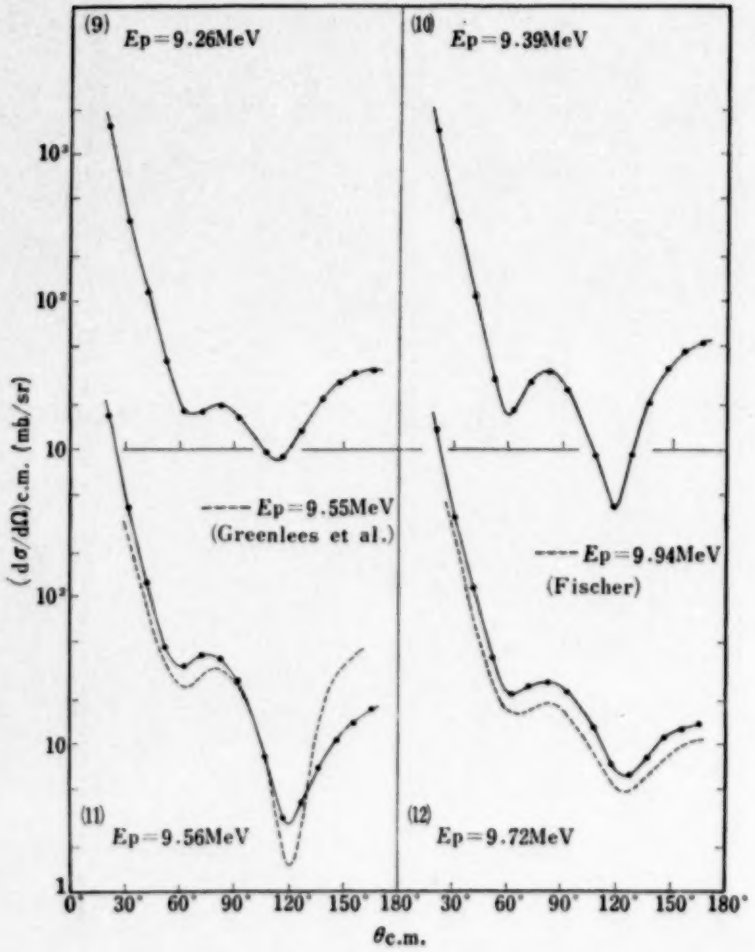

Fig. 4. (3) Angular distributions of elastic protons from magnesium.

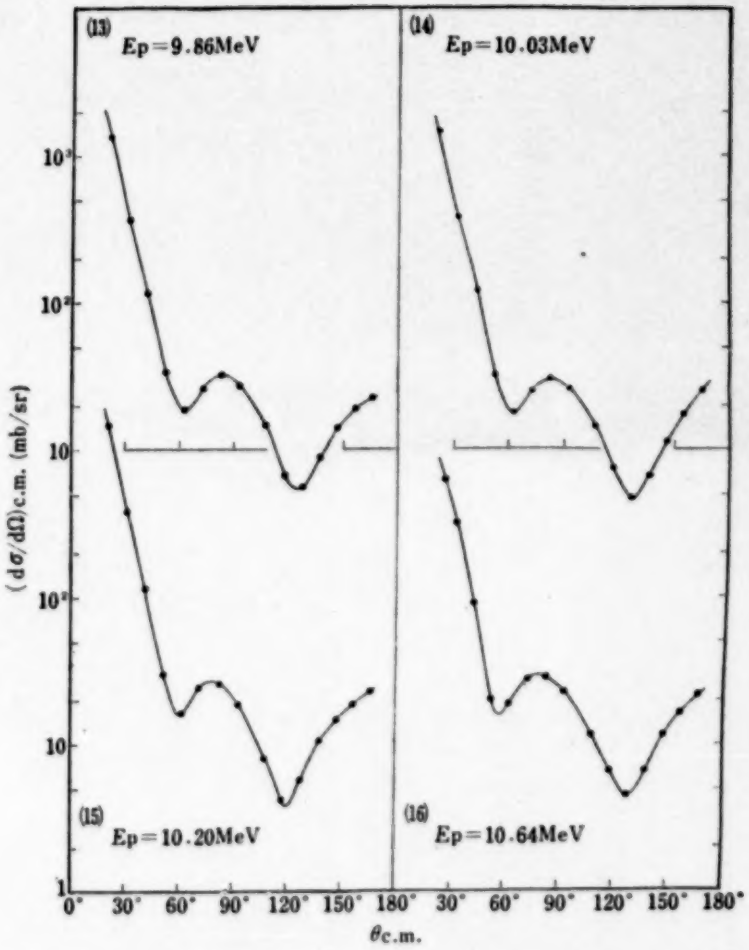

Fig. 4. (4) Angular distributions of elastic protons from magnesium.

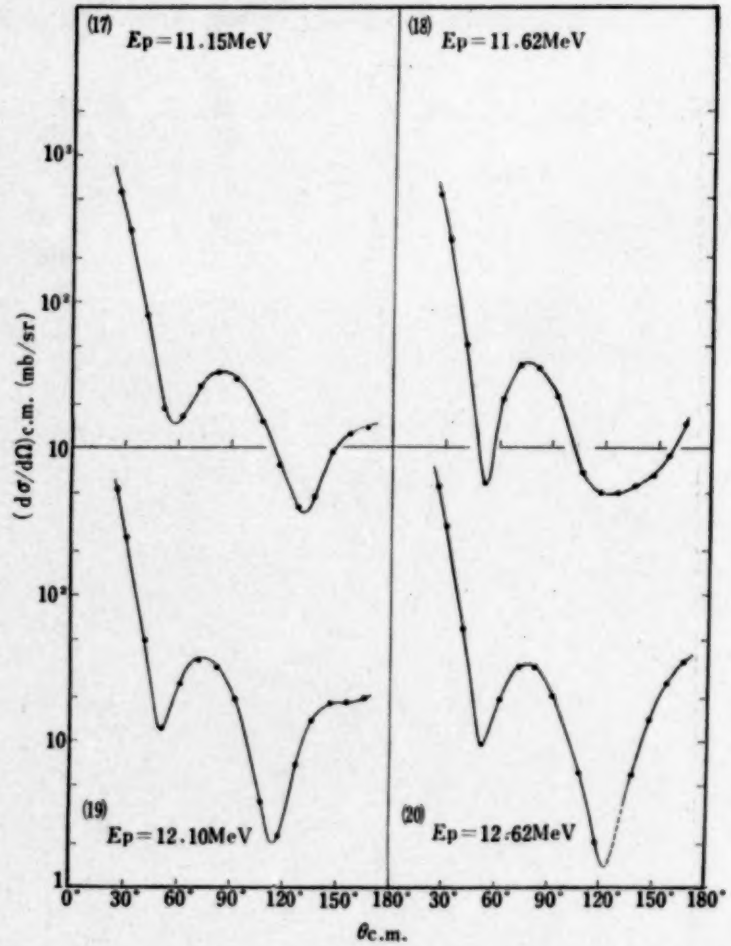

Fig. 4. (5) Angular distributions of elastic protons from magnesium.

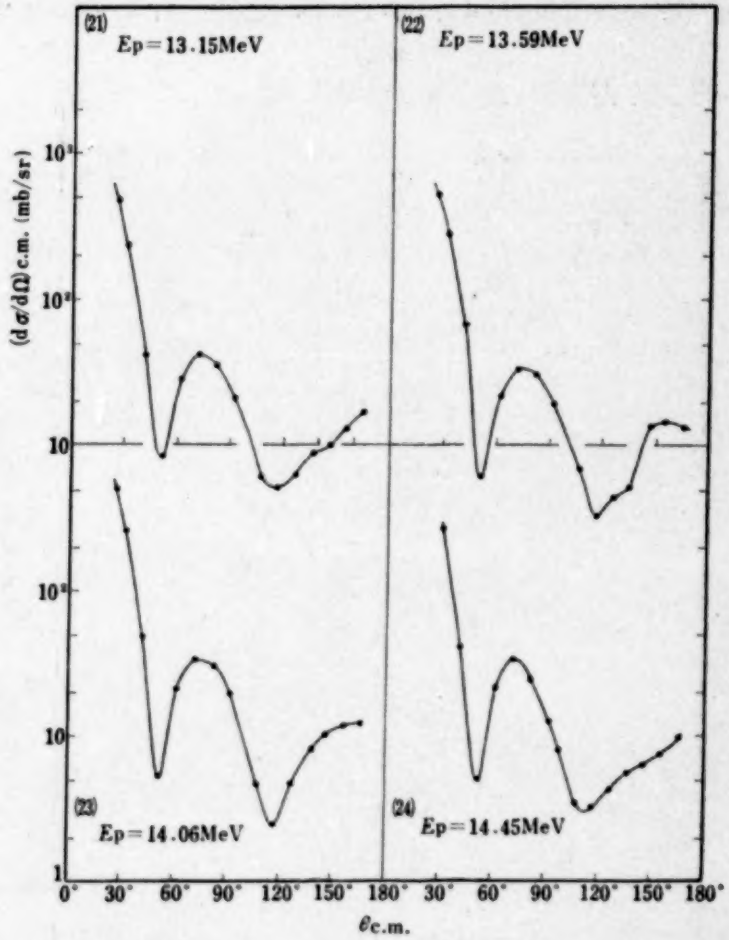

Fig. 4. (6) Angular distributions of elastic protons from magnesium.

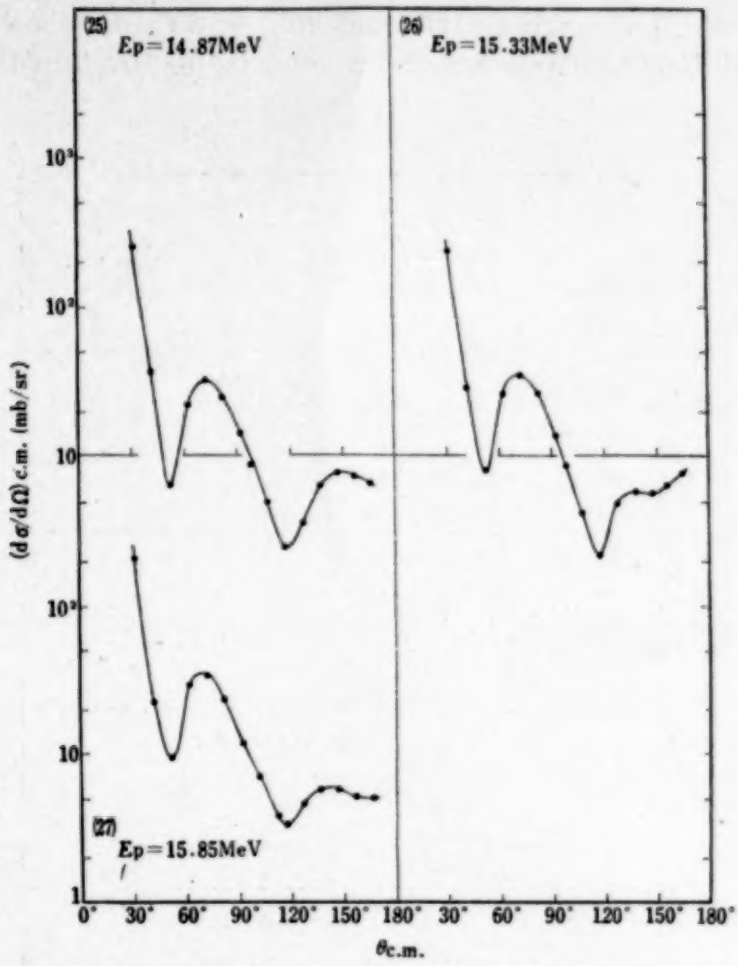

Fig. 4. (7) Angular distributions of elastic protons from magnesium.

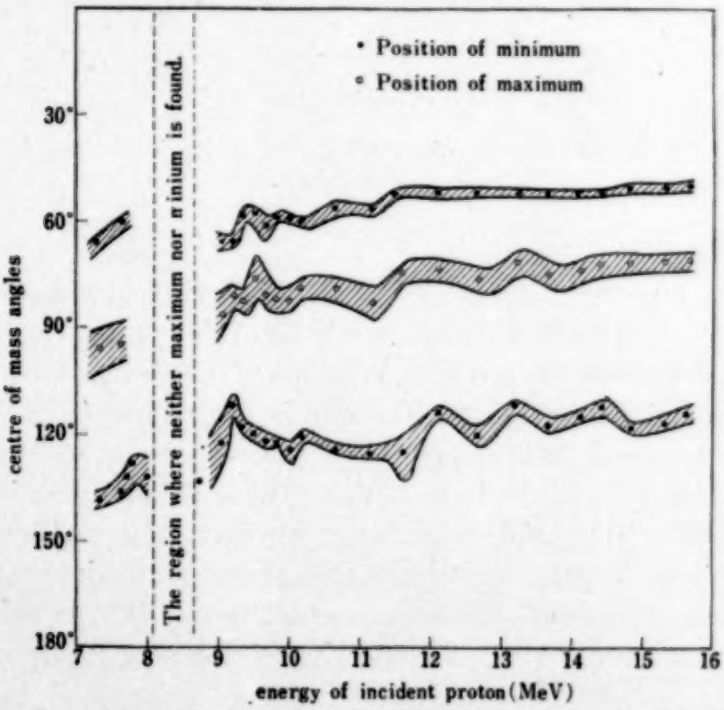
• Position of minimum
◦ Position of maximum
The region where neither maximum nor minium is found.
centre of mass angles
energy of incident proton (MeV)

Fig. 5. Positions of maxima and minima in the diffraction pattern for the elastic scattering of protons from magnesium.

155° and at 60°, but small at 125° and 90°. At 30°, the absolute values of variation $\Delta(d\sigma/d\Omega)$ are large but the fractions $\Delta(d\sigma/d\Omega)/(d\sigma/d\Omega)$ are not so large.

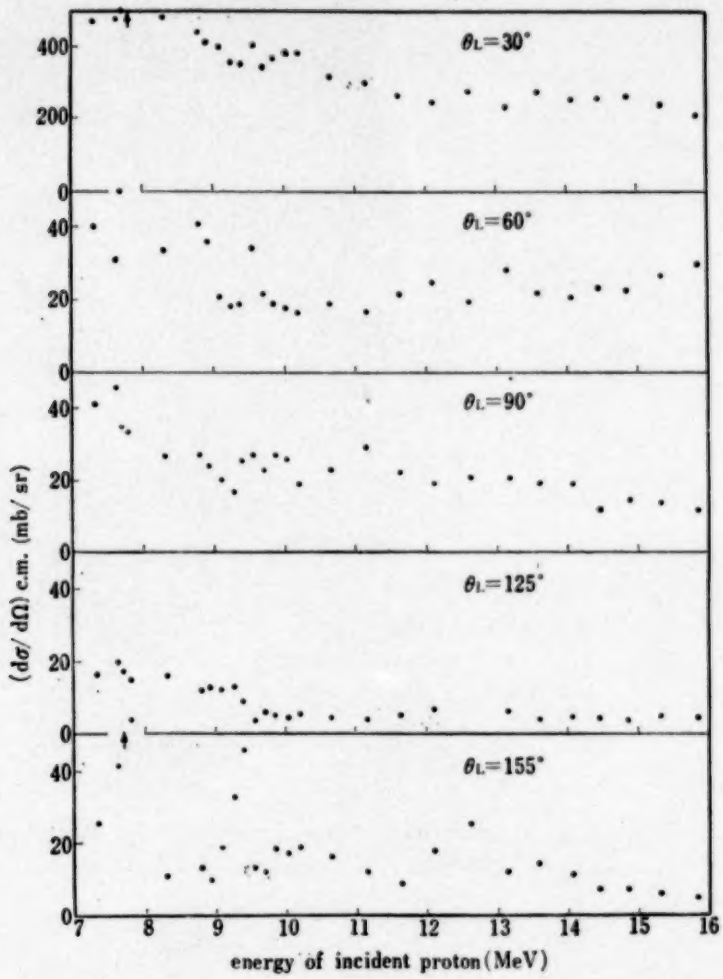

Fig. 6. Energy dependences of the differential cross section for the elastic scattering from magnesium.

3.3. INELASTIC SCATTERING

Results of the angular distribution for the inelastic scattering leading to the first excited state at 1.37 MeV are shown in fig. 7. The numerical values of the cross section have also been reported elsewhere [26]). We can tentatively divide the energy region into two parts. The one is the region (A), $E_p < 12$ MeV, where the angular distributions shape is highly dependent on the energy. The other is the region (B), $E_p > 12.5$ MeV, where the shape remains almost unchanged, while the differential cross section at given angles still varies with the energy. In the region (B), the distribution shows a maximum at a forward angle, a minimum near 90° and a maximum near 130°. In this region, the angular distribution for the elastic scattering is also very stable against energy

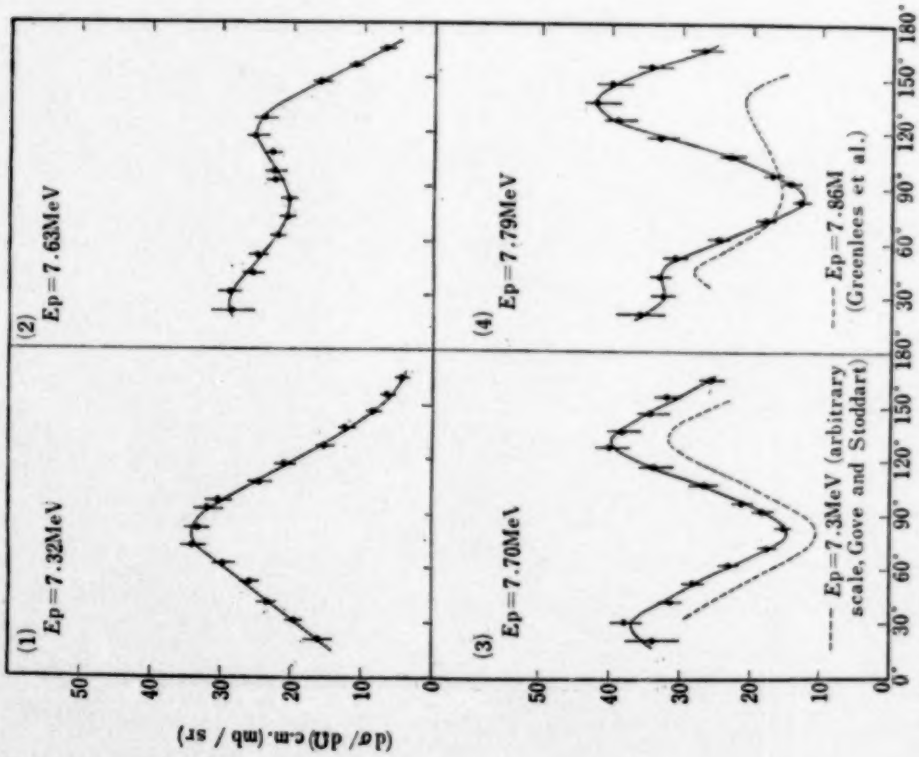

Fig. 7. (1) Angular distributions for the inelastic scattering of protons from magnesium-24.

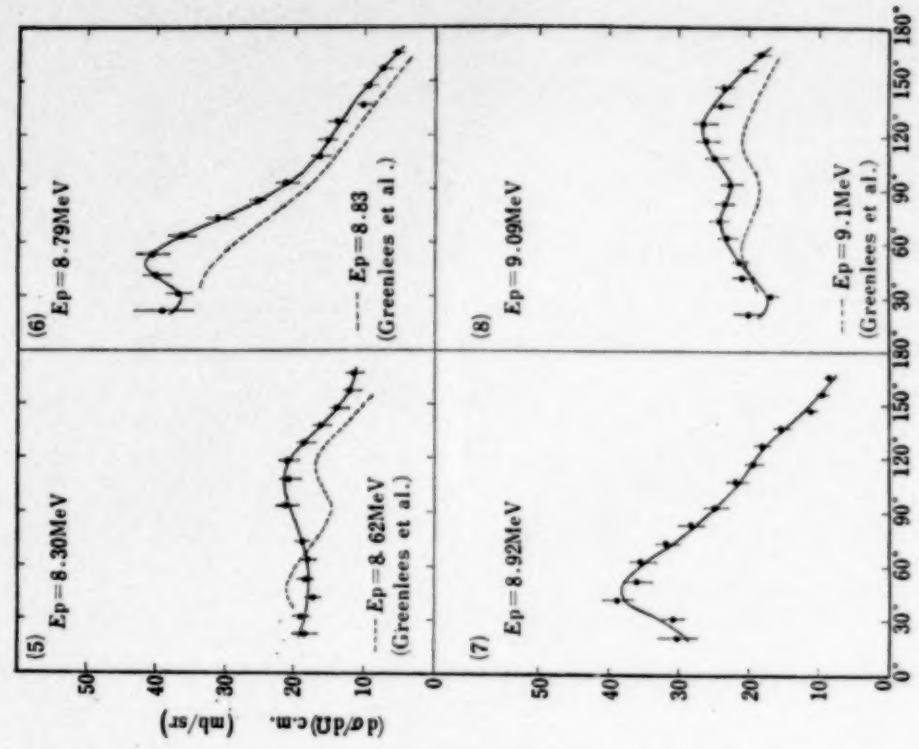

Fig. 7. (2) Angular distributions for the inelastic scattering of protons from magnesium-24.

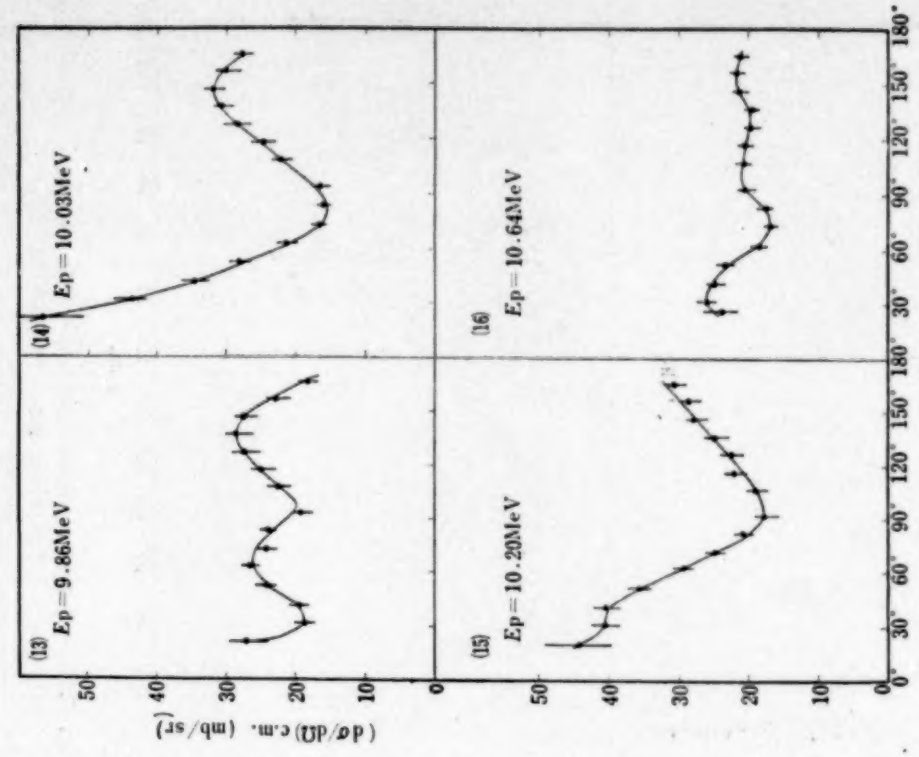

Fig. 7. (4) Angular distributions for the inelastic scattering of protons from magnesium-24.

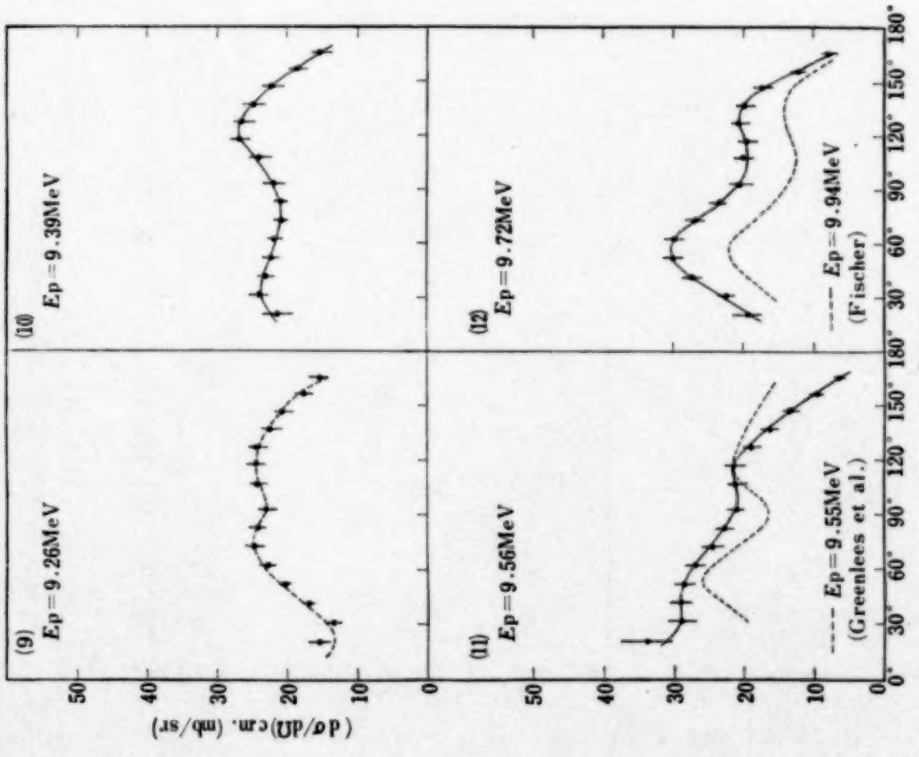

Fig. 7. (3) Angular distributions for the inelastic scattering of protons from magnesium-24.

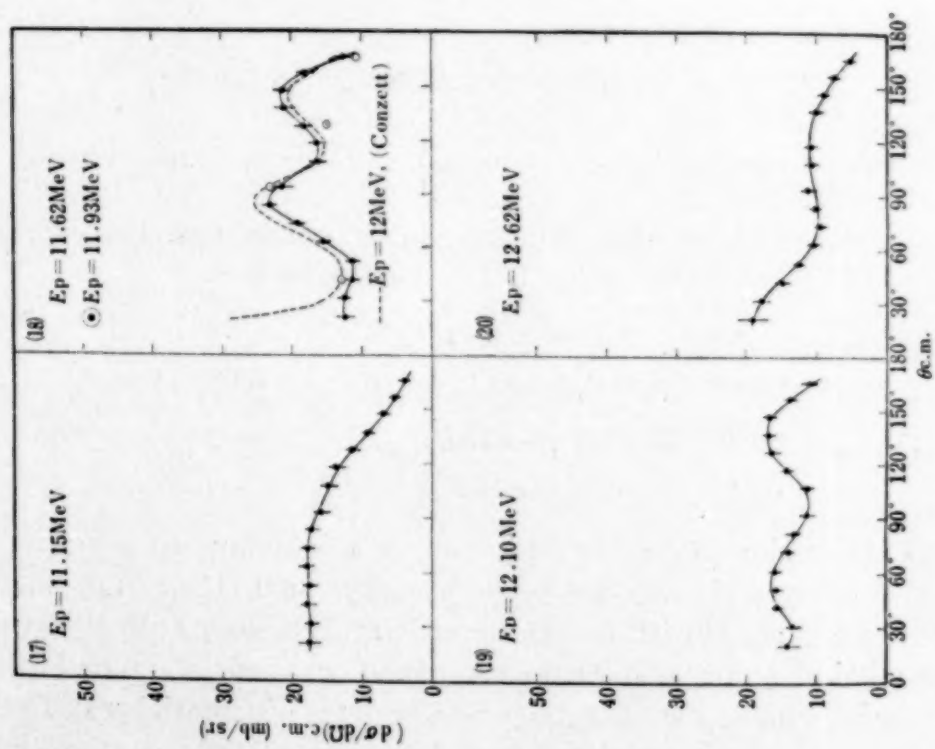

Fig. 7. (5) Angular distributions for the inelastic scattering of protons from magnesium-24.

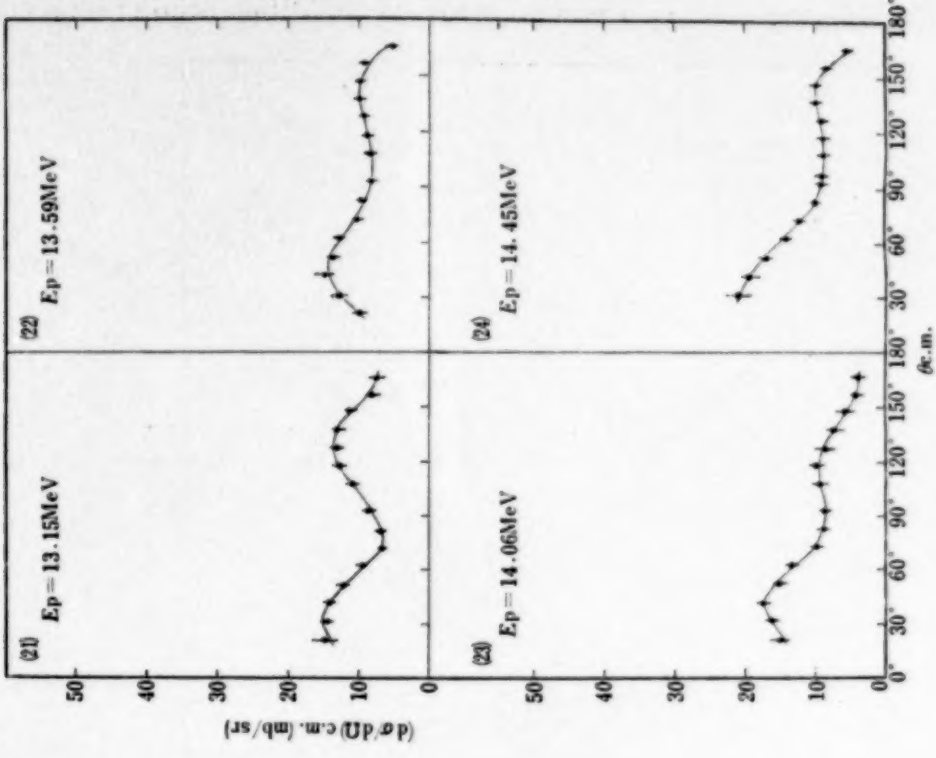

Fig. 7. (6) Angular distributions for the inelastic scattering of protons from magnesium-24.

change. We can expand the inelastic angular distribution in Legendre polynomials. Considering the experimental errors of the differential cross section

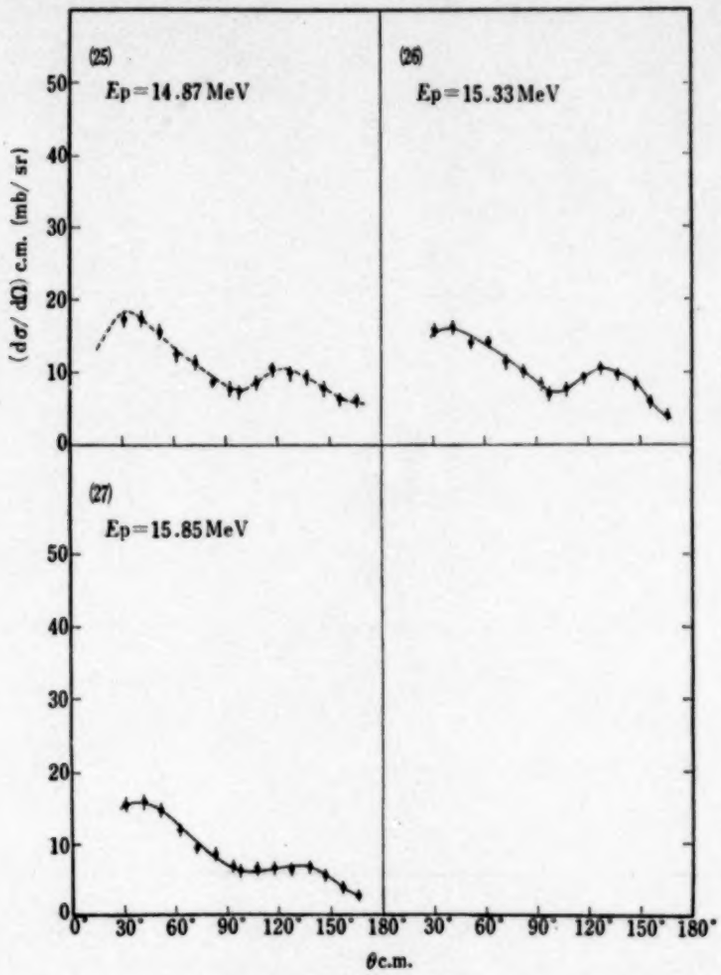

Fig. 7. (7) Angular distributions for the inelastic scattering of protons from magnesium-24.

the terms of order higher than 8th are almost meaningless. For example, fits are shown in (9) and (25) of fig. 7. The coefficients are

$$f(\theta)_{9.26} = 21.70\,P_0 - 2.07\,P_1 - 6.74P_2 - 0.49P_3 - 2.24P_4 + 3.53P_5 + 1.57P_6 + 0.62P_7 - 1.62P_8,$$

$$f(\theta)_{14.87} = 10.88P_0 + 4.85P_1 + 2.15P_2 + 0.33P_3 - 4.88P_4 - 1.15P_5 - 0.20P_6 - 2.38P_7 - 1.20P_8.$$

Of course, in the region (A) these coefficients are also highly dependent on the energy and those of odd order are not necessarily small. The results suggest that neither the analysis with the one level formula of resonance theory nor with the statistical assumption for the compound process is adequate in these phenomena. Fig. 8 shows the energy dependence of the differential cross section at given angles. It also includes the partial (integrated) cross section. From

the results shown in figs. 6 and 8, it is hard to assign definitely the levels of the compound nucleus. The only exception is at $E_p = 7.70$ MeV. which corresponds to the level of Al^{25} at 9.68 MeV. The fact that the variation at 90° is less remarkable than at other angles, may suggest that the reaction occurs through odd parity states. We must point out that the variation in partial cross section is

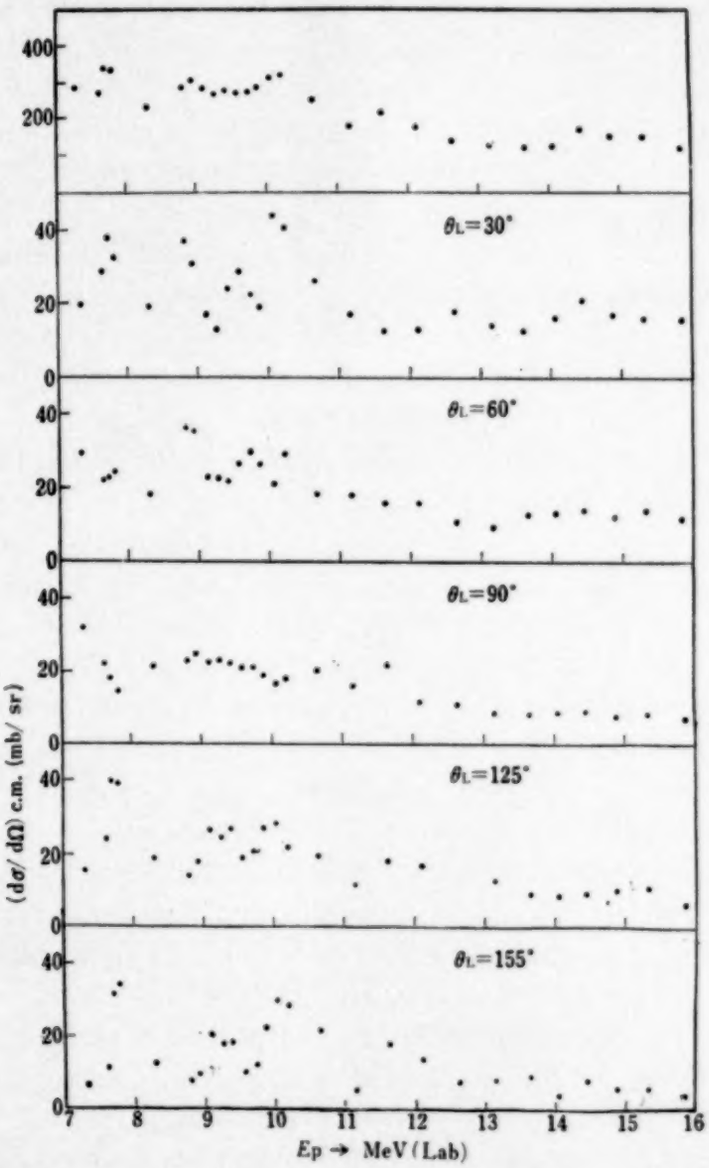

Fig. 8. Energy dependences in the cross sections for the inelastic scattering from magnesium.

rather smooth with energy. It is noted that we used a beam of energy spread as described in sect. 2.1 and also chose the energy points investigated optionally. The variations with energy might appear more frequently or steeper than represented in figs. 6 and 8, if a beam of finer spread and with finer intervals were used.

4. Comparisons

4.1. COMPARISON WITH OTHER EXPERIMENTS

Some authors have reported [27]) the emitted spectrum of inelastic protons from Mg^{24}. The level energies presented in this paper are not always consistent with their values. Fulbright, Lasson and Poulson [28]) measured the emitted spectrum of inelastic alpha particles from magnesium for the incident energy of 20 MeV. The spectrum is very similar to ours of $E_p = 15.7$ MeV. The groups which do not appear in the alpha particle scattering are 7.4 MeV and 11.5 MeV. Some levels presented here also correspond † to those obtained in the Na^{23} (d, n) Mg^{24} reaction [30]) and the beta-decay [27]) of Al^{24} and Na^{24}.

Yamabe *et al.* [1]) investigated the inelastic scattering of protons from magnesium at the vicinity of 5.5 MeV. They discussed the difficulty that the angular distributions may not be explained by the one level formula of resonance theory in such a low energy region. Seward [2]) investigated the inelastic scattering of protons in the energy region just below the present investigation. We can see from his results that just below 7.5 MeV the situation is nearly similar to that just above 7.5 MeV, as revealed in the present paper. He and Lackner *et al.* [11]) also showed that even in such an energy region, the angular correlation between the inelastic proton and the successive gamma-ray has a symmetry axis along a direction near that of the recoil axis ††. The differential cross section at 90° varies more remarkable below 8.0 MeV than above 8.0 MeV. Seward's result that the $(d\sigma/d\Omega)$ 90° reaches a maximum value of 60 mb/sr near 7.5 MeV agrees with our result which shows a maximum value of 46 mb/sr at 7.6 MeV. The discrepancy between those two cross section values is caused by the fact that Seward regarded the elastic scattering at 23° as the Rutherford scattering but it is not really so, as revealed in this experiment. Gove and Stoddart [3]) measured the angular distribution of the inelastic scattering at 7.3 MeV as shown in (3) of fig. 7. Their result is very similar to ours at 7.70 MeV. Greenlees *et al.* [5]) measured the elastic and the inelastic angular distribution at five energies, 7.86, 8.62, 8.83, 9.13 and 9.59 MeV. Generally speeking, their result agrees with ours, as shown in (4), (6), (8) and (11) of fig. 4 and (4), (6), (7), (8) and (11) of fig. 7. The agreement in the results for elastic scattering seems to be better than in that for inelastic scattering . This fact shows perhaps that the angular distribution shape for inelastic scattering is more sensitive to changes in energy than for elastic scattering. Baker *et al.* measured an inelastic angular distribution of a very particular shape at 9.6 MeV. It seems, however, to be similar to our result at 9.56 MeV. Conzett [8]) measured the angular distribution of the inelastic scattering at 12 MeV. Even though his

† see footnote to sect. 3.1.

†† Angular correlation studies in the energy range covered by this experiment have been performed recently in our laboratory. The results are roughly consistent with the direct interaction theory [37]).

distribution shape seems to be very unusual, our result at 11.62 MeV agrees very well with this except at extreme forward angles, as shown in (18) of fig. 7. We also measured the differential cross sections at four angles at 11.93 MeV in the check measurement and found that at this energy the cross section does not contradict Conzett's values. The angular distributions of the elastic and inelastic scattering obtained by Fischer at 9.94 MeV have no counterpart in our result, but ours at 9.72 MeV are very close to those of Fischer's. Our absolute values are larger by a factor of 1.4 than this in both the elastic and the inelastic scattering †. Gugelot and Phillips measured the inelastic angular distribution at 18 MeV. Their distribution shape shows a steep increase at forward angles, which is not found in our results. Such an abrupt change at the high energy region bewilders us somewhat. In a word, the result presented here agrees farely well with the results presented by other authors.

In the case of the scattering of alpha particles, Blair *et al.* [15]) made an experimental and theoretical investigation in view of the strong deformation of Mg^{24}. Our result does not agree with Blair's model as reported by McDaniels *et al.* [30]) In the energy region where the angular distribution shape is stabilized, the diffraction patterns of the elastic and the inelastic scattering of protons from magnesium are neither in nor out of phase to each other. But, as pointed out previously [25]), the angular frequency of diffraction is nearly the same in both scatterings.

4.2. COMPARISON WITH RESULTS FOR OTHER NUCLEI

The angular distributions for light even nuclei measured in our laboratory are presented in fig. 10 and 11.

4.2.1. Elastic scattering

From angular distributions of the diffraction type, we can draw such figures as fig.5 for C^{12}, O^{16} and Ne^{20}. These figures show that the positions of the maxima and the minima vary smoothly with energy in general with small fluctuations in position. In some energy regions which are characteristics of the nucleide, however, these angular positions become obscure or make abrupt changes. Such regions are 9—11 MeV for C^{12}, less than 11 MeV for O^{16}, near 8, 9 and 10.5 MeV for neon and 7.7 to 9 MeV for magnesium. Even outside of such anomalous regions, the cross section varies with energy especially at backward angles, and the fluctuation generally amount to a few hundred keV or 1 MeV. From figures like fig. 5, we can determine the average positions of the minima and the maxima over the energy range, when we neglect the anomalous regions. Fig. 9 shows such average positions for various nucleides. This figures shows that the regularity of positions of the minima and maxima, even over the anomalous region, is governed by some general rule, such as arising from a

† A similar discrepancy with his result occurs in the scattering from carbon [18]).

potential involving a wide range of mass number and incident energy. In the elastic scattering it is hard to find any characteristic nature for magnesium except in the anomalous regions.

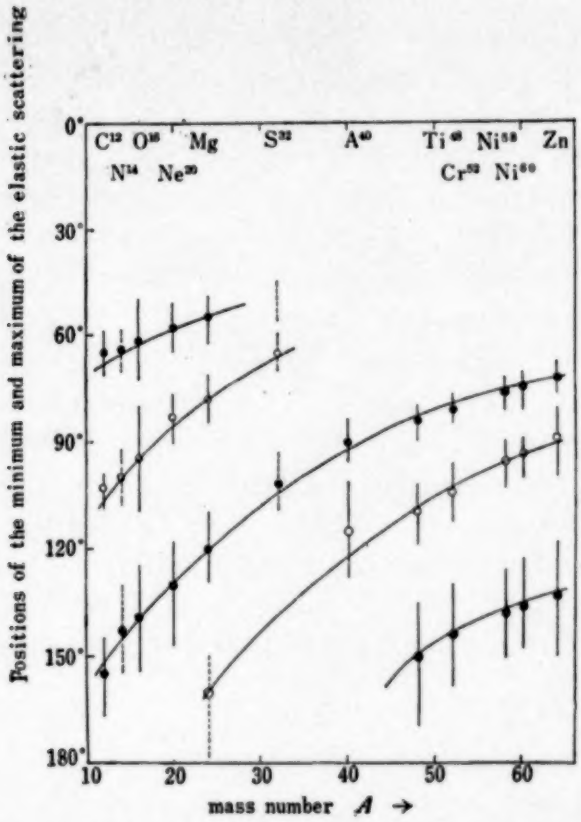

Fig. 9. Mass dependences of the positions of the maximum and the minimum of the elastic diffraction pattern. The average position of the minima over the energy range 7—14 MeV is denoted by ○; that of the maxima by ●. The bars indicate the ranges of energy variation and the dotted bars those ranges which are no certain.

4.2.2. Inelastic scattering

The total yield for the inelastic scattering is so large for C^{12}, Ne^{20} and Mg^{24} as to be comparable to πR^2. For the Ne^{20}, Mg^{24}, Si^{28} and S^{32} the emitted spectra resemble roughly one another. For C^{12} and O^{16}, the open channels are rather limited and for O^{16} the total yield is not considered to be so large. The partial (integrated) cross section varies with energy, but the variation is not so large as for the differential cross section at a given angle. Its energy average decreases gradually as the incident energy increases, and the angular distribution shape approaches the stabilized pattern which is characteristic of each nucleide. The pattern for Mg^{24} is not similar to that for C^{12} nor to those for the nuclei heavier than argon. For Mg^{24}, variations with energy of the angular distribution shape for inelastic scattering are more rapid than for C^{12}. The situation for Mg^{24} is similar to that for Ne^{20}.

5. Discussion

The optical model was a great success in the analysis of the elastic scattering and total cross sections for the nucleon-nucleus system. The results presented here regarding the elastic scattering in the region of $E_p < 12$ MeV, however, seem difficult to explain by a simply optical model [31]). On the other hand, they are also difficult to analyse by the one level formula of compound nucleus formation. As to the deviation from the simple optical model, we can consider two reasons. Firstly, the level density may not be large enough to secure that the necessary energy average [31–33, 36]) is performed by the beam energy spread realized in this experiment. Secondly, the channel interaction pointed by Yoshida [21, 22]) may play an important role. From the former point of view, we might fit our results to the prediction of the optical model if we average the cross section over a certain energy range. We are not willing to do so, however, because the energy points investigated have been selected optionally and their number is not large, so our data are not sufficient to give true average results. But in the region below 12 MeV, it appears that the average cross section gives us angular distributions which vary slowly with energy.

The discussion can also be extended to the inelastic scattering [33, 34, 36]). Some authors [2, 11]) reported, as mentioned before, the results on angular correlation measurements which prove the existence of the direct process even in the low energy region ($\approx$ 6 MeV). If the actual energy spread were not sufficient for the assumption of the optical model, it would not seem strange that the interference term between the direct process and the compound process plays a role, and the angular distribution changes with energy rapidly. From the results in the region $E_p < 12$ MeV, a stabilized angular distribution was not obtained, even when we average the cross section over 1 MeV. It was predicted [36]) that the channel coupling by direct interaction displays an "intermediate structure" and the cross section is represented by the sum of the contributions of the direct process and of the average compound process. From the result shown in fig. 10 and 11, we cannot point out eventual coincidences of anomalous regions between in the elastic and the inelastic scatterings with a few exceptions [18]) and the anomalies seem to happen more frequently in the inelastic scattering.

In the higher energy region ($E_p > 12$ MeV), the angular distribution shapes for both the elastic and the inelastic scattering have a stabilized pattern with small fluctuations of the cross section. For these features we may admit such a simple theoretical explanation as that given by the optical model and the distorted wave Born approximation.

The authors wish to thank Professor S. Kikuchi and Professor I. Nonaka for their encouragement and valuable suggestions. They are obliged to

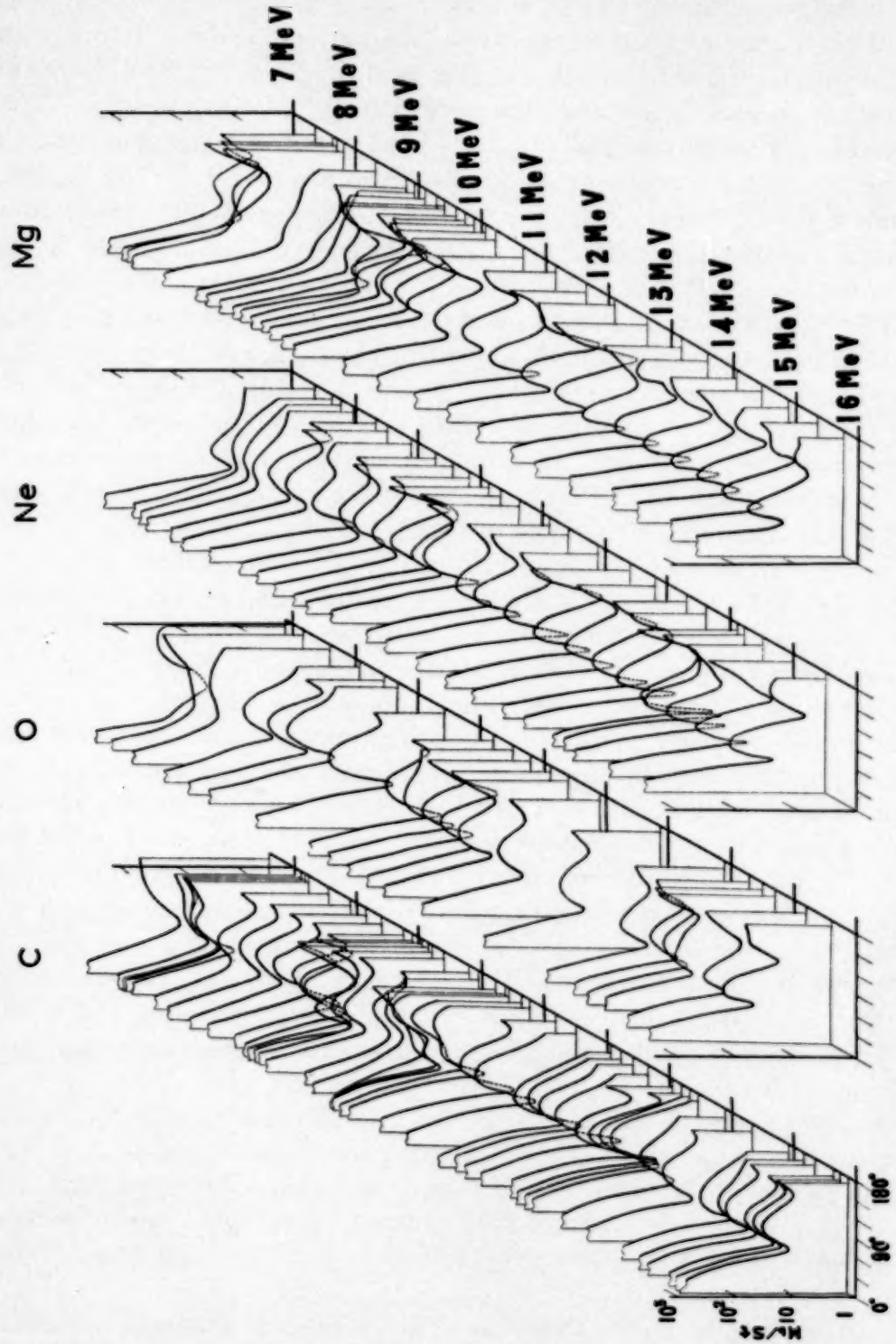

Fig. 10. Angular distribution for the elastic scattering of protons.

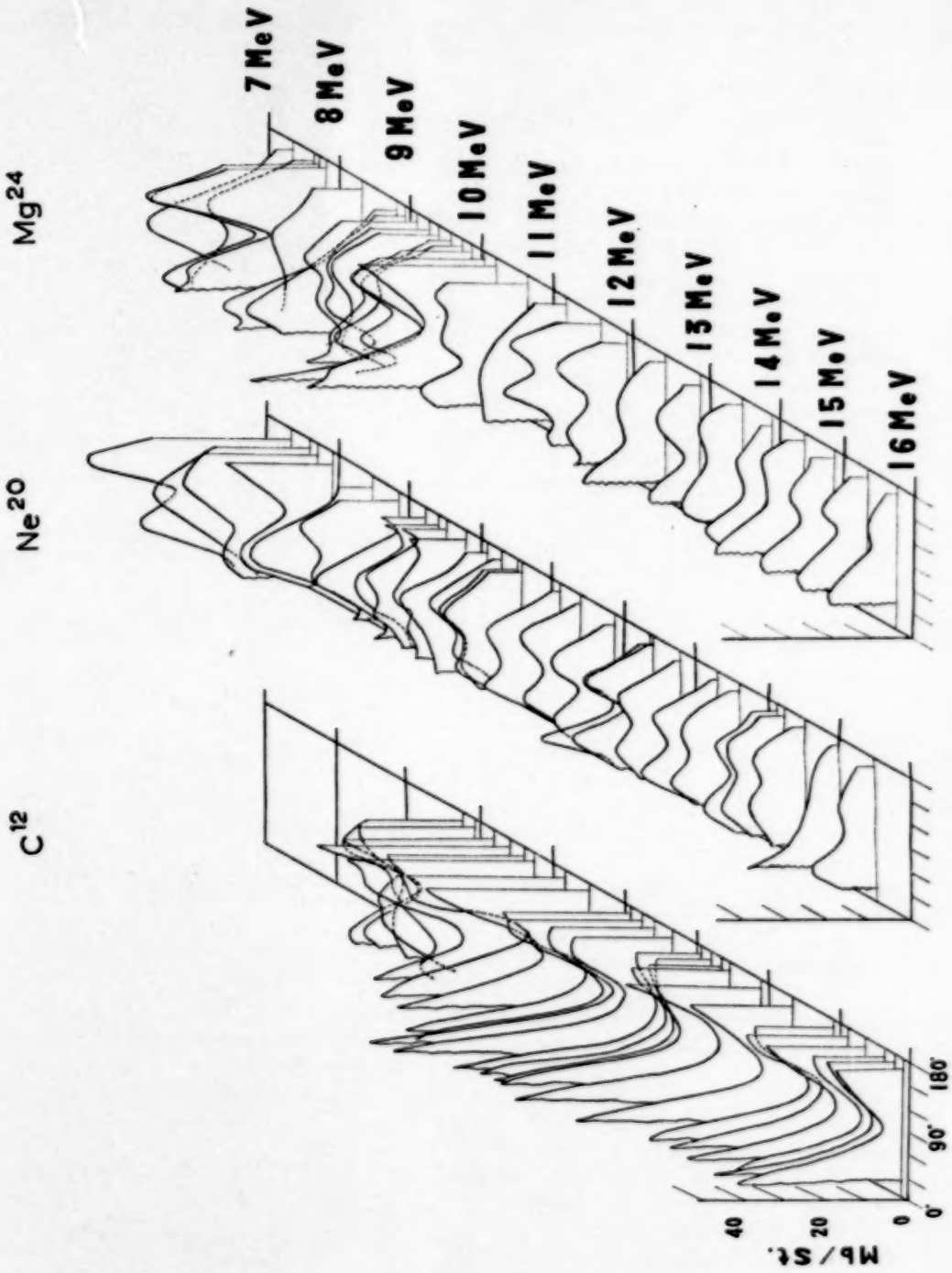

Fig. 11. Angular distribution for the inelastic scattering of protons leaving first 2^+ state.

Dr. R. M. Eisberg, Dr. M. Kawai, Dr. K. Kikuchi and Dr. K. Saito for their reading of the manuscript and suggestions. Thanks ar ealso due to Mr. T. Karasawa Mr. A. Suzuki, Mr. H. Ogawa and other members of the cyclotron crew and to Mr. Yoshimura and the staff of the electronic engineering division.

References

1) S. Yamabe, M. Kondo, T. Yamazaki and A. Toi, J. Phys. Soc. Japan **13** (1958) 777
2) F. D. Seward, Phys. Rev. **114** (1959) 514
3) H. E. Gove and H. F. Stoddart, Phys. Rev. **86** (1952) 572
4) C. J. Baker, J. N. Dodd and D. H. Simmons, Phys. Rev. **85** (1952) 1051
5) G. W. Greenlees, B. C. Haywood, L. G. Kuo and M. Petravic, Proc. Phys. Soc. **70** (1957) 331
6) G. W. Greenlees and A. E. Souch, Proc. Phys. Soc. **69** (1956) 686
7) G. E. Fisher, Phys. Rev. **96** (1954) 704
8) H. E. Conzett, Phys. Rev. **105** (1957) 1324
9) Y. Oda *et al.*, J. Phys. Soc. Japan **15** (1960)
10) P. C. Gugelot and P. R. Phillips, Phys. Rev. **101** (1956) 1614
11) H. A. Lackner, G. F. Dell and H. J. Hausman, Phys. Rev. **114** (1959) 560
12) H. Yoshiki, Phys. Rev. **117** (1960) 773
13) M. Takeda, J. Phys. Soc. Japan **15** (1960) 557
14) G. W. Greenlees and J. Lowe, private communication
15) J. S. Blair, G. W. Farwell and D. K. McDaniels, U.S. Atomic energy Commission contract A.T. (45–1)-293
16) C. Hu *et al.*, J. Phys. Soc. Japan **14** (1959) 861
17) S. Kobayashi, J. Phys. Soc. Japan **15** (1960) 1164, INSJ-33
18) Y. Nagahara, J. Phys. Soc. Japan **16** (1961)
19) Litherland *et al.*, Phys. Rev. **102** (1956) 208
20) G. Rakavy, Nuclear Physics **4** (1957) 375
21) S. Yoshida, Proc. Phys. Soc. **69** (1956) 668
22) S. Yoshida, Progr. Theor. Phys. **19** (1957) 169
23) S. Kikuchi *et al.*, J. Phys. Soc. Japan **15** (1960) 1
24) K. Kikuchi, S. Kobayashi and K. Matsuda, J. Phys. Soc. Japan **14** (1959) 121
25) S. Kobayashi, K. Matsuda, Y. Nagahara, Y. Oda and N. Yamamuro, J. Phys. Soc. Japan **15** (1960)
26) N. Yamamuro, S. Kobayashi, K. Matsuda, Y. Nagahara and Y. Oda, INSJ-29 (1960)
27) P. M. Endt and C. M. Braams, Rev. Mod. Phys. **29** (1957) 683
28) H. W. Fulbright, N. O. Lassen and N. O. R. Ponulson, Mat. Fys. Medd. Dan. Vid. Selsk. **31** No. 10 (1959)
29) F. A. ElBedervi and M. A. ElWahab, Nuclear Physics **3** (1957) 385;
Calvert, Yaffe, Litherland and Maslin, Proc. Phys. Soc. **68** (1955) 1008
30) D. K. Mc Daniels, J. S. Blair, S. W. Chen and G. W. Farwell, Nuclear Physics **17** (1960) 614
31) H. Feshbach, C. E. Porter and V. F. Weisskopf, Phys. Rev. **96** (1954) 448
32) F. L. Friedman and V. F. Weisskopf, Niels Bohr and the development of pnysics
33) G. E. Brown, Rev. Mod. Phys. **31** (1959) 893
34) T. Sasagawa, Prog. Theor. Phys. Suppl. **11** (1959) 69
35) M. Sano, T. Terasawa and S. Yoshida, Nuclear Physics **6** (1958) 20
36) K. Matsuda, T. Mikumo and H. Yamaguchi (1960) (preliminary result)
37) N. Yamamuro *et al.*, to be published

2.I: 4.D

Nuclear Physics **27** (1961) 25—27; © *North-Holland Publishing Co., Amsterdam*

Not to be reproduced by photoprint or microfilm without written permission from the publisher

THE E.C./β^+ RATIO IN Pr^{139}

O. BORELLO †, S. COSTA and F. FERRERO

Istituto di Fisica dell'Università, Torino

and

Istituto Nazionale Fisica Nucleare, Sez. di Torino

Received 4 April 1961

Abstract: The previously reported [1]) value of the E. C./β^+ ratio for Pr^{139} has been remeasured and found to be 4.8.

In a previous paper by Ferrero *et al.* [1]), the (γ, n) and (γ, 2n) cross sections in Pr^{141} were investigated, assuming for the E.C./β^+ ratio for Pr^{140} the value 0.852 given by Rasmussen *et al.* [2]) and for Pr^{139} the value 16 given by Stover [3]).

As some doubts have been raised about these values [4]), we have measured again the ratio

$$R = \left(\frac{\text{E.C.}}{\beta^+}\right)_{Pr^{139}} \Big/ \left(\frac{\text{E.C.}}{\beta^+}\right)_{Pr^{140}}.$$

A Pr_6O_{11} high purity (99.99 %) powder sample enclosed in a small aluminium container, with extremely thin walls, was irradiated by the X ray beam from the Turin 100 MeV Synchrotron. Both β^+ activities were measured by detecting the 0.51 MeV annihilation radiation produced in a Al converter, placed on a side of the sample, sufficiently thick to stop completely the β^+.

The NaI(Tl) (5 cm × 5 cm) crystal was looked by a 6292 Dumont photomultiplier, followed by a single channel pulse-height analyzer with the window centred on the 0.51 MeV line.

The 40 keV X-ray activity from E.C. was detected by means of a thin Be window NaI(Tl) (2 mm) crystal followed by an analogous electronic device.

The Pr^{140} and Pr^{139} half-lives were measured and found to be of the correct magnitudes.

Taking the arithmetical mean of several measurements we obtained

$$R = 5.47.$$

This result is not changed by L_I subshell electrons capture, if one assumes that the L_I contribution to E.C. is a few percent (about 10 %) of the K shell contribution.

† On leave from Universidade de S. Paulo. Brasil and fellow of the Conselho Nacional de Pesquisas, Rio de Janeiro, Brasil

We assume [5])

$$\left(\frac{\text{E.C.}}{\beta^+}\right)_{\text{Pr}^{140}} = 0.887.$$

Hence we have

$$\left(\frac{\text{E.C.}}{\beta^+}\right)_{\text{Pr}^{139}} = 4.8.$$

With these new figures, the (γ, n) and $(\gamma, 2\text{n})$ cross sections given in ref. [1]) should be multiplied respectively by 1.02 and by 0.35, thus obtaining the results of fig. 1.

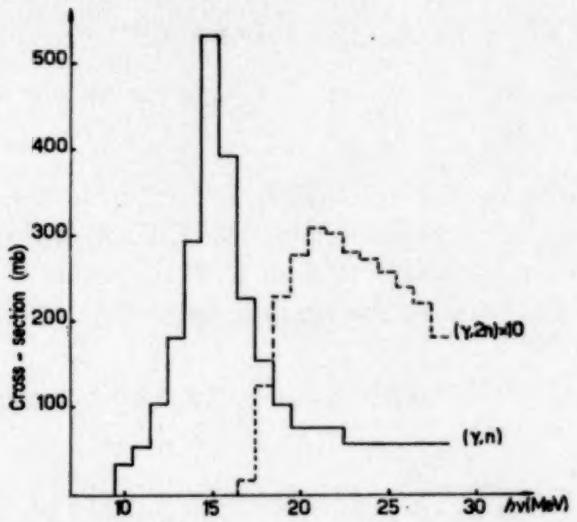

Fig. 1. The corrected (γ, n) and $(\gamma, 2\text{n})$ cross sections.

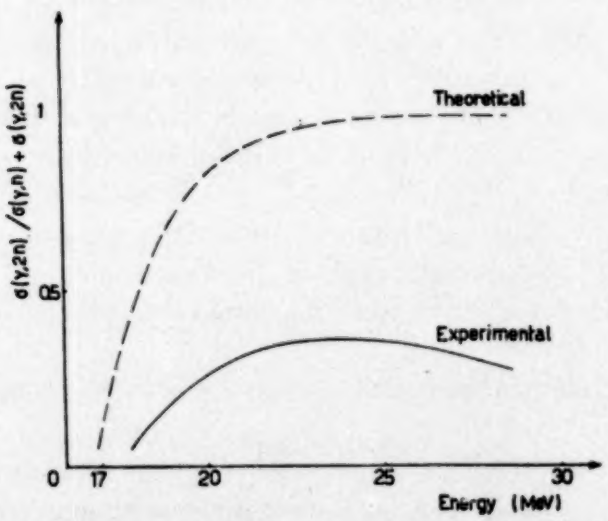

Fig. 2. Theoretical and experimental curves of the $(\gamma, 2\text{n})/(\gamma, \text{n}) + (\gamma, 2\text{n})$ ratio.

These values of the $(\gamma, 2\text{n})$ cross section turn out to be in agreement with the data by Carver and Turchinetz [4]) who found the maximum of the cross section

at approximately 20 MeV with a peak value of 40 mb, considering the $(E.C./\beta^+)_{Pr^{139}}$ ratio to be 5.2.

It is to be noted that the conclusions reached in ref. [1]) are qualitatively valid even taking into account the results of the present work. Indeed, the $(\gamma, n)+(\gamma, 2n)$ integrated cross sections up to 30 MeV are 3.0 MeV · b, a figure still greater than that given by the Levinger and Bethe dipole sum rule, i.e. 2.88 MeV · b. On the other hand, the disagreement between the statistical model predictions about the $(\gamma, 2n)/(\gamma, n)+(\gamma, 2n)$ ratio and the experimental data, is still more enhanced. In fig. 2 we have plotted the two curves, the theoretical one being the same as in ref. [1]).

To explain this disagreement it seems reasonable to suppose an appreciable direct photoneutron contribution to the (γ, n) process, even in such heavy nuclei as Pr^{141}.

We wish to thank professor R. Malvano for his constant advice and encouragement.

References

1) F. Ferrero, R. Malvano and E. Silva, Nuclear Physics **10** (1959) 423
2) D. Strominger, J. M. Hollander and G. T. Seaborg, Rev. Mod. Phys. **30** (1958) 585; J. Rasmussen, private communication
3) B. J. Stover, Phys. Rev. **81** (1951) 8
4) J. H. Carver and W. Turchinetz, Proc. Phys. Soc. **73** (1959) 110
5) D. S. Dzhelepov, I. F. Uchevatkin and S. A. Shestopalova, JETP **37** (1960) 611

2.B:3.B

Nuclear Physics **27** (1961) 28—37; © *North-Holland Publishing Co., Amsterdam*

Not to be reproduced by photoprint or microfilm without written permission from the publisher

ANGULAR CORRELATION STUDIES OF THE 358 keV → 81 keV CASCADE IN Cs^{133}

B. N. SUBBA RAO

Tata Institute of Fundamental Research, Bombay-5, India

Received 10 April 1961

Abstract: With the main aim of studying the nuclear structure effect on the internal conversion process of the *l*-forbidden 81 keV M1 transition, angular correlation measurements with the 358 and 81 keV gamma-rays, and with the 358 keV gamma-ray and the *K*-conversion electrons of the 81 keV transition have been performed. The results, after necessary corrections, are

$$W(\gamma\gamma;\theta) = 1+(0.046\pm0.011)P_2(\cos\theta)-(0.008\pm0.014)P_4(\cos\theta),$$

$$W(\gamma e_k^-;\theta) = 1+(0.014\pm0.008)P_2(\cos\theta)+(0.007\pm0.011)P_4(\cos\theta).$$

While gamma-gamma angular correlation alone could not choose between $\frac{1}{2}$ or $\frac{3}{2}$ spin assignment to the 439 keV state, the gamma-K-conversion electron angular correlation requires it to be only $\frac{3}{2}$. These angular correlation results lead to a 0.7 M1+0.3 E2 multipolarity for the 358 keV transition and $\delta^2_{\mathrm{II}}(\gamma\gamma) = 0.0043$ and $\delta^2_{\mathrm{II}}(\gamma e_k^-) = 0.0066$ for the 81 keV transition. These different mixing ratios for this transition indicate the possibility of the nuclear structure effect on the internal conversion process being operative. With the help of all these results, the nuclear structure effect parameter is deduced from the *K*-conversion coefficient of the 81 keV transition to be $\lambda = -1.28$ or $+253$. The various factors leading to uncertainties in λ are presented. Nuclear structure effect on particle parameters is considered.

1. Introduction

The scheme of levels in Cs^{133} based on the results of earlier authors [1–3]) is shown in fig. 1. The spin of the ground state has been determined [2]) to be $\frac{7}{2}$. The measured [2]) magnetic moment of the ground state of $+2.577$ nm is in accordance with the shell model orbital of $g_{\frac{7}{2}}$ for the 55th proton. The deviation of about 60 % from the pure single particle value (Schmidt's value) can be understood by taking into account a small admixture of other possible nuclear configurations [4]). This mixed nuclear configuration is also sufficient to explain the observed quadrupole moment [2]) of -0.003 b.

The first excited state at 81 ± 1 keV has a half-life [3]) of (6.3 ± 0.1) ns. From the conversion coefficient [1, 2]) of $\alpha^k = 1.49\pm0.08$ for this 81 keV transition, it is known to be an M1 transition with a possible admixture of E2 component. Thus, the 81 keV excited state is expected to be $\frac{5}{2}+$. The gyromagnetic ratio [3]), obtained by measuring the rotation of the angular correlation pattern of the 358 keV → 81 keV gamma-gamma cascade under the influence of an external magnetic field applied normal to the plane of the two counters, $g = 1.23\pm0.12$

corresponds to a magnetic moment of $\mu = +3.1 \pm 0.3$ n.m. This value of magnetic moment allows the 81 keV excited state to be identified as the $d_{\frac{3}{2}}$ shell model state. The retarded transition probability of the 81 keV excited state can then be understood in terms of l-forbiddenness ($\Delta l = 2$, $d_{\frac{3}{2}} \rightarrow g_{\frac{7}{2}}$) of the M1 transition together with a small amount of configuration mixing [5]) in both the levels concerned. Thus, the ground and first excited states are fairly well described by the spherical shell model and the 81 keV transition is described as l-forbidden to the same degree of validity.

In the case of such a retarded gamma transition, the dynamic nuclear structure effect [6]) should be expected to assume a measurable magnitude, if the internal conversion inside the nuclear volume is not correspondingly inhibited. Adopting a transition energy of 77 keV ($k = 0.15\ m_0 c^2$) and a mixing

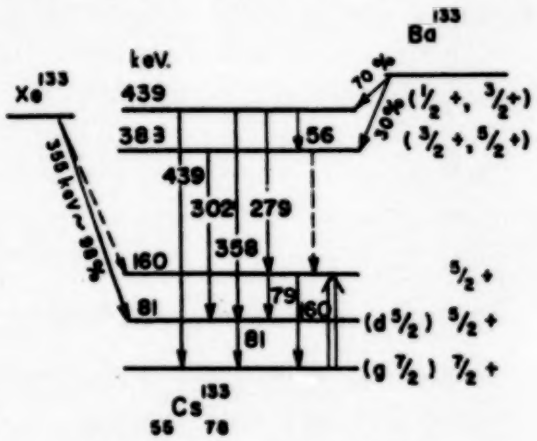

Fig. 1. Level scheme of Cs^{133}.

ratio of $\delta_{II}^2 = 0.025$, which is based on the gamma-gamma angular correlation work [3]) interpreted under the assumption of a spin of $\frac{1}{2}$ for the 439 keV state and an E2 multipolarity for the 358 keV transition, recently [7]) the nuclear structure effect parameter λ has been deduced from the observed conversion coefficient [1]) to be +6.5. However, there is no basis for the assumption of a spin $\frac{1}{2}$ for the 439 keV state. It could equally well be $\frac{3}{2}$, which would then require the determination of the mixing ratio of the 358 keV transition also, in order to obtain an accurate value of the mixing ratio for the 81 keV transition. The transition energy of 77 keV assumed in the above mentioned work [7]) leads to a theoretical conversion coefficient of $\beta_1^k = 1.60$. But all observed values for the transition energy [1–3]) indicate that the simpler β^--decay of Xe^{133} and Coulomb excitation studies of Cs^{133} lead to a transition energy of 81 ± 1 keV and that the studies of the decay of Ba^{133} lead to a value of around 79 keV. The half-life [3]) of the excited state determined by $\beta - e^-$ delayed concidences with Xe^{133} as well as the 358 keV gamma and the supposed 79 keV gamma delayed coincidences lead to the same value. In the absence of any evidence for the existence of a close-lying doublet of levels at 79 and 81 keV, the magnetic

spectrometer value [1]) of 81±1 keV from the simpler β^--decay of Xe^{133} will be adopted as more reliable. It is to be noted that a shift of the centroid of the line profile of the 81 keV transition can be expected in studies with Ba^{133} due to the existence of a not very weak 78 (±?) keV transition. This more correct transition energy of 81 keV leading to $\beta_1^k = 1.43$ results in a value of the nuclear structure parameter $\lambda = -0.16$. But another way of deducing this nuclear structure effect on internal conversion is to study the angular correlation involving the conversion electrons of the transition. Moreover, this gamma-*K*-conversion-electron angular correlation could be expected to supplement the gamma-gamma angular correlation in fixing the spin of the 439 keV state and the multipolarity of the 358 keV transition. Since a separation of 29 keV between the *K* and *L*-conversion electrons at a *K*-conversion electron line energy of 46 keV should be expected to give a complete separation even with a scintillation spectrometer, this work consisting of gamma-gamma and gamma-K-conversion electron angular correlation of the 358 keV → 81 keV cascading transitions was undertaken. This paper deals with the details of experiments and results of these angular correlation measurements and the nuclear structure effects in the *l*-forbidden 81 keV M1 transition.

2. Angular Correlation Measurements

The schematic arrangement used in gamma-electron angular correlations is shown in fig. 2. The gamma channel consisted of a 3.8 cm × 3.8 cm NaI(Tl) crystal optically coupled to a RCA 6810A photomultiplier. The electron detector was a 2 cm × 0.25 cm anthracene crystal covered with a 150 $\mu g/cm^2$ aluminium reflector. This phosphor was optically coupled to a perspex light guide with a shaped collector head ending in the cylindrical part. The full length of the light guide was 9 cm. The end of the cylindrical part was coupled optically as shown in fig. 2 to the RCA 6810A photomultiplier. The light guide was also provided with aluminium reflector over its full length. This electron detector assembly was enclosed in a vacuum chamber of 25 cm diameter. It was made of aluminium lined with a 0.2 cm perspex sheet to minimise electron scattering. The volume of the detector relative to that of the vacuum chamber minimises the scattering effects due to scattered electrons reaching the detector. Further the part of the chamber in which the source is situated was shaped as shown in fig. 2 in order to minimise scattering effects. A vacuum of about 0.08 mm of Hg was maintained . A resolution of about 16 % could be obtained with the light guide for the 630 keV total conversion line of Ba^{137m}. Without the light guide, resolution was around 14% corresponding to photon absorption of about 20 % by the light guide.

The high gain photomultipliers operated around 2800 V together with 404A limiters (with a standing plate current of 20 mA) were used in a conventional

Bell type fast-slow coincidence set up with connecting cables of about 92 Ω characteristic impedance and clipping cable of about 50Ω. The overall resolution time was around 26 ns.

In γ-γ angular correlation work, the same arrangement with the electron detector-vacuum chamber assembly replaced by 3.8 cm$\times$0.6 cm NaI(Tl) crystal was used. Source detector (bare face) distance was 7.5 cm for both movable and fixed counters. The source was an aqueous solution of barium

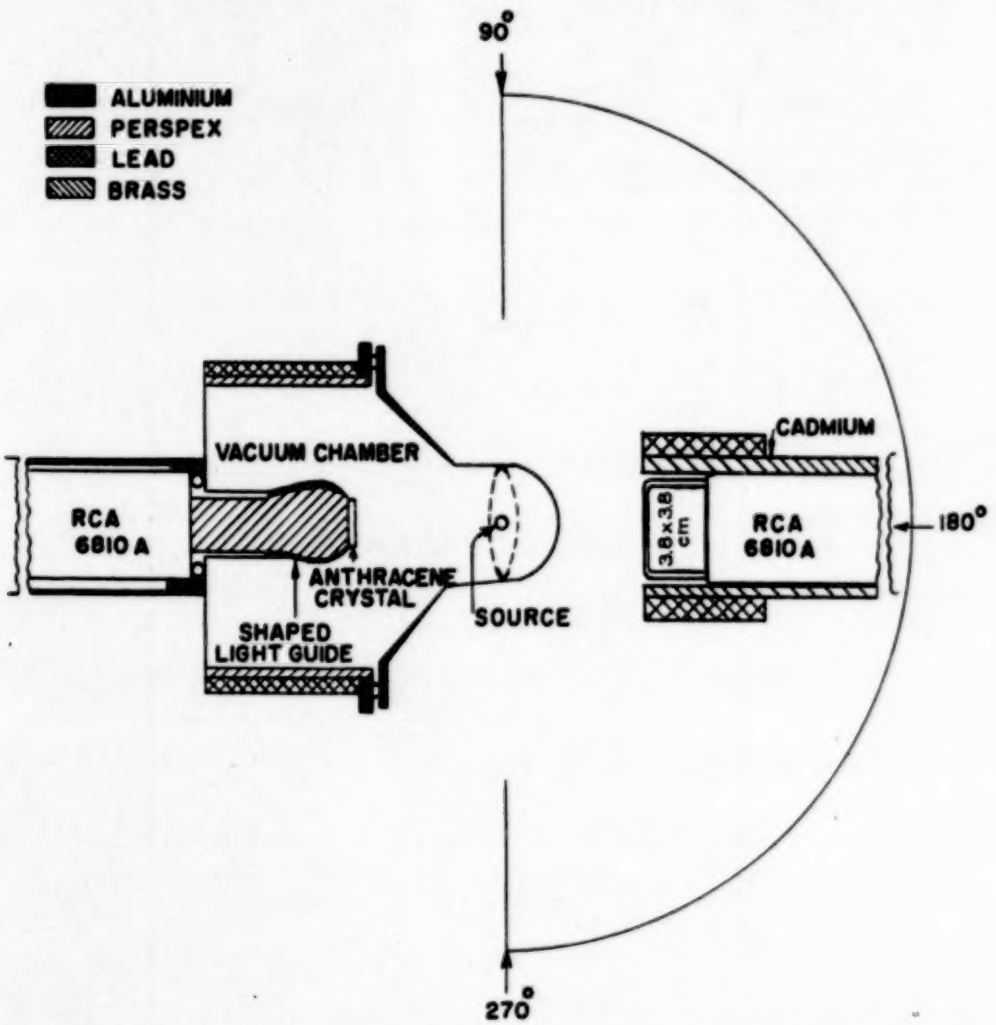

Fig. 2. Experimental arrangement for angular correlation measurements.

chloride contained in a perspex cylinder made conducting with aquadag (colloidal graphite) and the perspex cylinder was held in position in an aluminium holder.

In the gamma-electron angular correlation, the source detector distances were 9 cm in the electron channel and 11.5 cm in the gamma-channel. The source of barium nitrate was obtained from a carrier free chemical separation of caesium chloride (spectroscopically pure) bombarded for 5 h in a 7 μA beam of 19 MeV deuterons from the Birmingham cyclotron. Source was deposited over an area of 0.5 cm^2 on an aluminium backing of 150 μg/cm^2.

The gamma spectrum, electron spectrum and the conversion electron lines in coincidence with the photopeak of the 358 keV gamma -ray are shown in fig. 3. The channel settings in γ-γ angular correlation and γ-e_k^- angular

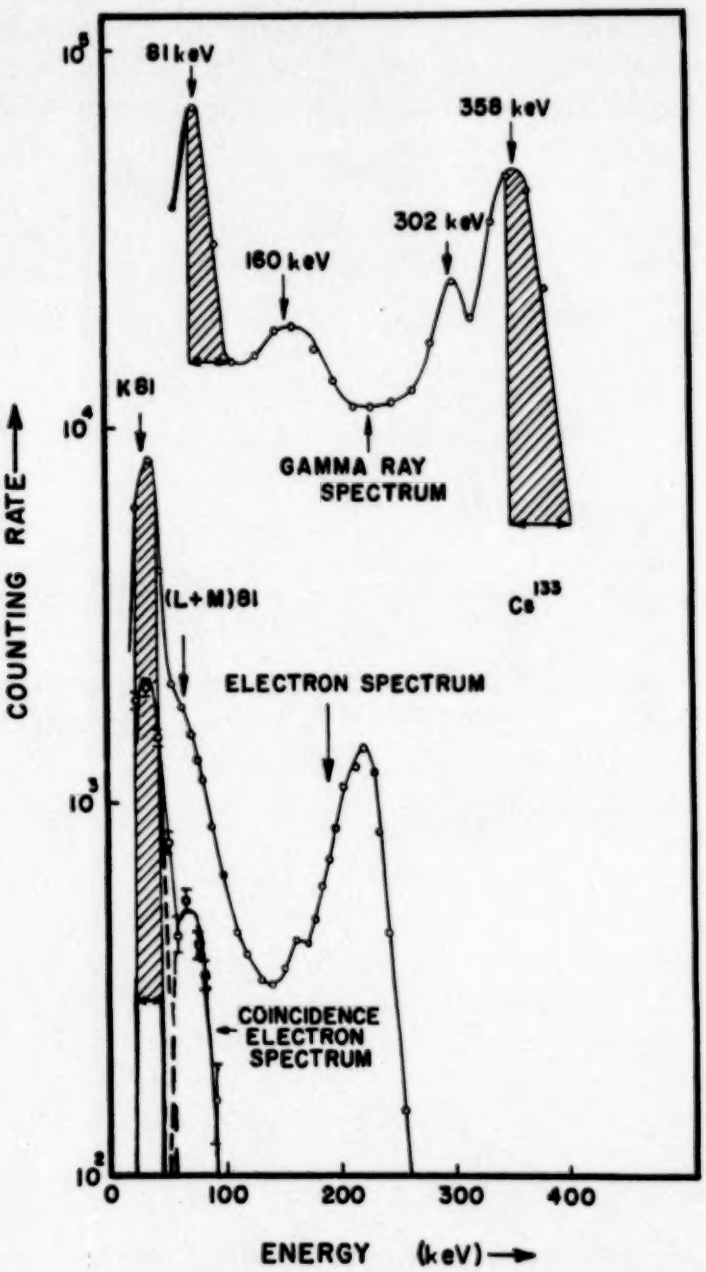

Fig. 3. Gamma and electron spectra and spectrum of conversion electrons in coincidence with the 358 keV gamm-ray.

correlation are shown in fig. 3. As was expected, K and $L+M$ lines of the 81 keV transition are well separated to allow a good angular correlation measurement.

In all these angular correlation measurements, the source was centred to about 0.5 % accuracy in the counting rate at the various angular positions of

the movable counter. Chance coincidences were determined periodically by introducing 125 ns delay in one of the channels. The chance rate was always in accordance with a resolution time of the coincidence system of 26 ± 4 ns. Chance coincidences were 2 to 3 % of the true coincidences.

The singles counting rates were constantly observed and channel settings were held constant throughout by periodic checkings of singles spectrum as well as from the singles counts which were never allowed to drift by more than 0.8 %. Possible effects due to slow drifts were further taken care of by a randomisation procedure in which angular settings were coverd in the sequence 180°, 270°, 150°, 210°, 180°, 90°, 240° and 120° in both sets of experiments. Further corrections were made by dividing the true coincidence rates by the appropriate singles counting rates. Coincidences were accumulated in each position for 5 min and 35 such runs were made until about 6500 counts could be obtained at each position. In the final analysis, coincidences at symmetric angular positions were checked. Following the statistical methods for treating such data, corrected coincidences at symmetric positions were added and adopted for further analysis.

The $\beta \rightarrow \gamma$ angular correlation [11]) of Co^{60} and the γ-γ angularcor relation of the 121 keV $\rightarrow$ 280 keV cascade in As^{75} were measured as a further check of the experimental set up with good agreement with observations by earlier authors.

In the gamma-*K*-conversion electron angular correlation, auxiliary runs were done for determining "scatter effects" due to scattered electron-coincidences or γ-γ coincidences. In these observations, the direct beam of electrons was cut of with 200 mg/cm^2 aluminium, still allowing the electrons scattered from the walls in the part of the source mounting and possibly from the walls of the chamber. These coincidences amounted to about 0.3 % of the true γ-e_k^- coincidences in the main runs and were isotropic in angle. Scatter effects and chance and background coincidences were subtracted out to obtain the all-corrected coincidence counting rates used in later analysis.

3. Results of Angular Correlation Measurements

By this procedure, the angular correlation data were fitted in both cases to

$$W(\theta) = 1 + a_2 P_2(\cos\theta) + a_4 P_4(\cos\theta). \tag{1}$$

The coefficients $A_2 = a_2/s_2^{\mathrm{I}} s_2^{\mathrm{II}}$ and $A_4 = a_4/s_4^{\mathrm{I}} s_4^{\mathrm{II}}$ were deduced, wherein s_2^{I}, s_4^{I} and s_2^{II}, s_4^{II} are the attenuation factors due to the finite solid angle effect for the two detectors. These factors were obtained for the experimental conditions in the present work by numerical integration of

$$J_t = \int_0^{\gamma} P_t(\cos\theta)(1 - e^{-\tau x(\theta)}) \sin\theta \, d\theta, \tag{2}$$

the notations and derivations of which have already been treated by Rose [8]), to be

$$s_2^{\mathrm{I}} = \frac{J_2^{\mathrm{I}}}{J_0^{\mathrm{I}}} = 0.965, \quad s_2^{\mathrm{II}} = \frac{J_2^{\mathrm{II}}}{J_0^{\mathrm{II}}} = 0.948, \quad s_4^{\mathrm{I}} = \frac{J_4^{\mathrm{I}}}{J_0^{\mathrm{I}}} = 0.992, \quad s_4^{\mathrm{II}} = \frac{J_4^{\mathrm{II}}}{J_0^{\mathrm{II}}} = 0.982,$$

in the case of γ-γ angular correlation with superscript I representing the channel in which the 81 keV gamma-ray was selected and II that in which the 358 keV photopeak was selected. Thus, we have

$$W(\gamma\gamma;\theta) = 1 + A_2 P_2(\cos\theta) + A_4 P_4(\cos\theta) \tag{3}$$

where $A_2 = 0.046 \pm 0.011$ and $A_4 = -(0.008 \pm 0.014)$. These coefficients are in good agreement with those of the earlier author [3]). Since a conducting surrounding and an aqueous solution have been employed in the present case, the agreement with the earlier measurements [3]) with solid and aqueous sources indicates that the 6 ns half-life for the 81 keV intermediate state does not attenuate the anisotropy of angular correlation in accordance with the conclusions of the earlier author [3]).

Assuming the two possibilities for $\frac{1}{2}+$or $\frac{3}{2}+$spin assignment to the 439 keV state and assuming that the 358 keV transition could be E2 or M1, the three curves A, B, C (c'') in fig. 4 are obtained from the function for the sequence $j_1 \xrightarrow{D \text{ or } 2} \frac{5}{2}+ \xrightarrow{D+2} \frac{7}{2}+$,

$$W(\gamma\gamma;\theta) = 1 + \frac{1}{1+\delta_{\mathrm{II}}^2} F_2(11 j_1 \tfrac{5}{2})[\delta_{\mathrm{II}}^2 F_2(22 \tfrac{7}{2} \tfrac{5}{2}) + 2\delta_{\mathrm{II}} F_2(12 \tfrac{7}{2} \tfrac{5}{2}) + F_2(11 \tfrac{7}{2} \tfrac{5}{2})] P_2(\cos\theta) + \frac{\delta_{\mathrm{II}}^2}{1+\delta_{\mathrm{II}}^2} F_4(22 j_1 \tfrac{5}{2}) F_4(22 \tfrac{7}{2} \tfrac{5}{2}) P_4(\cos\theta), \tag{4}$$

wherein the $P_4(\cos\theta)$ term vanishes if the 358 keV transition is a pure dipole. In this fig. 4, the coefficient A_2 is plotted against the mixing ratio of the 81 keV transition for the three possibilities $\frac{1}{2}+ \xrightarrow{2} \frac{5}{2}+$, $\frac{3}{2}+ \xrightarrow{2} \frac{5}{2}+$, $\frac{3}{2}+ \xrightarrow{D} \frac{5}{2}+$ (A, B, C, respectively) for the 358 keV transition. The experimental value of A_2 is in agreement with the three possibilities with different mixing ratio δ_{II}^2 for the 81 keV transition. Coefficient of the $P_4(\cos\theta)$ term is uncertain so that no complete information regarding the choice of the three possibilities can be derived from γ-γ angular correlation alone.

The gamma-K-conversion electron angular correlation data could be represented, after correcting for finite solid angle effects by

$$W(\gamma e_k^-;\theta) = 1 + (0.014 \pm 0.008) P_2(\cos\theta) + (0.007 \pm 0.011) P_4(\cos\theta). \tag{5}$$

There is no earlier γ-e_k^- angular correlation measurement with this isotope. Herein, the attenuation coefficients due to the finite solid angle were derived in the same way as described above and the computed values are $S_2^{\mathrm{I}} = 1$,

$S_2^{II} = 0.999$ and $S_4^{I} = S_4^{II} = 1$, in which I represents the electron channel and II the channel in which 358 keV photopeak is selected. This angular correlation function for the scheme

$$j_1 \xrightarrow{L} \tfrac{5}{2}+ \xrightarrow[e_k^-]{\text{M1+E2}} \tfrac{7}{2}+$$

is

$$\begin{aligned} W(\gamma e_k^-;\theta) = 1 &+ F_2(LLj_1\tfrac{5}{2})/(1+p^2)[p^2 b_2^{(2)}(e)F_2(22\tfrac{7}{2}\tfrac{5}{2}) \\ &+ 2pb_2 F_2(12\tfrac{7}{2}\tfrac{5}{2}) + b_2^{(1)}(\mathrm{m})F_2(11\tfrac{7}{2}\tfrac{5}{2})]P_2(\cos\theta) \\ &+ p^2/a+p^2)b_4^{(2)}(e)F_4(22j_1\tfrac{5}{2})F_4(22\tfrac{7}{2}\tfrac{5}{2})P_4(\cos\theta) \end{aligned} \qquad (6)$$

where $p^2 = (\alpha_2^k/\beta_1^k)\delta_{II}^2$, and α_2^k is the K conversion coefficient of the E2 component, β_1^k that of the M1 component, $b_2^{(2)}(e)$, $b_4^{(2)}$ (e) are particle para-

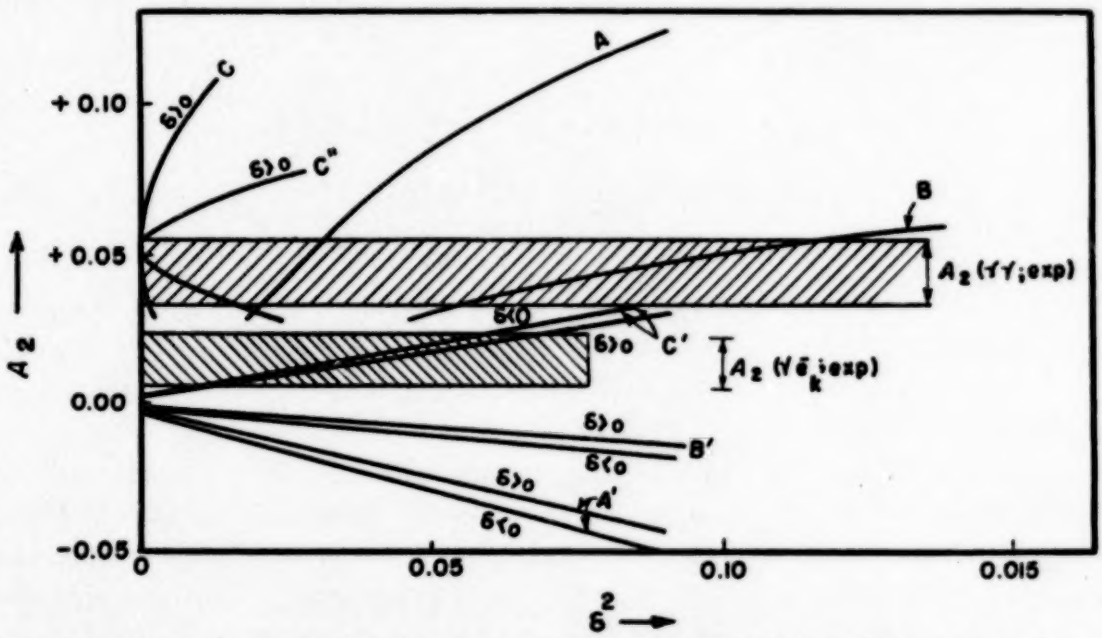

Fig. 4. Coefficient A_2 as a function of the mixing ratio δ_{II}^2 of the 81 KeV transition for decay schemes $(A, A') : \frac{1}{2} \xrightarrow{} \frac{2}{2} \frac{5}{2}$, $(B, B') : \frac{3}{2} \xrightarrow{} \frac{2}{2} \frac{5}{2}$, $(C, C') : \frac{3}{2} \xrightarrow{D} \frac{5}{2}$ for the 358 keV transition C'' is the same as C but with the scale of abscissa magnified by a factor of 10. The unprimed cases are for $\gamma-\gamma$ angular correlation and the once-primed cases are for $\gamma-e_k^-$ angular correlation.

meters for the electric component, b_2 being the M1, E2 interference particle parameter and $b_2^{(1)}$ (m) the particle parameter for M1 component. These particle parameters have been deduced from the computed values [9]) by extrapolation with the help of the limiting values and the recurrence relation between $b_4^{(2)}$ and $b_2^{(2)}$. For the three possibilities with $j_1 = \frac{1}{2}, \frac{3}{2}$ the lines A' B', C' corresponding to A, B, C for γ-γ angular correlation are plotted in fig. 4. It is seen from fig. 4 that γ-e_k^- angular correlation observations are in agreement only if the scheme of spins and multipolarities are $\frac{3}{2}+ \xrightarrow{D} \frac{5}{2}+ \xrightarrow{\text{M1+E2}} \frac{7}{2}+$ with $\delta_{II}^2 = 0.028 \pm 0.008$. The theoretical values of β_1^k and α_2^k for the 81 keV transition have been adopted in deriving δ_{II}^2 from p^2. But this mixing ratio is

very large compared with $\delta_{II}^2(\gamma\gamma) = 0.0001$ from γ-γ angular correlation for the same spin sequence. Since the pure dipole assignment for the 358 keV transition is only a simplification, M1 and E2 mixture was allowed next. Then the angular correlation functions for the above spin sequence take the form,

$$W(\gamma\gamma;\theta) = 1+\frac{1}{1+\delta_I{}^2}[\delta_I{}^2 F_2(22\tfrac{3}{2}\tfrac{5}{2})+2\delta_I F_2(12\tfrac{3}{2}\tfrac{5}{2})+F_2(11\tfrac{3}{2}\tfrac{5}{2})]$$
$$\times\frac{1}{1+\delta_{II}^2}[\delta_{II}^2 F_2(22\tfrac{7}{2}\tfrac{5}{2})+2\delta_{II}F_2(12\tfrac{7}{2}\tfrac{5}{2})+F_2(11\tfrac{7}{2}\tfrac{5}{2})]P_2(\cos\theta) \quad (7)$$
$$+\frac{\delta_I{}^2}{1+\delta_I{}^2}F_4(22\tfrac{3}{2}\tfrac{5}{2})\frac{\delta_{II}^2}{1+\delta_{II}^2}F_4(22\tfrac{7}{2}\tfrac{5}{2})P_4(\cos\theta).$$

Similarly, denoting the part of coefficients in A_2 and A_4 corresponding to the 358 keV by $A_2{}^I$ and $A_4{}^I$, we have

$$W(\gamma e_k{}^-;\theta) = 1+A_2{}^I\left(\frac{1}{1+p^2}\right)[p^2 b_2{}^2(e)F_2(22\tfrac{7}{2}\tfrac{5}{2})$$
$$+2pb_2F_2(12\tfrac{7}{2}\tfrac{5}{2})+b_2{}^{(1)}(\mathrm{m}F_2(11\tfrac{7}{2}\tfrac{5}{2})]P_2(\cos\theta) \quad (8)$$
$$+A_4{}^I(p^2/1+p^2)b_4{}^{(2)}(e)F_4(22\tfrac{7}{2}\tfrac{5}{2})P_4(\cos\theta).$$

With the help of these equations, $\delta_{II}^2(\gamma\gamma)$ and δ_{II}^2 $(\gamma e_k{}^-)$ for different values of $\delta_I{}^2$ were deduced. The results of γ-γ and γ-$e_k{}^-$ angular correlations agree if $\delta_I = -0.70\pm0.05$ with the corresponding values of $\delta_{II}(\gamma\gamma) = -0.065$ and $\delta_{II}(\gamma e_k{}^-) = -0.081$.

Thus, the spin of the 439 keV state is seen to be $\frac{3}{2}$ and not $\frac{1}{2}$ as had been assumed before. Also $\delta_I{}^2 = 0.50$ and $\delta_{II}^2 = 0.0043$. The parity of this 439 keV state should be positive since the spherical shell model which describes many observed properties quite satisfactorily, does not permit opposite parity low angular momentum states at such low excitation energies even if these states were looked upon not as single particle excitations but as due to the interaction between the single proton and the oscillating even-even core.

4. Nuclear Structure Effects in Internal Conversion

Having established these various parameters which were uncertain so far, and taking into account the correct energy of 81 keV for the transition, and the value of $\alpha^k = 1.49$, the nuclear structure effect parameter λ is deduced from [6])

$$\beta_1{}^k(\lambda) \approx \beta_1{}^k(1)[1-(\lambda-1)C(z,k)]^2, \quad (9)$$

where $C(z,k) = 7.91\times10^{-3}$ and $\delta_{II}^2(81\,\mathrm{keV}) = 0.0043$, to be $\lambda = -1.28$ in or $+2.53$ contrast to the value of $+6.25$ obtained under the many assumptions [7]) already discussed. While the mixing ratio of the transition has been obtained accurately

and unambigously in the present work, the transition energy needs to be determined more accurately by means of high resolution spectrometers because the existing uncertainty of about 1 keV in the transition energy makes the value of $\beta_1{}^k$ uncertain by about 0.05.

The particle parameters which have been employed in the angular correlation in the present work, are based on calculations under the point nucleus approximation [9]). The static and dynamic nuclear structure effects due to the finite size of the nucleus are particularly important [10]) for the interference parameter b_2 and the magnetic dipole parameter $b_2{}^{(1)}(\mathrm{m})$. Such effects are expected to be negligible for transitions resulting in the conversion electron continuum states of $d_{\frac{3}{2}}$ and $d_{\frac{5}{2}}$, so that $b_2{}^{(2)}(\mathrm{e})$ may be adopted to be unaffected without much error. However, theoretical calculations of the nuclear structure dependent particle parameters are available [10]) only for $Z = 78$. Adopting that the difference between the mixing ratios $\delta^2_{\mathrm{II}}(\gamma\gamma) = 0.0043$ and $\delta^2_{\mathrm{II}}(\gamma e_k{}^-) = 0.0066$ is due to these nuclear structure effects and assuming that, since the interference term involving b_2 is very small, all this effect is due to a correction necessary to the point nucleus value of $b_2{}^{(1)}$ (m), the coefficient A_2 in $W(\gamma e_k{}^-)$ requires, with $\delta^2_{\mathrm{II}}(\gamma\gamma) = \delta^2_{\mathrm{II}}(\gamma e_k{}^-) = 0.0043$, the corrected particle parameter $[b_2{}^{(1)}(\mathrm{m})]_{\mathrm{corr}}$, which is related to the point nucleus value $[b_2{}^{(1)}(\mathrm{m})]_{\mathrm{uncorr}}$ by

$$[b_2{}^{(1)}(\mathrm{m})]_{\mathrm{corr}}/[b_2{}^{(1)}(\mathrm{m})]_{\mathrm{uncorr}} \approx 1.5.$$

The actual value of the parameter λ can be deduced from the present work when theoretical calculations are available [12]).

The author is very thankful to Professor B. V. Thosar for his interest in this work and for some discussions. He is also thankful to the radiochemistry group at this Institute, in particular to Mr. A. T. Rane, for their help in carrier free chemical separation of barium activity from the caesium target.

References

1) I. Bergström *et al.*, Ark. for Fys. **5** (1952) 191, **7** (1954) 255
2) D. Strominger *et al.*, Rev. Mod. Phys. **30** (1958) 585
3) E. Bodenstadt *et al.*, Nuclear Physics **11** (1959) 584
4) H. Naya *et al.*, Supp. Progr. Theor. Phys. (Japan) **8** (1958) 33
5) A. Arima *et al.*, Progr. Theor. Phys. (Japan) **17** (1957) 567
6) E. L. Church and J. Weneser, Phys. Rev. **104** (1956) 1352
7) M. K. Ramaswamy, Phys. Rev. **119** (1960) 2021
8) M. E. Rose, Phys. Rev. **91** (1953) 610
9) L. C. Biedenham and M. E. Rose, Rev. Mod. Phys. **25** (1953) 729
10) E. L. Church *et al.*, Phys. Rev. **109** (1958) 1299
11) B. N. Subba Rao, Nuovo Cim. **20** (1961) 178
12) B. N. Sabba Rao, to be published

1.D.1:
6.D

Nuclear Physics **27** (1961) 38—40; © *North-Holland Publishing Co., Amsterdam*
Not to be reproduced by photoprint or microfilm without written permission from the publisher

REDUCED MATRIX ELEMENTS IN NUCLEAR SHELL THEORY

V. K. KEMBHAVI

Department of Physics, Karnatak University, Dharwar, India

Received 16 March 1961

Abstract: Using harmonic oscillator wave functions, reduced matrix elements have been expressed in terms of Talmi integrals and $3F_2$ series. The B coefficients of Brody, Jacob and Moshinsky are shown to be related to $3F_2$ series, and some recurrence relations for the B coefficients are obtained. A table of useful B coefficients is presented.

1. Introduction

It has been shown by Brody, Jacob and Moshinsky [1]) that matrix elements occurring in the harmonic oscillator shell model can be expressed in terms of what are known as B coefficients and Talmi integrals [2]) It is the purpose of this paper to point out that these B coefficients are related to $3F_2$ hypergeometric series, a connection which helps derivation of useful recurrence relations between the former.

If the radial wave function is expressed in terms of a confluent hypergeometric function

$$R_{nl} = \left[\frac{2\Gamma(n+l+\frac{3}{2})}{(\Gamma(l+\frac{3}{2}))^2 n!}\right]^{\frac{1}{2}} r^l \exp(-\tfrac{1}{2}r^2)\,{}_1F_1\left(\begin{matrix}-n\\ l+\frac{1}{2}\end{matrix}; r^2\right), \tag{1}$$

the "reduced matrix element" [1]) can be evaluated as

$$\langle nl||V(r)||n'l'\rangle = \left[\frac{\Gamma(n+l+\frac{3}{2})(\Gamma(n'+l'+\frac{3}{2})}{(\Gamma(l+\frac{3}{2})\Gamma(l'+\frac{3}{2}))^2 n!\, n'!}\right]^{\frac{1}{2}}$$
$$\times \sum_{\kappa=0}^{\infty} \frac{(-n)_\kappa \Gamma(\kappa+\frac{1}{2}(l+l'+3))}{(l+\frac{3}{2})_\kappa \kappa!}\, 3F_2\left(\begin{matrix}-n', -l-\kappa-\frac{1}{2}, -\kappa\\ l'+\frac{1}{2}, 1+n-\kappa\end{matrix}; -1\right) I_{\kappa+\frac{1}{2}(l+l')}, \tag{2}$$

where r is expressed in units of $(\hbar/m\omega)^{\frac{1}{2}}$.

Here $3F_2$ is a generalised hypergeometric series and $I_{\kappa+\frac{1}{2}(l+l')}$ is a Talmi integral. This is rendered possible because of the well known relationship between hypergeometric functions [3]).

$${}_1F_1\left(\begin{matrix}-n\\ l+\frac{1}{2}\end{matrix}; r^2\right) {}_1F_1\left(\begin{matrix}-n'\\ l'+\frac{1}{2}\end{matrix}; r^2\right) = \sum_{\kappa=0}^{\infty} \frac{(-n)_\kappa r^{2\kappa}}{(l+\frac{3}{2})_\kappa \kappa!}\, 3F_2\left(\begin{matrix}-n', -l-\kappa-\frac{1}{2}, -\kappa\\ l'+\frac{1}{2}, 1+n-\kappa\end{matrix}; -1\right) \tag{3}$$

Eq. (26) of Brody *et al.* can be rewritten as

$$\langle nl||V(r)||n'l'\rangle = \sum_{\kappa=0}^{n+n'} B(nl, n'l', \kappa+\tfrac{1}{2}(l+l'))I_{\kappa+\frac{1}{2}(l+l')} \tag{4}$$

$$= \sum_{\kappa=0}^{\infty} B(nl, n'l', \kappa+\tfrac{1}{2}(l+l'))f(0, \kappa, n+n')I_{\kappa+\frac{1}{2}(l+l')}, \tag{5}$$

where $f(0, \kappa, n+n')$ is a step function defined for $0 \leqq n+n'$ as follows:

$$f(0, \kappa, n+n') = \begin{cases} 0 & \text{if} \quad \kappa < 0, \\ 1 & \text{if} \quad 0 \leqq \kappa \leqq n+n', \\ 0 & \text{if} \quad \kappa > n+n'. \end{cases} \tag{6}$$

Comparing eqs. (2) and (5) the B coefficients can be readily expressed in terms of the $3F_2$ series as

$$B(nl, n'l', \kappa+\tfrac{1}{2}(l+l'))f(0, \kappa, n+n')$$
$$= \frac{(-1)^\kappa \Gamma(\kappa+\frac{1}{2}(l+l'+3))}{(n-\kappa)!\,\kappa!\,\Gamma(\kappa+l+\frac{3}{2})}\left[\frac{\Gamma(n+l+\frac{3}{2})\Gamma(n'+l'+\frac{3}{2})n!}{(\Gamma(l'+\frac{3}{2}))^2\, n'!}\right]^{\frac{1}{2}} \times 3F_2\left(\begin{matrix}-n', -l-\kappa-\frac{1}{2}, -\kappa; \\ l'+\frac{1}{2}, 1+n-\kappa\end{matrix}; -1\right). \tag{7}$$

Using the well known recurrence relations for the $3F_3$ series [4])

$$(n'+l'+\tfrac{1}{2})(n'+n-\kappa)3F_2\left(\begin{matrix}-n', -l-\kappa-\frac{1}{2}, -\kappa; \\ l'+\frac{1}{2}, 1+n-\kappa\end{matrix}; -1\right)$$
$$= 2\kappa(\kappa+l+\tfrac{1}{2})3F_2\left(\begin{matrix}-n'+1, -l-\kappa+\frac{1}{2}, -\kappa+1; \\ l'+\frac{1}{2}, 1+n-\kappa\end{matrix}; -1\right)$$
$$+(n'+n+l'+l+\kappa+1)(n-\kappa)3F_2\left(\begin{matrix}-n'+1, -l-\kappa-\frac{1}{2}, -\kappa; \\ l'+\frac{1}{2}, n-\kappa\end{matrix}; -1\right)$$
$$-\{n(n+l+\tfrac{1}{2})-n'(n'+l'+\tfrac{1}{2})\}3F_2\left(\begin{matrix}-n'+1, -l-\kappa-\frac{1}{2}, -\kappa; \\ l'+\frac{1}{2}, 1+n-\kappa\end{matrix}; -1\right),$$

we can easily deduce the following recurrence relation between the B coefficients:

$$\left[\frac{n'(n'+l'+\frac{1}{2})}{n(n+l+\frac{1}{2})}\right]^{\frac{1}{2}}(n'+n-\kappa)B(nl, n'l', \kappa+\tfrac{1}{2}(l+l'))$$
$$= (n'+n+l'+l+\kappa+1)B(n-1\,l, n'-1\,l', \kappa+\tfrac{1}{2}(l+l'))$$
$$-(2\kappa+l+l'+1)B(n-1\,l, n'-1\,l', \kappa+\tfrac{1}{2}(l+l'-2)) \tag{8}$$
$$-\{n(n+l+\tfrac{1}{2})-n'(n'+l'+\tfrac{1}{2})\}\left[\frac{1}{n(n+l+\frac{1}{2})}\right]^{\frac{1}{2}}B(nl, n'-1\,l', \kappa+\tfrac{1}{2}(l+l')).$$

If now, $n' = n, l' = l$ we get

$$(2n-p+l)B(nl, nl, p)$$
$$= (2n+p+l+1)B(n-1\,l, n-1\,l, p)-(2p+1)B(n-1\,l, n-1\,l, p-1) \tag{9}$$

where $p = \kappa+l$.

Putting $n' = n-1, l' = l+2$, we get the other useful recurrence relation:

$$\left[\frac{(n-1)(n+l+\frac{3}{2})}{n(n+l+\frac{1}{2})}\right]^{\frac{1}{2}} (2n-p+l+1)B(nl, n-1\,l+2, p+1)$$
$$= (2n+p+l+2)B(n-1l, n-2l+2, p+1)-(2p+3)B(n-1l, n-2l+2, p) \quad (10)$$
$$-\left[\frac{(l+\frac{3}{2})^2}{n(n+l+\frac{1}{2})}\right]^{\frac{1}{2}} B(nl, n-2\,l+2, p+1).$$

Using the recurrence relations (9) and (10), all the B coefficients can be computed. The recurrence relation (8) is of a general nature.

Tables of $B(nl, nl, p)$ have been computed by Brody *et al* [1]), But values of $B(nl, n'l', p)$, which are required in other physical situations such as evaluation of Coulomb energies of nuclei from shell model wave functions [5]), are not available for half integral values of p, A few useful coefficients are furnished in table 1 with a view to illustrating the facility of calculation when our formulae are used.

TABLE 1.

Values of $B(nl, n'l', p)$

p	n	l	n'	l'	$B\ (nl, n'l', p)$	p	n	l	n'	l'	$B\ (nl, n'l', p)$
0.5	0	1	0	0	0.92131768	2.5	1	1	1	0	2.85458907
	0	1	1	0	1.12837907		0	1	1	2	−1.52584700
	1	1	0	0	1.45673110		1	1	0	2	−1.80540651
	1	1	1	0	1.78412396		1	1	1	2	−5.79018224
							0	2	0	3	0.96503037
1.5	0	1	1	0	−1.50450542		1	2	0	3	1.80540651
	1	1	0	0	−1.16538488		0	1	0	4	0.71929119
	1	1	1	0	−3.80613112		1	1	0	4	1.13729920
	0	1	0	2	0.95153277						
	0	1	1	2	1.78015483	3.5	1	1	1	2	3.86012162
	1	1	0	2	1.50450542		1	2	0	3	−7.22162606
	1	1	1	2	2.81467194		1	1	0	4	−1.81967872
	0	0	0	3	0.62292444		0	3	0	4	0.97265919

I would like to thank Mr. K. M. Koliwad for his kind assistance in checking some of the results and Dr. N. V. V. J. Swamy for helpful discussions and a critical reading of the manuscript. I am grateful to Dr. T. A. Brody and Dr. M. Moshinsky for sending me tables of transformation brackets.

References

1) T. A. Brody, G. Jacob and M. Moshinsky, Nuclear Physics **17** (1960) 16
2) I. Talmi, Helv. Phys. Acta **25** (1952) 185
3) Erdélyi, Higher transcendental functions (McGraw-Hill Book Co., New York, 1953) vol. I, p. 187
4) W. N. Bailey, Quart. J. Math. Oxford **8** (1937) 113
5) N. V. V. J. Swamy, V. K. Kembhavi and D. G. Galgali, Phys. Rev. **120** (1960) 2069

2.B:
2.E:2.L

Nuclear Physics **27** (1961) 41—45; © *North-Holland Publishing Co., Amsterdam*

Not to be reproduced by photoprint or microfilm without written permission from the publisher

POLARIZATION IN C^{12} (p, p) SCATTERING FROM 5 TO 10.5 MeV

J. E. EVANS

Atomic Energy Research Establishment, Harwell, Berks

Received 27 March 1961

Abstract: The measurement of the polarization in C^{12} (p, p) scattering at three different energies, using a carbon polarimeter with the Harwell tandem generator, has been described [1]). The polarimeter, which has been made more efficient, has been calibrated using one of the three original measurements, and used to determine the polarization at several angles in the energy range from 5 to 10.5 MeV. The results provide data for using C^{12} as an analyser of proton polarization. They also provide a sensitive check on the accuracy of phase shift analyses of C^{12} (p, p) scattering [5]). Finally it is of interest to compare the gross behaviour below 10 MeV with optical model predictions.

1. The Polarimeter

The polarimeter (fig. 1) could be rotated inside a 76 cm diameter evacuated scattering tank. The proton beam from the tandem generator entered the tank

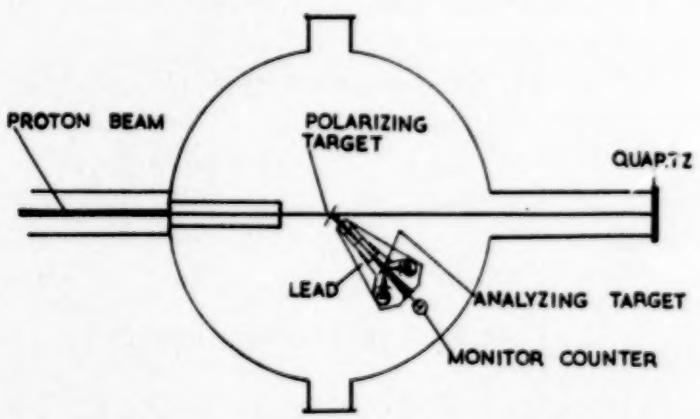

Fig. 1. Scattering tank with carbon polarimeter.

through two tantalum stops, the defining aperture being 6.3 mm × 2.3 mm. Slits were used in preference to circular apertures to minimize asymmetries due to fluctuations in beam position. The first target could be withdrawn to allow the beam to be caught on a marked quartz beyond the tank. The centres of the beam stops, the centre of rotation of the polarimeter and the mark on the quartz were all aligned.

Both targets were self-supporting carbon foils prepared from a suspension of

colloidal graphite in alcohol. The polarizing target was 2 mg/cm² and the analysing target was 6 mg/cm². The scattered beam entering the polarimeter passed through a collimator before striking the analysing target. The final aperture was 15 mm × 5 mm. The collimator was fitted with vacuum-tight Melanex windows (0.025 mm thick) at each end so that it would support at least $2\frac{1}{2}$ atm. xenon gas. The gas pressure could be varied from outside the scattering chamber so that the energy of protons striking the analysing target could be controlled.

After a second scattering, protons passed through two apertures, each 12 mm × 9 mm and fixed at 4.0 cm from the centre of the analysing target so that protons scattered through $48.0 \pm 0.5°$ passed through the centres of these apertures. The protons accepted by the apertures were then detected in CsI crystals (0.38 mm thick) supported inside reflecting enclosures, each viewed by a 5 cm EMI photo-tube disposed normally to the scattering plane. Protons which were not scattered a second time and passed through a 1.6 mm diameter aperture were detected in a third CsI scintillation counter, conveniently called the monitor counter.

After the second scattering protons were detected over a large solid angle so that measurement of the right/left ratio gave a product of polarizations $P_1\bar{P}_2$, where $\bar{P}_2$ was an average over the large solid angle. The quantity $\bar{P}_2$ was found using a known previously measured value [1]), for the polarization (P_1) at the first scattering. The proton resonance magnetometer on the tandem generator was used to arrange that the proton energy at the centre of the polarizing target was 6.04 MeV and the first scattering angle (θ_1) was set at 48°. It was known that P_1 was -0.79 ± 0.04. The collimator in the polarimeter was evacuated and the right/left ratio of twice scattered protons was found and used to calculate $\bar{P}_2$. The results for the ratio (outer counter)/(inner counter) were 2.97 ± 0.20 ($\theta_1 = +48°$) and 2.92 ± 0.20 ($\theta_1 = -48°$). These results indicate a value for $\bar{P}_2$ of -0.62 ± 0.04. This calibration was found to hold on a number of occasions during the course of the measurements.

2. Polarization Measurements

The quantity $\bar{P}_2$ was used to find other values of P_1, this being a justifiable procedure so long as the first scattered beam is always defined by sufficiently good geometry. The requirements for this have been calculated [1,2]) and were taken into account when deciding the size of the final collimator aperture. The analysing conditions of the calibration were realised in the measurements by using the appropriate pressure of xenon to slow down the polarized protons. The position of the counting rate peak in the monitor counter under calibration conditions was always found at the start of an experiment. After changing the beam energy and first scattering angle to the values for which P_1 was required, xenon was introduced until the monitor counter showed that the mean analysing

energy had been reduced to that at which $\bar{P}_2$ had been measured. The ratio (outer counter)/(inner counter) was measured for both positive and negative values of θ_1.

Two possible sources of error were investigated. The angular spread of the second scattered beam due to the xenon together with the fact that the angular distribution of protons from the polarizing target is not isotropic could produce asymmetry at high xenon pressures. This effect was sought using a gold first target with an incoming beam of 10 MeV and sufficient xenon to reduce the scattered beam to the calibration energy (about 5.5 MeV at the front surface of the analysing target). The asymmetry found was not statistically different from that obtained under calibration conditions with gold (i.e. close to zero).

The other possible error could arise due to straggling in the xenon. Under calibration conditions, with no xenon, the half width of the peak in the monitor counter was 5 %. But when measuring polarization at 10 MeV, although the peak was still symmetrical, the half width was 10 %. The variation of $\bar{P}_2$ as a function of analysing energy was investigated and found to be linear, and so errors due to this effect were ignored in comparison with those due to counting statistics and the uncertainty in $\bar{P}_2$ at the calibration energy.

3. Results

The results for the polarization are shown in fig. 2. The two dotted lines

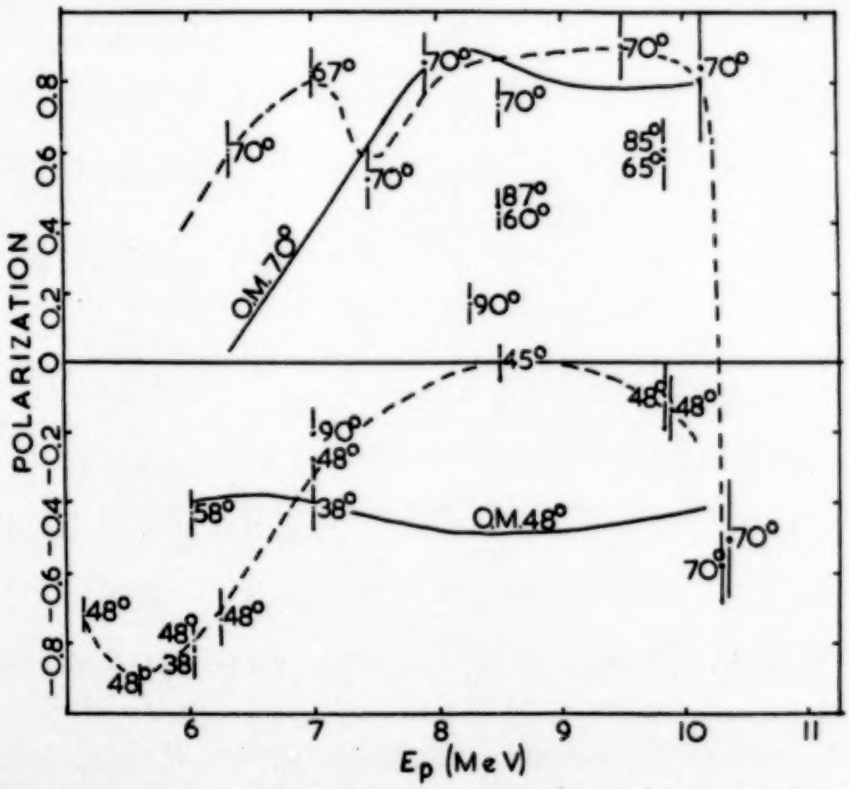

Fig. 2. C^{12} (p, p) polarization at various laboratory angles. The full lines show the results of the optical model calculations.

represent polarization at 48° and 70° using the Basle convention for the sign of polarization ($\mathbf{n} = \mathbf{K}_{in} \times \mathbf{K}_{out}$). At 48° the absolute value of the polarization falls off continuously above 5.6 MeV, approaching zero at 8.5 MeV then increasing again. These results smoothly fill in the gap between measurements made above and below this energy range by other workers at Rochester, Princeton and Osaka [3]).

The polarization at 70° is interesting. Its fairly smooth behaviour and high value between 7 and 10 MeV indicate the value of carbon as an analyzer in this region, especially when used in a calibrated polarimeter in the manner described above. The approximate positions of the resonances are known [4]). The dip at 7.5 MeV can be attributed to the resonance at that energy, because the width Γ of the resonance is of the order [4]) of 350 keV but the energy loss in the target was only about 100 keV.

The change in sign at 10.25 MeV could well be due to a resonance [4]) at 10.3 MeV ($\Gamma \approx 250$ keV). It was not possible, because of background difficulties, to find if $P(70°)$ recovered sign again above the resonance.

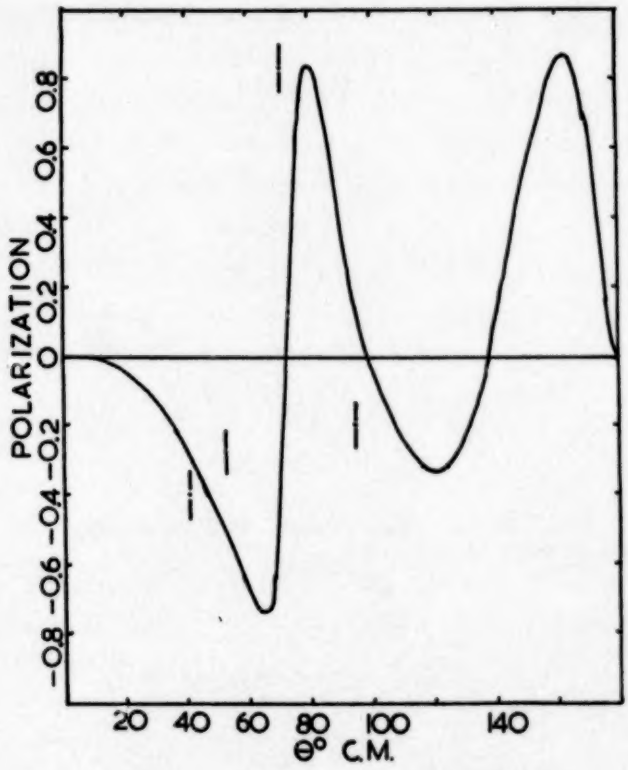

Fig. 3. Polarization in C^{12} (p, p) at 7 MeV as predicted by an optical model calculation.

It is of interest to compare the polarization outside of resonances with the expected optical model behaviour. An optical model calculation of the polarization in the range 6—10 MeV was carried out by Dr. P. E. Hodgson of the

Clarendon Laboratory using the following parameters (held constant over the energy range):

$$U = -50 \text{ MeV}, \quad W = -9 \text{ MeV}, \quad U_s = 9 \text{ MeV}, \quad r_0 = 1.3 \text{ fm}, \quad a = 0.65 \text{ fm}.$$

The potential contains the parameters as

$$V(r) = V_c(r) + (U+iW)V_{sw}(r_0, a) + \left(\frac{\hbar}{m_\pi c}\right)^2 U_s \frac{1}{r}\frac{d}{dr}[V_{sw}(r_0, a)] \quad \mathbf{l}\cdot\boldsymbol{\sigma},$$

where V_{sw} is the Saxon Woods potential.

The first maximum in the polarization at 70° at all energies is well reproduced (figs. 2 and 3). Fig. 3 at 7 MeV is typical of the calculations. The behaviour of the polarization at 48° is not as indicated by the first minimum of the diffraction pattern predicted by the optical model calculations. It is emphasized that no attempt was made to fit the data by varying the parameters.

Since this work was completed, a table of experimental results has been received from Professor Haeberli of the University of Wisconsin [6]). These show the polarization measured at 10° intervals from 20° to 140° at eight energies in the range 4.66 MeV to 8.66 MeV and the polarization at 50° measured at 29 different energies in the range 4.38 to 9.17 MeV. It is interesting that these results were obtained with a helium analyser, and that agreement with the present results is very substantial.

Dr. J. H. Montague collaborated in building the polarimeter and in some of the earlier experiments. Dr. E. B. Paul suggested mounting a polarimeter in the scattering tank, and encouraged the work. I am grateful to them both and to Dr. P. E. Hodgson for supplying the optical model calculations.

References

1) J. E. Evans, Helv. Phys. Acta, Supplementum VI (1961)
2) J. E. Evans, A.E.R.E. report R3347
3) S. Yamabe, M. Kondo, S. Kato, T. Yamazaki and J-Z. Ruan, J. Phys. Soc. Japan **15** (1960) 12, 2154
4) G. Dearnaley and A. B. Whitehead, unpublished
5) J. E. Evans and M. A. Grace, Nuclear Physics **15** (1960) 646

8.B

Nuclear Physics **27** (1961) 46—51; © *North-Holland Publishing Co., Amsterdam*

Not to be reproduced by photoprint or microfilm without written permission from the publisher

AN INTERPRETATION OF THE ISOBARIC SPIN SPACE

TH. A. J. MARIS

Instituto de Física, Universidade do Rio Grande do Sul, Pôrto Alegre, Brasil

Received 7 March 1961

Abstract: It is shown that the group of isobaric spin rotations is homomorphous with a certain group of Lorentz-invariant transformations of a 4-component spinor field. A simple interpretation of the isobaric spin operators of interacting fields as being quantities known from the Dirac theory seems possible.

1. Introduction

It has recently been remarked [1]) that one can interpret the isobaric spin degrees of freedom of a free fermion-isofermion field as a transformation property of a 4-component spinor by putting the "positive and negative mass states" of the Dirac field on the same footing.

In the present paper, these considerations are generalized for the case of an interacting fermion-isofermion field. From the following point of view the isobaric spin operators generate, together with the fermion gauge transformation and the charge conjugation, the complete group of unitary Lorentz-invariant symmetry transformations of an interacting 4-component spinor field, which is asymptotically free.

Except for a subsidiary condition for the spinor field, of which we do not yet see the full consequences, the present formulation goes over in the usual one by a simple transformation. The main point of interest might therefore be that starting from a 4-component spinor, one can obtain the isobaric spin degrees of freedom without introducing a foreign element into the theory. If the present interpretation were sound, questions on the properties of the isospace (like that of the number of its dimensions) would be answered and a relation between the isospin transformations of the strongly interacting particles and the γ^5 transformations of the leptons obtained.

Finally, following the ideas of Sakata and Markov, we briefly show that the introduction of an additional isospin-less Λ-field allows one to account for the occurrence of the known quantum numbers of all the strongly interacting particles without a priori introducing the isobaric spin space.

2. The Interacting Fermion Isofermion Field

Let us first consider an interacting *unquantized* 4-component spinor field which represents a fermion-isofermion of non-zero mass.

It is necessary to generalize the meaning of the operator $-(1/m)\gamma^\mu \partial/\partial x^\mu$, which plays an essential role in the interpretation of the isobaric spin of the free field [1]). For this purpose the operator γ^7 is defined by its representation in 4-momentum space

$$\gamma^7 = \frac{-i}{|K|}\gamma^\mu K_\mu, \tag{1}$$

$|K|$ being the absolute magnitude of the 4-momentum.

We now impose a subsidiary condition on our spinor field, namely that it does not contain Fourier components corresponding to imaginary masses. This condition seems not to be unnatural, as such components would tend to move with superlight velocities.

For the zero-mass components the definition (1) must be extended by a suitable limiting procedure, but its precise form is at present unimportant, as the components of exact zero mass will have an infinitesimal small weight for an interacting massive field.

The action of γ^7 is therefore very simple: it multiplies every Fourier component of a spinor by the sign of its mass. From this or eq. (1) it is clear that

$$(\gamma^7)^2 = 1. \tag{2}$$

This equation and the following ones are to be understood as being valid if both sides operate on a spinor obeying the subsidiary condition.

The operator γ^7 would seem to introduce an extreme non-locality in the theory. This situation is however somewhat similar to the one arising in the well-known separation of the positive and negative frequency components of a field. In fact one may find several other parallels between the present development which results in particles of opposite isobaric spins and that leading to particles and anti-particles. Suppose, for example, that in the case of a free scalar field one would limit oneself to solutions with only one sign of the frequency. It would then be necessary to introduce two fields, one for the particles and one for the antiparticles. Charge conjugation and the charge gauge transformation would be represented by transformations in the particle-antiparticle space, analogous to the transformations which are employed in the usual isobaric spin theory.

We proceed by defining

$$\gamma^6 = i\gamma^5\gamma^7. \tag{3}$$

In the following γ^1, γ^2, γ^3, γ^4 or γ^0 will be denoted by Greek superscripts and γ^5, γ^6, γ^7 by Latin ones. From eqs. (1), (2) and (3) it follows:

$$\{\gamma^i, \gamma^j\}_+ = 2\delta^{ij}, \tag{4}$$

$$\gamma^5\gamma^6 = i\gamma^7 \text{ and cycl.} \tag{5}$$

As proper Lorentz transformations do not mix positive and negative mass states, the γ^i are Lorentz invariants.

Most considerations of ref. [1]) can now immediately be generalized replacing $(i/m)\gamma^5\gamma^\mu\,\partial/\partial x^\mu$ and $-(1/m)\gamma^\mu\,\partial/\partial x^\mu$ by γ^6 and γ^7, respectively. The invariance of the theory under the isobaric spin rotations

$$\Psi'(x) = \mathrm{e}^{i\alpha^i\gamma^i}\Psi(x), \tag{6}$$

the α^i being real numbers, is again postulated. The projection operators for the fields with third components of the isospin equal to $\pm\frac{1}{2}$ are given by

$$\tfrac{1}{2}(1\pm\gamma^7). \tag{7}$$

The field is *quantized* with the usual equal time anticommutation rules for the two isobaric spin components

$$\begin{aligned}&\{\tfrac{1}{2}(1\pm\gamma^7)\psi_\alpha(x),\quad \tfrac{1}{2}(1\pm\gamma^7)\psi_\beta(x')\}_+ = 0,\\ &\{[\tfrac{1}{2}(1\pm\gamma^7)\psi_\alpha(x)]^\dagger, \tfrac{1}{2}(1\pm\gamma^7)\psi_\beta(x')\}_+ = \delta_{\alpha\beta}\delta_{+-}\delta(x-x').\end{aligned} \tag{8}$$

With the definition

$$\varphi = \gamma^7\psi, \qquad (\psi = \gamma^7\varphi), \tag{9}$$

one may write more symmetrically

$$\{\psi_\alpha^\dagger(x), \psi_\beta(x')\}_+ = \{\varphi_\alpha^\dagger(x), \varphi_\beta(x')\}_+ = 2\delta_{\alpha\beta}\delta(x-x'). \tag{10}$$

All other equal-time anti-commutators vanish.

The components of the isobaric spin operators T^1, T^2 and T^3, with the properties

$$[T^{i-4}, \psi] = -\tfrac{1}{2}\gamma^i\psi, \qquad [T^{i-4}, \varphi] = -\tfrac{1}{2}\gamma^7\gamma^i\psi, \tag{11}$$

$$[T^1, T^2] = iT^3 \text{ and cycl.}, \tag{12}$$

are given by

$$T^{i-4} = \tfrac{1}{4}\int_{t=t_0}(\psi^\dagger\gamma^i\psi+\varphi^\dagger\gamma^7\gamma^i\psi)\mathrm{d}^3x. \tag{13}$$

With the help of eqs. (4), (5) and (9), (10) one easily verifies that the T are hermitian, give zero when operating on the vacuum and fulfil the relations (12). The eqs. (11) are fulfilled for field operators located on the integration surface of constant time t_0. From this and the invariance postulate (6), it follows that the T are independent of t_0. By their hermiticity, zero eigenvalue for the vacuum and relations (11), the T are uniquely determined. Therefore they are Lorentz invariants, as their operations (11) have this property. For the case of the free field, one of course finds back the expressions of ref. [1]).

The parity transformations can be defined either by

$$\psi'(x) = \gamma^4 \psi(-x), \tag{14}$$

or by

$$\psi'(x) = \gamma^7 \gamma^4 \psi(-x), \tag{15}$$

depending on whether one wants to give the two isobaric spinor components a different or the same parity. To define the parity character we at present choose expression (15), which assigns to the neutron and proton equal parities in contradistinction to the transformation (14) which was taken in ref. [1]).

In table 1, bilinear expressions in the spinor field, which have a simple transformation character under both Lorentz and isospin transformations, are listed. The abbreviations in the two last columns have the usual meaning. The Lorentz-covariants which are scalars in isospace are built rather similarly to the commonly used ones. An isoscalar is changed into the corresponding isovector by the replacements $\psi \to \gamma^l \psi$ and $\varphi \to \gamma^7 \gamma^l \psi$. The covariants ($V^\mu$, S) and ($V^\mu$, V^l) are the fermion-and isospin-currents.

TABLE 1

Bilinear expressions in the spinor field

Bilinear covariant	Transformation character in	
	space-time	iso-space
$\bar{\varphi}\psi + \bar{\psi}\varphi$	S	S
$\bar{\varphi}\gamma^l\psi + \bar{\psi}\gamma^7\gamma^l\psi$	S	V^l
$i(\bar{\varphi}\gamma^5\psi + \bar{\psi}\gamma^5\varphi)$	P	S
$i(\bar{\varphi}\gamma^5\gamma^l\psi + \bar{\psi}\gamma^5\gamma^7\gamma^l\psi)$	P	V^l
$i(\bar{\psi}\gamma^\mu\psi + \bar{\varphi}\gamma^\mu\varphi)$	V^μ	S
$i(\bar{\psi}\gamma^\mu\gamma^l\psi + \bar{\varphi}\gamma^\mu\gamma^7\gamma^l\psi)$	V^μ	V^l
$i(\bar{\psi}\gamma^5\gamma^\mu\psi + \bar{\varphi}\gamma^5\gamma^\mu\varphi)$	A^μ	S
$i(\bar{\psi}\gamma^5\gamma^\mu\gamma^l\psi + \bar{\varphi}\gamma^5\gamma^\mu\gamma^7\gamma^l\psi)$	A^μ	V^l
$\bar{\varphi}\sigma^{\mu\nu}\psi + \bar{\psi}\sigma^{\mu\nu}\varphi$	$T^{\mu\nu}$	S
$\bar{\varphi}\sigma^{\mu\nu}\gamma^l\psi + \bar{\psi}\sigma^{\mu\nu}\gamma^7\gamma^l\psi$	$T^{\mu\nu}$	V^l

With the help of table 1, one may, in the usual way, construct quantities which are invariants under both Lorentz transformations and transformation (6). The resulting expressions can, assuming ψ to be the nucleon field, be translated into the usual language of the isospace by first using eqs. (4), (5) and (9) and then putting

$$\psi = \psi_{\text{proton}} + \gamma^5 \psi_{\text{neutron}}; \qquad \gamma^7 \psi \equiv \varphi = \psi_{\text{proton}} - \gamma^5 \psi_{\text{neutron}}. \tag{16}$$

The only feature reminiscent of the original formulation is then the subsidiary condition, which now demands that both ψ_p and ψ_n have only positive mass components.

The reversed substitution (16) transforms any 8-component isobaric spin invariant theory, which obeys the subsidiary condition, into a 4-component one that is invariant under the transformations (16), in particular under γ^5 transformations. It should however be noted that the γ^5 invariance of the usual nucleon weak interaction current is not represented by the simple γ^5 invariance of the 4-component formulation.

3. Concluding Remarks

It is now clear that, following the ideas of Sakata and Markov [2, 3]) one needs only a 4-component nucleon field and an isospinless Λ-field to account for the occurrence of all known quantum numbers of the strongly interacting particles, without postulating an isobaric spin space. The π-meson, for example, has the (P, V^l) symmetry of table 1, and the symmetry of the K-meson is given by

$$\overset{+}{K^0} \to \bar{\Lambda}\tfrac{1}{2}(1 \pm \gamma^7)N.$$

As is well known from the Sakata model, the hypercharge is the nucleon number, the strangeness the anti-Λ-number and the baryon number equals the $(\Lambda+N)$-number.

Finally, we want to remark that the interpretation of the isobaric spin degrees of freedom given above is based on the same idea on which other invariance operations known in physics are based: an arbitrariness in the definition of a measurable quantity, which can only be resolved by a concrete agreement, results in an invariance transformation between the possible choices. So, the translation, rotation and parity invariances originate from the arbitrariness in the location of the origin, in the orientation, and in the handedness of the coordinate system. The charge conjugation has its basis in the arbitrariness of the sign attributed to the charge of the electron. In the present interpretation the arbitrariness in the sign of the mass of a Dirac particle leads to the isobaric spin transformations.

The author is thankful to Professor D. Dillenburg, Professor Gerhard Jacob, Professor S. W. MacDowell and Professor M. A. Melvin for stimulating discussions and to Professor Saviniano de Castro Marques for the unique hospitality of his Institute. The stay of the author in Brasil has been made possible by the support of Comissão Supervisora do Plano dos Institutos (COSUPI), Conselho Nacional de Pesquisas, Brasil and the Division of Scientific Development of the Organization of the American States.

Note added in proof: Recently the author found the references [4–6]) in which the possibility of the representation of the nucleon by a 4-component spinor is shown. The identification in these papers of the isopin operations with the Pauli-Gürsey group is essentially different from that of the present treatment.

References

1) Th. A. J. Maris, Nuclear Physics **24** (1961) 356
2) S. Sakata, Prog. Theor. Phys. **16** (1956) 686
3) Markov, Rep. 6th Ann. Rochester Conf. High-Energy Nuclear Physics (1956)
4) G. Marx, Nuclear Physics **9** (1958/59) 337
5) G. Marx, Nuclear Physics **10** (1959) 468
6) H. P. Dürr, W. Heisenberg, H. Mitter, S. Schlieder und K. Yakazaki, Z. Naturf, **14a** (1959) 441

8.B

Nuclear Physics **27** (1961) 52—57; © *North-Holland Publishing Co., Amsterdam*

Not to be reproduced by photoprint or microfilm without written permission from the publisher

ON THE $K^+ + n \to K^0 + p$ SCATTERING AMPLITUDE POLES

V. AMAR and M. PAURI

Istituto di Fisica dell'Università, Milano

and

Istituto Nazionale di Fisica Nucleare, Sez. di Milano

Received 10 March 1961

Abstract: The process $K^+ + n \to K^0 + p$ is considered. The effects on this process of the introduction of the interaction $H' = 2fm_K[\bar{K}^+ K^0 \pi^+ + \bar{K}^0 K^+ \pi^-]$ proposed by Pais are examined by means of dispersion relations at fixed energy. A useful formula for the estimation of f_R is obtained by standard methods. A concrete possibility of discriminating between the models of Pais and of Gell-Mann is investigated. Finally, some consequences for isobaric conservation rules in the K-baryon interactions are discussed in connection with the possible existence of a vertex like $\bar{K}K\pi$, whether elementary or not.

1. Introduction

In a series of papers, Pais considered the possibility of grouping all the baryons in isobaric spin doublets (isospinors) giving a description of all the strong interactions known as "doublet approximation". This theory, however, leads to a set of conclusions which disagree with experimental results. In order to make the doublet approximation consistent with experiment, Pais [1]) proposed the introduction of an additional interaction $H' = 2fm_K [\bar{K}^+ K^0 \pi^+ + \bar{K}^0 K^+ \pi^-]$ assuming the $K^+ - K^0$ relative parity ($p(K)$) to be odd.

In this paper we intend to investigate, with the help of dispersive techniques, the consequences of such a hypothesis. For this purpose we shall deal with the $K^+ + n \to K^0 + p$ reaction using results of fixed energy dispersion relations [2]). This method allows us to deduce a formula which is suitable for the estimate of f_R and which will allow a numerical computation of f_R as soon as more accurate data on this process are available. This will show if the value obtained by Pais is of the correct order of magnitude.

We then discuss the possible features of the angular distributions of both the $K^+ + n \to K^0 + p$ and $K^+ + n \to K^+ + n$ reactions. We show that these features can be used as a test to determine whether the Pais theory, that of Gell-Mann or neither of these are correct. Finally we discuss some of the consequences of the existence of a $\bar{K}K\pi$ vertex, whether elementary or not, in particular concerning the I and I_3 conservation rules in K-baryon interactions.

2. Existence of a Forward Pole

Let $p_1, q_1, -p_2, -q_2$ be the nucleon and meson four-momenta, ingoing and outgoing respectively. The usual invariants are

$$\begin{aligned} s &= (q_2+p_2)^2 = (q_1+p_1)^2, \qquad t = (p_1+p_2)^2 = (q_1+q_2)^2, \\ u &= (q_1+q_2)^2 = (p_1+p_2)^2. \end{aligned} \tag{1}$$

By means of kinematical variables referred to the c.m. system for the $K+N \to K+N$ reaction they can be written as follows:

$$\begin{aligned} s &= (\sqrt{m_N{}^2+q^2}+\sqrt{m_K{}^2+q^2})^2 \equiv W^2, \\ t &= -2q^2(1-\cos\theta) \equiv -\Delta^2, \qquad u = 2m_N{}^2+2m_K{}^2-W^2+\Delta^2. \end{aligned} \tag{2}$$

These quantities are the squares of the c.m. energies for the reactions

$$\begin{aligned} &\text{a)}\ K+N \to K+N, \\ &\text{b)}\ K+\bar{K} \to N+\bar{N}, \\ &\text{c)}\ K+\bar{N} \to K+\bar{N}, \end{aligned} \tag{3}$$

respectively.

If we assume that the Mandelstam conjecture [3]) is justified, there will be, as is well known, poles in the matrix element $A(s, t, u)$ describing the three channels a), b) and c). These poles appear [4]) when the corresponding energy variables take the value of the square of the mass of a one-particle intermediate state having all its quantum numbers common with the initial and final states of the process in question. An inspection of the kinematical relations shows that when the energy is held fixed the remaining invariants are linearly related to $\cos\theta$ with real coefficients. One may speak, therefore, of a $\cos\theta$ complex plane in which the poles are in one-to-one correspondence with those of the momentum transfer variables.

As a consequence of the Pais interaction there is a pole at the value $\cos\theta \equiv \alpha_0 = 1+m_\pi{}^2/2q^2$ in the scattering amplitude $A(W, \cos\theta)$ for the process considered here. Thus, the scattering amplitude is expected [5]) to take the form

$$A(W, \cos\theta) = \frac{G(W, \cos\theta)}{\cos\theta-\alpha_0} + T(W, \cos\theta). \tag{4}$$

The function $G(W, \cos\theta)$ is the well known Born term, analytical over the whole $\cos\theta$-complex plane, and $T(W, \cos\theta)$ is the contribution to the scattering amplitude given by the other singularities. The cross section, then, is as

follows †

$$\frac{d\sigma}{d\Omega} = K(W)\frac{|G(W,\cos\theta)|^2}{(\alpha_0-\cos\theta)^2} \qquad (5)$$
$$+ \text{ terms containing at most first-order poles in } \alpha_0.$$

Straightforward calculations give the following result:

$$K(W)|G(W,\cos\theta)|^2 = \frac{f_R{}^2 g_R{}^2 m_K{}^2(1-\cos\theta)}{16\pi^2 q^2(p_{2,0}+q_{2,0})\sqrt{2q^2+m_N{}^2+m_K{}^2+2p_{2,0}q_{2,0}}}. \qquad (6)$$

The expression $F(\cos\theta) \equiv (\alpha_0-\cos\theta)^2 d\sigma/d\Omega$, which is obviously analytical in the neighbourhood of α_0, can be expanded in a power series like $\sum_{n=0}^{\infty} a_n \cdot (\alpha_0-\cos\theta)^n$, having a domain of analyticity determined by the nearest branch point. This can be found on considering the s, t boundary curves of the spectral functions [6]).

One ascertains by direct inspection that the only contribution to the s, t curves is given by the following diagram:

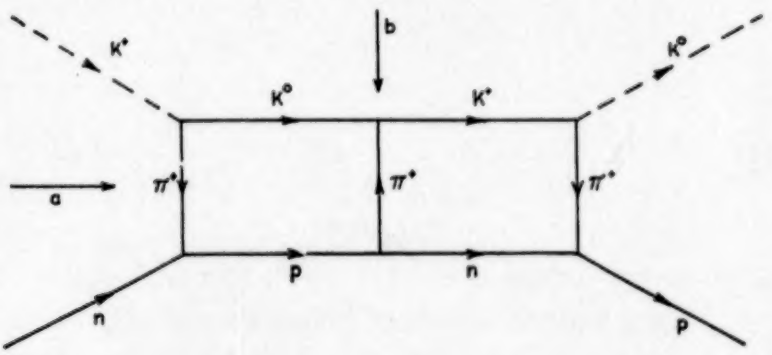

(7)

As regard the channels a) and b), this diagram contains the multiparticle intermediate state with lowest mass and enables us to work out the only boundary curve; its equation is

$$(t^2+9m_\pi{}^4)q^2-2tm_\pi{}^2(2m_\pi{}^2+5q^2) = 0, \qquad (8)$$

† We note that if only the Born term in the scattering amplitude is considered, it is possible to explain the "forward peak" reported in some recent papers on experimental work performed at energies between 120 and 130 MeV [10]). At this energy the position of the branch point is such that most of the experimental data ($\approx 80\%$) fall into the domain of analyticity of $\sum_{n=0}^{\infty} a^n(\alpha_0-\cos\theta)^n$. Nevertheless it seems that at energies between 150 and 250 MeV [11]), there may be evidence for a "backward peak." But this cannot be explained with the aid of the Born term alone, which always implies only a "forward peak". It seems that such a backward peak would be caused by a contribution from the cut opposite to that of the pole. Indeed the fraction of the experimental data falling into the domain of analyticity turns out to be less than half. It would be interesting to see whether there is a possible connection between the cut contribution and that fraction of the experimental data.

being asymptotic to the limiting values

$$t = 9m_\pi^2, \qquad s = (m_K+m_N)^2$$
$$q^2 = [s^2-2s(m_N^2+m_K^2)+(m_N^2-m_K^2)^2]\frac{1}{4s}. \tag{9}$$

The right cut in the $\cos\theta$-plane lies at the value $\cos\theta = 1+t/2q^2$, where t is fixed by the initial total energy (K+N state) and by its belonging to the boundary curve given above. The value of q for which all the experimental data fall into the domain of analyticity is easily shown to be $q \approx 1.485\ m_\pi$. With this value † of q, the pole lies at $\cos\theta \approx 1.22$ (K^+ lab. energy $\approx$ 70 MeV). Then the equation

$$a_0 = F(\alpha_0) = \frac{f_R^2 g_R^2 m_K^2(1-\alpha_0)}{16\pi^2 q^2(p_{2,0}+q_{2,0})\sqrt{2q^2+m_N^2+m_K^2+2p_{2,0}q_{2,0}}} \tag{10}$$

gives us the best estimate of f_R in terms of g_R.

The problem of determining the order of the polynomial that gives the best fit to the experimental data (and by which one can effectively extrapolate to $F(\alpha_0)$) has recently been considered by Taylor [7]). At the energy quoted above, polynomials up to second order seem to be sufficient.

To carry out an explicit calculation one needs rather accurate experimental data, not available at present. Poor statistics may in fact give rise to wrong conclusions as regards the numerical evaluation of f_R as well as the existence or non-existence of the π-pole [8]).

3. The Models of Pais and of Gell-Mann

We point out that the Gell-Mann model implies that p(K) is even (K^+-K^0 form an isodoublet), and that this excludes the presence of a forward pole. In fact, with the assumptions of parity conservation, invariance under spatial rotations and the pseudoscalar nature of the π meson, an even p(K) implies that no vertex exists like

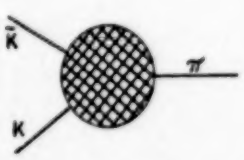

whether elementary or not. On the contrary, a hyperon backward pole exists in both the Pais and Gell-Mann theories, although a difference may come out in the value of the residue. This difference, at least in principle, could be used as

† Had we made calculations using only the asymptotes instead of the Mandelstam curves, the result would have been in $q \approx 1.3\,\mu$ and $\alpha_0 \approx 1.30$.

a test to decide between the two theories †. However, we expect that the existence of a close backward cut, at energies high enough to allow an extrapolation (between 1 and 2 GeV), will give difficulties in recognizing the pole, even if good experimental data becomes available.

On the other hand, it may be pointed out that other possibilities can be considered in order to choose between the Pais and the Gell-Mann theories. One of these is based on a comparison, at various energies, between the angular distributions of the given reaction and the elastic scattering $K^+ + n \to K^+ + n$. Similar shapes of these distributions would agree with the Gell-Mann and disagree with the Pais model (in fact, according to the Gell-Mann scheme, the forward pole is missing in both reactions and there is a first forward cut at $t = (2m_\pi)^2$). On the other hand, if the distributions were of different shapes, there would be agreement with Pais and disagreement with Gell-Mann (in fact, according to Pais the forward pole is missing only in the elastic scattering and there is a first cut at $t = (2m_\pi)^2$). Moreover, had the angular distributions similar shapes and were the existence of a forward pole recognizable in the charge-exchange process, neither the Pais nor the Gell-Mann theory would turn out to agree with experiment.

Finally, we point out that, independently of the Pais scheme or any other particular scheme, the existence of a vertex like (11) implies that (1) $p(K)$ must be odd, as Taylor already noticed, (2) no trilinear K-baryon interaction conserving I and I_3 can be constructed.

Point (2) requires some comment. As $p(K)$ is odd there are two possibilities:

a) K^+, (K^-) and K^0, $(\overline{K}^0)$ are isoscalars. This case, already considered by Pais, allows one immediately to conclude that I and I_3 cannot be conserved. Then we have here something more than point (2).

b) K particles are grouped in isodoublets as follows:

$$\begin{pmatrix} K^+ \\ K^- \end{pmatrix}, \qquad \begin{pmatrix} \overline{K}^0 \\ K^0 \end{pmatrix}.$$

This possibility allows us to obtain less restrictive conclusions than point a). One can, in fact, verify by direct inspection that charge conservation is incompatible with the I and I_3 invariance of a trilinear interaction and so justify point (2). This, however, does not exclude the possibility of a non-trilinear model which has the required symmetries. Moreover, with our group-

† On the basis of the Gell-Mann scheme, the calculation of the residue gives a result proportional to $g^2_{K\pi Y}$. On the other hand, in the Pais theory the result is proportional to GF_1, where G is a quantity depending on f_R and such as $\lim_{f_R \to 0} G(f_R) = 0$. Furthermore, whereas F_1 is essentially of the same order of magnitude as $g_{K\pi Y}$, G might be different. This is due to the fact that, since the Pais quantum numbers S_1 and S_2 take different values in the initial and final states, one $\overline{K}K\pi$ vertex is necessary, at least, in the diagrams connecting them; thus, no second order graph exists.

ing of K particles we have not modified the Gell-Mann-Nishijima characterization of each particle and the relation $I_3 = Q - \frac{1}{2}(S+N)$ must hold. This fact assures us that Q, S, N conservation guarantees the conservation of I_3 and consequently that a non-trilinear model conserving I_3, Q, S, N should exist. However, whether a model can be constructed which also conserves I is an open question. The above statements are based on the following usual assumptions beside the ones yet considered:

(i) $\mathrm{N} = \begin{pmatrix} \mathrm{p} \\ \mathrm{n} \end{pmatrix}$ is an isospinor,

(ii) $\boldsymbol{\pi} = \begin{pmatrix} \pi_1 \\ \pi_2 \\ \pi_3 \end{pmatrix}$ is an isopseudovector,

(iii) π-baryon interactions are charge independent.

All these considerations stress the importance of good experimental data about the $\mathrm{K}^+ + \mathrm{n} \to \mathrm{K}^0 + \mathrm{p}$ or any other suitable reaction.

We wish to express our thanks to Dr. A. Scotti and Professor F. Duimio for their friendly advice and criticism and to Professor L. M. Brown and Professor A. J. Hertz for having read the manuscript.

References

1) A. Pais, Phys. Rev. **112** (1958) 624
2) G. F. Chew, Phys. Rev. **112** (1958) 1380
3) S. Mandelstam, Phys. Rev. **112** (1958) 1344
4) G. F. Chew, Ann. Rev. Nucl. Sci. **9** (1959) **29**; UCRL 9289 -June 1960
5) J. G. Taylor, Nuclear Physics **9** (1959) 357
6) S. Mandelstam, Phys. Rev. **115** (1959) 1752
7) J. G. Taylor, Phys. Rev. **116** (1959) 768
8) G. Feldman and T. Fulton, Phys. Rev. Lett. **3** (1959) 64
9) A. Pais, Phys. Rev. **110** (1958) 574
10) O. R. Price, D. H. Stork and H. K. Ticho, preprint
11) D. Fournet Davis, N. Kwak and M. F. Kaplon, Phys. Rev. **117** (1960) 846

2.G

Nuclear Physics **27** (1961) 58—65; © *North-Holland Publishing Co., Amsterdam*

Not to be reproduced by photoprint or microfilm without written permission from the publisher

ALPHA-DEUTERON MODEL OF THE Li^6 NUCLEUS AND THE $Be^9(Li^6, \alpha)B^{11}$ REACTION

M. L. RUSTGI †

Division of Pure Physics, National Research Council, Ottawa, Canada

Received 4 April 1961

Abstract: The angular distributions of the particles emitted in (Li^6, α) and (Li^6, d) reactions are calculated under the assumption that they are stripping processes. An alpha-deuteron model of the Li^6 nucleus is used. The Coulomb effects of the interacting particles and the nuclear interaction between the outgoing particles are neglected. The derived formulae are compared with the experimental data of Leigh and Blair on the differential cross sections of the Be^9 (Li^6, α) B^{11} reaction. The general shapes of the calculated angular distributions are similar to those of the experimental data, but there is a lack of agreement between theory and experiment at large angles.

1. Introduction

It is now well known that the characteristic forward component in the angular distribution of the (d, p) and (d, n) reactions can be interpreted as due to a stripping process [1]. The angular distributions are then found to be directly related to the orbital angular momentum of the captured particle and the effective radius of capture. The backward peaking observed in some of the deuteron stripping reactions can be explained reasonably well in terms of the heavy-particle stripping process, as developed by Owen and Madansky [2]. The recent experimental work of J. J. Leigh and J. M. Blair [3] on the Be^9 (Li^6, α) B^{11} reaction for bombarding energies from 2.0 to 4.0 MeV also shows a forward and backward peaking and also an asymmetry about 90° in the angular distribution of the α particles. This leads them to suggest that perhaps the Be^9 nucleus strips the deuteron from the incoming Li^6 nucleus to leave an outgoing α-particle in a manner analogous to the (d, p) and (d, n) stripping reactions. Compound nucleus formation does not seem to be possible because the distance of closest approach turns out to be several times the nuclear dimension for the energies under consideration.

Recently several authors have made a theoretical study of reactions in which two or three nucleons are stripped from an incident α-particle. Their work can account reasonably well for the forward peaking in (α, p), (α, d) and (α, He^3) reactions ††.

† Present address: Physics Department, Banaras Hindu University, Varanasi (U.P.), India

†† Experimental work on (α, p) (α, d) and (He^3, p) reactions is given in ref. [4]).

In the present work, formulae are worked out for the differential cross section for the stripping of a deuteron or an alpha particle from an incident Li^6 nucleus. An alpha-deuteron model is assumed for the projectile [5]). The treatment is similar to that of El-Nadi [4]), who uses the first Born approximation together with the surface stripping assumption of Bhatia *et al* [1]). Since the Coulomb effects of the interacting particles and the nuclear interaction of the outgoing particles are neglected, the derived formula should be applicable when the energies of the incident particles are above the Coulomb barrier.

In sect. 2 a formula is derived for the differential cross section for the (Li^6, α) reaction. Sect. 3 contains a similar derivation for the (Li^6, d) reaction. In Sect. 4 a comparison is made of the derived formulae with the experimental data of Leigh and Blair [3]).

2. The (Li^6, α) Reaction

In the stripping theory of the (d, p) reaction, Bhatia *et al.* [1]) assume that the proton in the deuteron never comes into contact with the target nucleus, so that the neutron in the deuteron strikes the nucleus and is absorbed while the proton continues its initial motion undisturbed and emerges from the system. A similar assumption is made in the treatment presented below. Only the neutron and proton of the deuteron in the model used for the Li^6 nucleus are assumed to interact with the target nucleus while the α-particle is assumed to travel undisturbed.

The Born approximation for the differential cross section for the (Li^6, α) reaction is then given by

$$\sigma(\theta) = \frac{\mu_0 \mu_\alpha}{(2\pi\hbar^2)^2} \frac{k_\alpha}{k_0} \Sigma |I|^2, \tag{1}$$

where

$$I = \int \chi_f^*(\mathbf{r}_p, \mathbf{r}_n, \boldsymbol{\xi}) \exp[-i\mathbf{k}_\alpha \cdot \mathbf{r}'_\alpha] \chi_\alpha^*(\mathbf{r}_\alpha) [V(|\mathbf{r}_p - \boldsymbol{\xi}|) + V(|\mathbf{r}_n - \boldsymbol{\xi}|)] \cdot \chi_i(\boldsymbol{\xi}) \exp[i\mathbf{K}_0 \cdot \mathbf{r}_0] \chi_0(\mathbf{r}_0) d\mathbf{r}_p d\mathbf{r}_n d\mathbf{r}_\alpha d\boldsymbol{\xi}. \tag{2}$$

In eq. (1), we have

$$\mu_0 = \text{reduced mass of the } Li^6 \text{ nucleus} = \frac{M_0 M_i}{M_0 + M_i},$$

$$\mu_\alpha = \text{reduced mass of the } \alpha \text{ particle} = \frac{M_\alpha M_f}{M_\alpha + M_f},$$

where M_0, M_α, M_i and M_f are the masses of the Li^6 nucleus, α particle, initial nucleus and the final nucleus respectively; $K_0 = (\mu_0 V/\hbar)$ and $K_\alpha = (\mu_\alpha V_\alpha/\hbar)$, where V is the velocity of the incoming Li^6 nucleus in the centre-of-mass system and V_α is the velocity of the outgoing α particle relative to the centre-of-mass of the final nucleus; the summation sign implies the sum over final

states and average over the initial states. In eq. (2)

$$\mathbf{r}'_\alpha = \mathbf{r}_\alpha - \left[\frac{M_p+M_n}{M_t}\right]\mathbf{R},$$

where $\mathbf{R} = \frac{1}{2}(\mathbf{r}_p+\mathbf{r}_n)$; also χ_t, χ_α, χ_1, χ_0 are internal wave functions for the final nucleus, α particle, initial target nucleus and the incident Li^6 nucleus. It is assumed that the capture process of the neutron and proton from the Li^6 nucleus takes place close to the surface of the initial nucleus, or more precisely in some narrow shell just outside the surface, where one can roughly suppose the attraction of the nucleus for the proton and the neutron to outweigh that for the α particle. The other process in which the attraction of the nucleus for the alpha particle outweighs that for the neutron and the proton will be discussed in the next section. The mean radius of this shell is denoted by R_0 (usually referred to as the interaction radius). Replacing $\mathbf{r}_p = (r_p, \theta_p, \varphi_p)$ and $\mathbf{r}_n = (r_n, \theta_n, \varphi_n)$ by $\mathbf{R}_p(R_0, \theta_p, \varphi_p)$ and $\mathbf{R}_n(R_0, \theta_n, \varphi_n)$, respectively, in eq. (2) one obtains

$$I = \int \exp[-i\mathbf{K}_\alpha \cdot \mathbf{r}'_\alpha]\chi_\alpha^*(\mathbf{r}_\alpha)\chi_0(\mathbf{r}_0)\exp[i\mathbf{K}_0 \cdot \tfrac{1}{6}(\mathbf{r}_p+\mathbf{r}_n+4\mathbf{r}_\alpha)]d\mathbf{r}_p d\mathbf{r}_n d\mathbf{r}_\alpha \left\{\int \chi_t^*(\mathbf{R}_p, \mathbf{R}_n, \boldsymbol{\xi})[V(|\mathbf{r}_p-\boldsymbol{\xi}|)+V(\mathbf{r}_n-\boldsymbol{\xi})]\chi_1(\boldsymbol{\xi})d\boldsymbol{\xi}\right\}. \quad (3)$$

As in El-Nadi's paper [4]), the expression in the curly brackets in (3) can be expanded in states of given orbital angular momenta of the captured neutron and proton, i.e. in the form

$$\{\ \} = \sum_{LM} A_L I_{l(p)l(n)}(R_0) Y_L^{M*}(\Omega), \quad (4)$$

where Ω denotes the angular coordinates of the centre-of-mass of the captured neutron and proton,

$$Y_L^M(\Omega) = \sum_{m_p m_n} \begin{pmatrix} l_p & l_n & L \\ m_p & m_n & M \end{pmatrix} Y_{l_p}^{m_p}(\theta_p, \varphi_p) Y_{l_n}^{m_n}(\theta_n, \varphi_n), \quad (5)$$

and the two bracket symbol denotes the Wigner-vector-additon coefficients.

According to Kopaleishvili *et al.* [5]) the radial wave function for the Li^6 nucleus in the alpha-deuteron model may be written as

$$\chi_0(r_0) = N(\mathrm{Li}) \exp\left\{-\alpha^2 s^2 - \beta^2 t^2 - \gamma^2 \sum_{i>j=1}^{4} r_{ij}^2\right\}, \quad (6)$$

where $\mathbf{t}$ is the radius vector joining the centres of the alpha particle and the deuteron, $\mathbf{s}$ denotes the relative distance between the neutron and the proton of the deuteron in the Li^6 nucleus and r_{ij} is the distance between the i^{th} nucleon and the j^{th} nucleon in the alpha particle. The values of α, β and γ are given [5]) by $\alpha^2 = 0.075$ fm^{-2}; $\beta^2 = 0.0158$ fm^{-2} and $\gamma^2 = 0.158$ fm^{-2}. In

the notation of fig. 1(a) one can rewrite the wave function in the form

$$\chi_0(r_0) = N(\mathrm{Li})\exp\{-\alpha^2 s^2-\beta^2 t^2-2\gamma^2(u^2+v^2+2\rho^2)\}, \tag{7}$$

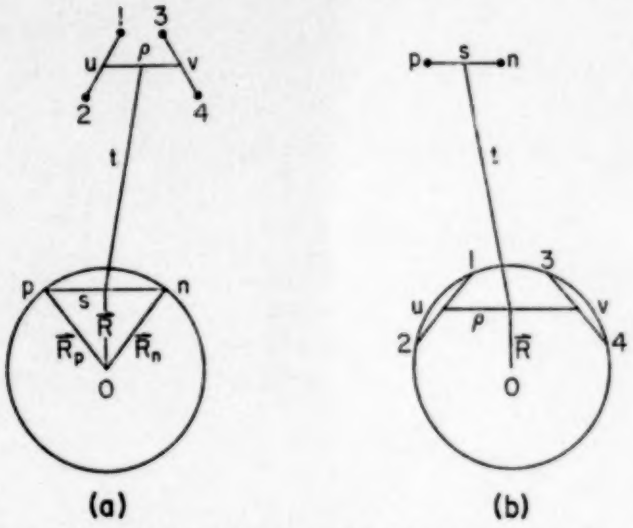

Fig. 1. The stripping of Li^6 nucleus by target nuclei. Fig. 1(a) shows the two-nucleon stripping in which the neutron and the proton of the deuteron in the Li^6 nucleus are captured and the alpha particle goes out. In fig. 1(b) the alpha particle is captured and the deuteron goes out.

where the normalization constant $N^2(\mathrm{Li}) = (8192\sqrt{2})\alpha^3\beta^3\gamma^9/\pi^{\frac{9}{2}}$. Similarly the wave function for the alpha particle, which is also assumed to be Gaussian [6]), may be written as

$$\chi_\alpha(r_\alpha) = N_\alpha \exp[-2\gamma^2(u^2+v^2+2\rho^2)], \tag{8}$$

and the normalization constant $N_\alpha^2 = (1024\sqrt{2}/\pi^{\frac{3}{2}})\gamma^9$.

The total exponent of the matrix element (eq. 2) is given by

$$X = -i\mathbf{K}_\alpha\cdot\mathbf{r}'_\alpha+i\mathbf{K}_0\cdot\tfrac{1}{6}(\mathbf{R}_p+\mathbf{R}_n+4\mathbf{r}_\alpha) = i\mathbf{Q}\cdot\mathbf{R}-i\boldsymbol{\kappa}\cdot\mathbf{t}, \tag{9}$$

where

$$\mathbf{Q} = \mathbf{K}_0-\frac{M_1}{M_t}\mathbf{K}_\alpha, \tag{10}$$

$$\boldsymbol{\kappa} = \mathbf{K}_\alpha-(\tfrac{2}{3})\mathbf{K}_0. \tag{11}$$

Substituting eqs. (7), (8) and (9) in the integral I, one gets

$$I = N(\mathrm{Li})N(\alpha)\sum_{LM}A_L I_{l(p)l(n)}(R_0)\int \mathrm{d}\mathbf{R}\,\mathrm{d}\boldsymbol{\rho}\,\mathrm{d}\mathbf{u}\,\mathrm{d}\mathbf{v}\,\mathrm{d}\mathbf{s}\,\mathrm{d}\mathbf{t}\,Y_L^{M*}(\Omega)$$
$$\cdot\exp[i\mathbf{Q}\cdot\mathbf{R}-i\boldsymbol{\kappa}\cdot\mathbf{t}-\alpha^2 s^2-\beta^2 t^2-4\gamma^2(u^2+v^2+2\rho^2)]. \tag{12}$$

The integration over Ω can be easily performed by expanding $\exp[i\mathbf{Q}\cdot\mathbf{R}]$ as a sum in spherical harmonics and making use of their orthogonal properties and of the surface stripping assumption

$$\int e^{i\mathbf{Q}\cdot\mathbf{R}}Y_L^{M*}(\Omega)\mathrm{d}\Omega = i^L[4\pi(2L+1)]^{\frac{1}{2}}j_L(QR_0)\delta_{M,0}. \tag{13}$$

The other integrals have the standard forms

$$\int_0^\infty e^{i\mathbf{b}\cdot\boldsymbol{\rho}} e^{-a^2\rho^2} d\boldsymbol{\rho} = \frac{\pi^{\frac{3}{2}}}{a^3} e^{-b^2/4a^2}, \tag{14}$$

$$\int_0^\infty e^{-Bs^2} d\mathbf{s} = \frac{\pi^{\frac{3}{2}}}{B^{\frac{3}{2}}}. \tag{15}$$

One thus obtains

$$I = N_{(\alpha)} N_{(\mathrm{Li})} \frac{\pi^8 f_{l(\mathrm{p})l(\mathrm{n})}(R_0)}{512\sqrt{2}\,\beta^3\alpha^3\gamma^9} \exp[-\kappa^2/4\beta^2] \sum_L A_L i^L [(2L+1)]^{\frac{1}{2}} j_L(QR_0). \tag{16}$$

Squaring eq. (16), substituting in eq. (1) and summing over the final states and averaging over the initial states, one gets for the differential cross section for the (Li^6, α) reaction

$$d\sigma = T^2 \frac{\mu_0\mu_\alpha}{(2\pi\hbar^2)^2} \frac{k_\alpha}{k_0} \frac{(2J_f+1)}{3(2J_1+1)} \exp[-\kappa^2/2\beta^2] \sum_L A_L{}^2 J_L{}^2(QR_0), \tag{17}$$

where

$$T = \frac{4\sqrt{2}\,\pi^2}{\alpha^{\frac{3}{2}}\beta^{\frac{3}{2}}} f_{l(\mathrm{p})l(\mathrm{n})}(R_0). \tag{18}$$

3. The (Li^6, d) Reaction

In the (Li^6, d) reaction, it is the α-particle from the Li^6 nucleus which is captured by the target nucleus while the deuteron travels undisturbed. In this case the matrix element I may be written as

$$\begin{aligned} I = \int d\mathbf{r}_1 d\mathbf{r}_2 d\mathbf{r}_3 d\mathbf{r}_4 d\mathbf{r}_d d\boldsymbol{\xi} \\ \chi^*(r_d)\exp[-i\mathbf{K}_d\cdot\mathbf{r}'_d]\chi_f{}^*(\boldsymbol{\xi},\mathbf{r}_1,\mathbf{r}_2,\mathbf{r}_3,\mathbf{r}_4)[V_1+V_2+V_3+V_4] \\ \exp[i\mathbf{K}_0\cdot\mathbf{r}_0]\chi_0(\mathbf{r}_0)\chi_1(\boldsymbol{\xi}) \end{aligned} \tag{19}$$

where

$$\mathbf{r}'_d = \mathbf{r}_d - \frac{M_1+M_2+M_3+M_4}{M_f}\mathbf{R}$$

and $\mathbf{R}$ is the radius vector defining the centre-of-mass of the four captured nucleons constituting the alpha particle in the Li^6 nucleus (fig. 1(b)). The other symbols have their usual meaning. The wave function of the deuteron will be approximated by the Gaussian form. The total exponent in the matrix element may be written as

$$\begin{aligned} Y &= -i\mathbf{K}_d\cdot\mathbf{r}'_d + i\mathbf{K}_0\cdot\tfrac{1}{6}(\mathbf{R}_1+\mathbf{R}_2+\mathbf{R}_3+\mathbf{R}_4+2\mathbf{r}_d), \\ &= i\mathbf{Q}\cdot\mathbf{R} - i\boldsymbol{\kappa}\cdot\mathbf{t}, \end{aligned} \tag{20}$$

where

$$\mathbf{Q} = \mathbf{K}_0 - \frac{M_1}{M_t}\mathbf{K}_d, \tag{21}$$

$$\boldsymbol{\kappa} = \mathbf{K}_d - \tfrac{1}{3}\mathbf{K}_0. \tag{22}$$

Here $\mathbf{R}$ is the radius vector of the centre-of-mass of the captured nucleons.

Assuming that the reaction takes place at the surface of the nucleus; as in the preceding section, one can make the following expansion:

$$\int \chi_t^*(\xi, \mathbf{R}_1, \mathbf{R}_2, \mathbf{R}_3, \mathbf{R}_4)[V_1+V_2+V_3+V_4]\chi_t(\xi)\mathrm{d}\xi = \sum_{LM} A_L f_{l_1 l_2 l_3 l_4}(R_0) Y_L^{M*}(\Omega), \tag{23}$$

where the angular coordinates of $\mathbf{R}$ are denoted by Ω.

Performing the other integrations as before one gets for the matrix element

$$I = N_{Li}N_d \frac{\pi^8 f_{l_1 l_2 l_3 l_4}(R_0) \exp\left[-\frac{\kappa^2}{4\beta^2}\right]}{\beta^3\gamma^9\alpha^3 64\sqrt{2}} \sum_L A_L (i)^L [2L+1]^{\frac{1}{2}} j_L(QR_0). \tag{24}$$

Squaring eq. (24), substituting in eq. (1) and summing over the final states and averaging over the initial states, one gets for the differential cross section for the (Li^6, d) reaction

$$\mathrm{d}\sigma = T^2 \frac{\mu_0\mu_d}{(2\pi\hbar^2)^2} \frac{k_d}{k_0} \frac{1}{3} \frac{(2J_t+1)}{(2J_1+1)} \exp[-\kappa^2/2\beta^2] \sum A_L^2 j_L^2(QR_0), \tag{25}$$

$$T = \frac{2\pi^{\frac{1}{2}} f_{l_1 l_2 l_3 l_4}(R_0)}{\beta^{\frac{3}{2}}\gamma^{\frac{9}{2}}},$$

where $\boldsymbol{\kappa}$ and $\mathbf{Q}$ are defined by eqs. (21) and (22).

It is thus seen that for the (Li^6, α) and (Li^6, d) reactions, the cross-section has the general form

$$\mathrm{d}\sigma \approx \exp(-\kappa^2/2\beta^2) \sum_L A_L^2 j_L^2(QR_0). \tag{26}$$

4. Discussion

In this section the formulae obtained in sect. 2 are compared with the experimental data of Leigh and Blair [3]). The allowed values of L for the $\frac{3}{2}^-$ ground state and $\frac{1}{2}^-$ first excited state of B^{11} are $L = 0$ or 2 (ref. [7])). In fitting experimental data with the formula (17) the following ratios of the coefficients were obtained:

ground state alphas for Li^6 energy (lab. system) of 3.5 MeV:

$$\frac{A_2}{A_0} = 10, \qquad R_0 = 6.0 \text{ fm};$$

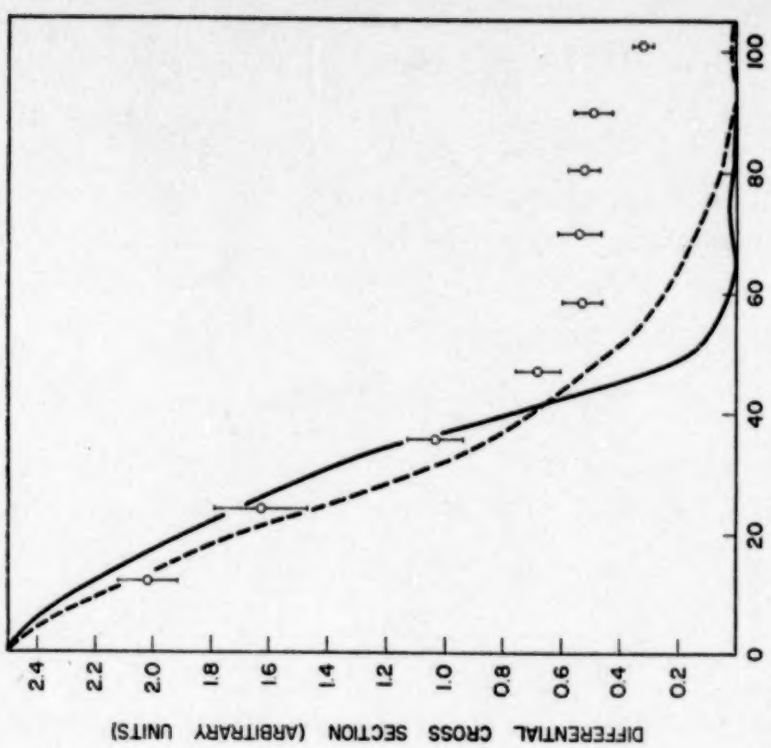

Fig. 3. Angular distribution of alpha particles for Li^6 energy (lab. system) of 3.5 MeV leading to the first excited state of B^{11}. The experimental points are those of Leigh and Blair [3]. The solid line represents the theoretical formula (26), with $A_2/A_0 = 1.73$ and $R_0 = 6.0$ fm. The broken line represents the same formula with $A_2/A_0 = 2.58$ and $R_0 = 5.12$ fm.

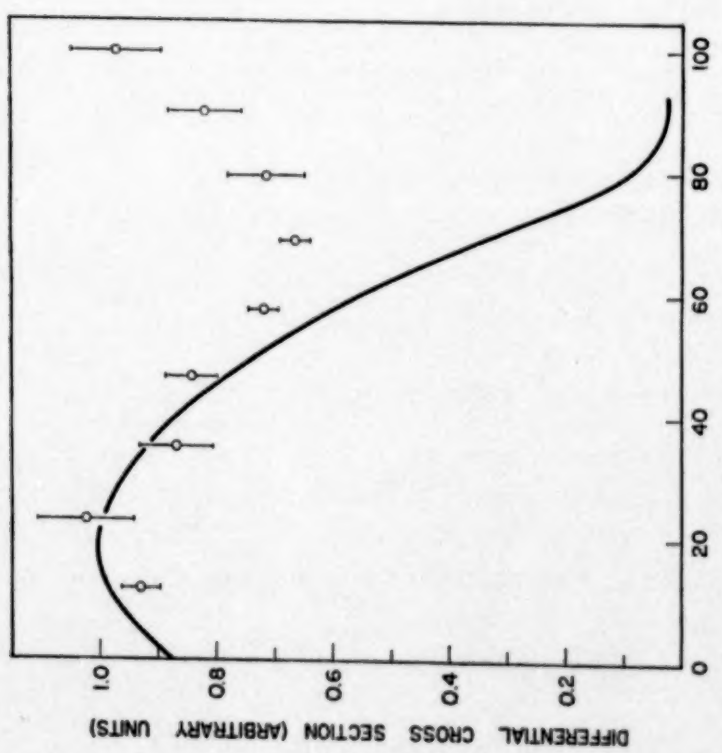

Fig. 2. Angular distribution of alpha particles for Li^6 energy (lab. system) of 3.5 MeV leading to the ground state of B^{11}. The experimental points are those of Leigh and Blair [3]. The solid line represents the theoretical formula (26), with $A_2/A_0 = 10$ and $R_0 = 6.0$ fm.

first excited state alphas for Li^6 energy (lab. system) of 3.5 MeV:

$$\frac{A_2}{A_0} = 2.58, \qquad R_0 = 5.12 \text{ fm};$$

$$\frac{A_2}{A_0} = 1.73, \qquad R_0 = 6.0 \text{ fm}.$$

A comparison of figs. 2 and 3 shows that a general agreement exists between the derived formulas and the experimental results of Leigh and Blair in the forward direction. Unfortunately no experimental data are available at present on the (Li^6, d) reaction. However, Leigh and Blair [8]) plan to do such experiments in the near future. It will be interesting to see whether the simple formula derived above fits the experimental observations.

The author is most grateful to the National Research Council for providing the facilities to carry out this work, and to Mrs. M. Helfenstein for doing the numerical work.

References

1) S. T. Butler, Proc. Roy. Soc. **208** (1951) 559;
A. B. Bhatia, K. Huang, R. Huby and H. C. Newns, Phil. Mag. **43** (1952) 485;
R. Huby, Proc. Roy. Soc. **215** (1952) 385;
F. L. Friedman and W. Tobocman, Phys. Rev. **92** (1953) 93;
W. Tobocman, Phys. Rev. **94** (1954) 1655;
R. G. Thomas, Phys. Rev. **100** (1955) 25;
S. T. Butler and O. Hittmair, Nuclear stripping reactions (John Wiley and Sons, Inc. New York, 1957);
A. G. Sitenko, Uspekhi Fiz. Nauk **67** (1959) 377 (translation: Soviet Phys. — Uspekhi **67** (1959) 195)
2) L. Madansky and G. E. Owen, Phys. Rev. **99** (1955) 1608;
G. E. Owen and L. Madansky, Phys. Rev. **105** (1957) 1766
3) J. J. Leigh and J. M. Blair, Phys. Rev. **121** (1961) 246
4) M. El-Nadi, Phys. Rev. **119** (1960) 242;
H. C. Newns, Proc. Phys. Soc. **76** (1960) 489;
M. El-Nadi, Phys. Rev. **120** (1960) 1360;
M. L. Rustgi, Nuclear Physics **25** (1961) 169
5) T. I. Kopaleishvili *et al.*, JETP (USSR) **38** (1960) 1758 (translation: JETP (Soviet Physics) **11** (1960) 1268)
6) T. Muto and T. Sebe, Progr. Theoret. Phys. (Kyoto) **18** (1957) 621
7) F. Ajzenberg-Selove and T. Lauritsen, Nuclear Physics **11** (1959) 1
8) J. J. Leigh and J. M. Blair, private communication

1.D.2:
1.E.4:
3.A

Nuclear Physics **27** (1961) 66—74; © *North-Holland Publishing Co., Amsterdam*
Not to be reproduced by photoprint or microfilm without written permission from the publisher

THE RESONANT SCATTERING OF GAMMA RAYS IN ^{177}Hf

W. D. HAMILTON † and B. S. SOOD ††
Department of Physics, Birmingham University

Received 17 April 1961

Abstract: Matched hafnium oxide and tantalum carbide scatterers were used to determine the intensities of resonant and fluorescent scattered γ-rays from the 113 keV and 321 keV levels in ^{177}Hf; the source of radiation was ^{177}Lu in the form of lutetium oxide. The resonant scattering condition was provided by the thermal broadening of the level widths, and the resonant fluorescent cross sections were found relative to the known Rayleigh scattering cross sections. The partial mean-lives for the γ-transitions have the values τ (113 keV; E2) $= 1.5 \pm 0.5$ nsec and τ (321 keV; E1) $= 17 \pm 5$ nsec.

When compared to the single particle estimates, these results indicate an enhancement factor of almost 330 for the 113 keV transition, but a hindering of 321 keV transition by a factor greater than 10^6. The results, in general, are consistent with previous investigations and may be interpreted on the basis of the Nilsson model.

1. Introduction

Recently in a survey of the intrinsic states of odd-A nuclei which have ellipsoidal shape, Mottelson and Nilsson [1]) have presented the accumulated evidence to show that the ^{177}Hf nucleus displays the collective rotational features which are characteristic of nuclei in the region $150 < A < 190$. These features have been sucessfully accounted for by considering the nucleons to exist in an axially symmetric but non-spherical potential, and by assigning an independent-particle motion to the last odd nucleon. The intrinsic configuration determines the spin and parity of the levels while the ellipsoidal nuclear shape and the corresponding charge distribution are related to the nuclear deformation parameter which in turn determines the strength of the quadrupole moment and the associated E2 transition probability.

The group of levels in each rotational band have the same parity, and successive levels differ in spin by one unit; the spin increases with level energy. The existence of a large quadrupole moment greatly favours E2 transitions between these levels and leds to a large E2 admixture with the M1 radiation which, from the single particle selection rules, might be expected to be the most probable transition.

Nuclei possessing rotational features are also typified by the existence of

† Present address: Physics Institute, Uppsala University, Sweden
†† Present address: Physics Department, Panjab University, India

low energy El transitions. These cannot be accounted for by the spherical shell model since the necessary spin and parity change will require inter-shell transitions and these greatly exceed the energy change which is of the same order as that between orbitals within the same shell. However, on the unified model transitions may occur between the levels of overlapping bands which have different parity. The transition probability will be determined by the selection rules associated with the intrinsic structure, (c.f. table I of ref. [1])), and it is usual for such El transitions to be greatly hindered compared with the single particle estimate of the spherical shell model.

Thus, in a strongly deformed nucleus the enhanced E2 and hindered E1 transitions might be expected to have comparable transition probabilities which are sufficiently large to allow the partial meanlives of the corresponding levels to be measured by the nuclear resonant scattering technique.

2. Level Structure of ^{177}Hf

The β-decay of ^{177}Lu as shown in fig. 1 was investigated by Marmier and Boehm [2]) and was later confimed by Ofer [3]), who examined the level structure from the stand point of the unified model. Ofer's results, for the most part, have been confirmed by the more recent angular correlation measurements made by Steffen [4]) and Klema [5]).

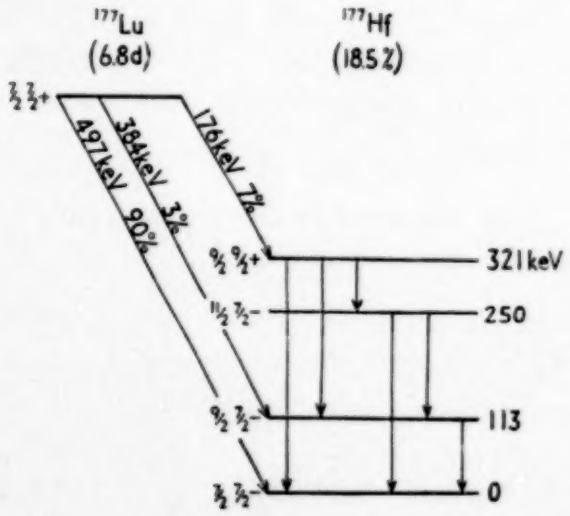

Fig. 1. The beta decay of ^{177}Lu as proposed by Ofer [3]).

The ground-state spin has been established as $\frac{7}{2}$ from atomic spectrum measurements [6]) and is in agreement with the calculations of Mottelson and Nilsson which also indicate that it has negative parity. The excited levels associated with the ground-state rotational band occur at 113 keV ($I = \frac{9}{2}^-$) and 250 keV ($I = \frac{11}{2}^-$). The angular correlation of the 208 keV—113 keV

γ-cascade yielded $\delta^2 = 25$ for the E2 : M1 ratio of the 113 keV transition while the results of the 72 keV—250 keV γ-cascade suggested that the 250 keV ground-state transition is pure E2.

The spin and parity of the 321 keV level has been determined as $\frac{9}{2}^+$ from the anisotropy of the 72 keV—250 keV γ-cascade [3]) and from the K electron conversion coefficient for the 72 keV transition. The level thus corresponds to a higher intrinsic excitation as predicted by the collective model.

The branching ratio for E1 transitions from the 321 keV level to rotational levels of the ground-state band is dependent solely on geometrical factors [7]), namely the Clebsch-Gordan coefficients. The theoretical branching ratio in order of increasing γ-ray energy is 1 : 250 : 4000, while the experimental ratio is 2 : 220 : 3 as found by Marmier and Boehm †. Chase and Wilets [8]) suggest that the large discrepancy arises because the E1 transitions are strongly forbidden according to the asymptotic quantum numbers. They have also calculated that the 321 keV transition is slower than the spherical independent-particle model transition by a factor probably less than 4×10^{-3}. Recently Klema has observed a 0.1 % M2 admixture in the 208 keV transition and this supports the strong E1 hindrance since M2 radiation is allowed by the selection rules given in table 1 of ref. [1]).

The mean-lives of the 133 keV and 250 keV levels have been determined from Coulomb excitation measurements [9, 10]) and are of the order 4×10^{-10} sec and 6×10^{-11} sec, respectively. Varapetian [11]) found that the mean-life of the 321 keV level was less than 6×10^{-10} sec. These values suggest that the E1 and E2 transition probabilities may be comparable and that the meanlives of the levels might be successfully determined from the resonant and fluorescent scattering cross-sections.

3. Experimental Conditions

The resonant scattering condition in the case of low energy transitions in heavy nuclei can be most conveniently provided by the thermal broadening of the emission and absorption lines. When only thermal broadening of the lines is present the differential resonant scattering cross section is given by [12])

$$\sigma(\theta)=3.6\times10^{-3}\,\frac{f(\theta)}{4\pi}\,\frac{I\Gamma_\gamma^{\,2}}{E_0^{\,3}\Gamma}\,g\left(\frac{A}{T}\right)^{\frac{1}{2}}\exp\left[-3\times10^{-9}\,\frac{A}{T}\left(\frac{32E_0}{A}\right)^2\right].$$

In this equation Γ_γ/Γ is the branching ratio for the ground-state decay, E_0 is the energy of the level which is resonantly excited, A is the atomic weight of the scattering isotope, I is its isotopic abundace, g is the ratio of the multiplicities of the ground to excited states, T is the mean effective temperature

† In order to compare these ratios the experimental results were corrected for internal conversion, from the tabulated coefficients by Rose, and the energy dependence of the E1 transition energy. The „reduced" transition intensities are then in the ratio 1 : 2.6 : 0.012.

of the source and scatterer in degrees Kelvin and $f(\theta)$ is the angular distribution function for the scattered radiation. E and Γ are in eV and $\sigma(\theta)$ is expressed in $cm^2 \cdot sr^{-1}$.

The dependence of $\sigma(\theta)$ on the mean effective temperature for the 113 keV and 321 keV transitions is shown in fig. 2. It is seen that the resonance effect for the 321 keV transition increases by the factor 35 on raising the source temperature from 20° C (room temperature) to 1000° C. The 113 keV transition

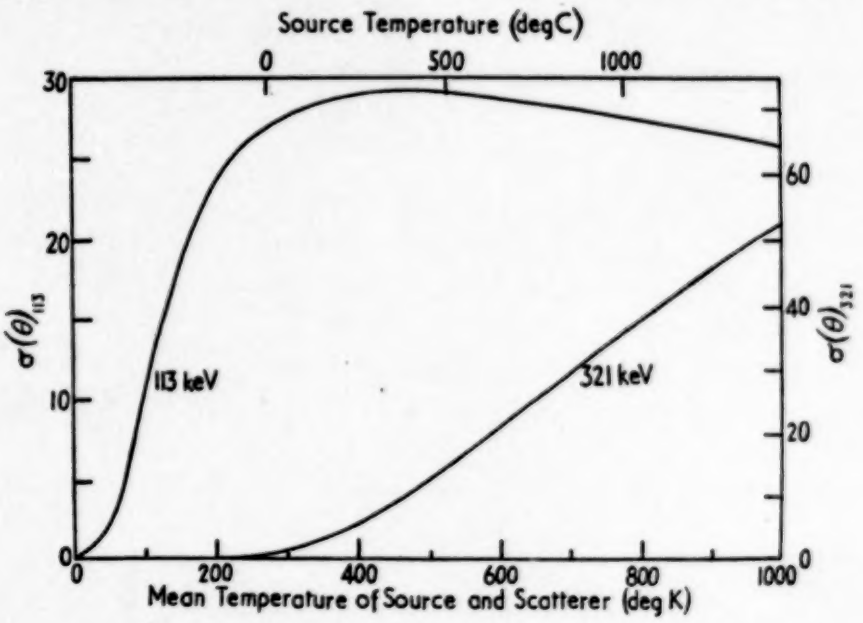

Fig. 2. The variation in the resonant scattering cross-section is shown as a function of the mean effective temperature of source and scatterer. The source and scatterer are assumed to have the same Debye temperature 240°, which is related to the effective and actual temperatures by the expression given by Lamb [14]). The cross-sections are expressed in arbitrary units; $\sigma(\theta)_{113}$ and $\sigma(\theta)_{321}$ refer to the 113 keV and 321 keV transitions, respectively.

shows no such marked change on increasing the temperature, but because of the lower transition energy the resonance cross section should be sufficiently large to allow the observation of the scattered radiation at room temperature. In each case it should be possible to observe the intensities of the resonant and Rayleigh scattered radiation when a matched comparison scatterer is used and to determine the resonant or fluorescent cross-section relative to the calculable Rayleigh cross section [13]).

4. Experimental Procedure

A comparatively large source strength of 400 mCur was required since only 1.3 % of the β—γ cascades from ^{177}Lu include the 321 keV ground state transition. The activity was produced by the neutron irradiation of 0.1 g of Lu_2O_3 at a pile factor of 12, i.e. 12×10^{11} neutrons $\cdot$ $cm^{-2} \cdot sec^{-1}$, for a period of one week in the BEPO reactor at Harwell.

The source was contained in a small quartz tube of internal diameter 3 mm. This was placed in a stainless steel tube. A chromal-alumel thermocouple was attached to the quartz tube to indicate the temperature when the steel tube was heated directly in the flame of a coal gas torch. The tube and torch were enclosed in a double walled asbestos-paper container to exclude direct air currents from the steel tube. This made it possible to hold temperature steady to within $\pm 10°$ C during the high temperature period, while the temperature for different periods was easily reproducible to within $\pm$ 30° C. The flow of air in the cavity wall of the asbestos container and the circulation of cold air around its outside kept the adjoining apparatus at room temperature.

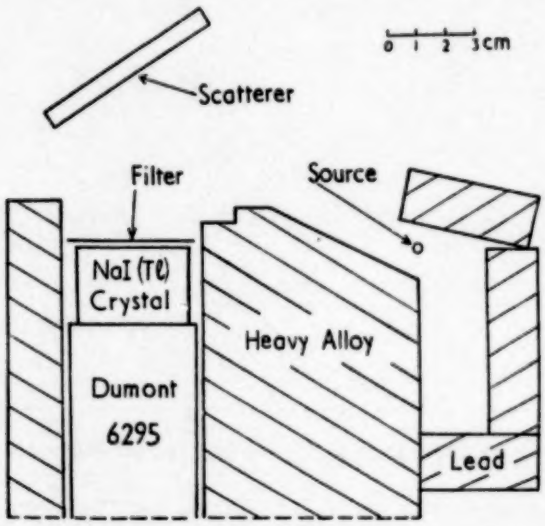

Fig. 3. The arrangement of source, scatterer and detector shown was used when recording the resonant scattering of the 113 keV transition for which the scattering angle θ was 120°.

Equivalent amounts of hafnium oxide and tantalum carbide were used to give identical Rayleigh scattering, The matched scatterers were made by compressing approximately 200 g of each powder to a pressure of 10^4 mm Hg to give thin brickettes. The brickettes measured 8 cm by 6.3 cm and were enclosed in celluloid containers which fitted into a light frame that enabled them to be exchanged rapidly and accurately replaced.

The scattered radiation was detected by a 2.5 cm thick by 3.7 cm diameter NaI(Tl) crystal mounted on a 6295 Dumont photomultiplier. The geometrical arrangement of source, scatterer and detector is illustrated in fig. 3. The source-scatterer and detector-scatterer separations were 11 cm and 6 cm, respectively, and the scattering angle was initially 110°. The 321 keV resonant and the 208 keV fluorescent radiation scattered from the 321 keV level was selected for detection by single channel pulse-height analysers set a 3 V wide channels, which covered at least the full width at half-height of the photo-

peaks. A 1 mm lead filter was placed in front of the crystal to reduce the detection of low energy photons and the associated build-up pulses.

The hafnium oxide and tantalum carbide scatterers were interchanged at 1 min intervals and the counting rates were recorded for a total period of 10 min for each scatterer when the source was at room temperature and at 950° C. Altogether 13 separate sets of results were taken and the counting rates were corrected for the contributions from the background and the non-elastic scattering.

The scattering angle was increased to 120° when recording the 113 keV radiation to discriminate against the intense Compton scattering of the 208 keV transition and the lead filter was replaced by a 0.5 mm copper foil which significantly reduced the low energy components of the scattered radiation. The scattered spectrum was recorded on a 100 channel pulse-height analyser and since the 113 keV elastic peak was masked by the Compton scattered peak of the 208 keV transition it was necessary to resolve the spectrum into its components. These were compared when the scatterers were alternatively hafnium oxide and tantalum carbide. The source remained at room temperature throughout the experiment.

The comparison of the spectra from both scatterers showed that they were matched to within the counting statistics.

5. Experimental Results

The graphical analysis of the scattered spectra in the 113 keV region indicated that a small resonant contribution to the elastic scattering occurred when tantalum carbide was replaced by hafnium oxide. It was estimated to be $\frac{1}{100}$ of the Rayleigh scattering. A statistical error of 35 % was set on this fraction, with a probable error of at least 30 % placed on the resonant cross-section and on all related values.

There was no significant contribution to the counting rate in the 3 V channel covering the 321 keV photo-peak, while in the channel positioned at 208 keV and increase of 250 counts/10 min was recorded when the source was hot. This value is the mean of 13 sets of results and the large statistical error of 30 % arises because of the smallness of the effect compared to the Rayleigh scattering. In comparing the number of fluorescent scattered 208 keV γ-rays with the number of Rayleigh scattered, a factor must be included to take account of the relative intensities of the 321 keV and 208 keV γ-rays incident on the scatterer. This was determined experimentally by direct observation of the source. After correcting for the relative efficiency of the counter for the two transitions the ratio of 208 keV : 321 keV γ-rays was determined as 60 : 1. This factor is smaller than the ratio 70 : 1 found by Marmier and Boehm; this is not un-

expected since the absorption by the source container would reduce the relative intensity of the lower energy γ-ray.

The resonant and fluorescent scattering cross-sections were obtained from the ratios of the resonant or fluorescent to Rayleigh scattered counts and the calculated Rayleigh cross-section. After substitution for the differential cross section in the equation, the partial level widths Γ_γ and the corresponding partial mean-lives τ_γ were found. The results are presented in table 1.

TABLE 1

Partial level widths Γ_γ and the corresponding partial mean-lives τ_γ

E_γ (keV)	$\frac{C_{res}}{C_{Ray}}$	$\sigma(\theta)_{Ray}$ (cm²/sr)	$\sigma(\theta)_{Res}$ (cm²/sr)	T (°K)	τ_γ (sec)
113	$\frac{1}{100}$	2.9×10^{-25}	2.9×10^{-27}	300	1.5×10^{-9}
208	$\frac{1}{150}$	4.8×10^{-26}	3.2×10^{-28}	790	2.5×10^{-10}

The partial mean-lives τ_γ were obtained from a comparison of the resonant and Rayleigh scattering intensities, the ratio of the latter is given in column 2. The differential Rayleigh cross-section $\sigma(\theta)_{Ray}$ was evaluated for $\theta = 110°$ when $E_\gamma = 208$ keV and for $\theta = 120°$ when $E_\gamma = 113$ keV. In column 5, T was the mean temperature of the source and scatterer.

From the intensity ratio [2]) of 70 : 1 for the 208 keV to 321 keV γ-decay modes, the partial mean-life of the 321 keV level for a ground state γ-transition is given by

$$\tau_\gamma(321\text{ keV}) = 1.7\times10^{-8}\text{ sec.}$$

When it is assumed that the 208 keV γ-decay mode represents $\frac{70}{81}$ of the alternative de-excitation process, either by internal conversion or by γ-decay to an intermediate level, then the total mean-life of the 321 keV level is

$$\tau(321\text{ keV}) = (2.2\pm0.7)\times10^{-10}\text{ sec.}$$

These results, which have been obtained from the 208 keV γ-ray partial mean-life, are naturally very sensitive to the relative γ-ray intensities.

It is convenient in the presentation of the results in table 2, to compare the experimental value of the reduced downward transition probability $B(\lambda;I_f\rightarrow I_i)$,

TABLE 2

Experimental values of the reduced downward transition probability and single particle estimates.

E_γ (keV)	$B(E\lambda;\ I_f\rightarrow I_i)$	$B(E\lambda;\ I_f\rightarrow I_i)/B(E\lambda)_{s.p.}$
113 (E2)	3.0	3.3×10^{2}
208 (E1)	2.8×10^{-6}	1.3×10^{-4}
321 (E1)	4.1×10^{-7}	5.2×10^{-7}

The enhancement factors of the reduced transition probability relative to the Weisskopf single particle estimate are given in column 3.

which depends solely on the nuclear matrix elements, with the single particle estimate.

In the evaluation of $B(E2)$ for the 113 keV transition it was assumed that the E2/M1 mixing ratio was $\delta^2 = 25$, while both the 208 keV and 321 keV transitions were considered to be pure E1.

The total mean-life of the 113 keV level, when the total conversion coefficient has the value $\alpha = 2.3$ is given by

$$\tau(113\text{ keV}) = (4.5 \pm 1.4) \times 10^{-10}\text{ sec.}$$

This compares favourably with the directly measured value [15] of 4.2×10^{-10} sec. When account is taken of the statistical factor representing the ratio of the multipolarities of the ground to excited states, the reduced upward transition probability has the value $B(E2) = 2.4$; this is in good agreement with those obtained from Coulomb excitation. The enhancement factor of 330 for the E2 transition is of the order expected for a strongly deformed nucleus.

The hindrance factor for the ground state transition is greater than 10^6, and is in good agreement with the values tabulated by Mottelson and Nilsson (cf. table 10 ref. [1]). If it is assumed that the M2 radiation in the transition is unhindered, then from a comparison of the E1 and M2 transition probabilities an admixture corresponding to $\delta^2 = 0.18$ for the M2 : E1 intensities would be expected to be present in the 321 keV transition. On the same basis the M2 admixture in the 208 keV transition is $\delta^2 = 6 \times 10^{-4}$. This is smaller than either the value of 10^{-2} reported by Wiedling [17]) or that of 10^{-3} found by Klema [5]). Very recently Vartapetyan [18]) has determined the total mean-life of the 321 keV level by a method in which the delayed coincidences between the 321 keV γ-ray and the preceding β-transition were measured. He obtained the result $(7 \pm 2) \times 10^{-10}$ sec and concluded that this value was consistent with 0.1 % M2 admixture in the 208 keV transition and with the 20 : 1 ratio for the relative intensity of the 208 keV to 321 keV γ-rays [11]). The present result of $\tau = (2.2 \pm 0.6) \times 10^{-10}$ sec, while of a similar order of magnitude, was derived on the basis of the ratio 70 : 1 for the relative intensities, which was roughly confirmed in the experiment.

The intensity ratio of E2 transitions between levels of the same rotational band is also dependent on the ratio of the Clebsch-Gordan coefficients, and in this case there is little deviation between the experimental and theoretical values for the ratio. Thus since the reduced transition probability for the 113 keV γ-ray is known, that corresponding to the 250 keV ($\frac{11}{2}^- \rightarrow \frac{7}{2}^-$) transition may be determined.

The partial mean-life of the 250 keV level was evaluated as

$$\tau_\gamma(250\text{ keV}) = 5.7 \times 10^{-11}\text{ sec.}$$

After correcting for the total internal conversion coefficient $\alpha = 0.1$, the total

mean-life is

$$\tau(250\ \text{keV}) = (5.2 \pm 1.6) \times 10^{-11}\ \text{sec.}$$

This value is approximately the mean of the Coulomb excitation measurements [9, 10]).

The γ-ray transition probabilities from the low lying levels of ^{177}Hf to the ground-state and their degree of hindrance or enhancement relative to the single-particle estimate for a spherical nucleus are consistent with the predictions for a strongly deformed nucleus. There is also good agreement between the present results and the earlier determinations for the mean-lives of the 113 keV and 250 keV levels, although in the case of the 321 keV level there appears to be some deviations.

The authors are most grateful to Professor P. B. Moon F.R.S. for his interest and helpful discussions during the course of the work, and one of them (W.D.H) acknowledges the receipt of a Research Studentship from the Ministry of Education for N. Ireland.

References

1) B. R. Mottelson and S. G. Nilsson, Mat. Fys. Skr. Dan. Vid. Selsk. **1**, No. 8 (1959)
2) P. Marmier and F. Boehm, Phys. Rev. **97** (1955) 103
3) S. Ofer, Nuclear Physics **3** (1957) 479
4) K. G. Steffen, Z. Phys. **147** (1957) 132
5) E. Klema, Phys. Rev. **109** (1958) 1652
6) D. R. Speck and E. A. Jenkins, Phys. Rev. **101** (1956) 1831
7) G. Alga, K. Alder, A. Bohr and B. R. Mottelson, Mat. Fys. Medd. Dan. Vid. Selsk. **29**, No. 9 (1955)
8) D. M. Chase and L. Wilets, Phys. Rev. **101** (1956) 1038
9) N. P. Heydenburg and G. M. Temmer, Phys. Rev. **104** (1956) 931
10) J. de Boer, M. Martin and P. Marmier, Helv. Phys. Acta **31** (1958) 578
11) H. Vartapetian, Ann. Phys. **3** (1958) 569
12) P. B. Moon, Proc. Phys. Soc. **64** (1951) 76
13) P. B. Moon, Proc. Phys. Soc. **63** (1950) 1189
14) W. E. Lamb, Phys. Rev. **55** (1939) 190
15) E. E. Berlovich, Isvest. Akad. Nauk, USSR Ser. Fiz. **20** (1956) 1438
16) S. A. Moszkowski, in Beta- and gamma-ray spectroscopy, ed. K. Siegbahn (North-Holland Publishing Company, Amsterdam, 1955)
17) T. Wiedling, Directional correlation measurements and some other related investigations of excited nuclei (Almqvist and Wiksells, Uppsala, 1956)
18) G. A. Vartapetyan, JETP **11** (1960) 1378

3.B

Nuclear Physics **27** (1961) 75—78; © *North-Holland Publishing Co., Amsterdam*

Not to be reproduced by photoprint or microfilm without written permission from the publisher

MEASUREMENT OF K CONVERSION COEFFICIENT OF 279 keV GAMMA RADIATION IN Tl^{203}

J. P. HURLEY and J. M. FERGUSON

U. S. Naval Radiological Defense Laboratory, San Francisco 24, California

Received 7 April 1961

Abstract: The K conversion coefficient of the 279 keV transition in Tl^{203} was determined by measuring the relative intensities of the 279 keV gamma ray and the K x-rays from a Hg^{203} source. Using the value $\omega_K = 0.955$ for the fluorescent yield, the conversion coefficient was determined to be $\alpha_K = 0.175 \pm 0.0036$.

1. Introduction

Previous measurements of the K conversion coefficient of 279 keV gamma ray in Tl^{203} made with beta spectrometers [1]) have yielded values near 0.16, while those measurements made with scintillation counters [2–4]) have given values close to 0.20. In addition neither of the two divergent groups of experimental measurements is consistent with the theoretical values of 0.179 and 0.175 derived from the tables of Rose [5]) and Sliv and Band [6]) and using the M1+E2 intensity ratio of 2.25 reported by McGowan and Stelson [7]). In view of these divergent results we decided to remeasure the 279 keV K conversion coefficient using a scintillation counter. In this method the coefficient α_K is measured by counting the number of K x-rays and the number of gamma rays from a Tl^{203} source, and is given by the expression

$$\alpha_K = \frac{1}{\omega_K} \frac{N_x}{N_\gamma},$$

where N_x is the number of x-rays, N_γ the number of gamma rays (after correction for attenuation and detector efficiency) and ω_K the fluorescent yield for the K x-ray.

2. Apparatus and Procedure

A Hg^{203} source obtained from the Oak Ridge National Laboratory was dissolved in weak HCl and deposited between the two films of rubber hydrochloride. The film thickness was 0.25 mg/cm². The detector was a Harshaw Type 16Ml316/A assembly consisting of an unshielded 10 cm by 10 cm NaI (Tl)

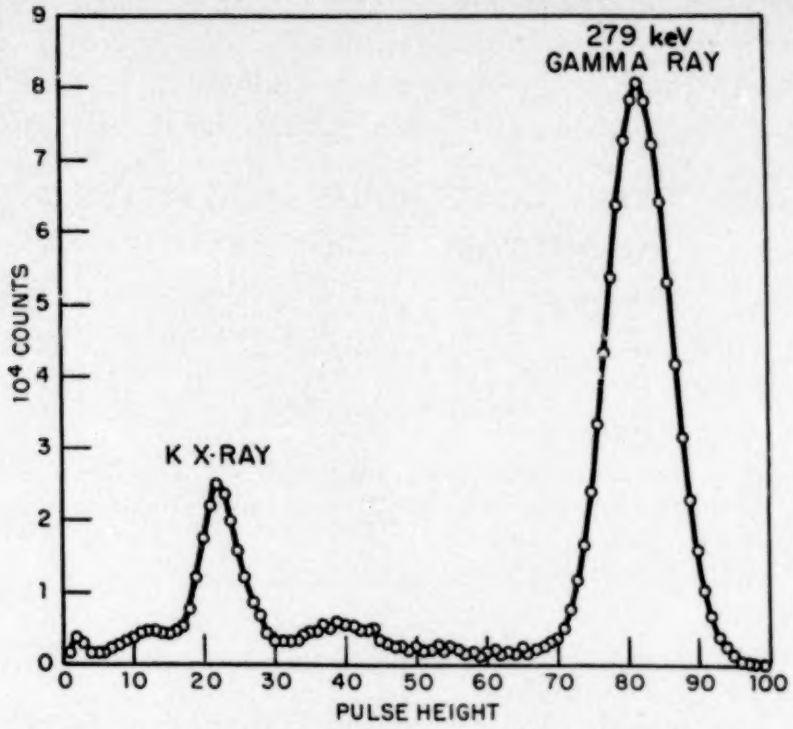

Fig. 1. Hg^{203} pulse-height spectrum taken with a 10 cm height, 10 cm diameter NaI(Tl) crystal. The spectrum of background radiation and radiation scattered into the crystal from the room were determined by a run made with a shadow shield between the source and crystal, and were subtracted from this run.

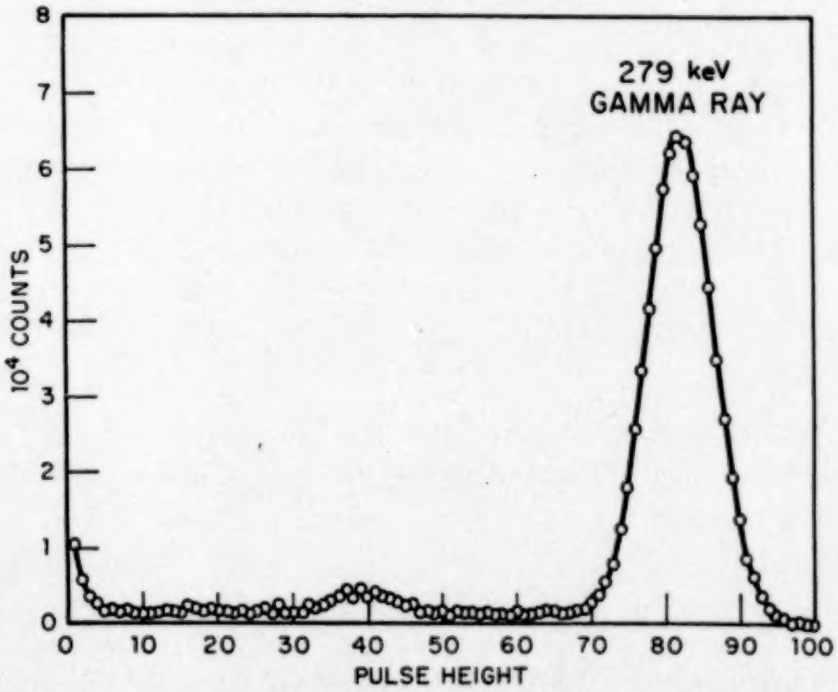

Fig. 2. Hg^{203} pulse-height spectrum taken with a 10 cm height, 10 cm diameter NaI(Tl) crystal. In this run a 0.038 cm Ta plate was placed between the source and absorber to selectively filter out the 74.6 keV x-ray. The background plus in-scattered spectrum were subtracted as described in fig. 1.

crystal and a Dumont 6363 photomultiplier. The source and detector, elevated to a distance of 76 cm above the floor, were separated by a distance of 121 cm.

Three pulse-height spectra were recorded on a Penco Type PA-3 100-channel analyzer. The first spectrum was measured using no auxiliary absorbers, the second spectrum was recorded with a 0.038 cm tantalum plate to selectively absorb the 74.6 keV x-ray, and the third spectrum was measured using a 2 cm lead shadow shield. The last distribution when subtracted from the first two yielded spectra corrected for scattered radiation and general room background. The statistical errors introduced by the subtraction process were smaller than 1 % in all cases. The corrected no-absorber spectrum is shown in fig. 1, while the corrected tantalum-filtered spectrum is shown in fig. 2.

3. Results

Following subtraction of the normalized tantalum absorber spectrum from the spectrum measured with no absorber, the number of counts under the resulting K x-ray full-energy and escape peaks was computed. The number of counts in the gamma-ray spectrum was then found by subtracting the x-ray contribution from the total spectrum. Both the x-ray and gamma-ray spectra were then corrected for detector efficiency [8]) and for attenuation in air [9]) and crystal package (aluminium, neoprene rubber, poleythylene and magnesium oxide †. The efficiencies were computed to be 100 % and 98 % and the attenuation factors were computed to be 0.896 and 0.965 for the x-ray and gamma ray, respectively. Using the value $\omega_K = 0.955$ for the fluorescent yield [10]), the conversion coefficient α_K was calculated to be

$$\alpha_K = 0.175 \pm 0.0036.$$

Because they were estimated to be $\ll$ 1 % and therefore not significant in this calculation, corrections were not made for source scattering, backscattering, bremsstrahlung, L shell x-ray and autoionization.

4. Discussion

Our experimental value of α_K is consistent with the theoretical conversion coefficient of Rose [5]) and Sliv and Band [6]) using the intensity mixture ratio measured by McGowan and Stelson [7]). Our value falls in the range between previous scintillation counter results [2–4]) and beta spectrometer measurements [1]).

It is noted that our result is in disagreement with those theoretical values calculated with selected mixture ratios of 1.44 as reported by Nijgh and

† Densities furnished by the Harshaw Chemical Co., Cleveland, Ohio.

Wapstra [11]) and 1.96 and 6.25 as reported by Deutch and Goldberg [12]) these values for δ^2 having been selected to secure the best fit with the experimental data.

References

1) G. J. Nijgh, A. H. Wapstra, L. T. M. Ornstein, N. Salomons-Grobben, J. R. Huizenga and O. Almen, Nuclear Physics **9** (1958) 528;
C. Nordling, K. Siegbahn, E. Solokowski and A. H. Wapstra, Nuclear Physics **1** (1956) 326;
A. H. Wapstra and C. J. Nijgh, Nuclear Physics **1** (1956) 245;
J. L. Wolfson, Can. J. Phys. **34** (1956) 256;
N. Marty, Compt. Rend. **240** (1955) 291;
A. H. Wapstra, D. Maeder, C. J. Nijgh and L. Th. M. Ornstein, Physica **20** (1954) 169;
S. Thulin and K. Nybo, Ark. Fys. **7** (1954) 289;
H. W. Wilson and S. C. Curran, Phil. Mag. **42** (1951) 762;
T. Azuma, Bull. Naniwa Univ. **3** (1955) 237;
R. K. Doerner and A. H. Weber, Phys. Rev. **99** (1955) 672;
F. O. Friel and A. H. Weber, Phys. Rev. **101** (1956) 1076
2) M. K. Ramaswamy and P. S. Jastram, Nuclear Physics **15** (1960) 510
3) R. L. Heath and P. R. Bell, Phys. Rev. **87** (1952) 176
4) S. A. E. Johansson, Ark. Fys. **3** (1952) 533
5) M. E. Rose, Internal conversion coefficients (North-Holland Publishing Co., Amsterdam 1958)
6) L. A. Sliv and I. M. Band, Coefficients of internal conversion of gamma radiation (USSR Academy of Sciences, Moscow-Leningrad, 1956 (K) and 1958(L))
7) F. K. McGowan and P. H. Stelson, Phys. Rev. **103** (1956) 1133
8) A. L. Stanford, Jr. and W. K. Rivers, Jr., Rev. Sci. Inst. **29** (1958) 406
9) G. W. Grodstein, U.S. Mational Bureau of Standards circular 583
10) A. H. Wapstra, G. J. Nijgh and R. van Lieshout, Nuclear Spectroscopy Tables (North-Holland Publishing Co., Amsterdam, 1959) p. 81
11) G. J. Nijgh and A. H. Wapstra, Nuclear Physics **9** (1958) 545
12) B. I. Deutch and N. Goldberg, Phys. Rev. **117** (1960) 818

2.B

Nuclear Physics **27** (1961) 79—93; © *North-Holland Publishing Co., Amsterdam*

Not to be reproduced by photoprint or microfilm without written permission from the publisher

THE USE OF POLARISED DEUTERONS TO STUDY THE D+D REACTIONS

J. R. ROOK † and L. J. B. GOLDFARB

Department of Theoretical Physics, The University of Manchester

Received 21 February 1961

Abstract: It is shown that further information on the spin transitions involved in the D+D reactions at low energies ($E_D \lesssim 1$ MeV) may be obtained by the use of polarised deuteron beams, but that a complete determination of the reaction matrix elements requires two double polarisation measurements. The selection rules on the spin transitions are discussed in terms of the internucleon forces and the earlier formulae giving the energy dependence of the cross sections and polarisation are slightly modified to give a further degree of freedom in fitting the experimental data.

1. Introduction

The reactions $D+D \rightarrow H^3+p$ and $D+D \rightarrow He^3+n$ have been the subject of considerable experimental studies [1])††. In this paper we are concerned with the information to be obtained from these studies at low bombarding deuteron energies, i.e. for laboratory energies $E_D \lesssim 1$ MeV. For these energies it is found, experimentally, that the angular distribution of the outgoing protons or neutrons can be represented adequately by

$$W_0(\theta) = W_0^0(1+\alpha P_2(\cos\theta)). \tag{1}$$

The quantities W_0^0 and α are energy-dependent parameters which were discussed, in terms of the barrier penetration factors of the initial deuterons, by Beiduk, Pruett and Konopinski [2]).

Formulae for the outgoing nucleon polarisation have been given by several authors [3]). At low energies these formulae reduce to

$$\mathbf{P}(\theta) = \frac{\mathbf{n}C\alpha P_2^1(\cos\theta)}{1+\alpha P_2(\cos\theta)}, \tag{2}$$

where α is the quantity appearing in eq. (1), and the associated Legendre function $P_2^1(\cos\theta)$ is as defined by Jahnke and Ehmde [4]). The unit vector $\mathbf{n}$ is normal to the plane of the reaction and is given by $\mathbf{n} = \mathbf{k}_1 \times \mathbf{k}_2 / |\mathbf{k}_1 \times \mathbf{k}_2|$, where $\mathbf{k}_1$ and $\mathbf{k}_2$ are propagation vectors for the initial and final beams, respec-

† Now at the Clarendon Laboratory, Oxford

†† The differential cross sections are given in the papers of ref. [1]) and the nuclear polarisation by those of ref. [6]).

tively. The work of ref. [2]) indicates that the quantity C does not depend on energy. A recent polarisation measurement [5]) at $E_D = 98$ keV disagrees with eq. (2) suggesting rather that the polarisation is fairly independent of energy at a centre-of-mass angle of 45°. In sect. 2 we generalise the consideration of the energy dependence given in ref. [2]) and provide a further degree of freedom in fitting the polarisation data. Our formula, given by eq. (2), in which C is energy dependent, improves the fit to the current polarisation data [6]), although not significantly if the results of ref. [5]) are ignored.

The second paper of ref. [2]) discusses these reactions in terms of the internucleon forces using the Wheeler resonating group method to obtain a formula for the cross section. In sect. 3 we use the Born approximation, without explicit reference to Wheeler's method, to derive a formula from which the higher-order corrections are more easily obtained. Our first-order formula differs from that of ref. [2]) in that certain kinetic-energy terms do not appear, but a slight modification of our formalism yields exactly the result of ref. [2]). Of particular interest in this treatment, is the possibility of a change in the channel-spin through the reaction, i.e. the possibility of singlet-triplet or triplet-singlet transitions, as they are forbidden in first order with the usual central and tensor internucleon forces. In sect. 2 we consider more fully the approximations under which these transitions are forbidden.

Sects. 4 and 6 contain a discussion of the information to be obtained using polarised deuterons. In particular it is found that measurements of the asymmetries arising in such experiments would lead to an estimate of the importance of triplet-singlet spin transitions. These may also be estimated by a comparison of the outgoing polarisation of the nucleon with that of the He^3 (or H^3) as is discussed in sect. 5. It is shown in sect. 4 that the use of tensor polarised deuterons would provide further information on the reaction matrix elements but would not determine them completely. In sect. 6 we consider the possibility of such a complete determination by means of double polarisation measurements.

2. Angular Distribution and Polarisation of the Outgoing Nucleon.

In presenting the results of our calculations, we adhere mainly to the notation of ref. [2]) and for completeness repeat some of their observations. In particular we note that the initial state consists of two identical bosons and hence must be symmetric under interchange of the deuterons. Thus for even orbital angular momentum l the channel spin S must be 0 (singlet) or 2 (quintet) and for odd l, S must be 1 (triplet). It is usual in treating this reaction to ignore quintet states as this would involve a close approach of the deuterons which is not likely because of the exclusion principle [2]). Since, however, the effective radius for the initial state of the reaction is ≈ 7 fm this may be a weak argument.

We limit ourselves to incoming s and p waves, and consider d waves only

in interference with s waves so as to give no term in $P_4(\cos\theta)$ in eq. (1). We also exclude outgoing f waves but otherwise there are no restrictions other than those arising from the conservation of parity and angular momentum.

We adopt the assumption of ref. [2]) that the energy variation of the matrix elements is entirely governed by the barrier penetration factors for the incoming deuterons. One may justify the neglect of the energy variation of the outgoing penetration factors by taking into account the fact that the Q-values of the reactions are 3.24 and 3.98 MeV for neutron and proton emission, respectively. (If the energy variation for the incident deuterons is large this assumption may become invalid.) Since the effective radius for the final state is smaller than that for the initial state, being ≈ 4 fm, it is reasonable to assume that the centrifugal barriers for final f and higher waves are large.

We write the reaction matrix with the phase conventions of Devons and Goldfarb [7]) as

$$\langle S_2 l_2 J|R|S_1 l_1 J\rangle,$$

where the suffices 1 and 2 refer to the initial and final state, respectively. The quantum number J refers to the total angular momentum of the system. We follow ref .[2]) and put

$$\begin{aligned} \langle 0JJ|R|0JJ\rangle &\equiv \alpha_J, \qquad \langle 0JJ|R|1JJ\rangle \equiv \beta_{JJ}, \\ \langle 1JJ|R|0JJ\rangle &\equiv \beta_J, \qquad \langle 1lJ|R|1lJ\rangle \equiv \alpha_{lJ}. \end{aligned} \tag{3}$$

It will be noted that β_{JJ} is zero if triplet-singlet transitions are forbidden and β_J is zero if singlet to triplet transitions are forbidden. The differential cross section can be written in terms of these parameters as

$$W_0(\theta) = \tfrac{1}{36}\lambda^2\{B_0 + B_1 P_2(\cos\theta)\}, \tag{4a}$$

where λ is the reduced wavelength of the bombarding deuterons in the centre-of-mass system and

$$B_0 = |\alpha_0|^2 + |\alpha_{10}|^2 + 3|\alpha_{11}|^2 + 3|\beta_{11}|^2 + 5|\alpha_{12}|^2, \tag{4b}$$

$$\begin{aligned} B_1 = \tfrac{3}{2}|\alpha_{11}|^2 + \tfrac{7}{2}|\alpha_{12}|^2 - 3|\beta_{11}|^2 + 10\,\mathrm{Re}(\alpha_2\alpha_0^*) \\ + 9\,\mathrm{Re}(\alpha_{12}\alpha_{11}^*) + 4\,\mathrm{Re}(\alpha_{12}\alpha_{10}^*). \end{aligned} \tag{4c}$$

When the polarisation of the outgoing nucleon is measured with detectors whose sensitivity is given by the vector $\mathbf{P}$, as defined in ref. [7]), the angular distribution is given by

$$W(\theta) = W_0(\theta) + W_1(\theta), \tag{5a}$$

where

$$W_1(\theta) = \tfrac{1}{36}\lambda^2 B_2 P_2^1(\cos\theta)\mathbf{P}\cdot\mathbf{n}. \tag{5b}$$

The quantity **n** is the unit normal defined above while B_2 is given by

$$B_2 = \tfrac{3}{2}\sqrt{2}\,\mathrm{Im}(\alpha_{11}\beta_{11}^*)+3\,\mathrm{Im}(\alpha_{11}\alpha_{12}^*) + \tfrac{3}{2}\sqrt{2}\,\mathrm{Im}(\beta_{11}\alpha_{12}^*)+2\,\mathrm{Im}(\alpha_{10}\alpha_{12}^*)+\frac{10\sqrt{5}}{3}\,\mathrm{Im}(\alpha_0\beta_2^*). \tag{5c}$$

As indicated above, we now assume the main energy dependence of $\lambda\!\!\!^{-2}B_0$, $\lambda\!\!\!^{-2}B_1$ and $\lambda\!\!\!^{-2}B_2$ is given by the appropriate barrier penetration factors for the initial two deuteron system. As a check on the validity of the WKB approximation used in ref. [2]), we have recomputed the barrier penetration factors given there, assuming boundary conditions appropriate for a hard sphere at the nuclear surface. We have also computed the energy dependence of the phase associated with the s and d wave interference, which is neglected in ref. [2]).

We denote the barrier penetration factor for a wave of orbital angular momentum l, by

$$\Omega_l = \sqrt{\sigma_l}\,\mathrm{e}^{i(\phi_l+\psi_l)},$$

where ψ_l is the phase shift appropriate for the motion of two like point charges. In terms of the usual regular and irregular Coulomb functions, $F_l(\rho)$ and $G_l(\rho)$ we have

$$\sigma_l = \frac{1}{kR}\,\frac{1}{F_l^2(kR)+G_l^2(kR)}, \tag{6a}$$

$$\mathrm{tg}\,\phi_l = -F_l(kR)/G_l(kR), \tag{6b}$$

where $k = 1/\lambda\!\!\!^{-}$ and R is the nuclear radius. The latter quantity is not well-defined in this reaction because of the considerable spread of the deuteron wavefunctions; but a value of 7 fm gives a fairly reasonable fit to the angular distributions. Investigations of the effect of different choices for the boundary conditions were undertaken in ref. [2]) showing that the energy dependence of the barrier penetration factors does not significantly depend on this choice.

The calculated penetration factors are shown in fig. 1. Where there is interference between different values of l, we show both the real and imaginary parts of $\Omega_l\Omega_{l'}^*$.

Comparing with the results of ref. [2]), it is observed that the curves are very similar, the only significant difference being the curve for σ_0 which is found to fall more quickly above the peak using the WKB approximation. A further point to notice is that $\mathrm{Re}(\Omega_2\Omega_0^*)$ behaves quite similarly to σ_1, as is pointed out by Beiduk *et al.* and that Im $(\Omega_2\Omega_0^*)$ is smaller but has a different energy variation. We thus see that the inclusion of this latter term provides a further degree of freedom in fitting eq. (5) to the experimental polarisation data.

We show in fig. 2 the recent nucleon polarisation measurements of refs. [5, 6]). The polarisation is seen to be very nearly constant between deuteron energies of 100 and 600 keV, although this mainly depends on Kane's work at 98 keV.

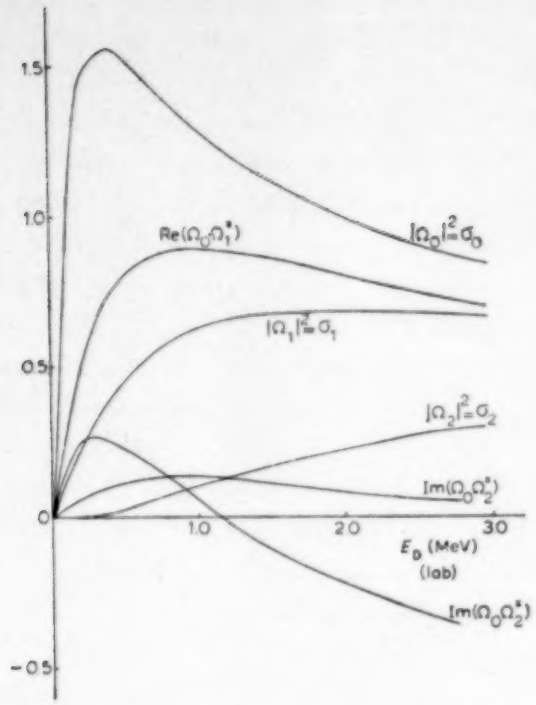

Fig. 1. Energy variation of barrier penetration factors for the two deuteron system assuming the boundary conditions appropriate for a hard sphere of radius 7 fm. The ordinate is in arbitrary units

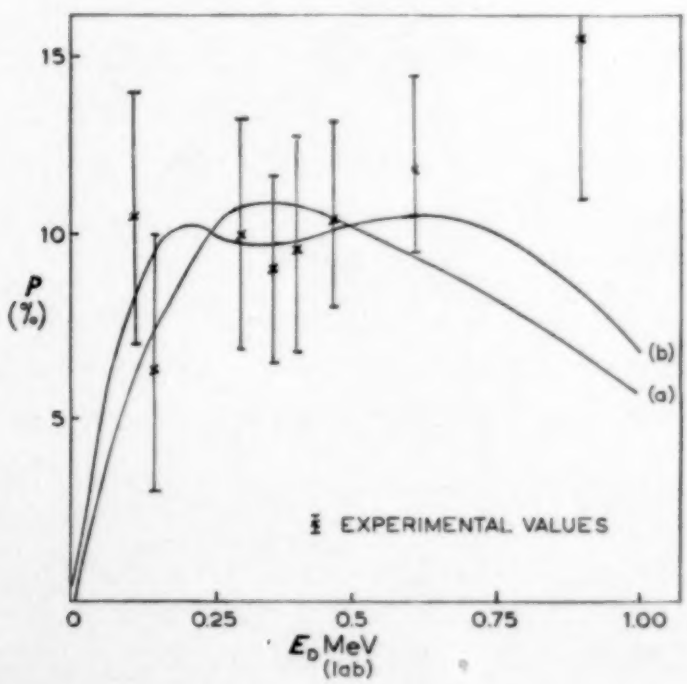

Fig. 2. Predicted energy variation of polarisation compared with the experimental points. (a) Best fit excluding Im $(\Omega_s\Omega_0^*)$. (b) Best fit including Im $(\Omega_s\Omega_0^*)$

This has been difficult to interpret on the basis of the work of ref. [2]) since, under their assumptions, the energy dependence of both $\lambda\!\!\!^{-2}B_1$ and $\lambda\!\!\!^{-2}B_2$ is proportional to σ_1 while the energy dependence of B_0 is directly measurable. Curve (a) in fig. 2 gives the polarisation obtained on the basis of ref. [2]). The introduction of $\mathrm{Im}(\Omega_2\Omega_0^*)$ provides another degree of freedom, as indicated above, so that a more constant polarisation can be obtained as shown by curve (b) in fig. 2. It will be observed that neither of the curves in fig. 2 fits the point at 900 keV but there is evidence at this energy of higher incident partial waves. It is quite possible that the slightly improved fit to the data is fortuitous, since we have simply provided an extra degree of freedom, more especially as we might expect β_2, corresponding to the singlet-triplet transition, to be quite small.

If we ignore Kane's data, we note that there is reasonable agreement with experiment if we set the coefficient of Im $(\Omega_2\Omega_0^*)$ equal to zero, although the fit is improved even in this case by the introduction of the extra term.

The general conclusion of this section is that a slight improvement to the fit of the polarisation data can be obtained if we take into account the variation in energy of the phase of the barrier penetration factor and if we further assume that the singlet-triplet term β_2 is not negligible.

3. Four-Body Approach

We use the Born approximation to evaluate the matrix elements. We write the Schrödinger equation for the entire system as

$$(T_1+T_2+T_3+T_4+V)\Psi = E\Psi, \tag{7}$$

where T_1, T_2, T_3 and T_4 are the kinetic-energy operators for the nucleons, using labels 1 and 3 for protons and 2 and 4 for neutrons, while V is the sum of the potentials. We now put

$$\Psi = \psi_0+\psi_1, \tag{8}$$

where ψ_0 is the wavefunction describing the initial two-deuteron state. We ignore for the time being the symmetries of the system and write ψ_0 as

$$\psi_0 = \phi_{D_1}(\mathbf{r}_1-\mathbf{r}_2)\phi_{D_2}(\mathbf{r}_3-\mathbf{r}_4)\chi(12-34), \tag{9}$$

where ϕ_{D_1} and ϕ_{D_2} represent spin-dependent deuteron wavefunctions, χ represents the wavefunction for the relative motion of the two deuterons and 12—34 represents $\frac{1}{2}(\mathbf{r}_1+\mathbf{r}_2)-\frac{1}{2}(\mathbf{r}_3+\mathbf{r}_4)$. Using eqs. (8) and (9) in eq. (7), multiplying by the complex conjugate of the triton wavefunction, ψ_T^* integrating over the coordinates of the nucleons occurring in ψ_T^* and summing over spin, we obtain

$$(T_{1-234}-E)\int \psi_T^*\psi_1 \mathrm{d}\tau_{234} = -\int \psi_T^*(V'\psi_0+V'''\psi_1)\mathrm{d}\tau_{234}. \tag{10}$$

The operator T_{1-234} represents the kinetic-energy operator for the emitted nucleon in the centre-of-mass system while V' and V''' are given by

$$V' = V_{13}+V_{14}+V_{23}+V_{24},$$
$$V''' = T_1+T_2+T_3+T_4-T_{1-234}-T_{CM}+V,$$

where T_{CM} is the kinetic energy of the centre-of-mass of the system. This latter quantity has no effect on the final result and we ignore it.

We now put

$$\psi_1 = \psi_T(234)\phi(r_0)+\psi_2, \tag{11}$$

where ψ_T, ψ_2 and ϕ are all spin-dependent and $\mathbf{r}_0$ is given by

$$\mathbf{r}_0 = \mathbf{r}_1-\tfrac{1}{3}(\mathbf{r}_2+\mathbf{r}_3+\mathbf{r}_4). \tag{12}$$

Inserting eq. (11) in eq. (10) we obtain

$$(T_{1-234}-E_F)\phi(\mathbf{r}_0) = -\int \psi_T^*(234)\{V'\psi_0+V''\psi_T\phi(\mathbf{r}_0) + (T_1+T_2+T_3+T_4+V-E)\psi_2\}d\tau_{234}, \tag{12}$$

where $V'' = V_{13}+V_{14}+V_{12}$ and E_F is the energy of the emitted proton in the centre-of-mass system. The solution of (12) representing outgoing waves only, obtained by the usual Green-function techniques, is

$$\phi(\mathbf{r}) = -\frac{m^*}{2\pi\hbar}\int \frac{e^{ik_f|\mathbf{r}-\mathbf{r}_0|}}{|\mathbf{r}-\mathbf{r}_0|}\psi_T^*(234)\{V'\psi_0 + V''\psi_T\phi(\mathbf{r}_0)+(T_1+T_2+T_3+T_4+V-E)\psi_2\}d\tau_{234}, \tag{13a}$$

where $\mathbf{k}_f$ is the wavevector for the outgoing nucleon in the centre-of-mass system and m^* is the reduced mass of the emitted nucleon. The differential cross section is thus given by

$$W(\theta) = \frac{k_f}{k_i}\frac{mm^*}{4\pi^2\hbar^4}\left|\int \chi_D^* e^{-i\mathbf{k}_f\cdot\mathbf{r}_0}\psi_T^*(234) \{V'\psi_0+V''\psi_T\phi(\mathbf{r}_0)+(T_1+T_2+T_3+T_4+V-E)\psi_2\}d\mathbf{r}_0 d\tau_{234}\right|^2, \tag{13b}$$

where χ_D is the spin wavefunction of the outgoing and $\mathbf{k}_i$ is the wavevector of the initial deuteron in the centre-of-mass system.

The effect of the symmetries of the system are now included. The initial two deuteron system must be symmetric under exchange of the two deuterons while it must be antisymmetric under exchange of either the protons or the neutrons. This means we multiply the initial state in (13a) by the operator $\frac{1}{2}\sqrt{2}\,(1-p_{13})$, where p_{ij} is the operator exchanging particles i and j. Similarly

we multiply the final state by the operator $\frac{1}{2}\sqrt{2}(1-\mathcal{P}_{13}+\mathcal{P}_{14}\mathcal{P}_{23}+\mathcal{P}_{12}\mathcal{P}_{34})$, the spin wavefunction of the outgoing system being antisymmetric in particles 2 and 4, as is appropriate for the ground state of the triton.

If the wavefunctions occurring in eq. (13a) are analysed into spin and orbital angular momenta the individual matrix elements, after removal of the magnetic quantum number dependence, become the α and β defined in sect. 2.

The integrand in (13b) consists of the sum of three terms. The first is analogous to that of ref. [2]), the only difference being the omission in our formula of terms representing the relative kinetic energy of the two deuteron system. We may make the correspondence complete if we assume that ψ_0 has the form of eq. (9) outside the nuclear radius and is a constant inside this radius. The effect is to add to the first term the operator $T_{12-34}-E_1$, where E_1 is the initial centre of mass bombarding energy and T_{12-34} represents the kinetic energy operator for the motion of two deuterons. These latter terms are in any event diagonal in channel spin and orbital angular momentum so they have no effect on the selection rules we discuss.

The second term represents the scattering of the outgoing nucleon in the field of the residual nucleus and higher orders can be obtained by iteration. The third term contains, in addition to the higher-order corrections to the second term, such factors as the distortion of the initial deuteron wavefunctions and compound-nucleus formation. An estimate of the former could be had either by the adiabatic approximation or by variational methods, while the latter would involve excited states of the α particle. The first term in eq. (13b) contains ψ_0 and hence $\chi(12-34)$ describes the motion of the deuterons in their mutual potential including the Coulomb force between the two protons. The inter-deuteron potential can be calculated by considering the inverse process, when it is found that the first order is just V' and the higher orders can be obtained by iteration in analogy with the proton-triton scattering. The authors of ref. [2]) attempt to evaluate the first term using a plane wave to represent the function χ, but taking into account the Coulomb force by the methods of sect. 2, obtain qualitative agreement with quite crude approximations.

We wish now to consider the information to be obtained concerning the spin couplings. We consider only the terms involving V' and V'' in eq. (13b). After iterating for $\phi(\mathbf{r}_0)$, using (13a) and similarly taking into account the two deuteron scattering, we note that $W(\theta)$ can be represented as the square modulus of a sum of terms of the type

$$\langle \mathrm{i}|V'|\mathrm{D}_1\rangle\langle \mathrm{D}_1|V'|\mathrm{D}_2\rangle \ldots \langle \mathrm{D}_n|V'|\mathrm{T}_m\rangle \ldots \langle \mathrm{T}_2|V''|\mathrm{T}_1\rangle\langle \mathrm{T}_1|V''|\mathrm{f}\rangle,$$

where i and f represent the initial and final states, while $\mathrm{D}_1 \ldots \mathrm{D}_n$ and $\mathrm{T}_1 \ldots \mathrm{T}_m$ represent the two deuteron and triton-proton states, respectively. The matrix elements up to $\langle \mathrm{D}_{n-1}|V'|\mathrm{D}_n\rangle$ represent two deuteron scattering while the terms from $\langle \mathrm{T}_m|V''|\mathrm{T}_{m-1}\rangle$ represent triton nucleon scattering. We thus see

that our theory is roughly equivalent to a distorted-wave Born approximation, which is valid when the coupling between the various channels is small.

We denote the initial two deuteron spin state with projection on the z axis equal to M by χ^0_{SM} and the final state by χ_{SM}. These can be written, after being appropriately symmetrised, in terms of two particle singlet (s_{ij}) and triplet (t_{ij}) states as

$$\chi^0_{00} = \frac{1}{\sqrt{12}}(3s_{13}s_{24}+t^0_{13}t^0_{24}-t^1_{13}t^{-1}_{24}-t^{-1}_{13}t^1_{24})$$

$$\equiv \frac{1}{\sqrt{12}}(3s_{14}s_{23}+t^0_{14}t^0_{23}-t^1_{14}t^{-1}_{23}-t^{-1}_{14}t^1_{23}),$$

$$\chi^0_{1M} = \frac{1}{\sqrt{2}}(s_{13}t^M_{24}+t^M_{13}s_{24}) \equiv \frac{1}{\sqrt{2}}(s_{14}t^M_{23}+t^M_{14}s_{23}),$$

$$\chi_{00} = s_{13}s_{24} \equiv \tfrac{1}{2}(s_{14}s_{23}+t^0_{14}t^0_{23}-t^1_{14}t^{-1}_{23}-t^{-1}_{14}t^1_{23}),$$

$$\chi_{10} = t^0_{13}s_{24} \equiv \tfrac{1}{2}(s_{14}t^0_{23}+t^0_{14}s_{23}-t^1_{14}t^{-1}_{23}+t^{-1}_{14}t^1_{23}),$$

$$\chi_{1\pm1} = t^{\pm1}_{13}s_{24} \equiv \tfrac{1}{2}[(s_{14}\pm t^0_{14})t^{\pm1}_{23}+t^{\pm1}_{14}(s_{23}\mp t^0_{23})].$$

We ignore quintet states and consider the possibility of singlet-triplet or triplet-singlet transitions. We assume the potential consists of two-particle interactions and that the spin couplings can be represented in terms of irreducible tensor operators T^{ij}_{kq}, as defined in ref. [8]), where i and j refer to the particle pair concerned. We make the further assumption that the potential does not couple two-particle singlet and triplet states. This is the case of the usual tensor and $\mathbf{L}\cdot\mathbf{S}$ forces which correspond to the cases $k = 2$ and $k = 1$, respectively.

We illustrate the calculations by considering the singlet to triplet transtions. Consider the matrix element

$$\langle\chi_{10}|T^{ij}_{kq}|\chi^0_{00}\rangle.$$

The potentials between the pairs 1—3 and 2—4 can be seen to have no effect since the potential is assumed not to couple two-particle singlet and triplet states. Considering now the pair 1—4; we have

$$\langle\chi_{10}|T^{14}_{kq}|\chi^0_{00}\rangle = \langle t^1_{14}|T^{14}_{kq}|t^1_{14}\rangle - \langle t^{-1}_{14}|T^{14}_{kq}|t^{-1}_{14}\rangle.$$

Using the Wigner-Eckart theorem, and ignoring common phase factors, we obtain

$$\langle t||T^{14}_k||t\rangle(11, k0|11)\{1-(-1)^k\}.$$

Since the matrix element vanishes for even values of k, the singlet-triplet transitions occur only through the $\mathbf{L}\cdot\mathbf{S}$ force in this approximation. The conclusions for the pair 2—3 are identical. We now consider the results in detail.

3.1 TRIPLET-SINGLET TRANSITIONS

These are not allowed in first order with the conventional two-body force; i.e. with central, tensor and $\mathbf{L}\cdot\mathbf{S}$ components. In higher orders we consider separately the two cases described above, i.e. the D—D scattering in the initial field, which may be large because of the large effective radius and low energies, and the triton-nucleon scattering in the final field, which may be somewhat smaller. Triplet-singlet transitions of the two deuteron system are forbidden to any order provided we limit our intermediate states to χ^0_{SM} ignoring quintet states. Triplet-singlet transitions of the triton-nucleon system are allowed only if we include a two particle $\mathbf{L}\cdot\mathbf{S}$ force.

3.2 SINGLET-TRIPLET TRANSITIONS

Similar arguments show that these transitions are allowed even in first order if we include a two particle $\mathbf{L}\cdot\mathbf{S}$ force. In higher orders the conclusions are as stated in subsect 3.1 for triplet-singlet transitions.

In conclusion we would say that the existence of such triplet-singlet or singlet-triplet transition is, to the extent to which our assumptions are valid, a consequence of the internucleon $\mathbf{L}\cdot\mathbf{S}$ force. We would expect the singlet-triplet (β_2) transitions to be more likely than the triplet-singlet (β_{11}) transitions as the former are allowed in first order.

4. Use of Polarised Deuterons

We describe the polarisation of the incident deuteron beam by use of the vector $\mathbf{Q}$ and the tensor with components Q_{xx}, Q_{xy}, etc. as defined in ref. [9]). Thus we have

$$\hbar\mathbf{Q} = \langle\mathbf{s}\rangle, \qquad \hbar^2 Q_{ij} = \tfrac{3}{2}\langle s_i s_j + s_j s_i\rangle - 2\hbar^2\delta_{ij},$$

where s is the spin operator associated with $s = 1$. The y axis in this case is taken to be along the unit vector $\mathbf{n}$ defined in sect. 2, while the direction of propagation of the beam determines the z direction. On the other hand, we describe the efficiency for detection of the outgoing polarisations by use of a y axis along $-\mathbf{n}$ and a z axis along the direction of the outgoing beam.

The angular distribution arising from an incoming polarised deuteron beam is found to be

$$W(\theta) = W_0(\theta) + W_2(\theta), \tag{14a}$$

where $W_0(\theta)$ is the angular distribution obtained when no polarisations are measured and $W_2(\theta)$ involves the deuteron polarisation. The explicit form for $W_0(\theta)$ is given in sect. 2 while $W_2(\theta)$ is given by

$$\begin{aligned} W_2(\theta) = {} & \tfrac{1}{36}\lambda^2\{Q_y[P_1^1(\cos\theta)B_3 + P_2^1(\cos\theta)B_4] \\ & + \tfrac{1}{2}P_2^2(\cos\theta)(Q_{xx} - Q_{yy})B_5 + P_2^1(\cos\theta)B_6 Q_{xz} \\ & + P_2(\cos\theta)Q_{zz}B'_5 + B_7 Q_{zz}\}, \end{aligned} \tag{14b}$$

where we have put $Q_{yz} = Q_{xy} = Q_x = 0$ and B are given by

$$\begin{aligned}
B_3 &= 3\sqrt{3}\,\mathrm{Im}(\alpha_0\beta_{11}^*),\\
B_4 &= \tfrac{3}{2}\mathrm{Im}(\alpha_{10}\alpha_{12}^*)+\tfrac{9}{4}\mathrm{Im}(\alpha_{11}\alpha_{12}^*),\\
B_5 &= \tfrac{3}{8}|\alpha_{12}|^2+\tfrac{3}{8}|\alpha_{11}|^2-\tfrac{3}{4}|\beta_{11}|^2-\tfrac{3}{4}\mathrm{Re}(\alpha_{12}\alpha_{11}^*),\\
B'_5 &= 2B_6-B_5,\\
B_6 &= \tfrac{1}{2}|\alpha_{12}|^2-\tfrac{3}{2}\mathrm{Re}(\alpha_{12}\alpha_{11}^*)+\mathrm{Re}(\alpha_{12}\alpha_{10}^*),\\
B_7 &= \tfrac{1}{4}(|\alpha_{12}|^2-3|\beta_{11}|^2-3|\alpha_{11}|^2+2|\alpha_{10}|^2).
\end{aligned} \tag{14c}$$

One notes, as is expected, that the deuteron polarisation of first and second rank gives rise, respectively, to the imaginary and real parts of products of matrix elements.

Each B can in principle be obtained by analysing the angular distributions from two sets of values of $\mathbf{Q}$ and Q_{ij}. A knowledge of B_3 would immediately give Im $(\alpha_0\beta_{11}^*)$ and lead to an estimate of β_{11}.

Recent experimental work by Pondrom [10]) at ≈ 700 keV has shown that at a lab angle of 45° the coefficient of Q_y is probably small. This may suggest that β_{11} is small although more experimental data is needed to resolve this question.

A knowledge of B_i would provide eight linear equations for the fourteen unknowns. These latter quantities are not independent, being connected by the equations

$$[\mathrm{Re}(\alpha_{11}\alpha_{12}^*)]^2+[\mathrm{Im}(\alpha_{11}\alpha_{12}^*)]^2 = |\alpha_{11}|^2|\alpha_{12}|^2, \tag{15}$$

and similar cases. If β_{11} and β_2 are negligible, and can indeed be equated to zero, then we require to solve for the nine combinations which appear in the equations for B_i. To do this, we have seven equations and, in addition, there are equations of type (15). Thus, these equations, may be solved in principle; however, the non-linearity of eq. (15) gives rise to non-unique solutions.

5. Polarisation of the Triton or He^3

It has been pointed out by Cini [11]) that we can obtain more information simply by measuring the polarisation of the He^3 (or H^3) which is emitted. This can be seen by merely interchanging the role of outgoing and residual particles and noting that we obtain the same formal expression for the polarisation. The matrix elements, however, have a different meaning since they are now associated with an alternate coupling to form the channel spin. The effect is that each of the terms in the equation for B_2 is multiplied by $(-1)^{S_2-S'_2}$. Thus, as found by Cini, the angular distribution in this case is given by eq. (5) with $\mathbf{n}$ now defined in terms of the momentum vector of the He^3 (or H^3),

and with B_2 replaced by B'_2, where

$$\begin{aligned} B'_2 = & -\tfrac{3}{2}\sqrt{2}\,\mathrm{Im}(\alpha_{11}\beta_{11}^*)+3\,\mathrm{Im}(\alpha_{11}\alpha_{12}^*) \\ & \tfrac{3}{2}\sqrt{2}\,\mathrm{Im}(\beta_{11}\alpha_{12}^*)+2\,\mathrm{Im}(\alpha_{10}\alpha_{12}^*)+\tfrac{10}{3}\sqrt{5}\,\mathrm{Im}(\alpha_0\beta_2{}^*). \end{aligned} \tag{5d}$$

By comparing the experimental values of B_2 and B'_2 we may obtain an estimate of the validity of the approximation of putting $\beta_{11} = 0$.

6. Double Polarisation Measurements

For a complete evaluation of the reaction matrix it is necessary that we perform double polarisation measurements. We have considered two possibilities, namely, either we measure both outgoing polarisations or we use a polarised deuteron beam and measure the polarisation of the outgoing nucleon.

6.1. MEASUREMENT OF BOTH OUTGOING POLARISATIONS

We measure both polarisations in the coordinate system of the outgoing nucleon, denoting by $\mathbf{P}$ and $\boldsymbol{\Pi}$ the polarisation efficiency of the detectors of the outgoing nucleon and H^3 (or He^3), respectively. We assume the y axis is along $-\mathbf{n}$. The angular distribution now becomes

$$\begin{aligned} W(\theta) = & \tfrac{1}{36}\lambda^2\{A+CP_2(\cos\theta)+zP_2{}^2(\cos\theta)T_a \\ & +xP_2{}^1(\cos\theta)T_y-yP_2{}^1(\cos\theta)(\mathbf{P}+\boldsymbol{\Pi})\cdot\mathbf{n} \\ & +P_2{}^1(\cos\theta)[(\mathbf{P}-\boldsymbol{\Pi})\cdot\mathbf{n}a+\mathbf{P}\times\boldsymbol{\Pi}\cdot\mathbf{n}b]\}, \end{aligned} \tag{16}$$

where

$$T_a = P_x\Pi_x-P_y\Pi_y, \qquad T_b = P_z\Pi_z, \qquad T_y = P_z\Pi_x+\Pi_zP_x.$$

Furthermore, we have

$$\begin{aligned} A = & (1+\tfrac{1}{3}\mathbf{P}\cdot\boldsymbol{\Pi})(5|\alpha_{12}|^2+3|\alpha_{11}|^2+|\alpha_{10}|^2) \\ & +(1-\mathbf{P}\cdot\boldsymbol{\Pi})(3|\beta_{11}|^2+|\alpha_0|^2) \\ & +2(T_a-2T_b)(-\tfrac{1}{6}|\alpha_{12}|^2+\tfrac{1}{2}|\alpha_{11}|^2-\tfrac{1}{3}|\alpha_{10}|^2), \\ C = & (1-\mathbf{P}\cdot\boldsymbol{\Pi})(-3|\beta_{11}|^2+10\,\mathrm{Re}(\alpha_2\alpha_0{}^*)) \\ & +(1+\tfrac{1}{3}\mathbf{P}\cdot\boldsymbol{\Pi})(\tfrac{7}{2}|\alpha_{12}|^2+\tfrac{3}{2}|\alpha_{11}|^2+9\,\mathrm{Re}(\alpha_{12}\alpha_{11}^*) \\ & +4\,\mathrm{Re}(\alpha_{12}\alpha_{10}^*))+2(T_a-2T_b)(-\tfrac{5}{2}|\alpha_{12}|^2+\tfrac{1}{4}|\alpha_{11}|^2 \\ & +\tfrac{1}{6}\sqrt{5}\,\mathrm{Re}(\alpha_{12}\alpha_{11}^*)-\tfrac{4}{3}\,\mathrm{Re}(\alpha_{12}\alpha_{10}^*)), \\ z = & -\tfrac{11}{12}|\alpha_{12}|^2-\tfrac{3}{4}|\alpha_{11}|^2+\tfrac{1}{6}\sqrt{5}\,\mathrm{Re}(\alpha_{11}\alpha_{12}^*), \\ x = & -|\alpha_{12}|^2+\tfrac{1}{3}\sqrt{5}\,\mathrm{Re}(\alpha_{12}\alpha_{11}^*)-\mathrm{Re}(\alpha_{12}\alpha_{10}^*), \\ y = & 3\,\mathrm{Im}(\alpha_{12}\alpha_{11}^*)+2\,\mathrm{Im}(\alpha_{12}\alpha_{10}^*)+20\sqrt{5}\,\mathrm{Im}(\beta_2\alpha_0{}^*) \\ a = & \tfrac{3}{2}\sqrt{2}\,\mathrm{Im}\,(\alpha_{12}\beta_{11}^*+\alpha_{11}\beta_{11}^*) \\ b = & \tfrac{3}{2}\sqrt{2}\,\mathrm{Re}\,(\alpha_{12}\beta_{11}^*+\alpha_{11}\beta_{11}^*). \end{aligned}$$

This experiment gives seven further quantities involving the real parts but only two involving the imaginary parts. Thus, together with the deuteron polarisation, there would be sufficient information to determine uniquely the real parts of products which occur. We would, however, only have three experimental quantities for the four imaginary parts but equations of the type (15) would determine them, although possibly not uniquely.

6.2. POLARISATION OF THE OUTGOING NUCLEON USING A POLARISED DEUTERON BEAM

With the conventions of refs. [7, 9]), we denote by $\mathbf{Q}$, Q_{ij} and $\mathbf{P}$ the vector and tensor polarisation of the deuteron beam, and the polarisation sensitivity of the detectors of the outgoing nucleons, respectively. The angular distribution can then be written as

$$W(\theta) = W_0(\theta)+W_1(\theta)+W_2(\theta)+W_3(\theta), \tag{17}$$

where $W_0(\theta)$ is the unpolarised angular distribution. The quantity $W_1(\theta)$ denotes the additional contribution when measurement is made in the outgoing polarisation with no incoming polarisation. The quantity $W_2(\theta)$ gives the addition arising from an incident polarised beam with polarisation insensitive detectors, while $W_3(\theta)$ involves both the incoming and outgoing polarisations. We put $Q_{yz} = Q_{xy} = Q_x = Q_z = P_z = P_x = 0$. In terms of the $d^k_{\kappa_2\kappa_1}(\theta)$ defined by Rose [12]), we define functions $\delta^k_{1\kappa_1}(\theta)$, by

$$\delta^k_{1\kappa_1}(\theta) = d^k_{1\kappa_1}(\theta)-(-1)^k d^k_{-1\kappa_1}(\theta). \tag{18}$$

An alternative definition can be obtained using the formula

$$d^k_{\kappa_2\kappa_1}(\theta) = (-1)^{k-\kappa_1} d^k_{-\kappa_2\kappa_1}(\pi-\theta),$$

thus we have

$$\delta^k_{1\kappa_1}(\theta) = d^k_{1\kappa_1}(\theta)-(-1)^{\kappa_1} d^k_{1\kappa_1}(\pi-\theta). \tag{18a}$$

In terms of these quantities, W_3 is given by

$$\begin{aligned} W_3 = {} & \tfrac{1}{36}\lambda^2[P_y Q_y\{A_1\delta^1_{11}(\theta)+A_2\delta^2_{11}(\theta) \\ & +A_3\delta^3_{11}(\theta)\}+P_y Q_{zz}\{A_4\delta^1_{11}(\theta)+A_5\delta^2_{11}(\theta) \\ & +A_6\delta^3_{11}(\theta)\}-Q_{zz}P_y P_2{}^1(\cos\theta)A_7 \\ & +\tfrac{1}{6}P_y(Q_{xx}-Q_{yy})\{A_8\delta^2_{12}(\theta)+A_9\delta^3_{12}(\theta)\}], \end{aligned} \tag{19}$$

where, considering s and p waves only,

$$A_1 = \tfrac{67}{5}|\alpha_{12}|^2 - \tfrac{9}{8}\mathrm{Re}(\alpha_{10}\alpha_{11}^*) - \tfrac{1}{4}\sqrt{2}\,\mathrm{Re}(\alpha_{10}\beta_{11}^*) - \tfrac{289}{160}\,\mathrm{Re}\,(\alpha_{10}\alpha_{12}^*) + \tfrac{27}{80}\sqrt{2}\,\mathrm{Re}(\beta_{11}\alpha_{12}^*),$$

$$A_2 = -\tfrac{27}{40}\,\mathrm{Re}(\alpha_{10}\alpha_{12}^*) + \frac{9\sqrt{2}}{80}\,\mathrm{Re}(\alpha_{11}\beta_{11}^*) - \tfrac{9}{8}\,\mathrm{Re}(\alpha_{11}\alpha_{12}^*) + \tfrac{9}{8}\sqrt{2}\,\mathrm{Re}(\beta_{11}\alpha_{12}^*),$$

$$A_3 = \tfrac{81}{10}|\alpha_{12}|^2 - \tfrac{49}{1000}\,\mathrm{Re}(\alpha_{11}\alpha_{12}^*) - \tfrac{21}{50}\sqrt{2}\,\mathrm{Re}(\beta_{11}\alpha_{12}^*),$$

$$A_4 = \tfrac{1}{4}\mathrm{Im}(\alpha_{10}\alpha_{11}^*)t + \sqrt{2}\,\mathrm{Im}(\alpha_{10}\beta_{11}^*) + \tfrac{17}{40}\,\mathrm{Im}(\alpha_{11}\alpha_{12}^*) - \tfrac{11}{20}\sqrt{2}\,\mathrm{Im}(\beta_{11}\alpha_{12}^*),$$

$$A_5 = \tfrac{3}{20}\mathrm{Im}(\alpha_{10}\alpha_{12}^*) - \tfrac{3}{2}\sqrt{2}\,\mathrm{Im}\,(\alpha_{11}\beta_{11}^*) - \tfrac{3}{4}\,\mathrm{Im}(\alpha_{11}\alpha_{12}^*) + \tfrac{3}{4}\sqrt{2}\,\mathrm{Im}(\beta_{11}\alpha_{12}^*),$$

$$A_6 = \tfrac{2}{5}\sqrt{2}\,\mathrm{Im}(\beta_{11}\alpha_{12}^*),$$

$$A_7 = \tfrac{9}{8}\sqrt{2}\,\mathrm{Im}(\alpha_{11}\beta_{11}^*) + \tfrac{3}{8}\,\mathrm{Im}(\alpha_{11}\alpha_{12}^*) - \tfrac{3}{8}\sqrt{2}\,\mathrm{Im}(\beta_{11}\alpha_{12}^*),$$

$$A_8 = \tfrac{27}{4}\sqrt{2}\,\mathrm{Im}(\alpha_{11}\beta_{11}^*) - \tfrac{9}{4}\,\mathrm{Im}(\alpha_{11}\alpha_{12}^*) + \tfrac{9}{4}\sqrt{2}\,\mathrm{Im}(\beta_{11}\alpha_{12}^*),$$

$$A_9 = \tfrac{3}{5}\sqrt{5}\,\mathrm{Im}(\beta_{11}\alpha_{12}^*).$$

One notes the appearance of three new combinations involving real parts and six involving imaginary parts. We have further introduced into the equations the real and imaginary parts of $\alpha_{10}\alpha_{11}^*$ and $\alpha_{10}\beta_{11}^*$. Hence this experiment would enable the imaginary parts to be determined unambiguously, but the real parts would possibly be non-unique by virtue of eq. (15).

7. Conclusion

If we believe the recent nucleon polarisation measurement of Kane, it would be necessary to include a sizeable singlet — triplet spin transition. These are expected to be large if the internucleon $\mathbf{L}\cdot\mathbf{S}$ potential is large while the triplet-singlet transitions would be expected to be smaller. To test this latter result, we would like to compare the H^3 (or He^3) polarisation with that of the nucleon in identical experiments, or to measure the effect of using vector polarised deuterons. It does not seem possible to assess the importance of the assumptions made without further explicit calculation.

The use of polarised deuterons leads to further information concerning the reaction matrix elements, principally about the real parts of bilinear combinations. If the quantity β_{11} is small there is some hope of determining all the elements of the reaction matrix although further physical assumptions may be necessary to remove all ambiguities. The magnitude of β_{11} is most readily estimated by measurement of the triton (or He^3) polarisation or by use of vector polarised deuterons. A double polarisation measurement does not lead to a completely unambiguous evaluation for $E_D \lesssim 1$ MeV although two types of such measurements will suffice.

References

1) G. Preston, P. F. D. Shaw and S. A. Young, Proc. Roy. Soc. Lond. **226** (1954) 206;
P. R. Chagnon and G. E. Owen, Phys. Rev. **101** (1956) 1798;
J. C. Fuller, W. E. Dance and D. C. Ralph, Phys. Rev. **108** (1958) 91
2) F. M. Beiduk, J. R. Pruett and E. J. Konopinski, Phys. Rev. **77** (1950) 622, 628
3) R. J. Blin-Stoyle, Proc. Phys. Soc. Lond. **64** (1951) 700, **65** (1952) 949;
M. Fierz, Helv. Phys. Acta **25** (1952) 629
4) E. Jahnke and F. Ehmde, Tables of functions (Dover Publications, New York, 1945)
5) P. P. Kane, Nuclear Physics **10** (1957) 429
6) F. M. McCormac, M. F. Steuer and F. L. Hereford, Phys. Rev. **104** (1956) 718;
I. I. Levintov, A. V. Miller and V. N. Shamshev, Nuclear Physics **3** (1957) 221 and 237;
P. S. Dubbeldam, C. C. Jonker and H. J. Boersma, Nuclear Physics **15** (1960) 452;
P. J. Pasma. Nuclear Physics **6** (1958) 141
7) S. Devons and L. J. B. Goldfarb, Handbuch der Physik (Springer Verlag, Berlin, 1958) Vol. XLII
8) A. R. Edmonds, Angular momentum in quantum mechanics (Princeton University Press, Princeton, 1957)
9) L. J. B. Goldfarb, Nuclear Physics **7** (1958) 622;
L. J. B. Goldfarb and J. R. Rook, Nuclear Physics **12** (1959) 494
10) L. Pondrom, private communication
11) M. Cini, Nuovo Cim. **8** (1952) 1007
12) M. E. Rose, Elementary theory of angular momentum (John Wiley and Sons, New York, 1957)

8.B

Nuclear Physics **27** (1961) 94—102; © *North-Holland Publishing Co., Amsterdam*

Not to be reproduced by photoprint or microfilm without written permission from the publisher

INTERPRETATION OF ISOBARIC MULTIPLETS IN TERMS OF THE SPACE-TIME REFLECTION GROUP

H. SOKOLIK

Magnetic Laboratory of the Academy of Sciences, Moscow, USSR

Received 14 December 1960

Abstract: The paper is concerned with a mathematical interpretation of Goldansky's scheme [1]). The number of spinor and scalar representations of the general Lorentz group is shown to be equal to the total number of mesons and baryons of the Gell-Mann scheme.

1. Introduction

The present paper deals with the classification of elementary particles according to the representations of the general Lorentz group $\mathscr{L}$, i.e., the direct product of the local Lorentz group $\mathscr{L}^+$ and the group of space-time reflections defined by T, P, I-operators corresponding to time, space and space-time reflections, respectively.

Elaborating upon the approach of refs. [2–5]) we shall use new ("anomalous") reflection group representations, defined, in contrast to the ordinary representations, by commuting T, P, I in the spinor case and by anticommuting T, P, I in the scalar and tensor cases.

Let a representation of $\mathscr{L}$ be determined by the weight numbers $(j_1 j_2)$ and $(j_2 j_1)$, where $(j_1 j_2)$ and $(j_2 j_1)$ are transformed into each other via T and P-reflections, (jj) being invariant with respect to the ordinary representations of the reflection group. At the same time, in terms of a more general theory, two (jj)-representations can be regarded as different and be transformed into each other with T, P-operators. This doubling of dimensionality can be interpreted [4, 6–8]) as the introduction of an isobaric spin. Our aim is to interpret the doublets of spinor and scalar particles in terms of 8-component "anomalous" spinors and 2-component "anomalous" scalars respectively.

2. Spinor Representations

According to ref. [9]) representations of $\mathscr{L}$ satisfy the following conditions:

$$\mathrm{TP} = \varepsilon_1 \mathrm{I}, \qquad \mathrm{PI} = \varepsilon_2 \mathrm{T}, \qquad \mathrm{TI} = \varepsilon_3 \mathrm{P}, \tag{1}$$

where $\varepsilon_i = \pm 1$ (the Wigner time reflection being of the form $\mathrm{T}_0 = \mathrm{TC}$).

It was shown in ref. [9]) that

$$\begin{aligned}&[M_{4j}, \mathrm{T}]_+ = [M_{4j}, \mathrm{P}]_+ = 0, \qquad [M_{4j}, \mathrm{I}]_- = [M_{ij}, \mathrm{I}]_- = 0,\\ &[M_{ij}, \mathrm{T}]_- = [M_{ij}, \mathrm{P}]_- = 0,\end{aligned} \tag{2}$$

where $M_{\alpha,\beta}$ ($\alpha, \beta = 1, 2, 3, 4$) are the generators of the local Lorentz group $\mathscr{L}^+$.

Substituting the expressions for $M_{\alpha,\beta}$ obtained in ref. [9]) into (2) and making use of the Schur Lemma [9]), we obtain

$$\begin{aligned}\mathrm{T} &= \begin{bmatrix} 0 & (-1)^{[l]+1} \\ (-1)^{[l]} & 0 \end{bmatrix},\\ \mathrm{P} &= \begin{bmatrix} 0 & (-1)^{[l]} \\ (-1)^{[l]} & 0 \end{bmatrix},\end{aligned} \tag{3}$$

(or vice versa) where $j_1+j_2 \geqq l \geqq |j_1-j_2|$ and 1 is a $(2l+1)\times(2l+1)$ unit matrix.

Hence it is clear that there can be only two classes:

a) proper representations determined by commuting T, P, I,

$$\mathrm{T} = \varepsilon_1 \begin{bmatrix} 0 & (-1)^{[l]} \\ (-1)^{[l]} & 0 \end{bmatrix}, \quad \mathrm{P} = \varepsilon_2 \begin{bmatrix} 0 & (-1)^{[l]} \\ (-1)^{[l]} & 0 \end{bmatrix},$$

$$\mathrm{TP} = \varepsilon_3 \mathrm{I},$$

$$\mathrm{T} = \eta_1 \begin{bmatrix} 0 & (-1)^{[l]+1} \\ (-1)^{[l]} & 0 \end{bmatrix}, \quad \mathrm{P} = \eta_2 \begin{bmatrix} 0 & (-1)^{[l]+1} \\ (-1)^{[l]} & 0 \end{bmatrix}, \tag{4}$$

$$\mathrm{I} = \eta_3 \begin{bmatrix} -1 & 0 \\ 0 & -1 \end{bmatrix};$$

b) projective representations [2]) given by

$$\mathrm{T} = \theta_1 \begin{bmatrix} 0 & (-1)^{[l]+1} \\ (-1)^{[l]} & 0 \end{bmatrix}, \quad \mathrm{P} = \theta_2 \begin{bmatrix} 0 & (-1)^{[l]} \\ (-1)^{[l]} & 0 \end{bmatrix},$$

$$\mathrm{TP} = \theta_3 \mathrm{I},$$

$$\mathrm{T} = \xi_1 \begin{bmatrix} 0 & (-1)^{[l]} \\ (-1)^{[l]} & 0 \end{bmatrix}, \quad \mathrm{P} = \xi_2 \begin{bmatrix} 0 & (-1)^{[l]+1} \\ (-1)^{[l]} & 0 \end{bmatrix}, \tag{5}$$

$$\mathrm{I} = \xi_3 \begin{bmatrix} 1 & 0 \\ 0 & -1 \end{bmatrix},$$

where $\varepsilon, \eta, \theta, \xi$ are the real or imaginary unit.

In the case of a spinor representation of $\mathscr{L}$ we can obtain from (4), (5) four different representations according to which the spinors (ξ_1, ξ_2); $(\xi_{\dot{1}}, \xi_{\dot{2}})$ are

transformed as follows:

$$\mathrm{T}=\gamma_4, \qquad \mathrm{P}=\gamma_4\gamma_5, \qquad \mathrm{I}=\gamma_5, \tag{6}$$

$$\mathrm{T}=i\gamma_5\gamma_4, \qquad \mathrm{P}=i\gamma_4, \qquad \mathrm{I}=\gamma_5, \tag{7}$$

$$\mathrm{T}=\gamma_4, \qquad \mathrm{P}=i\gamma_4, \qquad \mathrm{I}=i1, \tag{8}$$

$$\mathrm{T}=i\gamma_4\gamma_5, \qquad \mathrm{P}=\gamma_4\gamma_5, \qquad \mathrm{I}=i1, \tag{9}$$

with $j_1=\frac{1}{2}$, $j_2=0$.

The factors ε, η, θ, ξ are chosen so that after substituting (6)—(9) into the well-known expressions for a 4-vector

$$x_1=\xi_1\xi_{\dot{1}}+\xi_2\xi_{\dot{2}}, \qquad x_2=\xi_1\xi_{\dot{2}}+\xi_2\xi_{\dot{1}},$$
$$x_3=\xi_1\xi_{\dot{1}}-\xi_2\xi_{\dot{2}}, \qquad x_4=\xi_1\xi_{\dot{2}}-\xi_{\dot{2}}\xi_1,$$

we obtain the corresponding reflections

$$x'_i=-x_i, \qquad x'_4=x_4(\mathrm{P}), \qquad x'_i=x_i, \qquad x_4'=-x_4(\mathrm{T}), \qquad x'_\alpha=-x_\alpha(\mathrm{I}).$$

It follows from (6)—(10) and (4), (5) that there can be no other spinor representations.

It will be noted that (6) and (7) as well as (8) and (9) are related by the unitary transformation [10])

$$U=\exp\left[\tfrac{1}{4}i\pi\gamma^5\right]. \tag{10}$$

Since arbitrary representations of $\mathscr{L}$ can be determined by a direct product of spinor representations (6)—(9) it seems convenient to use spinor notations for this purpose [4]).

The basis vectors of the representations (j_1j_2) (j_2j_1) are determined by monomials [11])

$$\begin{aligned} Z^{j_1j_2p_1p_2}_{m_1m_2}&=\xi_1^{j_1+m_1}\xi_2^{j_1-m_1}\xi_{\dot{1}}^{j_2+m_2}\xi_{\dot{2}}^{j_2-m_2}\times(\xi_1\xi_2'-\xi_2\xi'_1)^{p_1}(\xi_{\dot{1}}\xi'_{\dot{2}}-\xi_{\dot{2}}\xi'_{\dot{1}})^{p_2},\\ Z^{j_2j_1p_2p_1}_{m_2m_1}&=\xi_1^{j_1+m_1}\xi_2^{j_1-m_1}\xi_{\dot{1}}^{j_2+m_2}\xi_{\dot{2}}^{j_2-m_2}\times(\xi_1\xi'_2-\xi_2\xi'_1)^{p_2}(\xi_{\dot{1}}\xi'_{\dot{2}}-\xi'_{\dot{2}}\xi'_{\dot{1}})^{p_1}\end{aligned} \tag{11}$$

(p_1, p_2 take on values 2,0 or 1).

According to ref. [4]) all representations of $\mathscr{L}$ can be obtained by substituting the transformations (6)—(9) of the spinors ξ, ξ' into (11):

$$\mathrm{T}=\begin{bmatrix}0&-1\\1&0\end{bmatrix}, \qquad \mathrm{P}=\begin{bmatrix}0&1\\1&0\end{bmatrix}, \qquad \mathrm{I}=\begin{bmatrix}1&0\\0&-1\end{bmatrix} \tag{12}$$

and

$$\mathrm{T}=\begin{bmatrix}0&i^{2j_2}\\(-1)^{2j_1}i^{2j_2}&0\end{bmatrix}, \qquad \mathrm{P}=\begin{bmatrix}0&(-1)^{2j_1}i^{2j_2}\\i^{2j_2}&0\end{bmatrix}, \qquad \mathrm{TP}=\mathrm{I}.$$

It will be noted that the group in question is not the full Lorentz group in the exact sense of the word, viz., $\mathscr{L}^+$ complemented by a single reflection T or

P. In fact, the space-time reflection $x'_\alpha = -x_\alpha$ can be replaced by the rotation $\exp(i\pi M_{43}) \exp(i\pi M_{21}) = -1$. The corresponding transformation for spinors will be

$$\exp[i\pi\gamma_{43}] \exp[i\pi\gamma_{21}] = \gamma_5,$$

where, in accordance with the conventional formula,

$$\gamma_{ik} = \tfrac{1}{2}[\gamma_i\gamma_k].$$

Thus, for the normal representations $\mathscr{L}$ the inversion I reduces itself to rotations (the general Lorentz group being equivalent to the full Lorentz group).

On the other hand, for (8), (9) the inversion I is given by $i1$.

This discrepancy can be accounted for, if and only if, "anomalous" representations are regarded as representations of the general Lorentz group. This points out to a more general character of $\mathscr{L}$, making it possible to introduce anomalous representations.

3. General Character of $\mathscr{L}$

Let us consider the spinor and scalar representations of $\mathscr{L}$. We shall need no other representations for our purposes, since all elementary particles have spin $\frac{1}{2}$ or zero. Let us first consider the "anomalous" scalar (0, 0); (0, 0), which may be obtained from (11) when $j_1 = j_2 = 0$, $p_1 = 1$, $p_2 = 0$, with ξ and ξ' being transformed according to normal and anomalous spinor representations respectively.

The representation is given by

$$Z^{00}_{10} = \xi_1\xi'_2 - \xi_2\xi'_1, \qquad Z^{00}_{01} = \xi_1\xi'_{\dot{2}} - \xi_2\xi'_{\dot{1}},$$

where Z^{00}_{10} and Z^{00}_{01} are transformed according to

$$\mathrm{T} = \begin{bmatrix} 0 & -1 \\ -1 & 0 \end{bmatrix}, \qquad \mathrm{P} = \begin{bmatrix} 0 & -i \\ i & 0 \end{bmatrix}, \qquad \mathrm{I} = \begin{bmatrix} i & 0 \\ 0 & -i \end{bmatrix},$$

or

$$\mathrm{T} = \begin{bmatrix} 0 & -i \\ i & 0 \end{bmatrix}, \qquad \mathrm{P} = \begin{bmatrix} 0 & 1 \\ 1 & 0 \end{bmatrix}, \qquad \mathrm{I} = \begin{bmatrix} i & 0 \\ 0 & -i \end{bmatrix}.$$

A more convenient form is

$$\begin{aligned} \mathrm{T} &= \begin{bmatrix} 1 & 0 \\ 0 & -1 \end{bmatrix}, \qquad \mathrm{P} = \begin{bmatrix} 0 & -i \\ i & 0 \end{bmatrix}, \qquad \mathrm{I} = \begin{bmatrix} 0 & i \\ i & 0 \end{bmatrix}, \\ \mathrm{T} &= \begin{bmatrix} 0 & -i \\ i & 0 \end{bmatrix}, \qquad \mathrm{P} = \begin{bmatrix} 1 & 0 \\ 0 & -1 \end{bmatrix}, \qquad \mathrm{I} = \begin{bmatrix} 0 & i \\ i & 0 \end{bmatrix}, \end{aligned} \tag{13}$$

where

$$\varphi = \begin{bmatrix} \xi' \, \mathrm{P}_1 \, \xi \\ \xi' \, \mathrm{P}_2 \, \xi \end{bmatrix}, \tag{14}$$

with

$$\mathrm{P}_1 = \begin{bmatrix} 0 & i\sigma_2 \\ i\sigma_2 & 0 \end{bmatrix}, \qquad \mathrm{P}_2 = \begin{bmatrix} 0 & -i\sigma_2 \\ i\sigma_2 & 0 \end{bmatrix}. \tag{15}$$

The direct product of (14) and (15) and the normal spinor representations (6), (7) yield

$$\mathrm{T} = \begin{bmatrix} \gamma_4 & 0 \\ 0 & -\gamma_4 \end{bmatrix}, \qquad \mathrm{P} = \begin{bmatrix} 0 & -i\gamma_5\gamma_4 \\ i\gamma_5\gamma_4 & 0 \end{bmatrix}, \qquad \mathrm{I} = \begin{bmatrix} 0 & i\gamma_5 \\ i\gamma_5 & 0 \end{bmatrix}, \tag{16}$$

$$\mathrm{T} = \begin{bmatrix} 0 & -\gamma_5\gamma_4 \\ \gamma_5\gamma_4 & 0 \end{bmatrix}, \qquad \mathrm{P} = \begin{bmatrix} i\gamma_4 & 0 \\ 0 & -i\gamma_4 \end{bmatrix}, \qquad \mathrm{I} = \begin{bmatrix} 0 & i\gamma_5 \\ i\gamma_5 & 0 \end{bmatrix}, \tag{17}$$

$$\mathrm{T} = \begin{bmatrix} i\gamma_5\gamma_4 & 0 \\ 0 & -i\gamma_5\gamma_4 \end{bmatrix}, \qquad \mathrm{P} = \begin{bmatrix} 0 & -\gamma_4 \\ \gamma_4 & 0 \end{bmatrix}, \qquad \mathrm{I} = \begin{bmatrix} 0 & i\gamma_5 \\ i\gamma_5 & 0 \end{bmatrix}, \tag{18}$$

$$\mathrm{T} = \begin{bmatrix} 0 & -i\gamma_4 \\ i\gamma_4 & 0 \end{bmatrix}, \qquad \mathrm{P} = \begin{bmatrix} \gamma_5\gamma_4 & 0 \\ 0 & -\gamma_5\gamma_4 \end{bmatrix}, \qquad \mathrm{I} = \begin{bmatrix} 0 & i\gamma_5 \\ i\gamma_5 & 0 \end{bmatrix}. \tag{19}$$

The 8×8 anomalous representations (16)—(19) can be reduced to two 4×4 anomalous representations (8) or (9).

Introducing the unitary transformation

$$U = \frac{1}{\sqrt{2}} \begin{bmatrix} 1 & \gamma_5 \\ 1 & -\gamma_5 \end{bmatrix}, \tag{19'}$$

it can, indeed, be shown that the transformed matrices (16) are of the form (8):

$$\mathrm{T} = \begin{bmatrix} \gamma_4 & 0 \\ 0 & \gamma_4 \end{bmatrix}, \qquad \mathrm{P} = \begin{bmatrix} i\gamma_4 & 0 \\ 0 & -i\gamma_4 \end{bmatrix}, \qquad \mathrm{I} = \begin{bmatrix} i1 & 0 \\ 0 & -i1 \end{bmatrix}. \tag{20}$$

It can likewise be shown that only the irreducible 8-component Dirac equation

$$\Gamma_i(\partial\Psi/\partial x_i) + im\Psi = 0,$$

where

$$\Gamma_i = \begin{bmatrix} 0 & \gamma_i \\ \gamma_i & 0 \end{bmatrix}, \quad \text{or} \quad \Gamma_i = \begin{bmatrix} 0 & -\gamma_i \\ \gamma_i & 0 \end{bmatrix},$$

is invariant with respect to (20). Similar results can be obtained for (17), (18) and (19).

In ref. [9]) it is shown that the invariance condition

$$\Gamma_i \frac{\partial}{\partial x_i} \psi + im\Psi = 0$$

is

$$[\mathrm{T}, \Gamma_4]_+ = [\Gamma_i, \mathrm{P}]_+ = 0, \quad [\Gamma_4, \mathrm{P}]_- = [\Gamma_i, \mathrm{T}]_- = 0, \quad [\Gamma_\alpha, \mathrm{I}]_+ = 0. \quad (21)$$

It can easily be shown that in the case of (16) and (18)

$$\Gamma_i = \begin{bmatrix} 0 & \gamma_5\gamma_i \\ \gamma_5\gamma_i & 0 \end{bmatrix} \quad \text{or} \quad \begin{bmatrix} 0 & -\gamma_5\gamma_i \\ \gamma_5\gamma_i & 0 \end{bmatrix}$$

satisfy the conditions (21). In the case of (17) and (19) the invariance conditions are fulfilled for

$$\Gamma_i = \begin{bmatrix} 0 & \gamma_i \\ \gamma_i & 0 \end{bmatrix} \quad \text{or} \quad \Gamma_i = \begin{bmatrix} 0 & -\gamma_i \\ \gamma_i & 0 \end{bmatrix}.$$

In the representation (16)—(19) the invariant spinor equations are given as $\Psi = \varphi \times \psi$,

$$\Gamma_i = \begin{bmatrix} \gamma_5\gamma_i & 0 \\ 0 & \gamma_5\gamma_i \end{bmatrix},$$

and in the cases (17) and (18) as

$$\begin{bmatrix} \gamma_i & 0 \\ 0 & \gamma_i \end{bmatrix},$$

and in this representation obviously satisfy the conditions (21).

It is noteworthy that though the irreducible anomalous spinors are of the 4-component kind (contrary to the assertion of ref. [8])) only the 8-component anomalous spinor is given by a relativistic wave equation of the type

$$\Gamma_i \frac{\partial}{\partial x_i} \Psi + im\Psi = 0.$$

Hence it follows that the real isodoublets with $m \neq 0$ should be represented by 8-component spinors.

It will be noted that the 4-component anomalous spinors can be interpreted in physical terms by introducing a new class of relativistic equations. For this purpose let us introduce a method similar to the Majorana theory [14]).

As was shown above, the 4-component representations by which transformation is made of the 4-component anomalous spinors forming the 8-component spinor Ψ,

$$\mathrm{T} = \begin{bmatrix} i\gamma_5\gamma_4 & 0 \\ 0 & i\gamma_5\gamma_4 \end{bmatrix}, \quad \mathrm{P} = \begin{bmatrix} \gamma_5\gamma_4 & 0 \\ 0 & -\gamma_5\gamma_4 \end{bmatrix}, \quad \Psi = \begin{bmatrix} \psi_1 \\ \psi_2 \end{bmatrix},$$

are connected through the transformation

$$\psi_2 = B\psi_1^*,$$

where

$$B = i\gamma_5\gamma_2, \qquad B[i\gamma_5\gamma_4]^*B^{-1} = i\gamma_5\gamma_4, \qquad B[\gamma_5\gamma_4]^*B^{-1} = -\gamma_5\gamma_4.$$

Thus the anomalous spinors $\psi_1\psi_2$ are analogues to the dotted and the undotted spinors of ref. [9]) related in the following way:

$$\xi_\tau^{\cdot} = C\xi_\tau^*, \qquad \text{where} \qquad C = \begin{pmatrix} 0 & 1 \\ -1 & 0 \end{pmatrix}.$$

Using $\psi_2 = B\psi_1^*$, we obtain

$$\gamma_i \frac{\partial}{\partial x_i}\psi + imB\psi^* = 0. \tag{23}$$

Eq. (23) gives an anomalous 4-component spinor. It can easily be checked that (23) is invariant with respect to the inversions

$$\mathrm{T} = i\gamma_5\gamma_4, \qquad \mathrm{P} = \gamma_5\gamma_4$$

and with respect to the transformations $\mathscr{L}^+$.

Using the relativistic equations of the type

$$\Gamma_i \frac{\partial}{\partial x_i}\Psi + im\Gamma_0\Psi^* = 0,$$

alongside with

$$\Gamma_i \frac{\partial}{\partial x_i}\Psi + im\Psi = 0$$

makes it possible to attach a physical meaning to 4-component anomalous spinors.

The direct product of anomalous scalars[13]) and anomalous spinors is reducible and splits into a sum of 4-component normal spinors. The proof of this property is similar to the one given above. Using

$$U = \frac{1}{\sqrt{2}}\begin{bmatrix} 1 & \gamma_5 \\ 1 & -\gamma_5 \end{bmatrix},$$

we obtain

$$\mathrm{T} = \begin{bmatrix} i\gamma_5\gamma_4 & 0 \\ 0 & i\gamma_5\gamma_4 \end{bmatrix}, \quad \mathrm{P} = \begin{bmatrix} i\gamma_4 & 0 \\ 0 & i\gamma_4 \end{bmatrix}, \quad \mathrm{I} = \begin{bmatrix} \gamma_5 & 0 \\ 0 & \gamma_5 \end{bmatrix}, \quad \Gamma_i = \begin{bmatrix} \gamma_i & 0 \\ 0 & \gamma_i \end{bmatrix},$$

or unitarily equivalent reducible representations. The normal scalar representations split into the scalar ones $\mathrm{T} = \mathrm{P} = 1$ and the pseudoscalar ones $\mathrm{T} = -\mathrm{P} = 1$.

4. Isomultiplets

Using the results obtained, it is possible to assign isomultiplets to the spinor and scalar representations of $\mathscr{L}$ considered above. The over-all description of the elementary particles was given in the papers by Goldansky, Heisenberg, and others [1, 12]).

According to refs. [1, 12]), each class of elementary particles contains one isotriplet, two isodoublets and three isosinglets. In the case of leptons the triplet and one of the singlets are excluded. In the present paper triplets are replaced by pairs of doublets. Thus $\Sigma^+\Sigma^0\Sigma^-\Lambda^0$ reduces to

$$[\Sigma^+, \Sigma^0+\Lambda_0/\sqrt{2}] \quad \text{and} \quad [\Sigma^0-\Lambda^0/\sqrt{2}, \Sigma^-].$$

The hyperon singlets $Z^+(s = 1)$ and $\Omega^-(s = -3)$ predicted by the Gell-Mann scheme are given by the normal 4-component spinors (6) and (7), while $[\Sigma^+, \Sigma^0+\Lambda^0/\sqrt{2}]$, $[\Sigma^0-\Lambda^0/\sqrt{2}, \Sigma^-]$, [p, n] and $[\Xi^0, \Xi^-]$ are described by 8-component anomalous spinors. To describe π and K-mesons we use anomalous scalar doublets transformed by the representations (14) and (15).

The doublets $[K^+, K^0]$ and $[\tilde{K}^0, K^-]$ are given by φ and $C\varphi^*$, where φ is transformed according to (14), while

$$C = \begin{pmatrix} 0 & 1 \\ -1 & 0 \end{pmatrix}.$$

The transformations T′, P′ and I′ referring to $(\tilde{K}^0, K^-)$ are of the form

$$CT^*C^{-1}, \qquad CP^*C^{-1}, \qquad CI^*C^{-1}.$$

The π-mesons given by the conjugate doublets

$$(\pi^+, \pi^0+\rho^0/\sqrt{2}) \qquad \text{and} \qquad (\pi^0-\rho^0/\sqrt{2}, \pi^-)$$

(ρ_0 being the hypothetic meson singlet) are described by the scalar doublet (15) and its conjugate in a similar way. The scalar and pseudoscalar $\tilde{\xi}\xi$ and $\tilde{\xi}\gamma_5\xi$ are used for describing $\mathscr{D}^+$ and $\mathscr{D}^-$ with strangeness ± 2 respectively [1, 13]).

In the case of leptons, μ^+ and μ^- are described by one of the normal spinors ψ and its conjugate $B\psi^*$. The doublets (e^+, ν^0) and $(\tilde{\nu}^0, e^-)$ are described by the anomalous 8-component spinor Ψ and its conjugate $\bar{B}\Psi^*$, where

$$\bar{B} = \begin{bmatrix} 0 & B \\ B & 0 \end{bmatrix}.$$

The author is indebted to Acad. Zeldovitch, Prof. Ivanenko and Dr. O. Germogenova for valuable discussions and helpful suggestions.

References

1) V. Goldansky, Nuclear Physics **6** (1958) 53
2) I. Gelfand and M. Zetlin, JETP **31** (1956) 1107
3) A. Brodsky and D. Ivanenko, JETP **36** No. 4, (1959)
4) H. Sokolik, JETP **36** No 4, (1959)
5) A. Brodsky and D. Ivanenko, Nuclear Physics **13** (1959) 447
6) I. C. Taylor, Nuclear Physics **3** (1957) 606
7) McLennan, Jr., Phys. Rev. **109** (1958) 986
8) V. I. Ogievetsky and Chou Kuang-chou, Nuclear Physics **10** (1959) 235
9) I. M. Gelfand and A. Yaglom, JETP **18** (1948) 703
10) I. Schwinger, Proc. Nat. Acad. Sci, USA **44** (1958) 223
11) E. Cartan, Leçons sur la theorie de spineurs
12) W. Heisenberg *et al.*, Zs. Naturforsch. **14a** (1959) 441
13) Wang Kang Chang, IXth Intern. Conf. on High Energy Physics, Kiev, 1959
14) Z. Tokuoka, Progr. Theoret. Phys. (suppl.) **13** (1960)

2.G

Nuclear Physics **27** (1961) 103—111; © *North-Holland Publishing Co., Amsterdam*

Not to be reproduced by photoprint or microfilm without written permission from the publisher

STUDY OF THE $O^{16}(d, n)F^{17}$ REACTION

O. DIETZSCH, Y. HAMA, E. W. HAMBURGER and F. C. ZAWISLAK †

Laboratório do Acelerador Eletrostático, Departamento de Física, Faculdade de Filosofia, Ciências e Letras da Universidade de São Paulo, São Paulo, Brasil ††

Received 4 April 1961

Abstract: The $O^{16}(d, n)F^{17}$ g.s. reaction has been investigated in the energy range from threshold (1.83 MeV) to 2.4 MeV. The deuteron beam was produced by the S. Paulo Electrostatic Accelerator; the neutrons were detected by a long counter. Yield curves were obtained at 3 angles and angular distributions at 7 energies. The angular distributions are isotropic near threshold but become quite anisotropic at higher energies; they are not symmetric about 90° and are suggestive of a direct reaction mechanism. An attempt was made to explain the experimental results by stripping theory, taking the distortion of the deuteron wave by the Coulomb field into account. At low energies the calculation yields results in agreement with experiment, but at higher energies a large discrepancy exists. This disagreement appears to be related to the existence of resonances in the yield curve at the higher energies.

1. Introduction

The mechanism of deuteron stripping reactions at bombarding energies above ≈ 10 MeV is reasonably well understood [1]). For this reason these reactions have been extensively used as a tool of nuclear spectroscopy [2]). At lower deuteron energies, however, the reaction mechanism is not as well understood because Coulomb effects and the competition of compound nucleus and direct interaction processes complicate the simple picture which is valid at higher energies. The present experiment was undertaken in order to study the reaction mechanism of low energy deuteron stripping.

The $O^{16}(d, n)$ reaction is an interesting choice for several reasons. It is one of the few (d, n) reactions which has a negative Q. Consequently there exists a deuteron energy range in which only one group of neutrons is produced, eliminating the need for a neutron spectrometer. The outgoing neutrons have low energies, up to 500 keV in this experiment, so that only a few partial waves contribute to the reaction; theoretical calculations are greatly simplified thereby. Finally the closed shell structure of O^{16} makes it a favourable target for the validity of the simple theory of stripping.

Neutron thresholds and the forward yield from this reaction in the same energy range have been obtained previously by Marion *et al.* [3]).

† On leave from Instituto de Física, Universidade do Rio Grande do Sul.

†† Work supported in part by the Conselho Nacional de Pesquisas (Brasil) and by the Rockefeller Foundation.

2. Experimental Arrangement

The deuteron beam was produced by the University of São Paulo Van de Graaff Accelerator and was magnetically analysed. The target was at ≈ 7 m from the machine. A circular tantalum aperture, 8 mm in diameter and situated 4 cm before the target, defined the illuminated area of the target. Between the aperture and the target an electrostatic suppressor was placed. The current deposited on the target was integrated by a circuit of the Higginbotham type [4]). The scattering chamber was made from a 10 cm diameter copper tube with 2 mm thick walls and was 12.5 cm high. It was located above a neutron pit, 3 m from the ground.

The angular distributions and yield curves were obtained with tungsten oxide targets, prepared by heating a clean tungsten blank in an oxygen atmosphere [3]). These targets had a thickness of about 50 keV for 2 MeV deuterons. A gas target was also used, in order to determine the absolute cross section scale and the thickness of the tungsten oxide targets. It was made of a copper cylinder with a 2.5 μm nickel foil entrance window and was 2.5 cm thick. Pressures ranged from 0 to 30 mm Hg.

The neutron detector was a conventional unshielded long counter [5]). The paraffin cylinder was 20 cm in diameter, 33 cm long and had eight 2 cm holes in its front face. It could be rotated about the target. Most of the data were taken with the front face of the counter at 31 cm from the target, so that the total angle subtended by the counter at the target was 35°. Because of the lower efficiency of the periphery of the counter, however, the actual angular resolution probably had a half width of ≈ 10°. The variation of the efficiency of the counter as a function of neutron energy in the range 300 keV to 2 MeV was determined by measuring the 0° excitation curve and the angular distributions of the neutrons from the T(p, n)He^3 reaction and comparing the results with those of Jarvis *et al.* [6]). The efficiency is constant from 300 keV to 1 MeV and drops by 15 % from 1 MeV to 2 MeV.

The deuteron energy was measured by a generating voltmeter, calibrated [3]) by the O^{16}(d, n) thresholds at 1.830 and 2.393 MeV. The counter ratio method [7]) was used to determine the thresholds. It is felt that the energies given in this paper are accurate within ±10 keV. The stability of the machine energy is probably also within ± 10 keV.

3. Results

3.1. EXCITATION CURVES

Fig. 1 shows the yield curves obtained at the laboratory angles 0°, 60° and 120°. Also shown are background runs obtained immediately after each yield curve by substituting the target by a clean tungsten blank. No data were

taken at energies above 2.4 MeV because two neutron groups are present in that energy range and the long counter cannot distinguish them.

The data at 0° can be compared with previous work by Marion *et al.* [3]). The

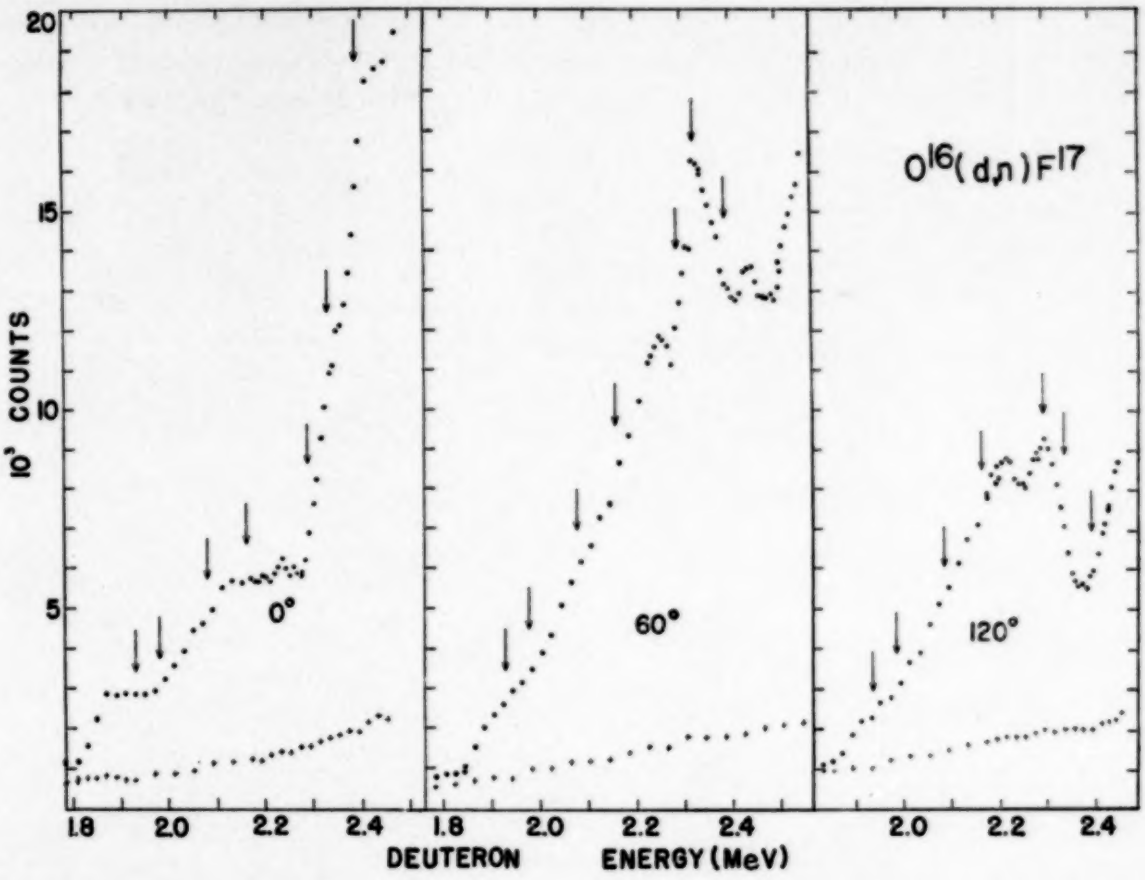

Fig. 1. Yield curves: counts per 24 μC *vs* deuteron energy, at 0°, 60° and 120° (lab. angles). Arrows indicate energies at which angular distributions were obtained. Crosses give background as measured by bombarding a clean tungsten blank. Below threshold (1.83 MeV) the background should coincide with the yield from the oxygen target. The observed difference is due to a carbon deposit on the target.

TABLE 1

Energies of the resonance peaks in MeV

Resonance	0°	60°	120°
2.22 [a])	2.23	2.25	2.21
2.34 [a])		2.33	2.29

[a]) from ref. [3]) at 0°

agreement is good. Marion *et al.* identified three resonances, at 2.22, 2.34 and 2.42 MeV, respectively. Our 0° data do not show the higher resonances probably because of target thickness effects. At 60° and 120°, however, both of the

lower resonances show up quite clearly. At 60° the third resonance, which is just above the threshold for the production of the second neutron group, was also identified.

It is interesting to note that the energies of the peaks change with angle, as shown in table 1. Such shifts are often ascribed to interference between compound nucleus and direct reactions. Since the resonances appear at all three angles they probably appear also in the total cross section (see fig. 4)

3.2. ANGULAR DISTRIBUTIONS

Angular distributions obtained at deuteron energies of 1.93, 1.98, 2.08, 2.16, 2.29, 2.33 and 239, MeV, from 0° to 150° (lab), are shown in figs. 2 and 3.

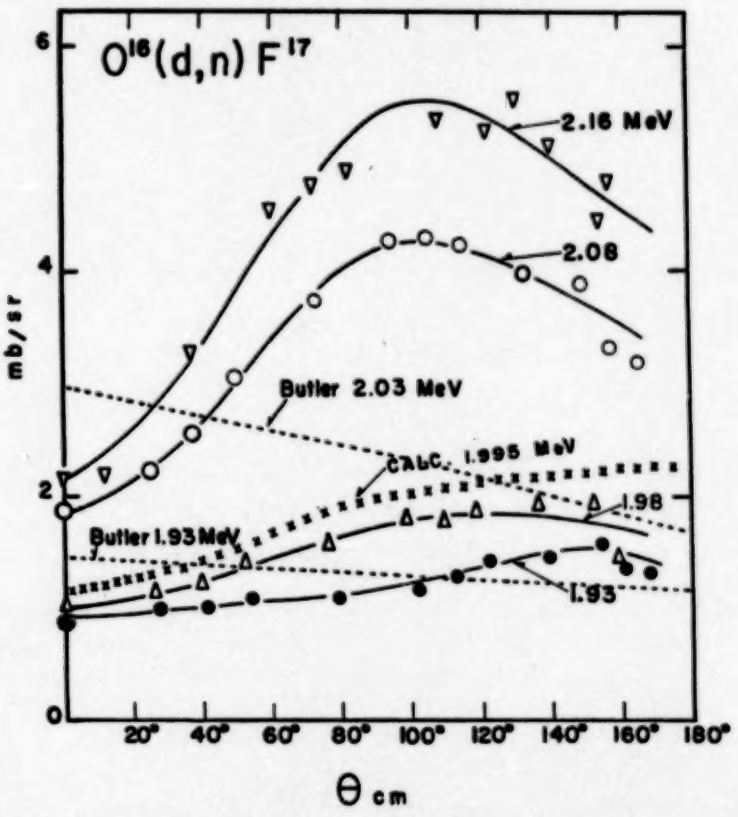

Fig. 2. Centre-of-mass differential cross sections for the O^{16}(d, n)F^{17} reaction at deuteron energies of 1.93, 1.98, 2.08 and 2.16 MeV. Curves are Legendre polynomial expansion fits to the experimental points. The curve labelled "calc." is theoretical (see text). Dashed curves are Butler curves for $E_d = 1.93$ and 2.03 MeV calculated from tables of Lubitz.

The following procedure was used to collect and process the data: At each energy alternate angular distributions were taken with the tungsten oxide target and with a tungsten blank, both at 90° to the incident beam. The reproducibility of the data (within $\approx \pm 5$ %) showed that a neutron monitor was not necessary. This procedure was repeated with the targets at 45° to the incident beam, in order to correct for the small neutron absorption in the target support.

The tungsten distributions were isotropic within ± 15 %. After background subtraction, the data were corrected for neutron scattering and absorption in the walls of the scattering chamber and in the target support. The correction was calculated from the amount of material in the different parts of the chamber and from the cross sections given by Hughes and Schwartz [8]). It was assumed that the scattered neutrons gave rise to an isotropic background. This approximation tends to overestimate the effect of the scattering. The scattered

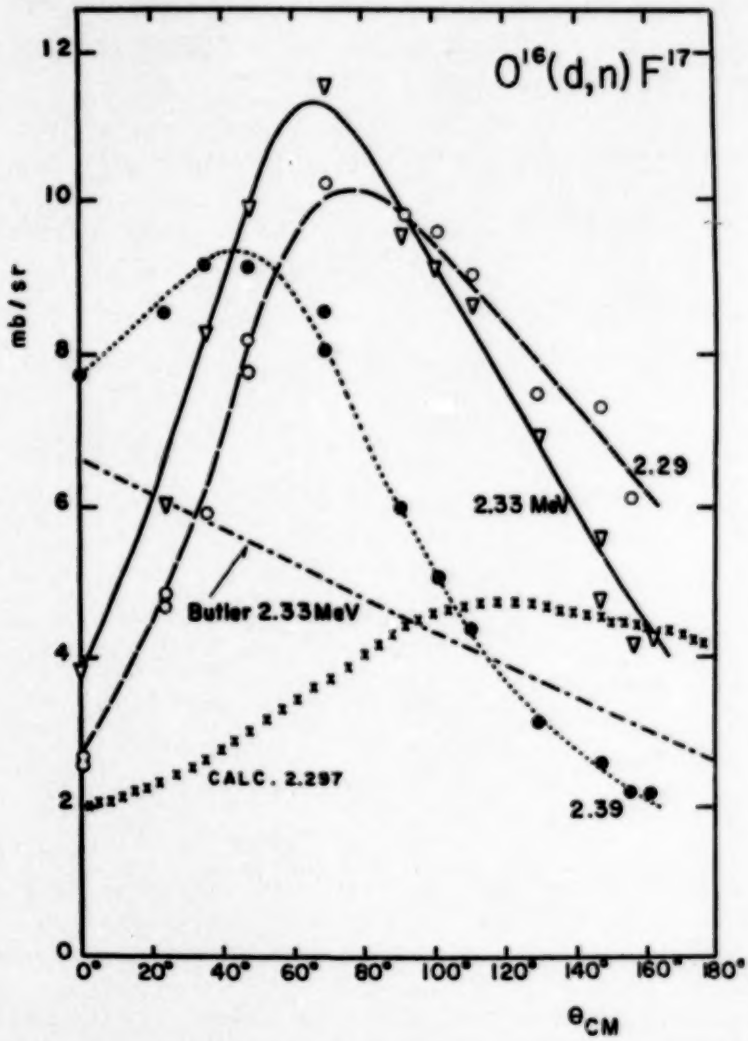

Fig. 3. Centre-of-mass differential cross sections for the O^{16}(d, n)F^{17} reaction at 3 deuteron energies near the 2.33 MeV resonance. The curve indicated by crosses is theoretical (see text). The lines are Legendre polynomial expansion fits to the experimental points. The Butler curve for E_d = 2.33 MeV is also shown.

background turned out to be from 15 % to 30 % of the total number of neutrons due to oxygen. Finally the data were transformed to the centre-of-mass system.

The experimental procedure was checked by measuring the angular distributions of the C^{12}(d, n)N^{13} reaction at 1.8 and 2.3 MeV, and comparing the results

with the work of Elwyn *et al.* [9]), obtained with time of flight techniques. In this reaction the neutron energies are larger and it is necessary to take into account, in addition to the corrections mentioned above, the variation of the counter efficiency with energy. Also the angular resolution of the counter must be considered, because the angular distribution have sharper peaks and valleys than in the O^{16}(d, n) reaction. After all corrections, our data agreed with that of Elwyn *et al.* within $\pm$ 10 % at 1.8 MeV and $\pm$ 15 % at 23. MeV.

It is estimated that relative cross sections quoted in this report are accurate to within $\pm$ 15 %, except at back angles, where the error may reach 30 %. Statistical errors were always small (< 3 %).

The relative normalization of the angular distributions in figs. 2 and 3 was obtained from the yield curves of fig. 1 after the corrections described above had been applied.

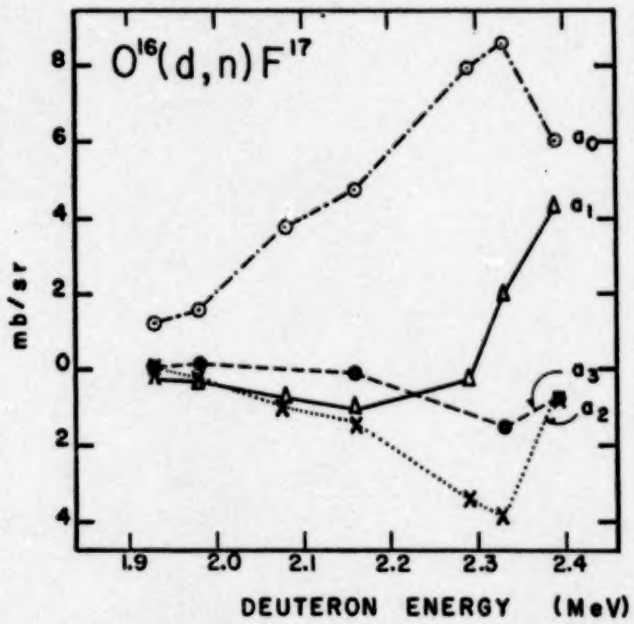

Fig. 4. Coefficients of the Legendre polynomial expansions of the angular distributions of figs. 2 and 3. The cross section is written $d\sigma/d\Omega = a_0 + a_1 P_1(\cos\theta) + a_2 P_2(\cos\theta) + a_3 P_3(\cos\theta) + a_4 P_4(\cos\theta) + a_5 P_5(\cos\theta)$. For a_4 and a_5, see text. The total cross section is proportional to a_0.

The lines drawn through the experimental points were obtained by fitting the data with expansions in Legendre polynomials up to the fifth order. The coefficients of the first four Legendre polynomials are plotted as a function of energy in fig. 4. The coefficient a_4 was always equal to a_3 within 0.05 mb/sr, while a_5 was smaller than 0.1 mb/sr always.

3.3. ABSOLUTE CROSS SECTION SCALE

Absolute cross sections were measured at deuteron energies of 2.1, 2.24 and 2.31 MeV at 0° and 60°, using a gas target filled with tank oxygen. The efficiency of the neutron counter was measured by using a calibrated 10 mc Ra

Be source as standard. It was assumed that the counter efficiency for the Ra-Be neutrons was 30 % lower than for the oxygen neutrons. The current integrator was calibrated with a source of known current. Background was found by bombarding the target at zero gas pressure, and the corrections previously described were made. The relative cross sections at the different angles and energies agreed with the solid target results. It is estimated that the absolute cross section scale is accurate within $\pm$ 30 %, due chiefly to uncertainty in the counter efficiency.

4. Discussion

None of the angular distributions is symmetric about 90°. Therefore, if the reaction proceeds via a compound nucleus, at least two levels of opposite parity must be contributing to the cross section. However, it is also possible that a direct reaction mechanism is dominant, specially in the energy region below the resonances. In particular, it is possible that the simple stripping mechanism, which is known to hold at energies of $\approx$ 10 MeV, be responsible for the angular distributions. The simple stripping formula first given by Butler [10]) can be deduced from the following basic assumptions:

(1) Plane wave Born approximation is applicable.

(2) The captured proton has a well defined angular momentum L;

(3) The outgoing neutron does not interact with the target nucleus.

(4) The reaction takes place outside of a sphere of radius R centered at the target, where R is of the order of the radius of the target. The Butler curves † for E_d = 1.93, 2.03 and 2.33 MeV are shown in figs. 2 and 3. The predicted differential cross section is approximately a linear function of angle ††. Warburton and Chase [12]) have pointed out that endothermic (d, p) and (d, n) reactions near threshold should proceed to a large extent by a stripping mechanism, but that distortion may change the angular distribution considerably from the plane wave (Butler) curves. It is clear that for the O^{16}(d, n) reaction near threshold the Butler theory does not apply.

Of the four assumptions underlying the Butler theory the one which is most clearly not applicable to low energy reactions is the plane wave approximation, i.e. the Coulomb field of the target will distort the deuteron wave.

Calculations were made to take into account the Coulomb field. The expression deduced by Tobocman [13, 14]) and by Thomas [15]) from the distorted wave Born approximation was used, but the distortion due to nuclear fields was neglected, only the Coulomb field was considered. In the notation of Tobocman

† Calculated from ref. [11]). Small curvatures near 0° and 180° have been neglected.

†† These curves show so little anisotropy compared to usual Butler curves because the transfer momentum $q = |\mathbf{K}_d - \mathbf{K}_n|$ varies very little from θ = 0° to 180° because K_n is small. Consequently the argument qR of the Bessel function $j_L(qR)$ which gives the oscillatory behaviour of the Butler curves, is almost constant.

(eqs. (1)—(4) of ref. [14]), $\alpha_\lambda = \beta_l = 0$. The neutron wave was, thus, taken to be plane. The radial integrals were calculated graphically to a precision of a few percent. Only neutron waves having orbital angular momentum up to $l_n = 3$ were considered; the contribution of $l_n = 3$ was already found to be negligible. Because of the vector coupling coefficients appearing in the expression for the cross section, the limitation on l_n also limits the angular momentum of the deuteron. The proton has $L = 2$ for the F^{17} g.s., which is a $d_{\frac{5}{2}}$ single particle state [2]).

Calculations were made at two energies chosen for convenience in interpolation in the tables of Coulomb functions [16]), 1.995 MeV and 2.297 MeV. There are two adjustable parameters in the cross section formula, the cut-off radius R and the reduced width θ^2 (in units of $3\hbar^2/2MR^2$). The results are not very sensitive to the radius R, as far as the shape of the angular distributions is concerned. θ^2 was fixed by requiring the calculated value of a_0 to agree with the experimental value given in fig. 4, at 1.995 MeV. The resulting value $\theta^2 = 0.053$ (for $R = 5$ fm), is in excellent agreement with the value [2, 17]) found at 15 MeV for the O^{16} (d, p)O^{17} reaction. The calculated angular distributions, for $R = 5$ fm, are shown in figs. 2 and 3, and the calculated values of the a_l for $R = 5$ fm and 3.5 fm are shown in table 2, together with experimental values obtained by interpolation in fig. 4.

TABLE 2

Calculated coefficients of Legendre polynomials, in mb/sr

E_d(MeV)	θ^2	a_0	a_1	a_2	a_3
1.995 exptal		1.9	−0.4	−0.4	0.1
calc $R = 5$ fm	0.053	1.9 [a])	−0.5	−0.18	−0.005
calc $R = 3.5$ fm	0.19	1.9 [a])	−0.63	−0.13	
2.297 exptal		8	0.2	−3.6	−1.3
calc $R = 5$ fm	0.053	4.0	−1.2	−0.9	0.1
calc $R = 3.5$ fm	0.19	4.3	−1.7	−0.82	

[a]) Value used for normalization to determine θ^2.

It is clear that at the lower energy the agreement with experiment is quite good, and leads one to believe that the assumptions made in the calculation are correct. At the higher energy the calculated angular distribution disagrees completely with experiment, both in absolute magnitude and in shape. It would seem that this disagreement is related to the existence of resonances in this energy range, which were neglected in the calculations.

The simplest improvement to be made in the calculation is to take the resonances into account by assuming appropriate non zero values for α_λ and β_l in eq. (4) of Tobocman and Kalos [14]). A preliminary attempt in this direction, assuming the 2.33 MeV resonance to be 3^- and neglecting the other resonances,

failed to improve the agreement with experiment. It became clear, however, that it is necessary to determine the spin, parity and widths of the resonances before more elaborate calculations are attempted. For that purpose the elastic scattering cross section O^{16}(d, d)O^{16} should be specially helpful and will be measured at this laboratory.

It is possible, however, that the distorted wave Born approximation is not sufficient to obtain agreement with experiment, and that interference of direct and compound nucleus processes must be taken into account [15]).

The authors are grateful for the advice and encouragement of O. Sala, R. A. Douglas, A. O. Hanson, J. Osada and T. Miyazima, and the help of K. Gohara, T. Polga and M. Capello.

References

1) N. Austern in Fast neutron physics, Vol. II edited by J. B. Marion and J. L. Fowler (to be published)
2) M. H. Macfarlane and J. B. French, Rev. Mod. Phys. **32** (1960) 567
3) Marion, Brugger and Bonner, Phys. Rev. **100** (1955) 46
4) W. A. Higginbotham and S. Rankowitz, Rev. Sci. Instr. **22** (1951) 688
5) A. O. Hanson and J. L. McKibben, Phys. Rev. **72** (1947) 673
6) G. A. Jarvis, A. Hemmendinger, H. V. Argo and R. F. Taschek, Phys. Rev. **79** (1950) 929
7) T. W. Bonner and C. F. Cook, Phys. Rev. **96** (1954) 122
8) D. J. Hughes and R. B. Schwartz, BNL 325 Report (1958)
9) Elwyn, Kane, Ofer and Wilkinson, Phys. Rev. **116** (1959) 1490
10) S. T. Butler, Proc. Roy. Soc. **208** (1951) 559
11) C. R. Lubitz, Numerical table of Butler-Born approximation stripping cross sections (University of Michigan, Ann Arbor, Mich., 1957)
12) E. K. Warburton and L. F. Chase, Jr., Phys. Rev. **120** (1960) 2095
13) W. Tobocman, Phys. Rev. **94** (1954) 1655.
14) W. Tobocman and M. H. Kalos, Phys. Rev. **97** (1955) 132
15) R. G. Thomas, Phys. Rev. **100** (1955) 25
16) Bloch *et al.*, Rev. Mod. Phys. **23** (1951) 147
17) E. L. Keller, Phys. Rev. **121** (1961) 820

1.E.1:
3.A

Nuclear Physics **27** (1961) 112—114; © *North-Holland Publishing Co., Amsterdam*
Not to be reproduced by photoprint or microfilm without written permission from the publisher

THE SPIN AND PARITY OF THE 648 keV RESONANCE IN Mg^{26} (p, γ)Al^{27}

ROLF NORDHAGEN
Fysisk institutt, Universitetet i Oslo, Blindern, Norway

Received 13 April 1961

Abstract: The spin and parity of the 648 keV resonance in Mg^{26}(p, γ)Al^{27} is discussed and tentatively assumed to be $\frac{1}{2}^-$.

The weak648 keV resonance found by proton bombardment of natural magnesium has recently been positively identified as belonging to the reaction Mg^{26}(p,γ) Al^{27}. This was done by the same group [1]) as originally reported the resonance, aided by the author of the present note. The identification was based on the appearance of the 0.84 MeV γ-ray from the first excited state of Al^{27} in the γ-radiation at 648 keV. This radiation was not due to the close-lying strong 661 keV resonance. Here also a 1.01 MeV γ-ray from the second excited state can be seen. The latter line is hardly present at 648 keV.

In the present note, the spin and parity of the 648 keV resonance are discussed. The discussion is entirely based on the careful study by Van der Leun of low lying resonances in the mass region $22 < A < 35$ and a close comparison with his results [2]).

The complete γ-ray spectrum from the 648 keV resonance could not be found, due to the close proximity of the strong wide F^{19}(p, $\alpha\gamma$) resonance at 672 keV and the Mg^{25}(p, γ) resonance at 654 keV. The only important feature which could be definitely established was, apart from the mentioned appearance of the 0.84 MeV line, the existence of a strong ground state transition. The total intensity of the resonance was estimated to be close to 10 % of the intensity of the 661 keV resonance. From Van der Leuns' work, a $(2J+1)\gamma$ of 1.4 eV for the latter resonance [3]) can be deducted, and thus the $(2J+1)\gamma$ of the 648 keV resonance is approximately 0.14 eV.

Van der Leun finds that in the four Mg^{26}(p, γ)Al^{27} resonances studied by him all levels decay by dipole transitions, and that enhanced E2 transitions are not present. In the odd-mass nucleide Al^{27} no isobaric spin selection rules hamper the dipole transitions, and it seems safe to conclude, as Van der Leun does, that only dipole transitions actually take part in de-exciting the resonant level. The existence of a transition to the Al^{27} ground state (spin $\frac{5}{2}^+$) then limits the resonant level spin to $\frac{3}{2}$, $\frac{5}{2}$ and $\frac{7}{2}$. The spin $\frac{7}{2}$ can be ruled out as cascades through the first excited state ($\frac{1}{2}^+$) are present.

We will then test the assumption $\Gamma_\gamma < \Gamma_p$ and thus $(2J+1)\gamma \approx (2J+1)\Gamma_\gamma \approx 0.14$ eV. For the time being we assume that the majority of the resonant level de-excitations takes place via the ground state transition ($\approx$8.9 MeV), and then study the possible strengths $|M|^2$ of the probable multipole transitions. In table 1 are listed the two possible values of Γ_γ and the corresponding transition strengths in Weisskopf units.

TABLE 1

Possible transition strengths of a 8.9 MeV 100 % ground state transition in the decay of the 648 keV resonance

Possible spins	Corresponding Γ_γ	$\lvert M\rvert^2$ in W.U.
$\frac{3}{2}$	0.035 eV	E1 : $1.1 \cdot 10^{-4}$ M1 : $2.3 \cdot 10^{-3}$
$\frac{5}{2}$	0.023 eV	E1 : $7.2 \cdot 10^{-5}$ M1 : $1.5 \cdot 10^{-3}$

Van der Leun finds an average $|M|^2$ of $1.7 \cdot 10^{-3}$ for E1 and of $2.5 \cdot 10^{-2}$ for M1 transitions, but observes a wide distribution ($\approx$ a factor 10) around these values.

The values found are just touching Van der Leun's lower limits and they fall below the distributions observed when we take into consideration that the resonance presumably decays only partly via the ground state transition. The assumption $\Gamma_\gamma < \Gamma_p$ thus does not seem to be in good agreement with the observations.

We then study the reduced proton widths θ_p^2 of a 0.03 eV wide level at 650 keV, using the same curves as Van der Leun for the barrier penetrability of the proton. For capture or protons with orbital angular momentum $l = 1$, we get $\theta_p^2 = 4.5 \cdot 10^{-5}$, $l = 2 : \theta_p^2 = 1.5 \cdot 10^{-4}$ and $l = 3 : \theta_p^2 = 3 \cdot 10^{-2}$.

Again we compare with Van der Leun's average, this time for θ_p^2 in the mass region $22 < A < 35$. It is found that θ_p^2 has an average of 7 % and lies roughly between 15 % and 1.5 %. It is seen that the value for $l = 3$ lies well within these limits.

The value $l = 3$ will give a spin for the resonant level of $\frac{5}{2}-$ or $\frac{7}{2}-$, and the latter is excluded by previous arguments. The spin $\frac{5}{2}-$ would give an E1 transition to the ground state whose width may be larger than the observed width. We may therefore tentatively conclude that the observed resonance at 648 keV in the reaction $Mg^{26}(p, \gamma)Al^{27}$ is a f-capture resonance with a spin $\frac{5}{2}-$. The small width may be due to a limitation by the proton width or by both Γ_γ and Γ_p being of the same order of magnitude. However, the assumption that the observed width is due to the width of a E1 or M1 transition, making possible both $\frac{3}{2}+$ or $\frac{5}{2}+$ for the resonance spin, cannot be completely excluded.

The author is greatly indebted to his colleagues [1]) for permission to publish this note.

References

1) S. L. Andersen, T. Holtebekk, O. Lönsjö and R. Tangen, Nuclear Physics **13** (1959) 310
2) C. Van der Leun, thesis, University of Utrecht (1958);
C. Van der Leun, P. M. Endt, J. C. Kluyver and L. E. Vrenken, Physica **22** (1956) 1223
3) H. E. Gove in Nuclear Reactions, ed. P. M. Endt and M. Demeur (North-Holland Publ. Co., Amsterdam, 1959) p. 302.

1.D.2:
1.E.4

Nuclear Physics **27** (1961) 115—133; © *North-Holland Publishing Co., Amsterdam*

Not to be reproduced by photoprint or microfilm without written permission from the publisher

ELECTRIC MONOPOLE TRANSITIONS IN COLLECTIVE NUCLEI

A. S. REINER

Physics Department, The Weizmann Institute of Science, Rehovoth, Israel †

Received 16 March 1961

Abstract: E0 transitions are studied in nuclei with phonon and rotation-vibration spectra under the usual assumptions of the Bohr-Mottelson model. The rate of E0 transitions in strongly deformed nuclei is shown to be proportional to the square of the zero-point fluctuation amplitude of the β-vibrations. This quantity can be determined from experimental data in several independent ways. Where sufficient data are available the various values found for this amplitude are compared. The agreement found indicates additional proof for the consistency of the model.

Expressions for the branching ratio of competing E0 and E2 transitions are derived. Because of the similarity between the E0 and E2 operators, the branching ratio in the strong-coupling model is essentially given by the square of the equilibrium deformation. Contributions to the E2 transiton probability due to the rotation-vibration interaction are included and found to be appreciable in some cases. Disagreement with experimental branching ratios is noted and possible reasons are discussed.

1. Introduction

Since the restatement by Church and Weneser [1]) that an electric monopole transition may proceed between any two states with the same spin and parity $I^{\pm}$, a revived interest in this type of transitions has resulted. Electron or pair emission by a monopole (E0) transition as the only decay mode had already been observed [2]) in the lighter nuclei like ^{16}O, ^{40}Ca, ^{72}Ge and ^{90}Zr. One is usually inclined to describe the ground and first excited 0^+ states in these neclei in terms of shell model configurations in which only a small number of particles partake.

The nuclei mentioned above will not be considered here, nor will ^{12}C, ^{42}Ca, ^{70}Ge, ^{140}Ca (see ref. [3])) where the 0^+ state appears as the second excited state (see, however, ref. [4])). Instead we shall treat E0 transitions in nuclei with collective features ††. The relevant states, which may decay by E0 conversion often do not belong to the lowest excited states of the spectrum. They form, however, an integral part of a phenomenological picture, the validity of which has been tested up to energies of 1.0—1.5 MeV. The composition of the relevant states

† Part of this work has been performed in 1957 during the author's stay at the Institute for Theoretical Physics in Copenhagen; the results appeared as part of a Ph. D. thesis (Amsterdam 1958, unpublished). Part of it has been sponsored by the Air Force Office of Scientific Research of the Air Research and Development Command, U.S. Air Force, through its European Office.

†† An extensive account of the experimental situation can be found in the review article by Marklund *et al* [5]).

is as such often better understood than that of the lowest excited 0^+ states in lighter nuclei. We shall therefore undertake a description of collective E0 transitions and investigate how well they fit within the same phenomenological framework.

We start in section 2 with a derivation of the collective E0 operator, which rests on the assumptions of the incompressibility of nuclear matter. The calculation of E0 transition probabilities is subsequently carried out in section 3 for the vibrational model and the strong-coupling model respectively. The great similarity in the operator which govern E0 and E2 transition cause competing E2 transitions to serve, both theoretically and experimentally, as a suitable standard to compare the intensity of an E0 transition. Accurate determination of E2 transition rates is therefore mandatory, for which reason rotation-vibration interactions are included in the strong-coupling model. These perturbations turn out to have surprisingly large effects on certain interband transitions.

Section 4 contains an extensive comparison between theoretical predictions and experimental material, which shows serious discrepancies. Higher order effects as well as the influence of octupole vibrations are considered and are found to be of minor influence. Attention is paid to the assumption of the incompressibility of nuclear matter.

2. The Collective Monopole Operator

The probability of E0 conversion by ejection of an atomic electron is given by the expression [1, 4, 6])

$$W_{\mathrm{K}}^{\mathrm{E0}} = B(Z)F(Z, E_{\mathrm{K}}, R_0)|M_{\mathrm{fi}}|^2. \tag{1}$$

The electronic transition is described by the first two factors, which in units $\hbar = m = c = 1$ read

$$B(Z)F(Z, E_{\mathrm{K}}, R_0) = B(Z)\alpha^2(Z\alpha)^3 \mathrm{e}^{\pi Z\alpha/p_{\mathrm{K}}}(\Gamma(2\gamma+1))^{-3} \times p_{\mathrm{K}}(E_{\mathrm{K}}+\gamma)|\Gamma(\gamma+i\alpha E_{\mathrm{K}}/p_{\mathrm{K}})|^2(4p_{\mathrm{K}}Z\alpha R_0^2)^{2\gamma-2}, \tag{2}$$

with $\alpha = e^2/\hbar c$ and where E_{K}, p_{K} denote energy and asymptotic momentum of the K electron in the continuum. If k (in units mc^2) denotes the available nuclear excitation energy and if B_{K} is the binding energy of the K electron, $E_{\mathrm{K}} = k+B_{\mathrm{K}}$. Out of the two factors BF in (2), the latter is common for all choices of ground state charge densities ρ_{00} which determine electronic wave functions. The factor $B(Z)$, on the other hand, depends on the specific choice made for ρ_{00}.

The radius R_0 in eq. (2) is a length parameter equal to the radius for a uniformly charged nucleus. It may for instance be defined by means of the

root-mean square radius for a homogeneous charge density ρ_{hom}, as

$$R_0 = [\tfrac{5}{3}\langle r^2\rangle_{\text{hom}}]^{\frac{1}{2}}.$$

The appearance of the parameter R_0, though undesirable, is difficult to avoid. Only for the model of a uniform nuclear ground state density can one without complicated calculations find the electronic matrix element. Its value, however, is undoubtedly correctly estimated by using ρ_{hom}, other "reasonable" charge densities ρ_{00} only weakly affecting the factor $B(Z)$. The function $B_{\text{hom}}(Z)$ used in the following varies smoothly and increases from 3.56 for $Z = 0$ to ≈ 3.8 for the heaviest elements [4, 6]). One may hope that the value of R_0 to be inserted in eq. (2) to give the correct value for BF is numerically $[\tfrac{5}{3}\langle r^2\rangle\rho_{00}]^{\frac{1}{2}}$ with a general ground state density ρ_{00}.

Returning to (1) we still have to define M_{fi}, the matrix element which accounts for the nuclear transition $\psi_i \to \psi_f$ [1, 4, 6]); we put

$$M_{fi} \equiv \tfrac{5}{3}\rho\langle r^2\rangle_{\rho_{00}} = \langle\psi_f|\int \mathrm{d}\mathbf{r} r^2 \rho_{\text{op}}(\mathbf{r})\left[1-\tfrac{3}{20}(Z\alpha)^2\left(\frac{r}{R_0}\right)^2+\ldots\right]|\psi_i\rangle, \quad (3)$$

where ρ is a dimensionless strength function. The quantity M_{fi} is thus approximately the second moment of the transition charge density ρ_{fi}. The small second term inside the brackets in eq. (3) corrects for the "long wavelength approximation" in which the electron wavefunction is taken to be a constant inside the nucleus. The correction, the numerical expression of which is given in eq. (3), is again appropriate to $\rho_{00} = \rho_{\text{hom}}$ and is negligible for all but the heaviest nuclei.

The various K/L, K/M . . . ratios, in which the probability of ejection of an L, M, . . . electron is compared with K electron conversion are in the long wavelength approximation independent of any nuclear model. The ratios are characteristic functions of Z and the de-excitation energy kmc^2 (see refs. [1, 4])).

A nuclear model enters into the calculation of M_{fi} through the transition charge density ρ_{fi}. In the collective model, for instance, one makes the essential simplification that ρ_{op} in eq. (3) can first be treated as a classical charge density $\rho_d(\mathbf{r})$. This deformed charge density is assumed to be related to a spherically symmetric charge distribution $\rho(r)$ in a hypothetical undeformed nucleus. This relation may for instance be established by following the nuclear fluid in the course of an incompressible flow [4, 7, 8]), in which case one is bound to choose $\rho(r) = \rho_{\text{hom}}$. Charge and matter densities are further assumed to have the same distribution and flow patterns. Each point r_0 in the spherical distribution reaches $\mathbf{r} \equiv r, \theta, \phi$ in the deformed body and is related to r_0 by

$$r = r(\theta, \phi) = r_0\left[1+\sum_{\mu=-2}^{2}\alpha_\mu Y_{2\mu}(\phi, \theta)+\frac{1}{4\pi}\sum_{\mu=-2}^{2}|\alpha_\mu|^2+\mathrm{O}(\alpha^3)\right], \quad (4)$$

where α_μ denote the five quadrupole deformation parameters. It is often

convenient to consider a coordinate system moving with the deformed body and oriented with respect to the coordinate system fixed in space by Eulerian angles θ_1. The ensuing transformation of the deformation parameters $\alpha_\mu \to a_\mu$ reads [7])

$$a_\mu = \sum_{\mu'} \alpha_{\mu'} D^{(2)}_{\mu'\mu}(\theta_1), \qquad a_{\pm 1} = 0, \qquad a_2 = a_{-2}. \tag{5}$$

The further substitution

$$a_0 = \beta \cos\gamma, \qquad a_{\pm 2} = 2^{-\frac{1}{2}}\beta \sin\gamma \tag{6}$$

defines a shape parameter β and the angle γ measuring deviations from axial symmetry. The equation of the surface (4) now reads

$$r = r(\theta') = r_0[1+\beta Y_{20}(\theta') + (4\pi)^{-1}\beta^2 + O(\beta^3)], \tag{7}$$

where θ' measures the angle between $\mathbf{r}$ and the symmetry axis, and r_0 is connected with R_0 by the relation $r_0 = (1-\beta^2/2\pi)R_0$, required by conservation of volume.

The distorted density to be inserted in eq. (3) is

$$\rho_d(\mathbf{r}) = \begin{cases} \dfrac{3Z}{4\pi R_0^3} & \text{if } \mathbf{r} \text{ is inside the surface } r = r(\theta') \\ 0 & \text{if } \mathbf{r} \text{ is outside the surface } r = r(\theta'). \end{cases} \tag{8}$$

We remark that the density (8) consists of two parts:

$$\rho_d(\mathbf{r}) = \rho_{\text{sph}}(r) + \rho_{\text{non-sph}}(\mathbf{r}), \tag{9}$$

of which only the first contributes to the integral in eq. (3). The non-spherical part of $\rho_d(\mathbf{r})$, however, influences in an indirect way the monopole transition rate, as will be discussed in the last section.

The actual substitution of (8) into (3) results in †

$$M_{fi} = \frac{5}{4\pi} Z\langle r^2\rangle \sigma(Z) \langle \psi_f|\beta^2|\psi_i\rangle, \tag{10}$$

with

$$\sigma(Z) = 1 - \tfrac{21}{50}(Z\alpha)^2 \frac{\langle r^4\rangle}{\langle r^2\rangle}. \tag{11}$$

The averages $\langle r^n\rangle$ are calculated for the homogeneous density ρ_{hom}.
From (10), M_{fi} is seen to be proportional with $\langle r^2\rangle$, which causes ρ (cf. ref. [3])) to be independent of the original charge density ρ_{hom} apart from the weak

† In the derivation of (10), the matrix element M_{fi} appears proportional to $R_0^2 = R^2(1+(2\pi)^{-1}\beta^2)$, where R is the average radius. The β^2 term was in ref. [4]) erroneously absorbed in the E0 operator. The resulting overestimate of $|M_{fi}|^2$ by a factor $(^7/_5)^2$ has also been noticed by Rasmussen in a publication which came to our attention after the completion of this work [8a]).

dependence on σ. The actual transition as described by $\langle\psi_f|\beta^2|\psi_i\rangle$ will be considered separately for nuclei having phonon spectra and rotation-vibration spectra.

3. The Calculation of Transition Probabilities

3.1. E0 TRANSITIONS IN VIBRATIONAL NUCLEI

No general description accounts with fair accuracy for the properties of low-lying states of so-called vibrational nuclei. One usually starts from a simple harmonic hamiltonian [7])

$$H = \sum_{\mu=-2}^{2} \left\{ \frac{|\pi_\mu|^2}{2B} + \tfrac{1}{2} B\omega^2 |\alpha_\mu|^2 \right\} \tag{12}$$

in terms of the quadrupole deformation α_μ present in (4) and their conjugate momenta π_μ. The vibrating mass is denoted by B while, $B\omega^2 = C$ is the effective surface tension.

Instead of α_μ, π_μ, it is convenient to define operators b_μ, $b_\mu{}^\dagger$ by

$$\alpha_\mu = (\hbar/2B\omega)^{\frac{1}{2}}(b_\mu + (-)^\mu b^\dagger_{-\mu}), \qquad \pi_\mu = i(\hbar B\omega/2)^{\frac{1}{2}}(b_\mu{}^\dagger - (-)^\mu b_{-\mu}). \tag{13}$$

States are built from the ground state $|0\rangle$ by operation with the operators $b_\mu{}^+$, each creating phonons with angular momentum and z component 2 and μ respectively. For the lowest states one has

$$\begin{array}{ll} \text{ground state:} & |0\rangle, \\ \text{first excited } 2^+ \text{ state:} & b_\mu{}^\dagger|0\rangle, \\ \text{second excited triplet} & \\ \text{with spins } I = 0,\ 2,\ 4, & \tfrac{1}{2}\sum_m \begin{pmatrix} 2 & 2 & I \\ m & M-m & M \end{pmatrix} b_m{}^\dagger b^\dagger_{M-m}|0\rangle. \end{array} \tag{14}$$

In order to evaluate the nuclear matrix element M_{fi} of eq. (10) one first writes $\beta^2 = \sum_\mu |\alpha_\mu|^2$ by means of (13) in terms of b operators as follows:

$$\beta^2 = (\hbar|2B\omega) \sum_\nu [b_\nu b_\nu{}^\dagger + b^\dagger_{-\nu} b_{-\nu} + (-)^\nu b_\nu b_{-\nu} + (-)^\nu b^\dagger_{-\nu} b_\nu{}^\dagger]. \tag{15}$$

Let us first consider the $0^{+\prime} \to 0^+$ transition (primes at spin quantum number indicate order of excitation). On using the appropriate states from (14) one easily verifies that

$$\rho(0' \to 0) = \frac{3}{4\pi} Z\sigma(Z)(\tfrac{5}{2})^{\frac{1}{2}} \left(\frac{\hbar}{B\omega}\right). \tag{16}$$

As to the $2^{+\prime} \to 2^+$ transition it is seen that the difference of creation and annihilation operators partaking in the states is odd, whereas the operator β^2 of eq. (15) is in this sense even. The $2^{+\prime} \to 2^+$ E0 transition is thus strictly forbidden in the pure phonon spectrum.

Since the $0^{+\prime}$ state may also decay to the 2^+ state by E2 γ-radiation, the experiment will usually compare the E0 electron intensity with the $0^{+\prime} \to 2^+$ E2 γ-transition probability. The latter reads [9])

$$W^{E2} = \frac{4\pi\alpha c}{75}\left(\frac{k_\gamma mc^2}{\hbar c}\right)^5 B(E2),$$
$$B(E2) = \left\{\frac{5}{4\pi} Z\langle r^2\rangle\right\}^2 \sum_{\mu, M_f} |\langle I_f M_f|\alpha_\mu{}^\dagger|I_1 M_1\rangle|^2. \tag{17}$$

The reduced transition probability $B(E2)$ for the $0^{+\prime} \to 2^+$ transition is thus seen to be, by use of (13) and (14),

$$B(E2, k_\gamma mc^2, \quad 0^{+\prime} \to 2^+) = \left\{\frac{5}{4\pi} Z\langle r^2\rangle\right\}^2 \frac{\hbar}{B\omega}. \tag{18}$$

Calling μ_K the intensity ratio for the K electrons and gamma rays emitted in the E0 and E2 transitions we have from (1), (10), (11), (16), (17) and (18) (note the conversion to the same time units!)

$$\mu_K \equiv \frac{W_K^{E0}(k, 0^{+\prime} \to 0^+)}{W^{E2}(k_\gamma, 0^{+\prime} \to 2^+)} = \frac{375}{8\pi\alpha} B(Z) F_K(Z, E_K, R_0)\sigma^2 k_\gamma{}^{-5} \frac{\hbar}{B\omega}. \tag{19}$$

The only parameter in (19) not directly known is $\hbar/B\omega$. It can be derived from Coulomb excitation of the 2^+ state for which the reduced transition probability reads

$$B(E2, 0^{+\prime} \to 2^+) = \tfrac{5}{2}\left[\frac{5}{4\pi} Z\langle r^2\rangle\right]^2 \frac{\hbar}{B\omega}. \tag{20}$$

Experiment shows that the phonon model can only hold in a qualitative way. But none of the simplest extensions seem to be consistent with experiment. We first mention that the simple asymmetric rotor model of Davydov and Fillipov [10]) can be excluded by the very absence of $0^{+\prime}$ states in the predicted spectrum. We have further made some calculations for the model of Wilets and Jean [11]), in which the equilibrium deformation is shifted from 0 to β_0. It is indeed possible to fix the spectrum with one value of β_0 which predicts, however, about equal strength for the $2^{+\prime} \to 2^+$ and $0^{+\prime} \to 0$ E0 transitions. Although the available data are very scarce (cf. table 1), it seems that the selection rule valid in the pure phonon model is only weakly violated.

Having no alternative simple theory at our disposal, we shall have to content ourselves with the estimates (16) and (19), and small compare them below with experimental results (section 4).

3.2. COLLECTIVE E0 TRANSITIONS IN ROTATION-VIBRATION SPECTRA

In spectra of this type one discerns four more or less independent excitation modes. Those are shape rotations, shape (β-) vibrations preserving axially

symmetry, γ oscillations around an axially symmetric equilibrium position, and finally excitations of the intrinsic structure. The pertinent lowest order wave functions are [9])

$$\Psi^0(\theta_i, \beta, \gamma) = \sqrt{\frac{2I+1}{8\pi^2}}\, D^I_{MK}(\theta_i)\psi_{n_\beta}(\beta)\psi_{n_\gamma}(\gamma)\chi_\alpha(x'_1). \tag{21}$$

The zeroth order description is of sufficient accuracy to account for the spectrum. Some E2 γ-transitions, however, with which we shall compare E0 transitions turn out to be unexpectedly sensitive to small interactions between the different modes. Out of these so-called rotation-vibration interactions we shall discuss only the perturbation between β vibrations and rotations, because we are primarily concerned with β bands. Moreover, γ vibrations of frequency $\omega_\gamma \approx \omega_\beta$ seem to be of less importance.

One thus considers the simple Hamiltonian

$$H = \frac{I(I+1)\hbar^2}{2\bar{\mathscr{I}}} - \frac{\hbar^2}{2B}\frac{\partial^2}{\partial\beta^2} + \tfrac{1}{2}B\omega_\beta^2(\beta-\beta_0)^2, \tag{22}$$

where $\bar{\mathscr{I}} = \mathscr{I}_0\beta^2$ denotes the moment of inertia, B again the mass parameter and β_0 the equilibrium deformation. The parameter $\mathscr{I}_0$ is proportional to the mass parameter B, but we shall as yet not make use of the "hydrodynamical" value [7])

$$\bar{\mathscr{I}} = \mathscr{I}_0\beta_0^2 = 3B\beta_0^2. \tag{23}$$

A zeroth order hamiltonian is obtained on putting $\bar{\mathscr{I}} \to \mathscr{I} = \mathscr{I}_0\beta_0^2$ while the remaining perturbation is expanded in powers of $(\beta-\beta_0)/\beta_0$ and can be treated as in the case of a vibrating diatomic molecule [9, 12]). The perturbation results in an increase of the equilibrium deformation amounting

$$a_I = \delta_I\beta_0 = \frac{I(I+1)\hbar^2/2\mathscr{I}}{\frac{1}{2}B\omega_\beta^2\beta_0^2 + 3I(I+1)\hbar^2/2\mathscr{I}}\beta_0, \tag{24}$$

while the modified rotation-vibration spectrum reads

$$\begin{aligned} E_{n_\beta, I} &= \frac{I(I+1)\hbar^2}{2\mathscr{I}}(1+\delta_I) + (n_\beta+\tfrac{1}{2})\hbar\omega_I, \\ \omega_I &= \omega_\beta\left(1 + \frac{3I(I+1)\hbar^2/2\mathscr{I}}{\frac{1}{2}B\omega_\beta^2\beta_0^2}\right)^{\frac{1}{2}} \approx (1+\tfrac{3}{2}\delta_I)\omega_\beta. \end{aligned} \tag{25}$$

The perturbed wave functions

$$\begin{aligned} \Psi &= D^I_{MK}(\theta_i)\psi_{n_\beta, I}(\beta)\psi_{n_\gamma}(\gamma)\chi_\alpha(x'_1), \\ \psi_{n_\beta, I} &= \left(\frac{\alpha_I^{\frac{1}{2}}}{\pi^{\frac{1}{2}}2^{n_\beta}n_\beta!}\right)^{\frac{1}{2}} e^{-\frac{1}{2}\alpha_I(\beta-\beta_0-\delta_I\beta_0)^2} H_{n_\beta}[\alpha_I^{\frac{1}{2}}(\beta-\beta_0-\delta_I\beta_0)] \end{aligned} \tag{26}$$

will be used in the calculation of transition probabilities. One notices that the set $\psi_{n_\beta, I}$ is orthogonal only for states with equal I.

From the form of the monopole operator in (10), it is seen that E0 transitions can proceed between states which differ only in the excitation of the β mode. In particular are forbidden for axially symmetric nuclei transitions between different γ bands. Matrix elements for single and double quantum transitions are easily found to be

$$\langle IMKn_\gamma n_\beta|\beta^2|I'M'K'n'_\gamma n_\beta-1\rangle = 2\beta_0 n_\beta^{\frac{1}{2}}\left(\frac{\hbar}{2B\omega_\beta}\right)^{\frac{1}{2}}(1+\tfrac{1}{4}\delta_I)\delta_{II'}\delta_{MM'}\delta_{KK'}\delta_{n_\gamma n'_\gamma}, \tag{27}$$

$$\langle IMKn_\gamma n_\beta|\beta^2|I'M'K'n'_\gamma n_\beta-2\rangle = n_\beta^{\frac{1}{2}}(n_\beta-1)^{\frac{1}{2}}\frac{\hbar}{2B\omega_\beta}(1-\tfrac{3}{2}\delta_I)\delta_{II'}\delta_{MM'}\delta_{KK'}\delta_{n_\gamma n'_\gamma}.$$

Substitution into (10) then yields the strength functions

$$\begin{aligned}\rho(I, n_\beta = 1 \to 0) &= \frac{3}{2\pi} Z\sigma(Z)(1+\tfrac{1}{4}\delta_I)(\hbar/2B\omega_\beta)^{\frac{1}{2}}\beta_0,\\ \rho(I, n_\beta = 2 \to 0) &= (1-\tfrac{5}{4}\delta_I)(\hbar/B\omega_\beta)^{\frac{1}{2}}(2\beta_0)^{-1}\rho(I, n_\beta = 1 \to 0).\end{aligned} \tag{28}$$

We recall that stability of the β vibrations requires the zero-point fluctuation amplitude $\xi = (\hbar/2B\omega_\beta)^{\frac{1}{2}}$ to be small with respect to the equilibrium deformation β_0. It is then seen that the crossover transition $\Delta n_\beta = 2$, although not strictly forbidden, is strongly hindered.

Determination of absolute electron yields using (28) requires knowledge of the amplitude $\xi = (\hbar/2B\omega_\beta)^{\frac{1}{2}}$, which can be obtained in several ways. Let us first consider the E2 γ-transition between states belonging to different β bands and separated in energy by $k_\gamma mc^2$. The transition probability (17) reads [9])

$$W^{E2}(k_\gamma; n_1 I_1 \to n_f I_f) = \frac{4\pi}{75}\alpha c\left(\frac{k_\gamma mc^2}{\hbar c}\right)^5\left[\frac{5}{4\pi}Z\langle r^2\rangle\right]^2\begin{pmatrix} I_1 & 2 & I_f\\ 0 & 0 & 0\end{pmatrix}^2|\langle n_f I_f|\beta|n_1 I_1\rangle|^2. \tag{29}$$

The last factor can be calculated by expansion of the (in general non-orthogonal) wave functions (26) in terms of the parameters $\delta_I \ll 1$. For $n_\beta = 1 \to 0$ transitions one finds in a straightforward manner

$$\begin{aligned}W^{E2}&(k_\gamma; n_\beta = 1 \to 0; I_1 \to I_f)\\ &= \frac{4\pi}{75}\alpha c\left(\frac{k_\gamma mc^2}{\hbar c}\right)^5\begin{pmatrix} I_1 & 2 & I_f\\ 0 & 0 & 0\end{pmatrix}^2\frac{\hbar}{2B\omega_\beta}\left[\frac{5}{4\pi}Z\langle r^2\rangle\right]^2 C_{1\to 0}(I_1 \to I_f).\end{aligned} \tag{30}$$

The factors C correct the E2 γ-transition probabilities for the rotation-vibration

interaction and read $[x_0 = \beta_0|(\hbar/B\omega_\beta)^{\frac{1}{2}}]$

$$\begin{aligned} C_{1\to 0}(0^{+\prime} \to 2^+) &\approx \{1+\delta_2(x_0^2-\tfrac{3}{4})\}^2, \\ C_{1\to 0}(2^{+\prime} \to 0^+) &\approx (1-\delta_2 x_0^2)^2, \\ C_{1\to 0}(2^{+\prime} \to 2^+) &\approx (1-\tfrac{3}{4}\delta_2)^2, \\ C_{1\to 0}(2^{+\prime} \to 4^+) &\approx \{1+\delta_2(\tfrac{7}{3}x_0^2-\tfrac{1}{16})\}^2. \end{aligned} \tag{31}$$

Any interband γ transition gives in principle the amplitude $\xi = (\hbar/2B\omega_\beta)^{\frac{1}{2}}$. Thus one has for instance

$$\xi = \left[\frac{B(\mathrm{E2},\, 0^+ \leftrightarrow 2^{+\prime})}{B(\mathrm{E2},\, 0^+ \leftrightarrow 2^+)}\right]^{\frac{1}{2}} \beta_0 \frac{1+\frac{1}{2}\delta_2}{1-\delta_2 x_0^2}. \tag{32}$$

It is again useful to compare the rates for E0 and competing E2 transitions. We define (cf. (19))

$$\begin{aligned} \mu_{\mathrm{K}}(I_1 \to I_f) &\equiv \frac{W_{\mathrm{K}}^{\mathrm{E0}}(k; I, n=1 \to I, n=0)}{W_\gamma^{\mathrm{E2}}(k_\gamma; I_1, n=1 \to I_f, n=0)} \\ &= \begin{pmatrix} I_1 & 2 & I_f \\ 0 & 0 & 0 \end{pmatrix}^{-2} \frac{75}{\pi\alpha} B(Z) F(Z, E_{\mathrm{K}}, R_0) \sigma^2(Z) \frac{\beta_0^2}{k_\gamma^5} \frac{1+\frac{1}{2}\delta_f}{C_{1\to 0}(I_1 \to I_f)} \end{aligned} \tag{33}$$

which is obtained from (1), (10), (28) and (30). It is seen that not only is μ independent of the charge-density ρ_{hom} (for not too heavy nuclei) but in contrast to the vibrational case (19) also of parameters like B and ω.

In the case no data regarding interband E2 γ-transitions are available one may invoke several alternative methods for a determination of the factor $(\hbar/2B\omega_\beta)^{\frac{1}{2}}$ occurring in the expression (28) for ρ.

It is for instance seen that the minute deviations of the spectrum (25) from the pure rotational spectrum, directly yields δ_2. Subsequently, one has

$$\xi' = (\hbar/2B\omega_\beta)^{\frac{1}{2}} \approx \left(\frac{\hbar\omega_\beta}{12\hbar^2/\mathscr{I}}\,\delta_2\right)^{\frac{1}{2}} \beta_0. \tag{34'}$$

We may at this stage use explicitly the hydrodynamical value (23) of $\mathscr{I} = 3B\beta_0^2$ by which ξ becomes independent of a known location of the $0^{+\prime}$ state,

$$\xi'' = (\tfrac{1}{8}\delta_2)^{\frac{1}{2}}\beta_0. \tag{34''}$$

Eqs. (34′) and (34″) can be combined to yield

$$\xi = \left(\frac{\Delta E_{\mathrm{rot}}}{2\Delta E_{\mathrm{vibr}}}\right)^{\frac{1}{2}}_{\mathrm{exp}} \beta_0. \tag{35}$$

Eq. (35) is useful if no accurate level positions are known in which case rather crude values of $\Delta E_{\mathrm{rot}} = 3\hbar^2/\mathscr{I}$ and $\Delta E_{\mathrm{vibr}} = \hbar\omega_\beta$ suffice for a tolerable estimate of ξ.

TABLE 1

Data on E0 transitions in vibrational nuclei. Results refer to calculated and observed values of $\rho(0^{+\prime} \to 0)$ and μ_K (eqs. (17) and (19)). Experimental estimates of $\rho(2^{+\prime} \to 2^+)$ are given and compared with $\rho(0^{+\prime} \to 0^+)$ estimated for those nuclei in spite of the yet unknown detection of the $0^{+\prime}$ state. Numbers in brackets are uncertain.

	E_{2^+}	E_{2^+}	$E_{0^{+\prime}}$	$C = B\omega^2$ (MeV)	$\rho(0^{+\prime} \to 0^+)$		$\rho(2^{+\prime} \to 2^+)$ ons.	μ_K	
					calc.	obs.		calc.	obs.
$^{106}_{46}$Pd	513	1120	1137	25 [17])	0.34	<0.14 [18])			
$^{112}_{48}$Cd	615	1310	($\approx$1400)	42 [17])	($\approx$0.27)				
$^{114}_{48}$Cd	559	1212	1308	36 [17])	0.27				
$^{152}_{64}$Gd	344.3	(756)	615.3	(31) [19]) (from Sm)	0.24			0.21 [a])	0.10 [20])
$^{192}_{78}$Pt	316.5	612.9		($\approx$30) (interpolated)	(0.27)		<0.02 [1])		
$^{196}_{78}$Pt	334	685		55 [19])	(0.14)		$0.009<\rho<0.05$ [1, 21])		
$^{198}_{78}$Hg	412	1089		88 [19])	(0.12)		<0.07 [1])		
$^{214}_{84}$Po	606	1378	1416	270 [19])	0.06	0.031 ± 0.025 [22])		0.006	$0.04<\mu<3.0$ [22])

Dr. Nathan has informed us of mistakes in the calculation of μ reported in ref. [20]), which explain the difference in the numbers given there and in the table above.

The next section is devoted to a comparison of the predictions with the experimental material.

4. Comparison between Theory and Experiment

4.1. VIBRATIONAL NUCLEI

We have assembled in table 1 data on E0 transitions in vibrational nuclei. Columns 2 to 4 mention the location of 2^+, $2^{+\prime}$ and $0^{+\prime}$ levels in keV, while in column 5 are entered the values for the surface tension $C = B\omega^2$ (in MeV). The quantities $\rho(0^{+\prime} \to 0^+)$, calculated from (16) and observed, together with $\rho(2^{+\prime} \to 2^+)_{\text{exp}}$ are found in columns 6—8. The last two columns contain the calculated and measured branching ratio (19).

Experiments on (d, t) and (d, p) reactions have recently brought into evidence several excited 0^+ states in vibrational nuclei [13]). Level positions are determined poorly as can be seen from comparison with other investigations which already revealed a $0^{+\prime}$ state (cf. ^{114}Cd, ref. [14])). We therefore mention only ^{112}Cd, where a prior weak indication as to the existence of a $0^{+\prime}$ state at 1400 or 1460 keV has now actually been confirmed [15]). ^{212}Po is not included in table 1 because of the conflicting evidence as to the spin value of the 1800 keV state [16]).

It is clear from the qualitative nature of the pure phononmodel that no more than indicative information can be attached to the theoretical predictions. It may, however, be meaningful to compare the limits set on $\rho(2^{+\prime} \to 2^+)$ with calculated values. No $0^{+\prime}$ states and $\rho(0^{+\prime} \to 0^+)$ values have been observed for those nuclei. But both from the general trend and the estimated $\rho(0^{+\prime} \to 0^+)$ values it is clear that the selection rule forbidding $2^{+\prime} \to 2^+$ E0 transitions appears only to be weakly violated. On this conclusion we rejected in subsection 3.1. the model of Jean and Wilets [10]).

4.2. ROTATION VIBRATION NUCLEI

We now turn to rotation vibration nuclei for which richer material and probably a more consistent description is available. Only a few typical nuclei are treated in detail. Data on remaining nuclei are calculated as sketched in the examples.

$^{152}_{62}$Sm

The marginal position of Sm as a still strongly deformed nucleus renders perturbation effects of unusual importance. This is reflected in particular in γ transition probabilities. (See also remark in ref. [20]), p. 213).

From data on the spectrum [20, 23]) found in table 2 one first derives through (28) the perturbation parameter

$$\delta_2 \approx \frac{3\hbar^2/\mathscr{I}}{\frac{1}{2}B\omega_\beta{}^2\beta_0{}^2} = 0.040.$$

Application of (34′) and (34″) then yields for the amplitude $\xi = (\hbar/2B\omega_\beta)^{\frac{1}{2}}$ 0.24 β_0 and 0.26 β_0 respectively.

Coulomb excitation to the 2^+ and $2^{+\prime}$ levels has been performed [23]) and one thus has an additional and independent experimental determination by use of (32). The result $(0.22\pm0.05)\beta_0$ is in agreement with the above estimates. Neglect of rotation-vibration interaction however, would have resulted in $\xi = (0.15\pm0.04)\beta_0$.

The theoretical strength function and branching ratios calculated from (28) and (33) are

$$\rho_{\text{th}} = 0.53, \qquad \mu_{\text{th}}(0^{+\prime} \to 2^+) = 0.032, \qquad \mu_{\text{th}}(2^{+\prime} \to 2^+) = 0.077.$$

Only $\mu_{\text{K}}(0^{+\prime} \to 2^+)$ has been measured [20]) directly to be † 0.013 ± 0.001. The second branching ratio has amongst others been deduced from simple branching ratios for interband transitions. If those are properly corrected for rotation-vibration interaction one reaches the estimate [25]) $\mu_{\text{exp}}(2^{+\prime} \to 2^+) \approx 0.03$.

The value for ρ deduced from branching ratios and the absolute measurement of $B(\text{E2}; 0^+ \to 2^{+\prime})$ yields

$$\rho = 0.33\pm0.05,$$

with error limits referring only to limits in the cross section for Coulomb excitation.

In principle, a complete set of data similar to that described above is available for ^{238}U, but is there subject to much greater experimental uncertainties.

$^{232}_{90}$Th

The first two members of the ground state band are found [26, 27]) at 50.1 and $\approx$ 163 keV approximately. In order to fit the smooth trend of observed δ_2 values one would expect the level at about 165 keV ($\delta_2 \approx 0.005$). One meets a similar situation in ^{238}U where the 4^+ level would fit much better at 146 keV than at 148 keV, which value is, however, rather uncertain [27]).

No $0^{+\prime}$ state being observed as yet, one has to invoke the $2^{+\prime}$ state for an estimate of ξ by use of (35); one gets $\xi = 0.18\beta_0$. Using the tentative value $\delta_2 = 0.005$ one would obtain from (34′) and (34″) the values $\xi = 0.14\beta_0$ and $\xi = 0.16\beta_0$ respectively, in line with all cases in which δ_2 is more accurately known. On the basis of these ξ values one then predicts

$$\rho_{\text{th}} = 0.31, \qquad \mu_{\text{K}}(0' \to 2) = 0.48, \qquad \mu_{\text{K}}(2' \to 2) = 1.3.$$

By Coulomb excitation, one could not yet resolve the $2^{+\prime}$ state at 773 keV from the first member of the γ vibrational band at [26, 28]) 780 keV. The strength of the $2^{+\prime} \to 0^+$ transition had therefore to be induced indirectly from the decay of the 2^+ complex to the 4^+ state at $\approx$ 163 keV, which is predicted to be

† In ref. [8a]) is cited the result of unpublished work indicating that μ has only half this value.

a nearly pure β transition. In conjuction with accurate data on Coulomb excitation of the 2^+ state [29, 30]) one then derives [28])

$$\rho_{exp} \approx 0.22, \qquad \mu_{exp}(2^{+\prime} \to 2) \approx 1.3, \qquad \xi \approx 0.11\beta_0$$

(see eq. (32) for ξ).

Coulomb excitation and conversion electron data[28, 31]) finally provide an alternative set of data

$$\rho_{exp} \approx 0.32, \qquad \mu_{exp}(2^{+\prime} \to 2) \approx 5.5, \qquad \xi \approx 0.08\beta_0.$$

Since, however, in the latter set, several intermediate steps are used, based on theoretical considerations, there is reason to judge the experiments employing γ transitions as the best available at present.

$^{232}_{92}U$

At least three members of the ground and first excited bands have been observed together with the E0 decay mode [32]). Unfortunately only lower limits on μ_K ratios are known, as yet preventing a test on the rule (27). Again the amplitude calculated from (34′) and (34″) agree reasonably well ($0.15\beta_0$ and $0.16\beta_0$ respectively). With $\beta_0 = 0.25$ one calculates $\rho_{th} = 0.40$, $\mu_K(0^{+\prime} \to 2) = 0.74$, to be compared with [32]) $\mu_{exp}(0^{+\prime} \to 2^+) \gtrsim 1.0$.

In table 2 are contained the results just discussed and those relevant to other nuclei with rotation-vibration spectra, where 0^+ excited states or E0 decay has been observed. The principal energy levels in keV with spins 2^+, 4^+, $0^{+\prime}$, $2^{+\prime}$ from which the perturbation parameter δ_2 and the rotation quantum $3\hbar^2/\mathcal{I}$ are derived, are entered in columns 2—7. In cases where as yet no $0^{+\prime}$ state has been detected, its position is estimated from the known location of the $2^{+\prime}$ state. In column 8 one finds the ratio of the amplitude ξ and β_0 directly measured in Coulomb excitation of the 2^+, $2^{+\prime}$ levels [32]). This value of ξ/β_0 is in columns 9 and 10 compared with the result obtainable from rotation-vibration interaction of eqs. (34′) and (34″), without and including knowledge of the hydrodynamical value (23) for the moment of inertia. The quantity $\delta_2 x_0^2$ (cf. (31)), which determines corrections on E2 transition probabilities and the equilibrium deformation β_0 are entered in columns 11, 12. The ρ values calculated from (28) using $\xi = (\hbar/2\beta\omega_\beta)^{\frac{1}{2}}$ from column 8 are found in column 13. Strength functions can be drawn from experiment if one branching ratio μ is known in conjunction with an interband E2 intensity (intensity ratios derivable from (30) are assumed to hold). In as much as ρ_{th}/ρ_{exp} differs from $(\mu_{th}/\mu_{exp})^{\frac{1}{2}}$ this is due to different ξ values employed: the amplitude obtained from rotation-vibration interaction is judged to be more reliable than the same quantity taken from Coulomb excitation data. The latter, however, naturally enters a determination of ρ_{exp}.

TABL

Theoretical and experimental data on E0 transitions in strongly deformed nuclei. Values in parenthesis r

	E_{2^+}	E_{4^+}	$E_{0^{+\prime}}$	$E_{2^{+\prime}}$	δ_2	$3\hbar^2/\mathcal{I}$	ξ/β_0		
							eq. (32)	eq. (34′)	eq. (34
$^{152}_{62}$Sm	121.79	366.36	885.0	811	0.04	126.9	0.22 [24])	0.24	0.26
$^{154}_{64}$Gd	123.07	371.07	678	816 [33])	0.039	128.1		0.23	0.26
$^{156}_{64}$Gd	88.92	288.2	(815?) [5])		0.011	89.8		(0.16)	0.19
$^{166}_{68}$Er	80.57	264.9	1460.2 [5])	1541.6	0.0058	81.1		0.16	0.16
$^{178}_{72}$Hf	93.15	306.8	1197 [34])		0.0052	93.6		0.13	0.16
$^{188}_{76}$Os	154.9	478	1086 [5])	(1306?) [5])	0.031	160.1		0.23	0.25
$^{230}_{90}$Th	52.8	173.8	634 [35])	676 [35])	(0.005)	(53.1)		0.13	0.16
$^{232}_{90}$Th	50.1	(163) [26, 27])	(725) [c])	773 [26, 28])	(0.005?)	(50.4)	(0.11) [26, 29])	0.14 [d])	0.16 [d] (0.18)
$^{232}_{92}$U	47.5	156.5	693 [32])	735 [32])	0.005	47.7		0.15	0.16
$^{234}_{92}$U	43.50	143.31	806 [36])	854 [36, 37, 38])	0.0050	43.7		0.15	0.16
$^{236}_{92}$U	44.9	(151)	(910) [c])	954 [38])		(45)			(0.16) [c]
$^{238}_{92}$U	44.7	(148) [27])	(990) [c])	1040 [38])		(45)	0.12 [26, 29])		(0.15) [c]
$^{238}_{94}$Pu	44.11	146.0	941.4 [39])	986	0.007	44.2		0.13	0.14
$^{240}_{94}$Pu	42.87	141.77	856 [40])	900 [40])	0.0078	43.0		0.13	0.15

[a]) μ_{exp} corrected for rotation-vibration interaction
[b]) See footnote page 126
[c]) Estimated from $2^{+\prime}$ level position
[d]) Assumed δ_2 value 0.005

Calculated and observed branching ratios $\mu(0^{+\prime} \rightarrow 2^+)$ are found in columns 15 and 16. Other branching ratios can easily be calculated from them and (30) and are only given if parallel experimental material is available.

Inspection of table 2 shows several remarkable facts. It is striking at first sight that the model of a vibrating axially symmetric rotor including the natural rotation-vibration interaction is amply proved by experiment to be consistent in several features though not in all. It is for instance clear from columns 8 and 9 that the two estimates (34′) and (34″) of the zero-point fluctuation amplitude generally agree. One may argue that the assumed proportionality $\mathcal{I}$ with β_0^2 already implies a harmonic Hamiltonian for the surface vibrations. Consequently the hydrodynamical relation $\mathcal{I} = 3B\beta_0^2$ should hold. But the fact that from two independent sets of experimental data one *derives* $\mathcal{I} \approx 3B\beta_0^2$ is unquestionably a proof of internal consistency. It is of interest to remark that inclusion of a perturbation through γ vibrations would lower the value of δ_β and increase the systematic differences in ξ values [5]). The observed inability of the full rotation-vibration interaction to account for the first details of the spectrum thus seems to indicate that the influence of γ vibrations is for some reason less than predicted.

to less certain data or to calculations based on uncertain data. A detailed description is given in the text.

$\delta_2 x_0^2$	β_0	ρ		$\mu_K(0' \to 2)$		$\mu_K(2' \to 2)$	
		calc.	obs.	calc.	obs.	calc.	obs.
0.37	0.28 [g])	0.53	0.33 0.24 [b])	0.032	0.013 ± 0.001 [20]) $\approx 0.0065 \pm 0.0005$ [b])	0.077	(0.03) [25])[a])
0.37	0.29 [g])	0.51		0.034	(≈ 0.02) [30])		
0.27	0.32 [g])	0.62					
0.11	0.32 [g])	0.53		0.0032			
0.17	0.26 [g])	0.46		0.0075	0.0076 ± 0.0025 [34])		
0.29	0.18	0.26		0.006			
0.17	0.24 [29])	0.25		0.60	(≈ 1.0) [35]) > 0.2 [35])		
0.14	0.25 [29])	(0.31) [d])	(0.22)	0.48		1.3	1.3 [28]) [a])
0.14	0.25	0.40		0.74	1.0 [32])	0.60($2' \to 0, 2, 4$) 0.59($4' \to 2, 4, 6$)	$\gtrsim 0.5$ [32]) $\gtrsim 0.04$ [32])
0.11	0.26 [29])	0.42		0.42	1.33 ± 0.08 [37])		
(0.09) [e])	0.27 [29])	($\lesssim 0.44$)		($\lesssim 0.29$)			
(0.09) [e])	0.27 [29])	($\lesssim 0.43$)	0.17	($\lesssim 0.21$)		($\lesssim 0.65$)	0.09 [32])
0.10	(0.27) [f])	0.39		0.31	(0.13) [39])		
0.10	(0.28) [f])	0.40		0.43	0.091 ± 0.023 [40])		

[e]) Calculated from eq. (35)
[f]) Extrapolated values
[g]) β_0 values taken from a compilation by Elbek

The consistency of the model is further confirmed by data on γ transitions. In as much as more or less reliable E2 intensities are known, those corroborate the ξ values found by spectral data. (See also section 5). A deficiency is to be found in the fact that moments of inertia in excited bands are systematically larger than in the lowest bands, an explanation of which lies outside the scope of the simple model.

We now arrive at the discussion of the predicted values (column 12). Since the values of $Z\xi$ are by experiment shown to be roughly constant, one infers from (28) that ρ is a smooth function, following variations in β_0 approximately linearly.

The presence of the factor Z in the theoretical expression for ρ suggests enhancement with respect to particle transitions. But contrary to other electromagnetic transitions the E0 single-particle strength

$$\rho \approx \langle \psi_{nl} | r^2 | \psi_{n'l} \rangle / \{ \tfrac{5}{3} \langle r^2 \rangle_{\rho_{00}} \}$$

is by no means a small unit. We recall in this context the suggestion [41]) that a proton making a transition in an harmonic oscillator well over two major shells could very well account for the exceedingly large observed strength

functions [2]) $\rho \approx \frac{1}{2}$ in ^{12}C and ^{16}O. It was shown on the other hand that only two of those excited states suffice to build a collective breathing mode. The conclusion is thus that either there is no enhancement in a collective transition, or the "single-particle" transition itself is somehow of a collective nature.

Leaving open the possibility of a peculiar behaviour of single-particle transitions, we now come to E0 transitions between two-particle configurations. As an example, we take ^{90}Zr, where the two 0^+ states involved are close to two orthogonal combinations of the $(2p_{\frac{1}{2}})_0^2$ and $(1g_{\frac{9}{2}})_0^2$ states [43]). Here as well as in the Ge isotopes, where the composition of the states is more obscure, one observes strength functions [2, 3]) $\rho \approx 0.09$. Although actual calculations for ^{90}Zr did not exactly reproduce the observed strength, the value of ρ_{Zr} seems to give insight as to the order of magnitude to be expected for "normal" E0 transitions of particle nature. Compared to this value both types of collective E0 transitions are predicted to be enhanced by a factor of order 30.

We finally arrive at a comparison between predicted and actually observed quantities. The last six columns of table 2 show serious discrepancies of two kinds. There is first one, which one may call systematic. Observed μ values fall short of predictions at least a factor 2.5 for Sm, which discrepancy becomes progressively smaller until the heavy elements are reached: with the exception of ^{238}U, theoretical branching-ratios become smaller than observed ratios. Values of μ for the Pu isotopes were until recently reported to be widely different. The observed values, although now showing about the correct ratio are again far smaller than the predicted μ ratios.

Discussion of the disagreement and tentative conclusions are presented in the following section.

5. Discussion and Conclusions

The above analysis has confirmed the adequacy of the model of a vibrating axially symmetric rotor as regards observed spectra. In a less general and conclusive way, evidence is also present as to agreement for γ intensities in intraband transitions. One is then tempted to trace the disagreements noted in μ and ρ values to an incorrect calculation of the E0 conversion probability in μ.

We shall therefore analyse the different steps in the calculations and consider additional effects. It will first be recognized that several possibilities could lead to changes in ρ itself. In fact all powers of β present in the spherically symmetric part contain a linear term $\propto \beta - \beta_0$ causing a non-vanishing contribution to ρ. Inclusion of the β^3 term for instance increases the calculated ρ value by about 10 %. Neglect of powers of β higher than the second seems justified within the approximations made.

Another possibility for the appearance of a term in the E0 operator linear in β, would be through the occurrence of octupole vibrations [44]). It requires,

however, a sizable octupole equilibrium deformation to produce a change in ρ as large as 10 %.

Higher order corrections in the quadrupole part of $\rho_d(\mathbf{r})$ of eq. (9) are also of some relevance. Inclusion of the β^2 term reduces β_0 as derived from Coulomb excitation when interpreted in terms of the linear terms only, as is usually done. The fractional change $1+\varepsilon\beta_0 = 1+\frac{5}{7}(5/4\pi)^{\frac{1}{2}}\beta_0$ appears doubled in a $n_\beta = 0 \leftrightarrow 1$ transition and the following implications result: ξ/β_0 values from Coulomb excitation have to be increased by $1+\varepsilon\beta_0$, which incidently brings them into even better agreement with ξ/β_0 derived from rotation-vibration interactions. The quantities ρ and μ on the other hand appear reduced by $1-\varepsilon\beta_0$ and $1-2\varepsilon\beta_0$ respectively.

All quantitative corrections discussed above appear to be of minor influence and some even cancel one another. Together with numerical uncertainties in the electronic matrix element and parameters like β_0 there may be room for theoretical corrections as large as 30—40 %.

It thus seems that the theory has to be changed basically. In that case one would naturally be led to the sole assumption made in the derivation of the E0 operator, viz. the assumption of incompressibility of nuclear matter.

To see the implications of this assumption it is again instructive to choose ^{90}Zr as illustration. The E0 matrix element M_{fi} there describes in a correspondence picture an oscillation between the spherically symmetric distributions built from the $(2p_{\frac{1}{2}})_0^2$ and $(1g_{\frac{9}{2}})_0^2$ states. Nuclear charge is in this case bound to be compressed and dilated in the course of the oscillation.

A more detailed picture has been used in the derivation of the collective E0 operator given in section 2. In the resulting charge distribution (9) are contained both a *spherical* and *non-spherical* part, the latter of which is not seen in the ground state distribution. It plays, however, a role in the radial oscillation between the densities in the two states, since charge may flow from ρ_{sph} to $\rho_{\text{non-sph}}$ and vice versa. It is this mechanism which explains the occurrence of 0^+ states in even nuclei far below the states describing collective compression modes [45]). Though there is no a priori reason for it, the stringent assumption of incompressible matter causes this flow to preserve density at each point. A comparison between the theory given and experiment is thus at least in part a test for the compressibility of nuclear matter. It would by no means be surprising to find that the compressibility of the dilute nuclear charge density in the transition region of a more realistic charge distribution indeed affects E0 rates.

It may be of interest to point at an analogous situation in the study of atomic isotope shifts, which are the static analogues of E0 transitions [4, 46]). Isotope shifts are also in a sense a measure of nuclear compressibility. There however, many features like the density of the valence electron at the nucleus or the possible influence of nuclear polarizability are only approximately

known and the test is thus less direct and subject to uncertainties.

The extent to which nuclear matter is compressible is probably best tested by means of inelastic electron scattering experiments [47, 48]). The present low resolution, however, will make it hard to get clean results. More accurate experiments in ordinary decay could, however, already substantiate a disagreement or show its absence within reasonable limits. Such experiments should be performed in nuclei like the U or Pu isotope where accurate level locations give already useful information and where 0^+ levels are excited in α decay. In addition to the $\mu(0^{+\prime} \rightarrow 2^+)$ ratio, a set of intensity measurements by Coulomb excitation to the 2^+, $2^{+\prime}$ levels is indispensable for the proof that a possible disagreement in μ values is not due to inconsistencies in γ branching ratios. If well-established dicrepancies would turn out to be of systematic nature only, it would justify a study of the influence of non-uniform charge distributions and of nuclear compressibility.

The author holds it a pleasure to thank Drs. Lipkin, Tassie and Glick for illuminating discussions and many useful remarks. He has also benefited from several communications of unpublished data.

References

1) E. L. Church and J. Weneser, Phys. Rev. **103** (1956) 1035
2) ^{16}O: Devons *et al.*, Proc. Phys. Soc. A **67** (1951) 134;
^{40}Ca: R. O. Bent *et al.*, Phys. Rev. **98** (1955) 1325;
^{72}Ge: J. J. Kraushaar *et al.*, Phys. Rev. **101** (1956) 139;
^{90}Zr: T. Yuasa and J. Labérique-Frollow, J. Phys. Rev. **17** (1956) 558, **18** (1957) 498;
Kloepper *et al.*, Phys. Rev. **114** (1959) 240
3) ^{12}C: G. Harris, J. H. Fregau and R. Hofstadter, Proc. Phys. Soc. A **67** (1954) 153;
^{42}Ca: I. Asplund and T. Wiedling, Arkiv for Fysik **15** (1959) 303;
^{70}Ge: D. Alburger, Phys. Rev. **109** (1958) 1222;
^{140}Ce: Dželepow *et al.*, Nuclear Physics **9** (1957/58) 665
4) A. S. Reiner, Ph. D. thesis, Amsterdam (1958, unpublished)
5) J. Marklund, B. van Nooyen and Z. Grabowski, Nuclear Physics **15** (1960) 533.
6) A. S. Reiner, Physica **23** (1957) 338
7) A. Bohr, Mat. Fys. Medd. Dan. Vid. Selsk. **26**, No. 14 (1952)
8) L. J. Tassie, Austral. J. of Physics **9** (1956) 407
8a) J. O. Rasmussen, Nuclear Physics **19** (1960) 85
9) A. Bohr and B. R. Mottelson, Mat. Fys. Medd. Dan. Vid. Selsk. **27**, No. 16 (1953)
10) A. S. Davidov and G. F. Fillipov, Nuclear Physics **8** (1958) 237
11) L. Wilets and M. Jean, Phys. Rev. **102** (1956) 788
12) L. Pauling, Quantum Mechanics (McGraw Hill New York)
13) B. L. Cohen and R. E. Price, Phys. Rev. **118** (1960) 1582
14) H. T. Motz, Phys. Rev. **104** (1956) 1353
15) R. K. Girgis and R. van Lieshout, Physica **25** (1959) 1200
16) G. T. Emery and W. Kane, Phys Rev. **110** (1960) 755;
G. Schupp *et al.*, Phys, Rev. **120** (1960) 189;
D. G. E. Martin and G. Parry, Proc. Phys. Soc. A **68** (1955) 1177;
F. Demichelis and R. A. Ricci, Nuovo Cim. **9** (1956) 96
17) F. K. McGowan and P. M Stelson, Phys. Rev. **110** (1958) 489

18) D. Alburger and B. Toppel, Phys. Rev. **100** (1955) 1357
19) K. Alder *et al.*, Rev. of Mod. Phys. **20** (1956) 432
20) J. Marklund, O. Nathan and O. B. Nielsen, Nuclear Physics **15** (1960) 199
21) T. R. Gerholm and B. G. Petterson, Phys. Rev. **110** (1958) 1119
22) M. Tutter, Z. für Physik **155** (1957) 360
23) J. Marklund, Nuclear Physics **9** (1958/59) 83
24) M. Birk, G. Goldring and Y. Wolfson, Phys. Rev. **116** (1959) 730;
R. K. Sheline, H. L. Nielsen and A. Sperduto, Nuclear Physics **16** (1960) 518
25) O. Nathan and S. Hultberg, Nuclear Physics **10** (1959) 118
26) F. K. MacGowan and P. H. Stelson, Paris Conf. 1958, (Dunod Paris); Phys. Rev. **120** (1960) 1803
27) F. S. Stevens, R. M. Diamond and I. Perlman, Phys. Rev. Letters **3** (1959) 435
28) F. E. Durham, D. H. Rester and C. M. Class, Phys. Rev. Letters **5** (1960) 202
29) Bell, Bjornholm and Severiens, Mat. Fys. Medd Dan. Vid. Selsk. **32**., No 12 (1960)
30) Skurnik, Elbek and Olesen, Nuclear Physics **22** (1961) 316
31) E. M. Bernstein, Bull, Am. Phys. Soc. **4** (1959) 9
32) S. Bjornholm, A. Knutsen and O. B. Nielsen, (to be published)
33) O. Nathan, private communication (1958)
34) G. J. Gallagher, H. L. Nielsen and O. B. Nielsen, (to be published)
35) E. Arbmann, S. Bjørnholm and O. B. Nielsen, Nuclear Physics **21** (1960) 406
36) C. J. Gallagher and, T. O. Thomas, Nuclear Physics **14** (1959) 1
37) S. Bjørnholm and O. B. Nielsen, to be pubished
38) F. E. Durham, D. H. Rester and C. M. Class, Proc. Kingston Conf. on Nuclear Structure (North-Holland Publishing Co., Amsterdam, 1960)
39) I. Perlman and F. Asaro, Kingston Conf. 1960 (unpublished)
40) Bunker *et al.*, Phys. Rev. **116** (1959) 143
41) J. P. Elliot, Phys. Rev. **101** (1956) 1212;
P. J. Richmond, Phys. Rev. **102** (1956) 751
42) R. A. Ferrell and J. Visscher, Phys. Rev. **102** (1956) 450, **104** (1956) 458
43) B. F. Bayman, A. S. Reiner and R. K. Sheline, Phys. Rev. **115** (1959) 1627;
I. Talmi and I. Unna, Nuclear Physics **19** (1960) 225
44) A. Bohr and B. Mottelson, Nuclear Physics **14** (1957) 529, (1958/59) 687;
V. Strutinsky, J. of Nucl. Energy **4** (1957) 523
45) A. M. Lane and E. D. Pendlebury, Nuclear Physics **15** (1960) 39
46) A. R. Bodmer, Nuclear Physics **9** (1958/59) 371
47) L. Tassie and A. S. Reiner, Bull. Am. Phys. Soc. **6** (1961)
48) L. Tassie, Nuovo Cim. Bull. Cim. Phys. Soc. **18** (1960) 525

1.D.2 *Nuclear Physics* **27** (1961) 134—143; © *North-Holland Publishing Co., Amsterdam*
Not to be reproduced by photoprint or microfilm without written permission from the publisher

THE SHAPE OF THE ATOMIC NUCLEUS AND ZERO SPIN EXCITED STATES

A. S. DAVYDOV, V. S. ROSTOVSKY and A. A. CHABAN
Department of Physics, Moscow State University, Moscow, USSR

Received 26 January 1961

Abstract: Collective excited states corresponding to rotation, β- and γ-oscillations of the surface of even nuclei are investigated. The probabilities for EO transitions between these states and E2 transitions from zero spin levels are calculated for spherical nuclei and non-spherical nuclei with $\gamma_0 = 0$ as well as $\gamma_0 \neq 0$. It is shown that the parameter γ in the theory of rotational states of non-axial nuclei can be identified with the most probable value of γ_m corresponding to zero oscillations of the nuclear surface about the equilibrium position.

1. Introduction

In a recent paper of Davydov [1]) collective excitations corresponding to quadrupole oscillations of the surface of even nuclei were investigated. The wave functions and energy of the collective excited states of non-spherical nuclei were calculated by simultaneously taking into account rotation of the nucleus and β and γ oscillations. It was shown that if the potential energy of the nucleus is minimum for $\gamma_0 = 0$, it is practically impossible to separate rotation and γ oscillations for all excited states with a non-vanishing spin. It was furthermore shown that excited states with zero spin can be divided into β and γ oscillations. In the present paper the wave functions for collective excited states derived in ref. [1]) are employed in a calculation of the probability of monopole electric transitions between various states.

Due to the zero oscillations of the surface of the nucleus, the most probable shape of the nucleus corresponds to $\gamma \neq 0$ even when the potential energy is minimum at $\gamma_0 = 0$. It will be shown in our paper that if the parameter γ encountered in Davydov and Chaban's paper [2]) on rotational-vibrational interaction is assumed to equal the most probable value of γ_m for the ground state of the nucleus, then in a good approximation the ratio of the excited state energies, the spins of these states and the probabilities for transitions between them can be deduced. These results signify that the phenomenological parameter γ introduced in our previous papers [2–4]) can be regarded as a parameter corresponding to the most probable value γ_m in the ground state of the nucleus. It will be shown that for small values of γ_m this interpretation permits one to determine the position of zero state levels in the case of β-as well as γ-oscillations.

2. The Most Probable Shape of the Nucleus and Collective Excitations

If the minimum of deformation potential energy of the nuclear surface corresponds to the value $\gamma_0 = 0$, then according to ref. [1]) the γ-oscillations wave function can be written in the form

$$\Phi(\gamma) = N \exp\left(-\frac{\gamma^2}{4\Gamma^2}\right), \qquad 0 \leqq \gamma \leqq \tfrac{1}{3}\pi, \tag{2.1}$$

where

$$\Gamma^2 = \frac{1}{2\sqrt{D}} = \mu^2 \frac{\omega}{2\omega_\gamma}. \tag{2.2}$$

Here

$$\mu = \beta_0^{-1}\sqrt{\hbar\omega/C} \tag{2.2a}$$

is the non-adiabaticity parameter introduced in ref. [2]); ω and ω_γ are respectively the β- and γ-oscillation frequencies; N is a normalization factor. Since $\omega = \sqrt{C/B}$ we find from (2.2) and (2.2a) that

$$\omega_\gamma = \hbar[2B\beta_0^2\Gamma^2]^{-1}. \tag{2.2b}$$

In γ space a volume element is $\sin 3\gamma \, d\gamma$ and therefore the most probable value of γ is defined by the equality

$$\gamma_m = \Gamma.$$

According to ref. [1]), for $\gamma_0 > 15°$ the oscillation wave function has the form

$$\Phi(\gamma) = N \, (\sin 3\gamma)^{-\frac{1}{2}} \exp\left[-\frac{(\gamma-\gamma_0)^2}{4\Gamma^2}\right].$$

The most probable value of γ is therefore identical to γ_0, i.e., $\gamma_m = \gamma_0$.

We shall now show that the most probable value derived above (for $\gamma_0 = 0$) can be identified with the parameter γ in the theory of non-axial nuclei [2–4]). Two zero spin levels of 1086 (0^+) keV and 1765 (0^+) keV were identified by King and Johns [5]) among the excited levels of the Os^{188} nucleus. It has been shown [2]) that from the experimental values of the energies of levels with spins 2, 4, 2 (or of any other three levels), one can determine for this nucleus the two parameters $\mu = 0.25$ and $\gamma = 19°$ in terms of which the energies of the other rotational levels and 0^+ level corresponding to β oscillations can be expressed. The theoretical value of the energy was found to agree satisfactorily with the experimental value of 1765 keV. If the lower, 1086 keV level is assumed to correspond to γ oscillations, we obtain from (2.2) the theoretical value

$$\gamma_m = \Gamma = \mu\sqrt{\frac{E_\beta}{E_\gamma}} = 0.25\sqrt{\frac{1765}{1086}} \approx 0.324 \approx 19°,$$

which is in good agreement with the effective value $\gamma_{eff} = 19°$ derived in ref. [2]). In accord with ref. [1]) it has been assumed that for $\gamma_0 = 0$ the energy of these oscillations is $2\hbar\omega_\gamma$. We thus arrive at the conclusion that the 1086 keV level in the Os^{188} nucleus corresponds to γ-oscillations and the 1765 keV level to β oscillations.

Marklund *et al.* [6]) mention that Bjørnholm and colleagues have detected 812 keV and 1045 keV 0^+ levels in U^{234}. The energy $E_1(2)$ is 43.5 keV. The value of μ can be determined from the formula

$$\mu \approx \sqrt{E_1(2)/E_\beta(0)} \tag{2.3}$$

as long as $\mu < 0.3$ and hence $\mu = 0.23$. If the first of the levels is assumed to refer to γ-oscillations one obtains $\Gamma = \mu\sqrt{E_\beta/E_\gamma} \approx 0.26 \approx 15°$.

The zero spin levels with energies 1462 keV and 2168 keV were found among the first excited states of Er^{166} by Wilson and Pool [7]). The energy of the first rotational state in this nucleus is $E_1(2) = 80.7$ keV. Assuming furthermore that $E_\beta(0) = 2168$ keV and $E_\gamma(0) = 1462$ keV, we find from formula (2.3) that $\mu = 19$. Thus $\Gamma \approx 0.232 \approx 13.5°$ which agrees well with the effective value $\gamma_{eff} = 12.4°$.

As has been previously noted [1]) the coupling between the γ-oscillations and rotation is especially strong for $\gamma_0 = 0$. We shall now show that in this case for $\gamma < 15°$ (when $\gamma_m = \Gamma$) the results of the theory which takes into account γ oscillation-rotation coupling are the same as those of the adiabatic theory of non-axial nuclei developed in refs. [3, 4]), providing the value $\gamma_m = \Gamma$ is ascribed to the phenomenological parameter γ in the formulas for the excited state energies presented in the above-mentioned papers. As a matter of fact, it has been shown [1]) that for non-spherical nuclei with $\gamma_0 = 0$ the energy of excited spin 3 levels can be expressed by the formula

$$E_{n\lambda}(3) = n\hbar\omega + 2\hbar\omega_\gamma(\lambda+\tfrac{1}{2}) + \frac{3\hbar^2}{2B\beta_0^2}, \qquad n, \lambda = 0, 1, 2, \ldots,$$

if the interaction between β-oscillations on the one hand and rotation and γ-oscillations on the other is neglected.

Inserting in the preceding expression the value of ω_γ from (2.2b) we obtain the following expression for the energy of the first excited state of spin 3:

$$E_{00}(3) = \frac{\hbar^2}{2B\beta_0^2\Gamma^2} + \frac{3\hbar^2}{2B\beta_0^2},$$

provided $n = \lambda = 0$. On the other hand it has been shown [3]) that according to the adiabatic theory of rotational states the energy of spin 3 levels is

$$E_{ad}(3) = \frac{18\hbar^2}{4B\beta_0^2\,\mathrm{sm}^2(3\gamma_m)} \approx \frac{\hbar^2}{2B\beta_0^2\gamma_m^2} + \frac{3\hbar^2}{2B\beta_0^2}, \qquad \text{if } \gamma_m < 15°.$$

Thus $E_{00}(3) = E_{ad}(3)$.

For $\gamma_m < 15°$ the quantum number K is a comparatively good quantum number. According to ref.[1]) (see eq. (4.11)) in this case the energy of excited states of spin I with a projection K is

$$E_{n\lambda}(IK) = n\hbar\omega + \hbar\omega_\gamma(2\lambda + \tfrac{1}{2}K) + \frac{\hbar^2[I(I+1) - \frac{3}{4}K^2]}{6B\beta_0^2},$$

when coupling between γ-oscillations and rotation is taken into account.

Inserting the value of ω_γ from (2.2b) we find for the case $n = \lambda = 0$ that

$$E_{00}(IK) = \frac{\hbar^2 K}{4B\beta_0^2\Gamma^2} + \frac{\hbar^2[I(I+1) - \frac{3}{4}K^2]}{6B\beta_0^2}. \tag{2.4}$$

On the other hand, in the adiabatic theory of rotational states, the spin 2 energy levels (e.g., $\gamma_m < 15°$) are defined by the formulas

$$E_1(2) = \frac{9\hbar^2\left(1 - \sqrt{1 - \frac{8}{9}\sin^2(3\gamma_m)}\right)}{4B\beta_0^2\sin^2(3\gamma_m)} \approx \frac{\hbar^2}{B\beta_0^2}, \tag{2.5}$$

$$E_2(2) = \frac{9\hbar^2\left(1 + \sqrt{1 - \frac{8}{9}\sin^2(3\gamma_m)}\right)}{4B\beta_0^2\sin^2(3\gamma_m)} \approx \frac{\hbar^2}{2B\beta_0^2\gamma_m^2} + \frac{\hbar^2}{2B\beta_0^2}. \tag{2.6}$$

For $\Gamma = \gamma_m$ these formulas, as one would expect, are identical to formula (2.4) with $I = 2$, $K = 0$ and $I = 2$, $K = 2$ respectively.

In particular, from (2.5) and (2.6) the following approximate formula for estimating γ_m^2 obtains:

$$\frac{E_2(2)}{E_1(2)} = \tfrac{1}{2}\left(1 + \frac{1}{\gamma_m^2}\right) \approx \frac{1}{2\gamma_m^2}. \tag{2.7}$$

By using (2.2b) and (2.5) an approximate formula for nuclei with $\gamma_m < 15°$ can be derived from (2.6):

$$2E_2(2) - E_1(2) \approx 2\hbar\omega_\gamma \approx E_\gamma(0). \tag{2.8}$$

By comparing the figures in the last two columns in table 1 it can be seen

TABLE 1

Spin 2 energy levels and γ-oscillational level

Nucleus	$E_1(2)$	$E_2(2)$	$2E_2(2) - E_1(2)$	$E_\gamma(0)$	Ref.
Er^{166}	80.7	788	1495.3	1462	[7])
Os^{188}	155	633	1111	1086	[5])

that the equation is valid for the Er^{166} and Os^{188} nuclei. This indicates that it is correct to ascribe the corresponding excited states of zero spin to γ oscillations.

The examples presented above thus indicate that the parameter γ in the theory of non-axial nuclei [2-4]) can be equated to the most probable value $\gamma_m = \Gamma$ providing relation (2.8) is approximately valid. If (2.8) does not hold, the potential energy minimum will not correspond to $\gamma_0 = 0$. Then $\gamma_m = \gamma_0$. In this case, as Davydov has shown [1]), the energy of the first zero spin excited state is defined by the expression

$$E_\gamma(0) \approx \hbar\omega_\gamma = \frac{\hbar^2}{2B\beta_0^2\Gamma^2}.$$

The energy of this level may thus be close to that of the level

$$E_2(2) = \frac{9\hbar^2\left(1+\sqrt{1-\frac{8}{9}\sin^2(3\gamma_m)}\right)}{4B\beta_0^2\sin^2(3\gamma_m)}.$$

The first two zero spin excited levels with energies of 1135 keV and 1305 keV in the Gd^{114} nucleus found by Groshev *et al.* [8]) and Cohen and Price [9]) may possible refer to γ and β oscillations. According to Davydov and Chaban [2]) this nucleus is characterized by the values $\mu = 0.54$ and $\gamma_{eff} = 22.5°$. Thus in this nucleus $\gamma_m = \gamma_0 = 22.5°$ and the parameter $\Gamma = \mu\sqrt{\omega/2\omega_\gamma} = \mu\sqrt{E_\beta(0)/2E_\gamma(0)}$ will equal either 20.5° or 23° depending on which of the discovered levels refers to γ oscillations. Thus in the Gd^{114} nucleus the value of Γ and equilibrium value γ_0 are of the same order of magnitude.

3. Electric Monopole Transitions Between Zero Spin States

The part of the operator for electric monopole transitions between collective nuclear excitations which depends on the internal coordinates of the nucleus is defined by the expression

$$\mathcal{M}(\mathrm{E0}) = \frac{3Z}{4\pi}\left(\frac{4\pi}{5} + \beta^2 + \frac{5\sqrt{5}}{21\sqrt{\pi}}\beta^3\cos 3\gamma\right), \tag{3.1}$$

where Z is the nuclear charge. Formula (3.1) can be used to calculate the nuclear parameter ρ (strength parameter) corresponding to a transition between nuclear states Φ_i and Φ_f,

$$\rho = \langle\Phi_f|\mathcal{M}(\mathrm{E0})|\Phi_i\rangle. \tag{3.2}$$

The constant additive term in (3.1) does not contribute to the matrix element. The role of the other two terms depends on the nature of the nuclear states between which the transition occurs.

3.1. SPHERICAL NUCLEI

Consider first E0-transitions in spherical nuclei ($\beta_0 = 0$). The excited states in this case are uniformly spaced, the distance between the levels being $\hbar\omega$.

We introduce the following wave functions [1]):

$$|0n\lambda\rangle = N_{n\lambda} y^{\frac{1}{4}(2+3\lambda)} e^{-\frac{1}{2}y} P_\lambda (\cos 3\gamma) F(-n, 3\lambda+\tfrac{5}{2}, y), \tag{3.3}$$

where

$$y \equiv \beta^2/\beta_{00}^2, \qquad \beta_{00}^2 \equiv \hbar/\sqrt{BC}, \tag{3.4}$$

P_λ is a Legendre polynomial, $F(-n, \alpha, y)$ a hypergeometric function and

$$N_{n\lambda} = \left\{\frac{3(2\lambda+1)\Gamma(n+3\lambda+\frac{5}{2})}{n!\beta_{00}[\Gamma(3\lambda+\frac{5}{2})]^2}\right\}^{\frac{1}{2}} \tag{3.5}$$

corresponds to a zero spin state excitation energy

$$E_{n\lambda}(0) = \hbar\omega(2n+3\lambda), \qquad n, \lambda = 0, 1, 2, \ldots. \tag{3.6}$$

The functions (3.3) are defined in space with a volume element

$$d\tau = \sin 3\gamma \, d\gamma \, d\beta, \qquad 0 \leqq \beta < \infty, \; 0 \leqq \gamma \leqq \tfrac{1}{3}\pi. \tag{3.7}$$

The operator (3.1) and the functions (3.3) can be employed to determine the matrix element for the E0-transition between the first excited β-oscillation state of zero spin and the ground state (transition energy $2\hbar\omega$)

$$\rho(0_\beta \to 0) = \langle 010|\mathcal{M}(\mathrm{E0})|000\rangle = -\frac{3Z}{4\pi}\sqrt{\tfrac{5}{2}}\beta_{00}^2. \tag{3.8}$$

The matrix element for E0-transition between a zero spin γ-vibrational state and ground state is

$$\rho(0_\gamma \to 0) = \langle 001|\mathcal{M}(\mathrm{E0})|000\rangle = \frac{75Z}{8\sqrt{42\pi}^{\frac{1}{2}}}\beta_{00}^3. \tag{3.9}$$

Thus the ratio of the E0-transition matrix elements of the type indicated above is

$$\frac{\rho(0_\gamma \to 0)}{\rho(0_\beta \to 0)} = -\frac{25}{2\sqrt{105\pi}}\beta_{00} \approx -0.69\beta_{00}. \tag{3.10}$$

The matrix element for transitions between a zero spin γ-vibrational state and the corresponding β-vibrational level is equal to

$$\rho(0_\gamma \to 0_\beta) = -\left(\frac{15}{\pi}\right)^{\frac{1}{2}}\frac{Z\beta_{00}^3}{8\sqrt{7}}. \tag{3.11}$$

The forms of the normalized wave functions of the first two excited spin 2 states of energies $\hbar\omega$ and $2\hbar\omega$ are (see ref. [1])) respectively

$$\Psi_{21} = \left(\frac{16}{15\sqrt{\pi}\beta_{00}}\right)^{\frac{1}{2}} e^{-\frac{1}{2}w} y^{\frac{3}{2}} \Phi_{21}(\gamma, \theta_i),$$
$$\Psi_{22} = \left(\frac{32}{105\sqrt{\pi}\beta_{00}}\right)^{\frac{1}{2}} e^{-\frac{1}{2}w} y^{2} \Phi_{22}(\gamma, \theta_i), \tag{3.12}$$

where

$$\Phi_{21}(\gamma, \theta_i) = \frac{\sqrt{15}}{4\pi}\left\{D^2_{M0}\cos\gamma + \frac{D^2_{M2}+D^2_{M,-2}}{\sqrt{2}}\sin\gamma\right\},$$
$$\Phi_{22}(\gamma, \theta_i) = \frac{\sqrt{15}}{4\pi}\left\{D^2_{M0}\cos 2\gamma - \frac{D^2_{M2}+D^2_{M,-2}}{\sqrt{2}}\sin 2\gamma\right\}.$$

These functions can be used to find the E0 transition matrix element between states Ψ_{22} and Ψ_{21}

$$\rho(22 \to 21) = \frac{15\sqrt{5}}{8\sqrt{14}\pi^{\frac{1}{2}}} Z\beta_{00}^3. \tag{3.13}$$

3.2. NON-SPHERICAL NUCLEI WITH A MINIMUM POTENTIAL ENERGY AT $\gamma_0 = 0$

In non-spherical nuclei in which the potential energy has minimum at $\gamma_0 = 0$ it is found that for small values of μ ($< 1/3$) and Γ ($< 15°$), states with an energy

$$E_{n\lambda}(0) = n\hbar\omega + 2\lambda\hbar\omega_\gamma, \qquad n, \lambda = 0, 1, 2, \ldots \tag{3.14}$$

can described by the wave functions

$$\Psi^0_{n\lambda} = \frac{H_n\left(\frac{\beta-\beta_0}{\mu\beta_0}\right) F(-\lambda, 1, \gamma^2/2\Gamma^2)}{[2^n n!\mu\beta_0\sqrt{\pi}]^{\frac{1}{2}}\Gamma} \exp\left\{-\tfrac{1}{2}\left[\frac{\gamma^2}{2\Gamma^2} + \left(\frac{\beta-\beta_0}{\mu\beta_0}\right)^2\right]\right\}, \tag{3.15}$$

where H_n is a Hermite polynomial and the $F(-\lambda, 1, x)$ are hypergeometric functions. Functions (3.15) are prescribed in space $\beta, \gamma(0, \infty)$ with a volume element $d\tau = \gamma d\gamma d\beta$.

By employing (3.15) the nuclear matrix element for E0-transitions from the first zero spin β-vibrational level to the ground state (transition energy $E_\beta = \hbar\omega$) can be found:

$$\rho(0_\beta \to 0) = \frac{3\sqrt{2}}{4\pi} Z\mu\beta_0^2. \tag{3.16}$$

The corresponding transition (transition energy $E_\gamma = 2\hbar\omega_\gamma$) form the first γ-vibrational level to the ground state is much less probable as its nuclear matrix element is

$$\rho(0_\gamma \to 0) = \frac{45\sqrt{5}}{28\pi^{\frac{1}{2}}} Z\Gamma^2\beta_0^3 = \frac{45\sqrt{5}}{28\pi^{\frac{1}{2}}} Z\frac{E_\beta}{E_\gamma}\mu^2\beta_0^3. \tag{3.17}$$

The E0-transition matrix element between the first β-vibrational level of zero spin and the corresponding γ-vibrational level is

$$\rho(0_\beta \to 0_\gamma) = \frac{135\sqrt{5}}{28\sqrt{2}\pi^{\frac{3}{2}}} Z \frac{E_\beta}{E_\gamma} \mu^2 \beta_0^3.$$

3.3. NON-SPHERICAL NUCLEI WITH $\gamma_0 > 10°$

In the approximation of small non-adiabaticity and for a small value of Γ, the energy of zero spin states in nuclei with $\gamma_0 > 15°$ is defined by the formula

$$E_{n\lambda}(0) = n\hbar\omega + \lambda\hbar\omega_\gamma.$$

The corresponding wave functions are

$$\Psi_{n\lambda}(\beta,\gamma) = \frac{H_\lambda\left(\frac{\gamma-\gamma_0}{\Gamma\sqrt{2}}\right) H_n\left(\frac{\beta-\beta_0}{\mu\beta_0}\right)}{[\pi 2^{\lambda+n+\frac{1}{2}} \lambda! n! \mu\beta_0 \Gamma \sin 3\gamma]^{\frac{1}{2}}} \exp\left\{-\tfrac{1}{2}\left[\frac{(\gamma-\gamma_0)^2}{2\Gamma^2} + \left(\frac{\beta-\beta_0}{\Gamma\beta_0}\right)^2\right]\right\}. \quad (3.18)$$

These functions are defined in β, γ space with a volume element $d\tau = \sin 3\gamma \, d\gamma \, d\beta$.

Using (3.18) we find that the matrix element for E0- transition from the first vibrational zero spin level to the ground state is the same as (3.16). The E0-transition matrix element from the first γ vibrational state to the ground state is defined by the expression

$$\rho(0_\gamma \to 0) = -\frac{15\sqrt{5}}{28\pi^{\frac{3}{2}}} \sqrt{\frac{E_\beta}{2E_\gamma}} Z\mu\beta_0^3 \sin 3\gamma_0. \quad (3.19)$$

Finally, for the E0-transition matrix element between the first β-vibrational and first γ-vibrational levels we obtain the expression

$$\rho(0_\beta \to 0_\gamma) = -\frac{45\sqrt{10}}{56\pi^{\frac{3}{2}}} Z \sqrt{\frac{E_\beta}{2E_\gamma}} \mu^2\beta_0^3 \sin 3\gamma_0. \quad (3.20)$$

From (3.19) and (3.16) we get

$$\left|\frac{\rho(0_\gamma \to 0)}{\rho(0_\beta \to 0)}\right| = \frac{5\sqrt{5}}{7\sqrt{2\pi}} \sqrt{\frac{E_\beta}{2E_\gamma}} \beta_0 \sin 3\gamma_0 \approx 0.64 \frac{\Gamma}{\mu} \beta_0 \sin 3\gamma_0. \quad (3.21)$$

4. Zero Spin States and Electric Quadrupole Transitions

In order to obtain more complete information on the properties of collective zero spin excitations corresponding to β- and γ-oscillations of the nuclear surface we shall consider E2 transitions from these levels to spin 2 levels.

The E2 transition operator has the form

$$Q_{2\mu} = Q_0 \frac{\beta}{\beta_0}\left(D^2_{\mu 0}\cos\gamma + \frac{D^2_{\mu 2}+D^3_{\mu,-2}}{\sqrt{2}}\sin\gamma\right), \qquad Q_0 = \frac{3ZR^2\beta_0}{\sqrt{5\pi}}. \tag{4.1}$$

For $\gamma_0 = 0$ and $\Gamma < 15°$ the wave functions of states with spin I ($n = 0$, $\lambda = 0$) correspond approximately to states with a definite value of K (only even values)

$$\Psi_{IK}(\beta, \gamma, \theta_i) = |IK\rangle \left(\frac{\gamma^2}{2\Gamma^2}\right)^{\frac{1}{2}K} \frac{\exp\left\{-\frac{1}{2}\left[\frac{\gamma^2}{2\Gamma^2} + \left(\frac{\beta-\beta_0}{\mu\beta_0}\right)^2\right]\right\}}{\Gamma\left[\mu\beta_0\sqrt{\pi}\left(\frac{K}{2}\right)!\right]^{\frac{1}{2}}}, \tag{4.2}$$

where

$$|IK\rangle = \left[\frac{2I+1}{16\pi^2(1+\delta_{K0})}\right]^{\frac{1}{2}} \{D^I_{MK}(\theta_i) + (-1)^I D_{M,-K}(\theta_i)\}. \tag{4.3}$$

The reduced E2 transition probability is given by the expression

$$B(\mathrm{E2}; 0 \to 2K) = \frac{5}{16\pi}\sum_{M\mu}|\langle\Psi_{2K}|Q_{2\mu}|\Psi^0_{n\lambda}\rangle|^2.$$

Inserting into this expression $\Psi^0_{n\lambda}$ from (3.15) for $n = 0$, $\lambda = 1$, and $n = 1$, $\lambda = 0$ and function Ψ_{2K} from (4.2) for $K = 0$ and $K = 2$, we get

$$B(\mathrm{E2}; 0_\beta \to 20) = \frac{5Q_0^2}{32\pi}\mu^2, \qquad B(\mathrm{E2}; 0_\beta \to 22) = \frac{5Q_0^2}{16\pi}\mu^2\Gamma^2, \tag{4.4}$$

$$B(\mathrm{E2}; 0_\gamma \to 20) = \frac{5Q_0^2}{16\pi}\Gamma^4, \qquad B(\mathrm{E2}; 0_\gamma \to 22) = \frac{5Q_0^2}{8\pi}\Gamma^2. \tag{4.5}$$

For a more accurate calculation of the reduced probabilities it should be kept in mind that K is not a good quantum number. The wave functions of the two spin 2 states can be represented by a linear combination of states with $K = 0$ and $K = 2$. These functions can be determined by solving the set of equations (4.7) in ref. [1]) by perturbation theory methods; the solutions with a definite value of K presented above may be employed as the zero approximation. We then obtain

$$\begin{aligned}\Psi_1(2) &= \Psi_{20} + \frac{4\sqrt{2}}{3}\Gamma^3\Psi_{22},\\ \Psi_2(2) &= \Psi_{22} - \frac{4\sqrt{2}}{3}\Gamma^3(\Psi_{20}+\Psi^1_{20}),\end{aligned} \tag{4.6}$$

where Ψ_{20} and Ψ_{22} are defined by (4.2) and the function

$$\Psi^1_{20} = |20\rangle \frac{1-\frac{\gamma^2}{2\Gamma^2}}{[\mu\beta_0\sqrt{\pi}]^{\frac{1}{2}}\Gamma} \exp\left\{-\tfrac{1}{2}\left[\frac{\gamma^2}{2\Gamma^2}+\left(\frac{\beta-\beta_0}{\mu\beta_0}\right)^2\right]\right\}$$

corresponds to an excited state with $I = 2$, $K = 0$, $n = 0$ and $\lambda = 1$. The E2-transition probabilities calculated with the aid of functions (4.6) yield the following relations:

$$\frac{B(\mathrm{E2};\, 22 \to 21)}{B(\mathrm{E2};\, 22 \to\ \ 0)} = \tfrac{10}{7}\,(1+8\Gamma^2), \qquad \frac{B(\mathrm{E2};\, 0 \to 22)}{B(\mathrm{E2};\, 0 \to 21)} = 2\Gamma^2(1-2\Gamma^2),$$

$$\frac{B(E2;\, 0_\beta \to 22)}{B(\mathrm{E2};\, 0_\beta \to 21)} = 2\Gamma^2(1-2\Gamma^2), \qquad \frac{B(\mathrm{E2};\, 0_\gamma \to 21)}{B(\mathrm{E2};\, 0_\gamma \to 22)} = \tfrac{1}{2}\Gamma^2(1-\tfrac{20}{3}\Gamma^2).$$

The functions (4.6) can also be used to calculate the nuclear matrix element for E0 transitions between 22 and 21 states:

$$\rho(22 \to 21) = -\frac{30\sqrt{10}}{7\pi^{\frac{3}{2}}} Z\beta_0^3\Gamma^5, \qquad \text{if} \qquad \gamma_0 = 0.$$

References

1) A. S. Davydov, Vestnik Moskovskogo Universiteta, vypusk phys. **1** (1961) 65; Nuclear Physics **24** (1961) 682
2) A. S. Davydov and A. A. Chaban, Nuclear Physics **20** (1960) 499
3) A. S. Davydov and G. F. Filippov, JETP **35** (1958) 440; Nuclear Physics **8** (1958) 237
4) A. S. Davydov and V. S. Rostovsky, JETP **36** (1959) 1788; Nuclear Physics **12** (1959) 58
5) W. J. King and M. W. Johns, Can. Journ. Phys. **37** (1959) 755
6) I. Marklund *et al.*, Nuclear Physics **15** (1960) 533
7) R. G. Wilson and M. I. Pool, Phys. Rev. **119** (1960) 262
8) L. V. Groshev *et al.*, Proc. Intern. Conf. on Nuclear Structure, Kingston, August 29-September 3, 1960 (University of Toronto Press)
9) B. L. Cohen and R. E. Price, Phys. Rev. **118** (1960) 1582

7.C

Nuclear Physics **27** (1961) 144—147; © *North-Holland Publishing Co., Amsterdam*

Not to be reproduced by photoprint or microfilm without written permission from the publisher

ON THE MECHANISM OF INTERACTION OF FAST PROTONS WITH NUCLEI

K. D. TOLSTOV

High Energies Laboratory, Joint Institute for Nuclear Research, Dubna, USSR †

Received 28 December 1960

Abstract: The paper discusses the results of the publications concerned with the interaction of 9 GeV protons with photoemulsion nuclei. The comparison drawn with recourse to data on nucleon-nucleon collisions warrants the conclusion that the cascade mechanism of interaction with nuclei is valid.

The mechanism of interaction with nuclei of fast nucleons in cosmic rays has been the subject of many experimental and theoretical investigations. Two alternative schemes have been suggested for explaining the experiments: the cascade mechanism of consecutive nucleon-nucleon collisions and the tunnel mechanism, i.e., the simultaneous interaction of an incident particle with a group of nucleons of the nucleus in a tube of nuclear substance along the path of the particle. Accelerators yielding particles of energy ≈ 10 eV made a definite solution of this problem possible for this energy region, since our knowledge of the energy of an incident particle eliminates quite a few difficulties.

In ref. [1]) it was concluded, on the strength of the analysis of the fission by 8.7 GeV protons of a group of light nuclei of photoemulsion (C, N, O) as well as silver and bromium nuclei, that the cascade mechanism of nucleon-nucleon interactions actually occurs in experiment. In this investigation the angular and momentum spectra of nuclear fission products were determined and the particles identified by their masses. This made it possible to determine the average number of consecutive collisions equal to 2 for the averaged nuclei of photoemulsion ($\bar{A} \approx 30$) or to 1.4 for light nuclei ($A = 14$). The energy spent in the generation of mesons and the fission of the medium nuclei was found equal to 5.1 ± 0.8 GeV, and the energy carried away by the fast nucleon equal to 3.0 ± 0.5 GeV. This means that their sum 8.1 ± 1 GeV agrees with the energy of the initial proton. Accordingly, the fraction of energy lost by the proton in a single collision with the nucleon of the nucleus was found equal to 0.4 ± 0.1; in later work [2, 3]) concerned with the study of proton-nucleon collisions, the figures coincided: 0.39 ± 0.02.

† Reported at the Conference on Physics of Elementary Particles Uhzgorod, May 18, 1960.

The tunnel mechanism contradicts experimental results, as is shown in ref. [1]), since this mechanism ought to give a larger number of fast particles and an essentially broader angular distribution. The authors of ref. [2]) also concerned with the interaction of 8.7 GeV protons with nuclei also arrive at the conclusion that their results do not contradict the cascade mechanism.

The authors of ref. [4]) also lay emphasis on the cascade mechanism, but conclude that the broadening of angular distributions with increasing multiplicity of fast particle generation corresponds to a pattern of interaction intermediate between the concepts of consecutive and simultaneous interactions of the initial nucleon with the nucleons of a nucleon †.

E. Friedländer, on the other hand, who also dealt with the interaction between nuclei in photoemulsion and 9 GeV protons [5]) infers that experiment fully agrees with the tunnel mechanism. It seems worthwhile therefore to discuss the experimental data and conclusions of ref. [4]).

(i) Only a particular kind of events with a number of relativistic particles was selected. The momenta of the particles were not measured and the speed of the centre of gravity γ_c, indispensable for finding the number of nucleons in the tunnel, was determined only by the emission angles of the particles, which is not reliable.

(ii) The histograms in fig. 5, making it possible, in the author's opinion, to classify interactions with different magnitudes ν, where ν is the number of nucleons of the nucleus in the tunnel, give no errors along the ordinate-axis representing the distribution function $\phi[\xi(\nu)]$ of the events; yet these errors are rather large since only 300 events are divided into two groups, 10 intervals of ν in each. The function $\xi(\nu)$ is evaluated by the Costangoli formula, which is not rigorous. Nor were the errors along the axis $\xi(\nu)$ given, which are essential in the case of narrow peaks and minima in the histogram.

(iii) The rigidity coefficient K is determined without measuring the momenta of the secondary particles under the assumption of the transversal momentum $1/P_\perp = 0.94/\mu$, (where μ is the mass of a pion, according to data on cosmic rays). This coefficient was found equal to $K = 0.33 \pm 0.02$ and it is claimed that it is in extremely good agreement with the results of ref. [5]). It is shown in refs. [1–3]), however, that the rigidity coefficient in p-n-collisions are equal to 0.4. Consequently, we cannot regard the magnitude $K = 0.3$ as reliable since if we do, we must assume that the rigidity coefficient decreases in the tunnel mechanism when free energy in c.m.s. is larger and the number $\bar{n}_s$ grows.

(iv) The tunnel mechanism and the growth of $\bar{n}_s$ with contradicts the conservation of large energy in one particle, all the more so since this particle, as is shown in ref. [1]), is a nucleon, and on the average, one nucleon per interaction

† G. B. Zhdanov, a co-author of ref. [4]), reported at the Dubna conference, May 1960, that the continuation of the investigation and the analysis of the results led to the conclusion of the soundness of the cascade mechanism.

for in the case of collision with a group of nucleons the excitation energy in the c.m.s. is larger and the velocity of the centre system is less.

(v) Throughout his argument the author neglects secondary interactions in the nucleus, though the possible path of the particles in the nucleus and the known cross sections for mesons and nucleons call for taking account of the secondary interactions. In ref. [7]) the Monte Carlo method was used for calculating the nuclear cascade and it was shown that the results of the calculation agree with the experimental data of ref. [1]).

Apart from the above comparisons, it is necessary to bear in mind that the mechanism of fast nucleon-nucleus interaction must depend on the properties of nucleon-nucleon collisions. E. Feinberg [8]) considered the conditions requiring for the introduction of the tunnel mechanism. It was assumed that the magnitude of the transversal momentum of the recoil nucleon $P_\perp \approx \mu$, where μ is the meson mass. Then the longitudinal momentum $P_\parallel$ is equal to

$$P_\parallel \approx \frac{M^2 \nu\varepsilon}{2E(E-\nu\varepsilon)} + \frac{\nu\mu^2}{2\varepsilon} + \tfrac{1}{2}[\theta_M{}^2(E-\nu\varepsilon)+\theta_M{}^2\nu\varepsilon], \tag{1}$$

where θ_M and θ_μ are the angles of the emission of the nucleon and π-meson, ν is the number of mesons, ε is the energy of mesons and M and E are the mass and the initial energy of the nucleon. It was shown in accordance with eq. (1) in ref. [8]) that the tunnel mechanism may set in when $\theta_M \approx \theta_\mu \approx M/E$ and $\nu\varepsilon \ll E$ or $\nu\varepsilon \approx (E-\nu\varepsilon)$. If on the other hand $\theta_\mu \approx \sqrt{M/E}$ which corresponds to isotropy in the c.m.s. and

$$\nu\varepsilon > 2\frac{\mu E}{M}, \tag{2}$$

then the pattern of consecutive collisions applies. The characteristics of p-n-collisions at 9 GeV known at present [1–3]) make it possible to elucidate this; in the c.m.s. we observe a sharp anisotropy of the nucleons, while the anisotropy of the mesons is comparatively small. The experimental value is $\theta_{\mu\frac{1}{2}} \approx 16°$, while $\theta_\mu = \sqrt{M/E} = 17°$. The energy losses $\nu\varepsilon = 0.4$. This means that the inequality (2) is valid. Consequently, by comparing with experiment, we have a case when the conditions necessary for the mechanism of consecutive nucleon-nucleon collisions are fulfilled. Let us note that the experimental value $P_\perp = 0.37 \pm 0.025$ GeV is nearly three times as large as was assumed in ref. [8]) as the initial condition for introducing the tunnel model.

In view of the above it should be concluded that the inference of ref. [1]) on the validity of the cascade mechanism for nucleon-nucleus collisions is correct for the energy region 10 GeV.

References

1) V. S. Barashenkov *et al.*, Nuclear Physics **14** (1960) 522
2) N. P. Bogachev *et al.*, JETP **38** (1960) 432
3) Vang Chou Feng *et al.*, preprint JINR P—526
4) G. B. Zhdanov *et al.*, JETP **37** (1959) 620
5) E. Friedländer, Nuovo Cim. (1959) 796
6) G. L. Bayatyan *et al.*, JETP **36** (1959) 690
7) V. S. Barashenkov *et al.*, Nuclear Physics (in the press)
8) E. L. Feinberg, JETP **28** (1955) 211

7.A

Nuclear Physics **27** (1961) 148—159; © *North-Holland Publishing Co., Amsterdam*

Not to be reproduced by photoprint or microfilm without written permission from the publisher

SCATTERING OF π-MESONS ON K-MESONS AT LOW ENERGIES

P. S. ISAEV and M. V. SEWERYNSKI

Laboratory of Theoretical Physics, Joint Institute for Nuclear Research, Dubna, USSR

Received 20 January 1961

Abstract: Explicit expression for s- and p-phase shifts of π-K-scattering are obtained in the effective-range approximation.

1. Approximate Equations for Scattering Amplitudes

Approximate equations for π-K-scattering partial amplitudes were obtained in ref. [1]). Obtaining exact solutions for these equations involves considerable difficulties at present: firstly it is necessary to know the s- and p-phase shifts of pion-pion scattering; secondly, so far there has been no reliable rule for selecting the physical solution out of the solutions obtained by the iteration method on electronic ccmputors.

It is possible, however, to obtain in rough approximation, one of the possible solutions of the set of equations (25—26) and (30—33) of ref. [1]) for the region of low energies, viz. the solution $T_l^{\frac{1}{2}} = T_l^{\frac{3}{2}}$, where $T_l^I(q^2)$ is the partial amplitude of π-K-scattering depending on the square of the momentum of the π-meson q^2 in the c.m.s. in a state of isobaric spin I and orbital momentum $l = 0$ or 1. This solution can well be used as first approximation in solving more precise equations by the iteration method on electronic computors, since the type of solution found by this method is known to depend largely on the choice of the first approximation.

Let us assume that $T_l^{\frac{1}{2}} = T_l^{\frac{3}{2}}$. Then the set of equations (25—26) from ref. [1]), for the π-K-scattering partial amplitudes averaged over all angles, will be written as

$$\operatorname{Re} T_l(q^2) = \operatorname{Re} T_l(0) + \frac{1}{16\pi^2} \mathrm{P} \int_0^\infty \mathrm{d}x \, \frac{\sqrt{x}}{W(x)} \{[n_l(x, q^2) - n_l(x, 0)]|T_0(x)|^2 + 3[\varphi_l(x, q^2) - \varphi_l(x, 0)]|T_1(x)|^2\}, \quad (1)$$

while the set of equations (30—33) from ref. [1]) for the π-K-scattering amplitudes, in the case of backward scattering, will be of the form

$$\operatorname{Re} T_0(q^2) = \operatorname{Re} T_0(0) + \frac{1}{8\pi^2} \mathrm{P} \int_0^\infty \mathrm{d}x \, \frac{\sqrt{x}}{W(x)} \left\{ \frac{|T_0(x)|^2}{x(x-q^2)} [x(V(x, q^2) - V(x, 0)) + q^2 V(x, 0)] \right. \quad (2)$$

$$\left. + 3 \frac{|T_1(x)|^2}{x(x-q^2)} [x(L(x, q^2) - L(x, 0)) + q^2 L(x, 0)] \right\},$$

$$\operatorname{Re} T_1(q^2) = \frac{1}{24\pi^2} \mathrm{P} \int_0^\infty \mathrm{d}x \frac{\sqrt{x}}{W(x)} \left\{ \frac{|T_0(x)|^2}{x(x-q^2)} [x(C(x, q^2) - C(x, 0)) + q^2 C(x, 0)] \right.$$

$$\left. + 3 \frac{|T_1(x)|^2}{x(x-q^2)} [x(Q(x, q^2) - Q(x, 0)) + q^2 Q(x, 0)] \right\}. \quad (3)$$

In eqs. (1), (2) and (3) n_l, φ_l, V, L, C and Q are the complex functions of the variables q^2 and x (the full notations of which are given in ref. [1])); and $W(x)$ is the total energy of the π-K-system.

It is noteworthy that the p-phase shift of π-π-scattering does not enter into eqs. (1—3), which gives more latitude in the choice of the explicit expressions for the s-phase shift of π-π-scattering, since the self-consistency of the s- and p-phase shifts is now unnecessary.

In the present paper the expression for the s-phase shift has been taken from ref. [2]).

The π-π-scattering s-phase shifts enters into eqs. (1—3) through the exponent $\exp [u(q^2, z_1) - u(x, z_1)]$. Calculation shows that taking account of the s-phase shift leads to values close to unity for the exponent: deviations do not exceed 5 % up to the values $x \approx 10\mu^2$ (μ being the π-meson rest mass) in eq. (1), and do not exceed 15 % for the same values of x in eqs. (2) and (3). At values of $x \gtrsim 10\mu^2$ the subtraction procedure should have a strong effect and the integral contribution to eqs. (1)—(3) in the region $x > 10\mu^2$ be negligible small.

It is natural, therefore, to put $\exp [u(q^2, z_1) - u(x_1 z_1)] = 1$, for the sake of simplicity, throughout the range of the variable x. Under the same assumption, viz. that the principal contribution from the integrals over x in eqs. (1)—(3) must come from the region of low x, the following expressions for the functions n_l, φ_l, V, C, L, Q and W can be used:

$$n_l(x, q^2) = \frac{1}{x-q^2} \int_{-1}^{+1} P_l(z_1) \mathrm{d}z_1, \qquad \varphi_l(x, q^2) = \frac{1}{x-q^2} \int_{-1}^{+1} z_1 P_l(z_1) \mathrm{d}z_1;$$

$$V(x, q^2) = 1, \qquad L(x, q^2) = 0, \qquad C(x, q^2) = 0,$$

$$Q(x, q^2) = 1, \qquad W(x) = \sqrt{(M+\mu)^2 + x\left(2 + \frac{M}{\mu}\right)},$$

where M is the mass of the K-meson.

Substituting these approximate expressions into eqs. (1)—(3) we obtain in both cases the same set of splitting equations

$$\operatorname{Re} T_0(q^2) = \operatorname{Re} T_0(0) + \frac{q^2}{8\pi^2} \mathrm{P} \int_0^\infty \mathrm{d}x \frac{\sqrt{x}}{W(x)} \frac{|T_0(x)|^2}{x(x-q^2)}, \quad (4)$$

$$\operatorname{Re} T_1(q^2) = \frac{q^2}{8\pi^2} \mathrm{P} \int_0^\infty \mathrm{d}x \frac{\sqrt{x}}{W(x)} \frac{|T_1(x)|^2}{x(x-q^2)}. \quad (5)$$

2. Imaginary Part of Amplitudes

The connection of the isobaric spin states T^I with the scattering phases is of the form

$$T^I = \frac{8\pi W(x)}{\sqrt{x}} \sum_{l=0}^{\infty} (2l+1) \exp\{i\delta_l^I\} \sin\delta_l^I P_l(z_1). \tag{6}$$

Hence it is easy to obtain the following relation:

$$\frac{\operatorname{Im} T_l(x)}{|T_l(x)|^2} = \frac{\sqrt{x}}{8\pi W(x)}. \tag{7}$$

3. The s-Scattering

The solution of eq. (4) will be searched in the form

$$T_0(q^2) = \frac{b}{v(q^2)}, \tag{8}$$

where $\operatorname{Re} v(0)$ is the magnitude describing the scattering length and b is a certain constant.

From (8) it follows that the analytical properties of the function $v(q^2)$ are determined by the analytical properties of the function $T_0(q^2)$. Using the condition (7) we obtain the explicit relation † for $v(q^2)$

$$v(q^2) = \operatorname{Re} v(0) - \frac{bq^2}{8\pi^2}\int_0^{\infty} \frac{\sqrt{x}}{W(x)} \frac{\mathrm{d}x}{x(x-q^2)}, \tag{9}$$

† When in eq. (9) the subtraction is performed not at 0 but a certain point $0 \geqq q_0^2 > -\nu/\lambda$ and the integral is cut off at a certain value of the parameter L, we have the following equation for the function $v(q^2)$:

$$v(q^2) = \operatorname{Re} v(q_0^2) - \frac{1}{8\pi^2\sqrt{\lambda+\frac{\nu}{q^2}}} \ln \frac{\sqrt{\lambda+\frac{\nu}{q^2}} - \sqrt{\lambda+\frac{\nu}{L}}}{\sqrt{\lambda+\frac{\nu}{q^2}} + \sqrt{\lambda+\frac{\nu}{L}}} + \frac{1}{4\pi^2\sqrt{\lambda+\frac{\nu}{q_0^2}}} \left(\frac{\pi}{2} - \operatorname{arc\,tg} \frac{\sqrt{\lambda+\frac{\nu}{L}}}{\sqrt{\lambda+\frac{\nu}{q_0^2}}} \right) - \frac{i}{8\pi\sqrt{\lambda+\frac{\nu}{q^2}}}. \tag{10a}$$

(In eq. (10a) the positive values of q_0^2, viz. $\nu/\lambda > q_0^2 \geqq 0$, should be substituted instead of q_0^2). It is advisable to use expression (10a) for comparing the results of the given paper with those of ref. [3]).

or

$$v(q^2) = \operatorname{Re} v(0) - \frac{b}{8\pi^2\sqrt{\lambda+\frac{\nu}{q^2}}} \ln \frac{\sqrt{\lambda+\frac{\nu}{q^2}}-\sqrt{\lambda}}{\sqrt{\lambda+\frac{\nu}{q^2}}+\sqrt{\lambda}} - \frac{ib}{8\pi\sqrt{\lambda+\frac{\nu}{q^2}}}, \qquad (10)$$

where $\nu = (M+\mu)^2$ and $\lambda = 2+M/\mu$.

From (8) and (10) it is clear that T_0 actually contains only one constant, namely $b/\operatorname{Re} v(0)$. Therefore, in the following we shall put the quantity b equal to unity.

Then we must demand that the function $v(z)$ should differ from zero all over the plane of the complex variable z. Hence it follows that the subtraction constant † can assume only positive values, i.e. $\operatorname{Re} v(0) > 0$.

From expression (10) the following expression for the s-phase shift is obtained

$$\frac{q}{\sqrt{\nu+\lambda q^2}} \operatorname{ctg} \delta_0 = 8\pi \operatorname{Re} v(0) - \frac{1}{\pi\sqrt{\lambda+\frac{\nu}{q^2}}} \ln \frac{\sqrt{\lambda+\frac{\nu}{q^2}}-\sqrt{\lambda}}{\sqrt{\lambda+\frac{\nu}{q^2}}+\sqrt{\lambda}}. \qquad (11)$$

For comparing the s-phase shift obtained in the given paper with that obtained in ref. [3]), it should be assumed in (10a) that the quantity $q_0^2 = \mu^2$ (which closely corresponds to the subtraction point of ref. [3]). The results of the comparison are given in fig. 1 (some difference is due to the choice of the approximation expression for the $W(x)$).

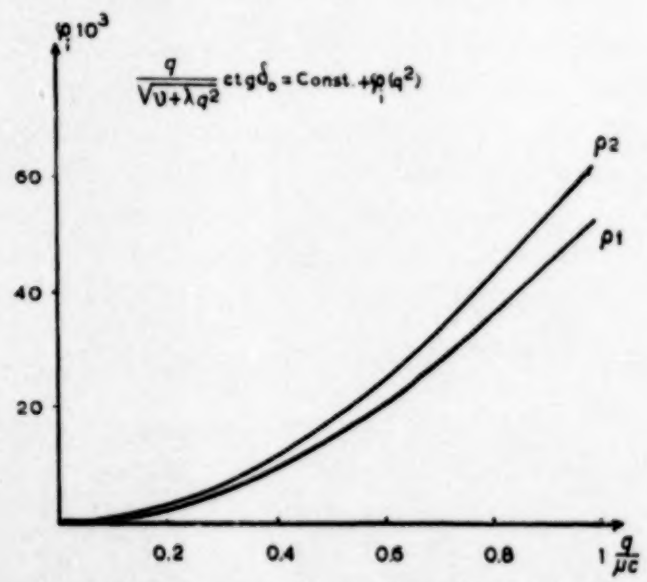

Fig. 1. Comparison of results for s-waves obtained in ref. [3]) (φ_1) and the present paper (φ_2)

† Similar restrictions imposed on the coupling constant were considered in refs. [3, 4]). These restrictions can be obtained in our work as well if we introduce the subtraction at a suitable point and demand that the function $v(q^2)$ have no zero in the region $-\mu^2 \leqq q^2 \leqq 0$.

It is important to emphasize that the region of change of the constant Re $v(0)$ depends explicitly on the choice of the subtraction point. Given a suitable choice of the constants, eq. (11) practically coincides with the expression for the s-phase of ref. [5]).

4. The p-Scattering

Eq. (5) contains no inhomogeneous term, and therefore the account of the negative cut is necessary in finding the solution by the inverse function method. Indeed, if we search the solution of eq. (5) in the form

$$T_1 = \frac{q^2}{F(q^2)} \tag{12}$$

use the expression

$$\operatorname{Im} F(q^2) = -\frac{q^3}{8\pi W(q^2)}$$

and assume, as in the case of the s-phase shift that the analytical properties of the function $F(q^2)$ are determined by those of the function $T_1(q^2)$, we obtain, by writing the Cauchy theorem for the function $F(q^2)$ and performing two subtractions,

$$\operatorname{Re} F(q^2) = A + Bq^2 - I(q^2), \tag{13}$$

where

$$A = \operatorname{Re} F(0), \qquad B = \frac{\partial \operatorname{Re} F(q^2)}{\partial q^2}\bigg|_{q^2=0}, \qquad I(q^2) = \frac{q^4}{8\pi^2} \mathrm{P} \int_0^\infty \frac{\sqrt{x}\,\mathrm{d}x}{x(x-q^2)W(x)}.$$

An elementary check, however, shows that the solution (13) gives 0 for the function $F(q^2)$ in the region $q^2 < 0$. To prevent the appearance of 0 in this region it is necessary either (a) to take account of the influence of the negative cut † or (b) to introduce a cut-off which leads to a third constant.

For our purpose (obtaining an approximate solution of eq. (5) in the region of small q^2) it is sufficient to introduce the cut off L under the condition $q^2 \ll L$.

In this case the solution assumes the form

$$\frac{q^3}{\sqrt{v+\lambda q^2}} \operatorname{ctg} \delta_1 = 8\pi(A + Bq^2) - \frac{q^2}{\pi\sqrt{\lambda + \frac{v}{q^2}}} \ln \frac{\sqrt{\lambda + \frac{v}{q^2}} - \sqrt{\lambda + \frac{v}{L}}}{\sqrt{\lambda + \frac{v}{q^2}} + \sqrt{\lambda + \frac{v}{L}}}. \tag{14}$$

† It can be shown [6]) that taking account of the influence of the negative cut under certain assumptions reduces to the emergence of an additional factor $x^\alpha (0 < \alpha < \frac{1}{2})$ in the denominator of the integrand $I(q^2)$. In this case the integral $I(q^2)$ proves to be convergent and the constants A and B can be chosen in a way preventing $F(q^2)$ going to zero for all $q^2 < 0$.

In the region $q^2 \approx 0$, the last term in eq. (14) tends to zero more rapidly than the second term and eq. (14) can be written in the form

$$\frac{q^3}{\sqrt{\nu+\lambda q^2}} \operatorname{ctg} \delta_1 \approx 8\pi A \left(1+\frac{B}{A} q^2\right), \tag{15}$$

which is in good agreement with the result of ref. [5]).

5. Conclusion

The problem of π-K-scattering has recently been investigated quite intensely. Two approaches are employed in these investigations: (a) The perturbation theory method [5]) and the kindred Chew-Low method [7]) and (b) the method of Mandelstam double representations [1, 3, 4]). Under the latter method the attempts to investigate π-K-scattering differ somewhat: in ref. [3]) the investigation is performed with the aid of the "classical" Mandelstam representations; in ref. [4]) the Cini-Fubini method [8]) is used; and in ref. [1]) use is made of the method of symmetrizing and antisymmetrizing the amplitudes to obviate the difficulties involved in the kinematic cut [2]). Yet in all three cases obtaining precise solutions for π-K-scattering is immensely difficult and the solutions can be obtained only after various simplifications. In particular, the solutions in refs. [3–4]) were sought in the effective-range approximation. The comparison of solutions for the s and p-phase shifts obtained in the given paper and in refs. [3–5]) shows that the results coincide.

Thus, the solutions (11) and (15) obtained in rather rough approximation can nevertheless prove useful in the following two cases:

a) They can be regarded as valid with a good degree of reliability for π-K-scattering in the energy region of the incident π-mesons $< \mu c^2$.

b) The solutions (11) and (15) can be used as the first approximation for solving more precise equations from ref. [1]) by the iteration method on electronic computors.

The authors are grateful to Professor H. Y. Tzu, A. Efremov and L. Solovyov for stimulating discussions.

References

1) P. S. Isaev and M. V. Sewerynski, preprint JINR P-550; Nuclear Physics **22** (1961) 663
2) A. V. Efremov *et al.*, JETP **39** (1960) 438
3) B. M. Lee, Phys. Rev. **120** (1960) 325
4) M. Gourdin, Y. Noirot and Ph. Salin, Nuovo Cim. **18** (1960) 651
5) S. Okubo, Phys. Rev. **118** (1960) 357
6) A. V. Efremov, private communication
7) G. Costa and L. Tenaglia, Nuovo Cim. **18** (1960) 368
8) M. Cini and S. Fubini, Ann. Phys. **3** (1960) 352

2.J

Nuclear Physics **27** (1961) 154—165; © *North-Holland Publishing Co., Amsterdam*

Not to be reproduced by photoprint or microfilm without written permission from the publisher

THE RATIO OF ASYMMETRIC TO SYMMETRIC FISSION IN p-WAVE NEUTRON FISSION OF U^{235}

J. G. CUNINGHAME, G. P. KITT and E. R. RAE

Atomic Energy Research Establishment, Harwell, Berks

Received 27 March 1961

Abstract: Radiochemical measurements have been made of the peak-to-valley ratio of the mass-yield curve for neutron induced fission of U^{235} at neutron bombarding energies from 65 keV to 14 MeV, with emphasis on the region about 125 keV. In this region, where p-wave interactions predominate, the peak-to-valley ratio was found to be $\approx$ 45 % higher than for thermal neutron fission, contrary to the trend suggested by the channel theory of fission.

1. Introduction

The interpretation of the phenomena observed in the fission of heavy nuclei has been strongly influenced since 1955 by the "channel theory" proposed in that year by Aage Bohr [1]). Much work, both theoretical and experimental, has been devoted to the study of the implications of this theory, and a review of the present position concerning some of these studies has been given recently by Griffin [2]).

The aspect of the channel theory with which the present work is concerned is the correlation to be expected in neutron induced fission of even compound nuclei, between the mass distributions observed and the spin and parity of the compound states. The argument for the existence of such a correlation is that in the moment when the compound nucleus becomes unstable towards fission, it still can exist in a number of more or less clearly defined quantum states, and if there is not too much excess energy available, then it will be constrained to proceed towards fission principally by way of the lowest available state which possesses the appropriate spin and parity. Hence the symmetry properties of these lowest available states should influence the whole fission process. If we examine the nature of these low lying states, on the assumption that they are similar to those in a stable heavy even nucleus, we find that they consist firstly of a ground state rotational band of levels of assignment 0^+, 2^+, 4^+ etc. At an energy of a few hundred keV higher will lie the first shape vibrational level (pear shaped vibration) on which will be built a second rotational band of odd spin, odd parity states 1^-, 3^-, 5^- etc. At somewhat higher energies will come other more complex rotational vibrational levels, and finally at around 1 MeV, the first particle state due to the unpairing of two nucleons. Above this the level

structure will be extremely complicated. Now the rotational states based on the 0^+ ground state will have wave functions which are symmetric with respect to the parameter describing the pear shaped vibration, while those based on the 1^-, first excited vibrational state, will have antisymmetric wave functions. Hence one would expect that fission proceeding via the even parity band would show a more symmetric mass distribution (higher valley in the mass-yield curve) than that proceeding via the odd parity band. Further, one could argue plausibly that states of the character 1^+, 3^+ or 2^- 4^-, which belong to neither

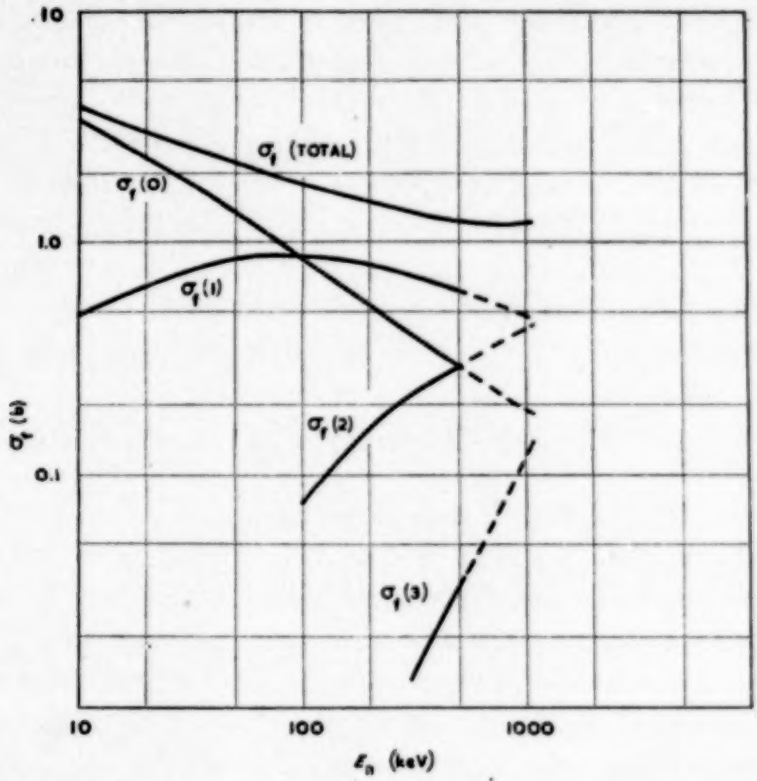

Fig. 1. Calculated partial wave fission cross-sections for neutron fission of U^{235}.

band, would contain wave functions of both the symmetric and antisymmetric type (as functions of the pear shaped vibration parameter) so that their mass distributions might be intermediate in character between the other two groups.

Following up this argument one might expect that the resonances observed in the slow neutron (s-wave) fission of U^{235}, which consist of 3^- and 4^- states, might divide into two classes according to their fission mass distributions, the 4^- states having rather higher valleys than those of the 3^- class. There is some experimental evidence for the division of the mass curves into two groups [3]), but the difference in the valley heights is small, and no spin measurements have been made to show whether the groups correlate with the two spin states. The present paper is concerned with the case in which the neutron energy is increased so that p-wave interactions become probable, and levels of character

2^+, 3^+, 4^+ and 5^+ are excited, in addition to 3^- and 4^-. Under these circumstances one might expect that the presence of the 2^+ and 4^+ states would lead to mass distributions appreciably more symmetric than the mean of the s-wave distributions. In fact the opposite has been observed.

In 1958, Rae, Margolis and Troubetskoy [4]) calculated the neutron capture and inelastic scattering cross sections of U^{235} up to 1.1 MeV on the basis of the statistical theory of nuclear reactions. In the course of these calculations, the partial wave fission cross sections (up to $l = 3$) for U^{235}+n were computed, and these are shown for neutron energies up to 1100 keV in fig. 1. The curves are dashed for energies above 500 keV, because above that energy they depend slightly on assumptions concerning the low-lying level structure of U^{235}. It will be observed that the p-wave cross section rises rapidly with energy and becomes equal to the s-wave cross section for a neutron energy of 100 keV. From there on to 500 keV, the p-wave component represents always at least 50 % of the total fission cross section, the d-wave having risen to equal the s-wave component by 500 keV. On the basis of these curves, radiochemical determinations of the peak-to-valley ratio have been made on U^{235} for neutrons of energy between 65 keV and 14 MeV with emphasis on the region around 125 keV.

2. Experimental

2.1. PRODUCTION OF NEUTRONS

Neutrons of 65 keV energy were produced by the T (p, n) reaction using protons produced by a Van de Graaff accelerator, which were directed on to a water-cooled zirconium tritide target. The fact that the experiment was carried out 5 keV above the threshold, necessary in order to get a sufficiently large neutron yield, results in the large neutron energy spread of 65^{+30}_{-25} keV. Neutrons of 125, 200 and 300 keV energy were produced using the Li (p, n) reaction on thin (10 keV) Li targets. The fission targets used intercepted a 60° cone of neutrons, and the spread of neutron energy was assumed to be + 5 keV− (5 keV+ energy spread of high energy group at 60°).

Neutrons of 540 and 1000 keV energy were made in the same way, but using a 40 keV Li target. The energy spread now becomes + 20 keV−(20 keV+ energy spread of high energy group at 60°).

Neutrons of 14 MeV energy were made by the T (d, n) reaction using a Cockcroft-Walton generator.

2.2. FISSION TARGETS

2.2.1. Thermal neutron irradiations

Six runs were carried out in the Bepo pneumatic irradiation tube (Au/Cd ratio ≈ 3) using 0.2 mg samples of natural uranyl nitrate, made from very pure uranium metal and wrapped in aluminium foil (99.99 % pure) ≈ 7 mg/cm^2

thick. Four runs were carried out in the Bepo thermal column, (Au/Cd ratio measured just after one of the irradiations ≈ 600), using ≈ 0.5 g samples of very pure UO_3 in a polythene container. A further two runs were carried out in the thermal column using 150 mg samples of U^{235} metal (from the same piece of foil as the U^{235} metal used in some of the Van de Graaff runs) in aluminium cans.

2.2.2. Machine Runs

Two types of targets were used. In some runs ≈ 5 g of U^{235} as trioxide were packed tightly into pure copper cans, 15 mm in diameter, 15 mm long and 0.25 mm wall thickness. Each can was surrounded by a 1 mm thick cadmium sheath and aligned in the centre of the neutron beam so that the end of the copper can nearer to the Li target was 10 mm from it. In other runs 93 % U^{235} metal was cut into discs 15 mm in diameter and ≈ 0.125 mm thick, and 5 g of these discs were packed into a 1 mm thick cadmium can.

2.3. IRRADIATIONS

All irradiations were for exactly 2 h. For machine runs a continuous check of neutron flux on the target was kept by means of a neutron counter placed about 2 m behind the target. In all cases the flux was substantially constant.

For pile runs the flux was not monitored directly, but the pile power was noted to be constant throughout all the runs.

2.4. CHEMISTRY

2.4.1. Molybdenum — silver runs

The chemistry was identical for all runs apart from the single difference mentioned in (i) below, as was the timing where appropriate. The following is a summary of the procedure:

(i) The irradiated sample was dissolved in concentrated hydrochloric acid containing known amounts of molybdenum and silver carriers plus a few drops of palladium hold-back carrier. In the case of the Bepo pneumatic tube irradiations the aluminium cover was dissolved with the target, and for all the pile runs 5 g of natural UO_3 were added to make the chemistry identical with that of the machine irradiated samples. The machine samples were merely dissolved directly in the hydrochloric acid.

ii) A few drops of bromine were added and the excess boiled off.

(iii) Exactly $19\frac{1}{2}$ min from the end of the irradiation, concentrated nitric acid was added to the boiling uranium solution. This caused immediate precipitation of the silver chloride, which was boiled for 1 min and then centrifuged off.

(iv) The silver was washed, dissolved and re-precipitated after the addition of palladium carrier. It was then redissolved and allowed to stand until at least

130 min from the end of the irradiation before being purified by a chloride/sulphide cycle method. In the case of runs where U^{235} was used an addition to the method was made in the form of two barium nitrate scavenges to remove alpha contamination. The silver was finally mounted as silver chloride.

(v) Molybdenum was separated from the uranium and then purified by an α-benzoin oxime, hydroxide scavenge, perchlorate method. Two barium nitrate scavenges were added in the case of the U^{235} runs. It was finally mounted as oxinate.

2.4.2. Zirconium — molybdenum — cadmium runs

The chemistry was again identical for all runs. After irradiation the sample was allowed to stand for 100 min to allow Cd^{115} to grow in. The chemical procedure was then as follows:

(i) The sample was dissolved in 5 ml concentrated nitric acid containing molybdenum, zirconium and cadmium carriers, cooled, bromine added and boiled off.

(ii) It was then diluted to $\approx$ 2N in nitric acid, made $\approx$ 1N in hydrofluoric acid and allowed to stand for 10 min.

(iii) Zirconium was then purified by barium fluozirconate cycles coupled with neodymium fluoride scavenges and zirconium mandelate precipitates. It was finally mounted as zirconium mandelate.

(iv) Molybdenum was separated and purified as before.

(v) Cadmium was purified by a series of sulphide precipitates with iron hydroxide and palladium sulphide scavenges, and mounted as the oxinate. Barium nitrate scavenges were included to remove alpha contamination.

2.5. COUNTING

The final precipitates of zirconium, molybdenum, silver and cadmium were mounted by filtration on to weighed filter paper discs which were later stuck to thick aluminium counting trays. The sources were 1.6 cm in diameter and were as similar as possible. Zirconium sources weighed 45 mg, molybdenum sources 25 mg, silver sources 10 mg and cadmium sources 12 mg.

Sources were counted in a number of identical methane flow proportional counters with windows 0.7 mg/cm^2 thick. These counters had backgrounds ranging between 1.3 and 2.1 counts per minute when used as β counters and about 0.01 counts per minute when used as α counters. For the Van de Graaff irradiations, initial count rates after removal of background ranged from 2—3 counts per minute for cadmium, from 3 to 30 counts per minute for silver, from 150 to 1500 counts per minute for molybdenum and much higher for zirconium. Counts rates in thermal and 14 MeV runs were much higher.

Molybdenum sources were counted for 15 d, zirconium sources for 45 d, silver sources for 60 d and cadmium sources for 90 d.

The only corrections applied to the counts were the following:

(i) Conversion of counts recorded to count rate at the end of the irradiation. This was carried out by the Ferranti Mercury computer using a least squares exponential curve fitting programme. The correct half-lives were fed into the computer and the computed result showed the standard deviation of the answer, together with a parameter related to χ^2 which indicated the accuracy of the fitting to the half-lives given.

TABLE 1

Results of all Mo^{99}/Ag^{113} runs

1	2	3	4	5	6	7
Target	Target weight	Type of irradiation	Neutron energy (keV)	Practical ratio [a])	Mean value [a])	True value [a])
Nat. uranyl nitrate	≈0.2 mg	pneumatic tube	thermal	59.2±0.38 58.9±0.39 57.2±0.42 59.3±0.37 59.8±0.56 58.1±0.45 58.2±0.25 56.7±1.53 55.7±0.25 58.0±0.33 58.4±0.17 58.6±0.22	58.2±1.12	551± 11
Nat. UO_3	≈0.5 g	thermal column				
U^{235} metal	≈150 mg					
U^{235} metal	≈5 g	A.W.R.E. Van de Graaff	65^{+30}_{-25}	101 ±16	101 ±19.4	956±186
$U^{235}O_3$ (first sample)	≈5½ g	A.E.R.E. Van de Graaff	125^{+5}_{-35}	107.6±7.3 86.6±4.1 86.3±4.6 73.4±5.9 70.5±11.7 86.6±4.1 86.3±4.6	84.8±11.1	803±107
U^{235} metal	≈5 g	A.W.R.E. Van de Graaff				
$U^{235}O_3$ (second sample)	≈5½ g					
U^{235} metal	≈5 g	A.W.R.E. Van de Graaff	200^{+5}_{-38}	48.4±7.5	48.4±9.2	458± 87
$U^{235}O_3$ (first sample)	≈5½ g	A.E.R.E. Van de Graaff	300^{+5}_{-42}	48.4±3.2	48.4±6.2	458± 59
			540^{+20}_{-48}	41.4±0.7	41.4±4.5	392± 44
			1000^{+20}_{-87}	42.7±1.2	42.7±4.8	404± 46
		A.E.R.E. Cockcroft Walton	14000	0.466±0.001	0.466±0.050	4.41±0.48

[a]) See footnote [b]) to table 2

(ii) Chemical yield.

(iii) A small relative absorption correction referring all zirconium sources to a 45 mg precipitate, all molybdenum sources to a 25 mg precipitate, all silver sources to a 10 mg precipitate and all cadmium sources to a 12 mg precipitate.

2.6. CALCULATIONS

The ratio of the corrected count rate at the end of the irradiation for Mo^{99}/Ag^{113}, Zr^{97}/Mo^{99} or Zr^{97}/Cd^{115g} was taken as the "practical" ratio. The values so obtained for the thermal fission cases were then compared with the "true" values of the appropriate ratio of the fission yields in thermal fission obtained either directly or by interpolation from ref. [5]). Hence a "counting factor" was obtained for any particular pair of nucleides, by which the practical ratio for that pair of nucleides at any other neutron energy could be multiplied in order to obtain an accurate comparison of the ratio of the fission yields between that energy and thermal. The thermal neutron fission yields used were as follows:

Zr^{97} — 5.9 %, Ag^{113} — 0.011 %

Mo^{99} — 6.06 %, Cd^{115g} — 0.0097 %.

3. Results

The Mo^{99}/Ag^{113} ratio was measured at neutron energies, thermal, 65, 125, 200, 300, 540, 1000 and 14000 keV and the Zr^{97}/Mo^{99} and Zr^{97}/Cd^{115g} ratios at thermal and 125 keV.

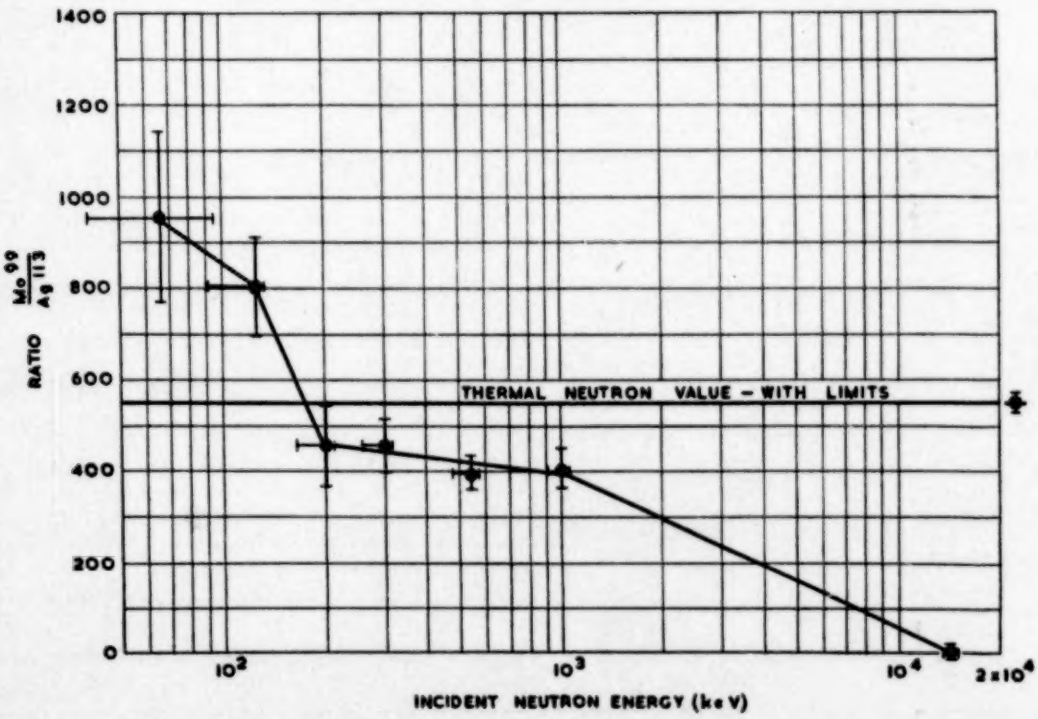

Fig. 2. Peak-to-valley ratios for U^{235} neutron fission.

TABLE 2

Results of all Zr^{97}/Mo^{99} and Zr^{97}/Cd^{115g} runs

1	2	3	4	5	6	7
Neutron energy keV	Practical ratio [b] Zr^{97}/Mo^{99}	Practical ratio [b] Zr^{97}/Cd^{115g}	Mean value [b] Zr^{97}/Mo^{99}	Mean value [b] Zr^{97}/Cd^{115g}	True value [b] Zr^{97}/Mo^{99}	True value [b] Zr^{97}/Cd^{115g}
thermal	7.81±0.012 7.75±0.015 7.85±0.023 7.82±0.015	270± 1.2 278± 1.6 276± 1.9 275± 1.9	7.81 ±0.04	275 ± 3.5	0.974 ±0.005	625 ± 8
125 [a]	9.01±0.075 8.25±0.035	350±14 362±35	8.63 ±0.38	356 ± 26	1.08 ±0.05	809 ± 61

[a]) The two runs at 125 keV were carried out with $U^{235}O_3$ targets weighing ≈ 5 g each and the four thermal runs with natural UO_3 targets weighing ≈ 0.6 g each. The latter were irradiated in the thermal column of the reactor.

[b]) The errors quoted are standard deviations and have been calculated as follows:
(I) The errors quoted in column 5 of table 1 and columns 2 and 3 of table 2 are the computer standard deviations and represent the standard deviations of the counting data only (including counter background uncertainties). They are thus individual figures for each ratio for each run.
(II) To obtain a final standard deviation quoted in columns 6 and 7 of table 1 and columns 4, 5, 6 and 7 of table 2 the following method was used:
(i) The final standard deviation in the thermal neutron case was computed from all the experimental results.
(ii) The experimental percentage variance was calculated from the spread of the experimental results at 125 keV from all the results for each pair of nucleides.
(iii) From this experimental variance at 125 keV, was subtracted the mean of the individual counting variances for the same results.
(iv) This difference between this mean counting variance and the total experimental variance was considered to be the variance due to all factors other than counting factors *for all machine irradiations* for the particular nucleide ratio.
(v) To calculate the standard deviation for a result at some neutron energy where only one experiment was performed, this common variance was then added to the counting variance for that particular energy and the square root of the total taken.

All the results for the Mo^{99}/Ag^{113} runs are given in table 1 and the mean values are plotted in fig. 2. The results for the Zr^{97}/Mo^{99} and Zr^{97}/Cd^{115g} runs are given in table 2.

4. Discussion

4.1. POSSIBLE SYSTEMATIC EFFECTS

The results show a large increase in the ratio of asymmetric/symmetric fission below 200 keV incident neutron energy. The measured value of this ratio at 125 keV incident neutron energy is approximately 45 % above the thermal neutron value. Because of this rather surprising result, it was thought essential to consider possible systematic effects with extreme care. These possibilities are discussed below.

4.1.1. Fine structure in Mo^{99}

Mo^{99} is just barely in the fine structure region in U^{235} fission. One might postulate that the change in peak-to-valley ratio was due solely to a fine structure change in Mo^{99} giving an increase in its fission yield at 125 keV not caused by a reduction in symmetric fission (no such effect occurring, however, at 200 keV and upwards). If this were so, one would expect the ratio of Zr^{97} (not affected by fine structure changes) to Mo^{99} to decrease proportionately. In fact, this ratio shows a small increase at 125 keV of about 11 % over its thermal value. This increase is a little outside the standard deviations concerned, but there are insufficient data to state with certainty that it is a real effect. Whatever the truth about this, it clearly shows that a fine structure change cannot be the cause of the increased peak-to-valley ratio.

Further confirmation of this is obtained from the Zr^{97}/Cd^{115g} ratio, which also shows a large increase at 125 keV. In this connection, it is worth noting that if it is assumed that the small change in the Zr^{97}/Mo^{99} ratio is due to experimental error, the percentage drop in the valley as shown by the Zr^{97}/Cd^{115g} ratio becomes 44 %. This is to be compared with a drop of 46 % indicated by the change in the Mo^{99}/Ag^{113} ratio.

4.1.2. Variation in isomer ratio Ag^{113m}/Ag^{113g}

If this ratio changed drastically at 125 keV compared with its value both at thermal energies and at 200 keV and upwards, so that the metastable state was particularly favoured at 125 keV, an apparent increase of the ratio Mo^{99}/Ag^{113g} would result. No direct test of such a possible effect can be made, owing to the short half-life of Ag^{113m}, but there would have to be a similar variation in the ratio Cd^{115m}/Cd^{115g} to account for the fact that the Zr^{97}/Cd^{115g} ratio also increases at 125 keV. It seems unlikely that both isomer ratios would be changed by approximately the same amount at the same energy.

4.1.3. Variation in independent yields

A very high independent yield (amounting to $\approx$ 30 % of the total chain yield) occurring at Cd^{113} and In^{115} in the 125 keV case (but not at higher neutron energies) could account for our results. This supposition, however, is considered too unlikely to merit further consideration.

4.1.4. Differential effect between thermal (reactor) and other (machine) runs

U^{235} had to be used for all the machine runs, whereas most reactor runs used natural uranium for convenience. However, two reactor runs were carried out using U^{235} and showed no change in the practical ratio obtained.

A further check is provided by the true ratio obtained for the run using 14 MeV neutrons. Our result of 4.41 ± 0.48 agrees very closely with the measured Russian value of 4.5 (ref. [6])). It also agrees reasonably well with the

results obtained directly, and by interpolation, from the much earlier work reported by Katcoff [5]). This result is ≈ 5.2.

4.1.5. Some effect of the target geometry or composition

In five of the machine runs at 125 keV, two different specimens of $U^{235}O_3$ packed into cans 15 mm long were used. In the other two, U^{235} metal approximately of the same total weight and diameter was used. The final result is a mean of all seven determinations, and does not show any statistical effect of target composition or geometry.

4.1.6. Contamination of Mo^{99} *in* 125 keV *runs by* Np^{239} *due to peaks in* U^{238} (n, γ) *cross-section at this energy*

This possibility arises because the U^{235} used contained 7 % of U^{238}. No peak is known in this cross-section at 125 keV. Attempts to check the purity of the Mo^{99} sources by gamma spectrometry failed because of the low intensity of the sources.

However, repurification of some of the Mo^{99} sources after counting showed no change in specific activity, and no such error can arise in the case of the Zr^{97}/Cd^{115g} ratio.

4.1.7. Variation in pile neutron spectrum

The Au/Cd ratio in the pneumatic tube (used for six thermal irradiations) was ≈ 3, and in the thermal column (used for a further six) was ≈ 600. There is no significant difference between the two sets of results.

4.1.8. (n, γ) *reactions on impurities in target materials*

If a target material used for machine measurements contained sufficient Mo impurity, the reaction Mo^{98} (n, γ) Mo^{99} would increase the Mo^{99} value and hence the peak-to-valley ratio. If the capture cross-section for Mo^{98} at 125 keV is assumed to be of the same order as its thermal value (0.13 b), the total Mo content of the U^{235} used would have to be ≈ 10 % in order to produce 10 % of the observed Mo^{99} counts. Spectrographic analysis of the U^{235} used shows less than 40 p.p.m. of total Mo.

Similarly, if the target material used for the thermal measurements contains an impurity whose daughter produced by (n, γ) reaction contaminated the final Ag^{113} source, and could not be distinguished from it by half-life, the Ag^{113} would be high and hence the practical thermal neutron ratio obtained would be too low.

A survey of all nucleides, both naturally radioactive, and produced by neutron reactions, or as daughters of nucleides produced by neutron reactions, whose half-lives were between 2 h and 10 h was made. If it is assumed that the target material contained 1 % of the element concerned and that the rigorous silver purification used only decontaminated it by a factor of 100, then in order to

produce 10 % of the observed Ag^{113} count rate, capture cross-section multiplied by the isotope abundance of the nucleide concerned would have to be 20 b. The only nucleides which cannot be eliminated by this criterion are Eu^{152} and Dy^{165}. In the target material, 50 p.p.m. of total Eu and 300 p.p.m. of total Dy would have to be present to produce 10 % of the observed Ag^{113} counts assuming a decontamination factor of 10^2. Actual analysis of the uranium showed < 0.001 p.p.m. of these elements present.

It should also be noted that our results have been obtained using two completely different sources of natural uranium and three different sources of U^{235}.

4.2. POSSIBLE INTERPRETATIONS OF RESULTS

If we accept the above arguments as evidence that the increased peak-to-valley ratio observed at neutron bombarding energies of 60 to 125 keV is genuine, several possible explanations suggest themselves.

(i) It may be that what is demonstrated is that the peak-to-valley ratio observed with thermal neutrons is anomalously low. At higher neutron bombarding energies, the mass distribution is averaged over many states of the compound nucleus U^{236}, and a true mean behaviour is observed. On the other hand, the behaviour observed at thermal energies is based on, at most, a few such states, and it could be that these states are not typical s-wave states. The experimental evidence on this point is confusing. The Los Alamos Radiochemistry Group [7]) found that epicadmium neutrons produced a rather higher ($\approx$ 15 %) peak-to-valley ratio than was produced by thermal neutrons. Nasahoglu *et al.* [8]) reported that the peak-to-valley ratio produced by thermal neutrons is the same within $\pm$ 20 % as that produced by a moderated pile beam. Roeland, Bollinger and Thomas [9]) found a 35 % drop in the peak-to-valley ratio produced by epithermal neutrons over that produced by thermal neutrons. This measurement has however, been criticised on the grounds that the beam contained a proportion of fast neutrons giving rise to a high symmetric component.

Finally, the more recent Los Alamos work reported by Griffin [2]) indicates that the peak-to-valley ratio averaged over the resonances up to a neutron energy of 60 eV differs only slightly from that produced by thermal neutrons, and is, if anything, lower.

While these experimental results are inconclusive, it would seem most unlikely that the peak-to-valley ratio averaged over the s-wave resonance region is $\approx$ 50 % higher than is observed in thermal fission, as would be necessary in order to explain our results.

(ii) The second explanation which suggests itself is that the odd parity normally associated with the U^{235} ground state is incorrect. This suggestion is attractive in that the observed behaviour would be as predicted by the channel theory. It would, however, upset the systematics postulated by

Mottelson and Nilsson [10]) and would require a rearrangement of the single particle levels calculated for heavy odd-neutron deformed nuclei.

(iii) If neither of the above explanations is acceptable, we are forced to assume that some new effect occurs in U^{235}+n which depresses the symmetric fission probability for neutron energies around 100 keV despite the predictions of the channel theory. In this case one might expect to observe this effect even more strongly in neutron induced fission of the even parity nucleides U^{233} and Pu^{239}.

The authors wish to thank Dr. A. T. G. Ferguson of A.E.R.E. and Mr. D. Akers of A.W.R.E. for very many helpful discussions in connection with the Van de Graaff irradiations. They also wish to thank the operators of the two Van de Graaffs for their unfailing co-operation. The authors also wish to thank Dr. E. S. Troubetskoy for making available the calculations on partial wave cross sections for neutron fission of U^{235}.

References

1) Aage Bohr, Proc. Int. Conf. At. En. (United Nations, New York, 1956) Vol. **2**, p. 911
2) J. J. Griffin, Proc. Int. Conf. Nuc. Structure, Kingston, 1960 (North-Holland Publishing Co., Amsterdam, 1960) p. 843
3) G. Cowan, A. Turkevich and C. Brown, Phys. Rev. **122** (1961) 1286
4) E. R. Rae, B. Margolis and E. S. Troubetskoy, Phys. Rev. **112** (1958) 492
5) S. Katcoff, Nucleonics **16**.4 (1958) 78
6) A. I. Protopopov *et al.*, Atomnaya **5** (1958) 130
7) L. A. S. L. Radiochemistry Group, Phys. Rev. **107** (1957) 325,
8) R. Nasahoglu, S. Raboy, G. R. Ringo, L. E. Glendenin and E. P. Steinberg, Phys. Rev. **108** (1957) 1522
9) L. W. Roeland, L. M. Bolinger and G. E. Thomas, Proc. Int. Conf. At. En. (United Nations, New York, 1958) Vol **15**, p. 551
10) B. R. Mottelson and S. G. Nilsson, Mat. Fys. Skr. Dan. Vid. Selsk. **1**, No. 8 (1959)

2.F

Nuclear Physics **27** (1961) 166—176; © *North-Holland Publishing Co., Amsterdam*

Not to be reproduced by photoprint or microfilm without written permission from the publisher

SURFACE DIRECT INTERACTION OF 14 MeV NEUTRONS WITH FLUORINE

E. KONDAIAH, M. L. JHINGAN and C. BADRINATHAN

Tata Institute of Fundamental Research, Colaba, Bombay 5, India

Received 4 April 1961

Abstract: The energy and angular distribution of charged particles arising when 14 MeV neutrons are incident on a foil of Teflon are studied using nuclear emulsion detector. The energy distribution showed three peaks at 530, 220 and 120 μm ranges. The energies of these peaks assuming them to be comprising of protons, deuterons or tritons are given and they agree with those to be expected from known levels of the final nuclei.

In general the emission at forward angles is found to be much more than at backward angles and is (5.5 ± 0.5) times that at backward angles for all the three groups taken together. Experimental angular distributions of all the three groups are given. In two cases, these distributions are compared with theoretical distributions assuming surface direct interactions to be taking place. The agreement between theory and experiment is good enough to draw conclusions regarding parities of the levels involved.

The energy and angular distributions of one of these groups indicate a new level in O^{19} at 4 MeV.

1. Introduction

In a previous paper [1]) studying the ratio of cross-sections of (n, α) to (n, p) reactions in fluorine, it was concluded that the major part of (n, p) cross-section

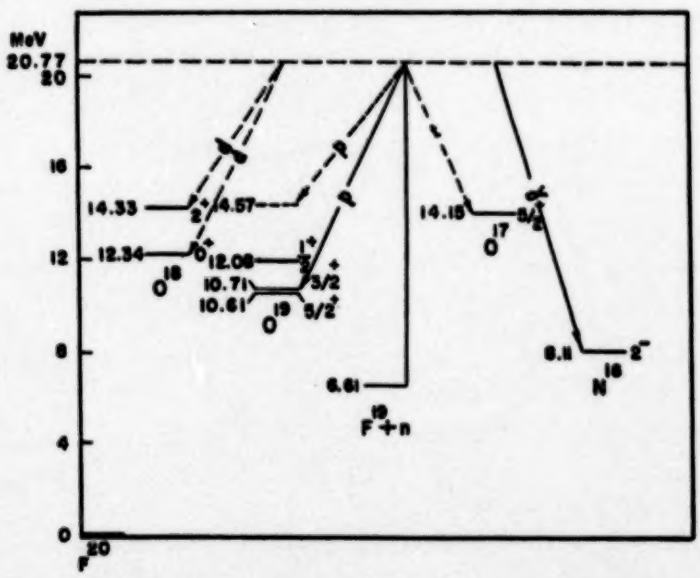

Fig. 1. Some energy levels of the resulting nuclei in (F^{19}+n) reactions. Zero MeV corresponds to F^{20} ground state.

arises from direct interactions. The results of the present paper confirm this conclusion and also show that the direct interaction involved is mainly the surface direct interaction. It is assumed that the odd proton in the fluorine nucleus lies out in the surface and is comparatively free so that Austern, Butler and McManus' theory [2]) can predict the angular distributions correctly. Ribe [3]) studied (n, d) reaction in fluorine using 14 MeV neutrons and has shown that direct interaction could account for the angular distribution in this pick up process. The results presented here agree with this conclusion.

Fig. 1. gives the levels of the resulting nuclei when 14 MeV neutrons are incident on a fluorine nucleus with which the present work is concerned. The zero energy line is taken to be the ground state of F^{20} which is taken as the reference line.

2. Experiment and Observations

14.165 MeV neutrons were obtained from T (d, n) He^4 reaction using the cascade generator of this Institute; neutrons at right angles to the deuteron beam were used. A Teflon $(CF_2)_n$ ribbon of 33 mg/cm^2 thickness was used as target in an arrangement similar to that of Allan [4]). This arrangement has the advantage of recording outgoing particles in all directions simultaneously. The geometrical arrangement of the neutron source, the Teflon target and the nuclear emulsion detector is given in fig. 2.

When the reaction chamber was used without any lining, the charged particles arising in the brass walls of the chamber were so large that they completely masked the contributions from the thin Teflon target. After lining the walls with lead, the background has come down to about 80 % of the actual effect due to Teflon. The background is taken into account in all the cases. The reaction chamber was evacuated to a pressure of 1 mm of mercury.

C-2 nuclear emulsions of 200 μm thickness were used as detectors. Background measurements were made under identical conditions but with the Teflon foil removed. Only 1 cm $\times$ 1 cm area in the centre of each plate was scanned so that the detector could be taken as a point detector for all practical purposes. The tracks were measured with a Lietz Ortholux microscope having a magnification of 850. Only those tracks with dip angles in the range 6° to 10° were taken into account. Those tracks originating in the surface of the emulsion only were measured to avoid tracks due to neutrons. At these low energies, it is not possible to distinguish between the different charged particles, namely, protons, deuterons, tritons, alpha particles, helium-3 etc. in the emulsions used. However, tracks with a length less than 60 μm were discarded, thus excluding alpha particles from F^{19} (n, α) N^{16} and C^{12} (n, α) Be^9 reactions as well as deuterons arising in C^{12} (n, d) B^{11} and protons arising in C^{12} (n, p) B^{12} reactions. Consequently, the tracks recorded comprised protons from the F^{19} (n, p) O^{19}

reaction, deuterons from the F^{19} (n, d) O^{18} reaction and perhaps some tritons from the F^{19} (n, t) O^{17} reaction. The Q-values of other reactions are such that they need not be considered here.

For the angular distribution measurements, the observations are grouped into angular intervals of 10°. The theoretical angular distributions [2]) are in centre-of-mass system, but these are converted into laboratory system for comparison with the experimental values.

3. Corrections Applied

Fig. 2 gives the geometry of the experimental arrangement. The distance between the centre of the plate and the target is 7.6 cm and that between the

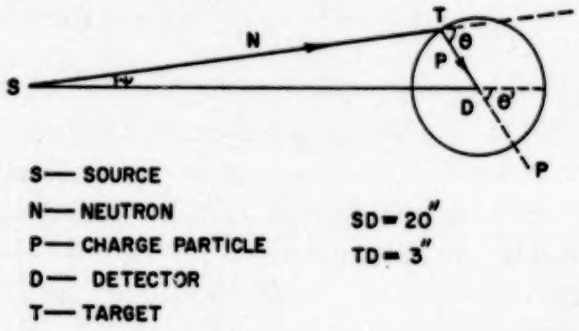

Fig. 2. Geometry of the experimental arrangement.

centre of the plate and the neutron source is 50 cm. Consequently, the angle ψ is different for different angles θ. The angle between the incident neutron N and the outgoing particle P is θ. whereas θ' is the actually measured angle. The angle θ is given by

$$\theta = \theta' + \psi.$$

The angle ψ is calculated for various values of the measured angle θ' and θ is evaluated.

Secondly, even though the target elements contributing particles at the detector, are at the same distance from the detector (taking the detector as a point detector †), they are at different distances from the source of neutrons. Hence, the intensity of neutrons incident on the target elements are different for different values of θ. This is corrected using the inverse square law.

Thirdly, the target is not thin enough to neglect loss of energy inside the target for the outgoing charged particles. For groups A and B of fig. 3, the

† The detector actually extended 5 mm on either side of the centre of the plate. This gives rise to some uncertainty in θ. But the observations for the angular distributions are grouped into intervals of 10° and hence this uncertainty in θ is neglected. The contribution of this uncertainty to the recorded intensity is negligilble.

effective thickness of the target is taken as 16.5 mg/cm² (that is half the thickness of the Teflon target). Group C of fig. 3 is too low in energy to correct in this way. However, considering this group to be either deuterons or tritons, an effective thickness of 12.3 mg/cm² for the case of deuterons and 5.8 mg/cm² for the case of tritons have been used to obtain the corrected energies. This assumes that deuterons originating at a thickness larger than 24.6 mg/cm² and tritons originating at a thickness larger than 11.6 mg/cm² in the Teflon target will not give contribution to group C of fig. 3.

4. Theoretical Angular Distributions

Austern, Butler and McManus [2]) have given the theory of direct interactions for (n, p) reactions especially taking into account the surface effects. This theory is very well suited for those cases where a comparatively free proton can exist outside a closed shell. The present report is part of a programme to make experimental investigation of all such cases.

The 9th proton in F^{19} can be considered as a comparatively free proton outside the closed shell at 8. The energy of the neutrons used in the present case, namely 14 MeV, is also very appropriate to observe the surface effects as it is neither so large that the nucleus becomes transparent to the neutrons used nor so low that compound nucleus effects predominate.

According to the simplest picture of a surface direct interaction, the proton is ejected from a state of lowest binding while the incident neutron is captured into a similar state of the residual nucleus characterised by a definite orbital angular momentum. It is assumed that the interaction between the two particles takes place only outside the nucleus, that is, where only the least bound states of the initial and final nuclei are important. In a case like this, according to Austern *et al.* [2]), the angular distribution is given by

$$\sigma \propto |r_{np}(\tfrac{1}{2}k)|^2 \varepsilon^2(r_0)(2l_p+1) \times \Sigma_l C^2_{l_n,\, l_p}(l,\, 0;\, 0,\, 0)\{J_l(Qr_0)\}^2,$$

where l is restricted to the values

$$(l_n+l_p) \geqq l \geqq |l_n-l_p|,$$

and to conserve parity can take only odd or even values in this range. In this expression $Q = |\mathbf{Q}|/\hbar$, where $|\mathbf{Q}|$ stands for the difference in the linear momenta of the ingoing neutron and outgoing proton, J_l is the spherical Bessel function which gives the angular variation and C is a Clebsch-Grodan coefficient.

The ground state of F^{19} is known to be a $\frac{1}{2}^+$ state. The magnetic moment of F^{19} fits with the value expected if the 9th proton were in the $2s_{\frac{1}{2}}$ state [5]). So, it is quite likely that the 9th proton in F^{19} is in the $2s_{\frac{1}{2}}$ state, giving $l_p = 0$. In such a case, l_n, the orbital angular momentum of the orbit into which the neutron is captured in an (n, p) reaction, is directly given by the value of l that

gives the best fit to the observed angular distribution of the outgoing protons. For example, from known spins and parities of O^{19} levels (fig. 1), the odd neutron in O^{19} (for ground state as well as first excited state at 96 keV) can be taken to be in a d-state. This means that in the reaction F^{19} (n, p) O^{19} leading to the ground and/or first excited state of O^{19}, the proton angular distribution should fit the theoretical distribution calculated for l given by

$$l = l_n - l_p = 2 - 0 = 2.$$

The results shown in fig. 5 are in agreement with this.

5. Results

5.1. ENERGY DISTRIBUTION

Fig. 3 gives the range distribution of the outgoing charged particles. It comprises of three distinct groups.

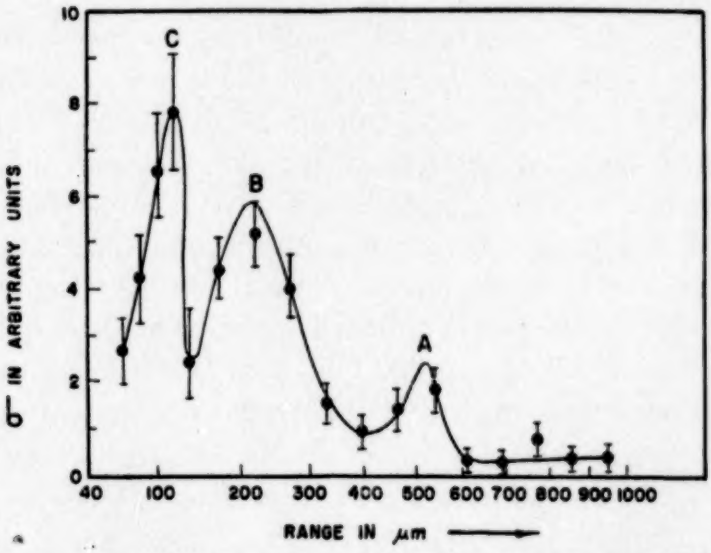

Fig. 3. Range distribution of charged particles from (F^{19}+n) reactions.

5.1.1. Group A

This group has a range around 530 μm. Taking this to be a proton group and correcting for the loss of energy inside the target, the energy of this group is obtained as 10.0$\pm$0.5 MeV. This agrees with the known Q-values of the F^{19} (n, p) O^{19} reaction leading to the ground and/or first excited at 96 keV of O^{19}. No other reaction can account for this group A.

5.1.2. Group B

This group has a range around 220 μm. If this is taken as a proton group, it corresponds to an energy of 6.2$\pm$0.5 MeV after correcting for the loss of energy inside the target. If this is the correct interpretation, it means that this

group of protons leads to a level in O^{19} at about 4 MeV, which is so far not reported.

However, as is mentioned above, deuterons cannot be ruled out. If this group is a deuteron group, its energy comes out to be 7.5 MeV after correcting for the loss of energy inside the target. This agrees with the known Q-value of the F^{19} (n, d) O^{18} reaction leading to the ground state of O^{18}. Ribe [3]) has reported such a deuteron group.

Thus, on range measurements alone, it is not possible to say whether group B is a proton group leading to a level in O^{19} at about 4 MeV or a deuteron group leading to the ground state of O^{18}. However, the angular distribution studies reported below indicate that group B consists of both protons and deuterons.

5.1.3. Group C

This group has a range around 120 μm. It is either a proton group of about 4 MeV, a deuteron group of 6 MeV or a triton group of 6.9 MeV.

From the Q-value of the F^{19} (n, t) O^{17} reaction based on nuclear masses, one would expect tritons of about 5.6 MeV energy leading to the ground state

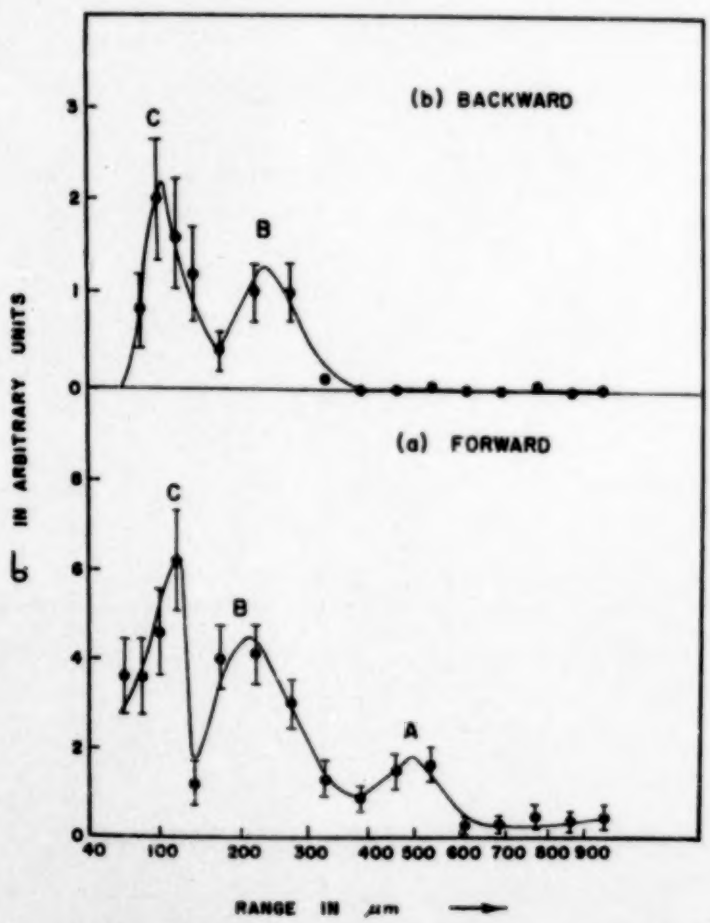

Fig. 4. Range distribution of charged particles from (F^{19}+n) reactions. (a) at forward angels. (b) at backward angles.

gives the best fit to the observed angular distribution of the outgoing protons. For example, from known spins and parities of O^{19} levels (fig. 1), the odd neutron in O^{19} (for ground state as well as first excited state at 96 keV) can be taken to be in a d-state. This means that in the reaction F^{19} (n, p) O^{19} leading to the ground and/or first excited state of O^{19}, the proton angular distribution should fit the theoretical distribution calculated for l given by

$$l = l_n - l_p = 2 - 0 = 2.$$

The results shown in fig. 5 are in agreement with this.

5. Results

5.1. ENERGY DISTRIBUTION

Fig. 3 gives the range distribution of the outgoing charged particles. It comprises of three distinct groups.

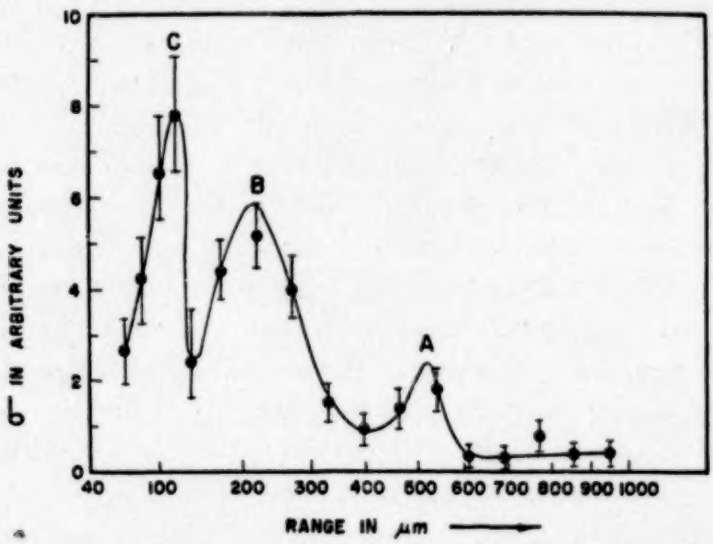

Fig. 3. Range distribution of charged particles from (F^{19}+n) reactions.

5.1.1. Group A

This group has a range around 530 μm. Taking this to be a proton group and correcting for the loss of energy inside the target, the energy of this group is obtained as 10.0 ± 0.5 MeV. This agrees with the known Q-values of the F^{19} (n, p) O^{19} reaction leading to the ground and/or first excited at 96 keV of O^{19}. No other reaction can account for this group A.

5.1.2. Group B

This group has a range around 220 μm. If this is taken as a proton group, it corresponds to an energy of 6.2 ± 0.5 MeV after correcting for the loss of energy inside the target. If this is the correct interpretation, it means that this

group of protons leads to a level in O^{19} at about 4 MeV, which is so far not reported.

However, as is mentioned above, deuterons cannot be ruled out. If this group is a deuteron group, its energy comes out to be 7.5 MeV after correcting for the loss of energy inside the target. This agrees with the known Q-value of the F^{19} (n, d) O^{18} reaction leading to the ground state of O^{18}. Ribe [3]) has reported such a deuteron group.

Thus, on range measurements alone, it is not possible to say whether group B is a proton group leading to a level in O^{19} at about 4 MeV or a deuteron group leading to the ground state of O^{18}. However, the angular distribution studies reported below indicate that group B consists of both protons and deuterons.

5.1.3. Group C

This group has a range around 120 μm. It is either a proton group of about 4 MeV, a deuteron group of 6 MeV or a triton group of 6.9 MeV.

From the Q-value of the F^{19} (n, t) O^{17} reaction based on nuclear masses, one would expect tritons of about 5.6 MeV energy leading to the ground state

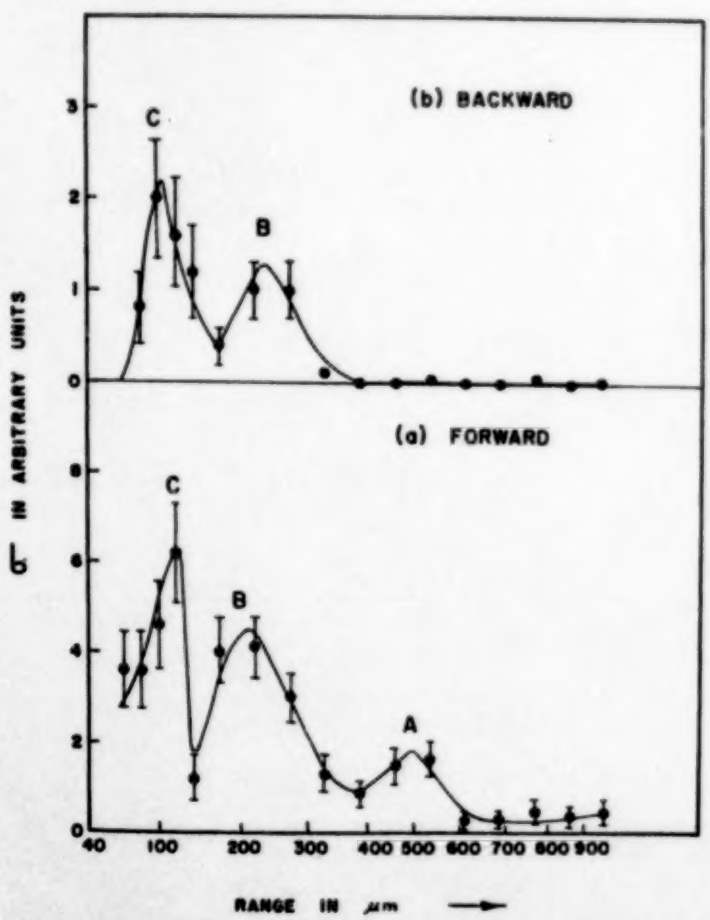

Fig. 4. Range distribution of charged particles from (F^{19}+n) reactions. (a) at forward angels. (b) at backward angles.

of O^{17}. As the energy of group C, if it were a triton group, would be higher than 5.6 MeV by about 1.3 MeV, it is unlikely that it is a triton group.

If group C is a deuteron group, its energy fits with the known Q-value of the first excited state in O^{18} at 1.982 MeV, within experimental errors.

If this group is a proton group, its energy is such that a new level in O^{19} at about 6 MeV has to be postulated. As O^{19} levels in this region are not yet known from other reactions, nothing definite can be stated about this.

As Ribe [3]) has found a deuteron group leading to the 1.982 MeV level in O^{18}, in the reaction F^{19} (n, d) O^{18} using 14 MeV neutrons, it is likely that this group C is the same deuteron group.

5.2. EMISSION AT FORWARD AND BACKWARD ANGLES

Figs. 4(a) and (b) give the energy spectra of the outgoing charged particles in the forward and backward angles, respectively. A glance at these two figures shows that group A is emitted entirely at forward angles and is absent at backward angles. This clearly shows that it arises entirely from direct interac-

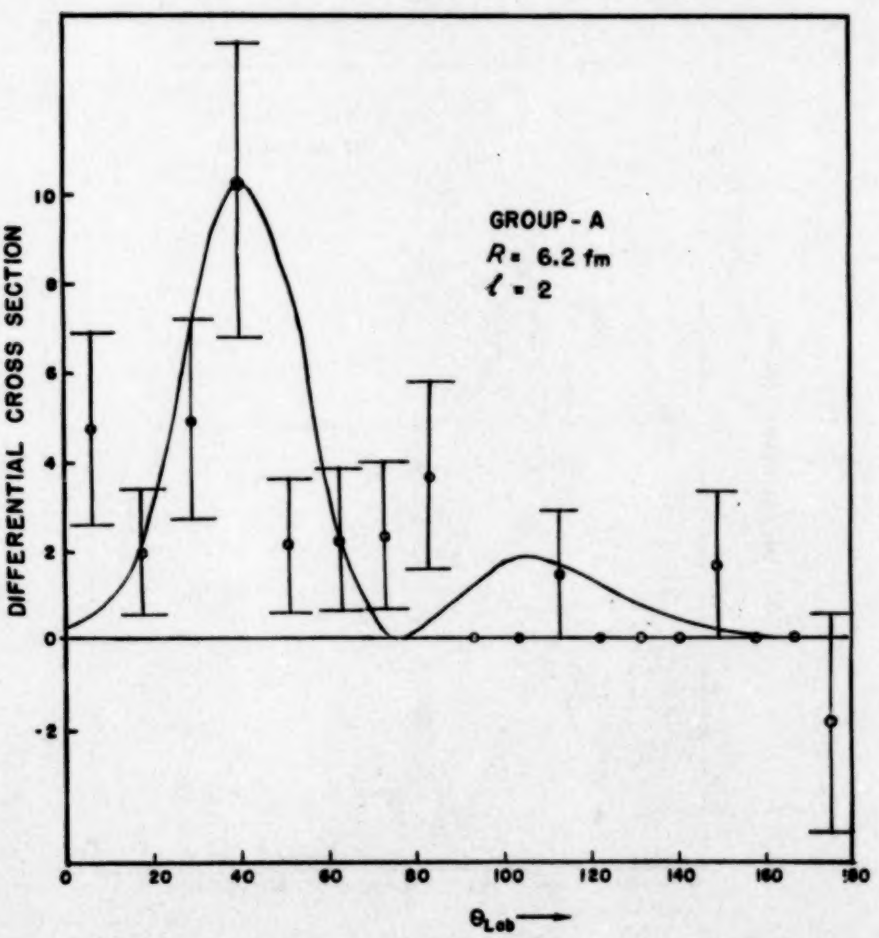

Fig. 5. Angular distribution of group A. The solid line curve is the theoretical curve for protons based on surface direct interactions.

tions and not from a compound nucleus process. The ratio of forward to backward emissions for groups B and C are 4.1 ± 0.4 and 5.3 ± 0.6, respectively; this ratio for all the three groups taken together is 5.5 ± 0.5. This shows that we are primarily concerned with direct interactions in the present case.

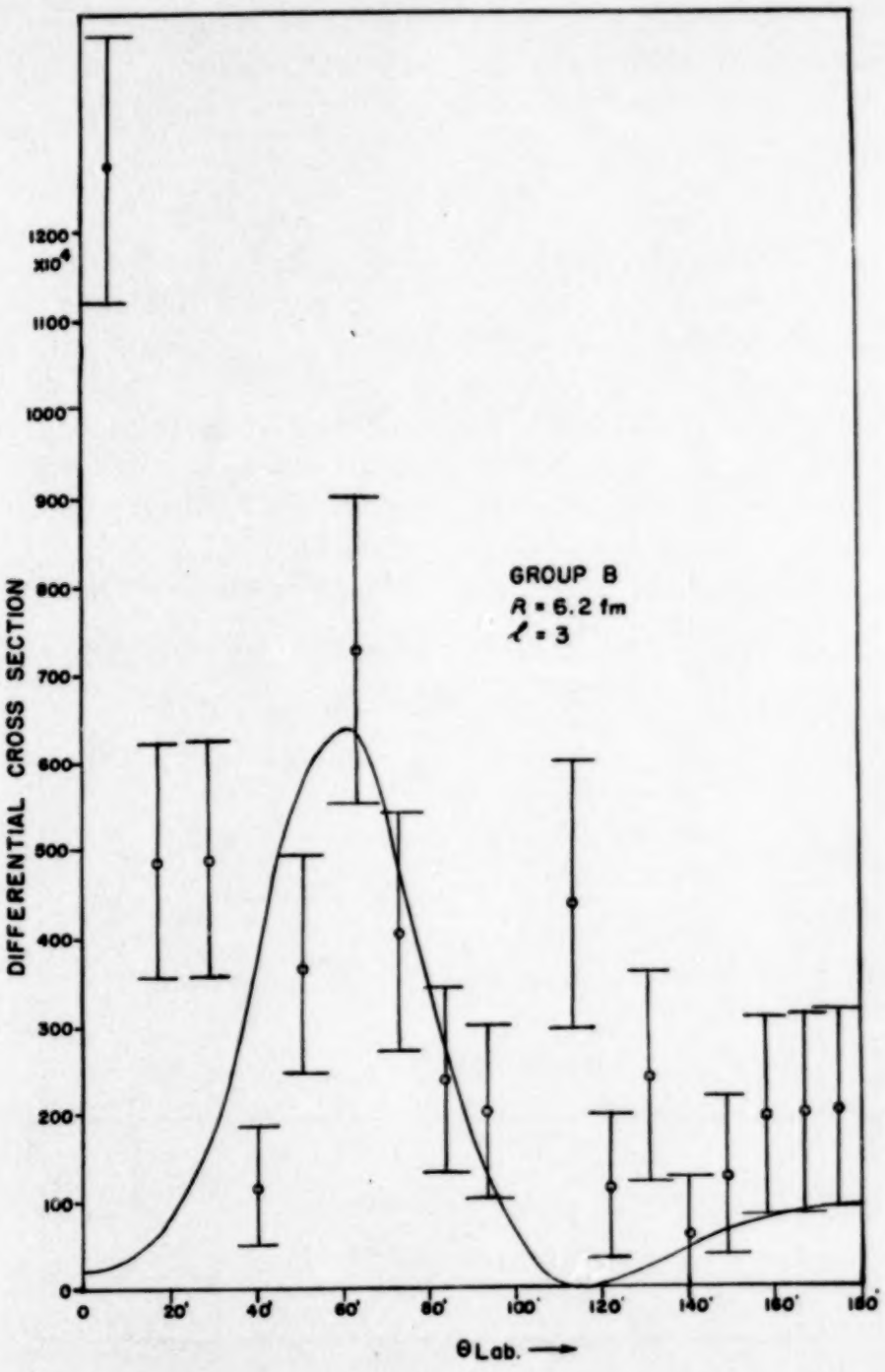

Fig. 6. Angular distributions of group B. The solid line curve is the theoretical curve for protons based on surface direct interactions.

5.3. ANGULAR DISTRIBUTIONS

5.3.1. Group A

Fig. 5 gives the angular distribution of group A. The experimental points with statistical errors are shown. The continuous curve drawn is the theoretical distribution for $l = 2$ taking an interaction radius $R = 6.2$ fm. The curve is normalised at its peak point. The agreement between the experimental points and the theoretical curve is satisfactory as far as the main peak is concerned. Other values of l and R were tried and found not to give so good a fit.

5.3.2. Group B

Fig. 6 gives the angular distribution of group B. As mentioned above, this group may be comprising deuterons as well as protons. According to Ribe [3]), the angular distribution at 14 MeV incident neutron energy is such that the cross-section for the (n, d) reaction at angles greater than 30° is very small. Taking this result as correct and assuming that the points at and above 30° in fig. 6 are due mainly to protons, it is possible to fit these points to the theoretical distribution calculated for $l = 3$ using $R = 6.2$ fm. Again the agreement between theory and experiment is quite satisfactory.

At present this appears to be the most likely explanation for the compar-

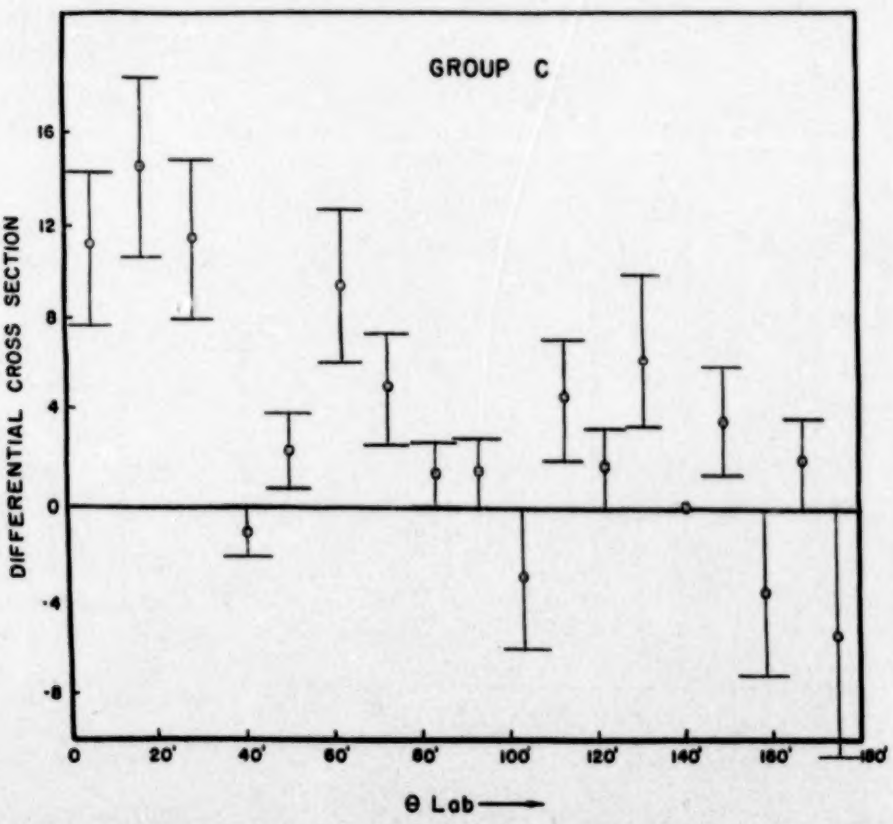

Fig. 7. Angular distribution of group C.

atively large number of tracks in the region 30° to 100°. If group B were to consist of only deuterons there should not have been so many tracks in the region 30° to 100°, on the other hand it is unlikely that group B consists of protons only and no deuterons since Ribe [3]) has established such an energy deuteron group using a proportional-cum-scintillation counter assembly that can distinguish between deuterons and protons.

5.3.3. Group C

Fig. 7 gives the angular distribution of tracks in this group. As this group can consist of tracks due to protons, deuterons as well as tritons and also as the energy of the tracks of this group is low, it is thought that no useful purpose can be served by comparing this experimental distribution with theory. However, the angular distribution definitely shows that it is peaked at forward angles; thus even this low energy group is due primarily to direct interactions rather than to compound nucleus.

6. Discussion

From the results presented above, it is obvious that protons leading to the ground and/or first excited state in O^{19} are entirely due to direct interaction. The fact that the angular distribution of this group fits well with $l = 2$ curve of surface direct interaction theory, as is to be expected, encourages one to deduce the level parameters for the 4 MeV level in O^{19}. As is mentioned above, it is preferable to assume that group B consists of both protons and deuterons. Consequently, the angular distribution shown in fig. 6 for this group gives the orbital angular momentum of the captured neutron as

$$l_n = l + l_p = l + 0 = 3.$$

This means that the 4 MeV level in O^{19}, reported here, is probably an f state and has negative parity.

From the results presented here, one can obtain a lower limit to the ratio of the F^{19} (n, p) O^{19} reaction to the F^{19} (n, d) O^{18} reaction, both reactions leading to the ground states. This ratio is greater than 0.25; this appears to be larger than the value to be expected from the results of Ribe [3]).

Lastly, figs. 3 and 4 do not show any indication of a proton group leading to the 1.469 MeV level in O^{19}. Such a group is to be expected at a range of 375 ± 25 μm. If such a group is present, its intensity should be less than that of group A which is the proton group leading to the ground and/or first excited state in O^{19}.

7. Conclusions

7.1. PROTON GROUPS

Proton groups leading to O^{19} levels at 0 and/or 96 keV as well as 4 MeV have been found from F^{19} (n, p) O^{19} reaction. Comparison of the angular distributions

of these groups with surface direct interaction theory showed that the ground and/or the 96 keV levels of O^{19} are d states whereas the 4 MeV level is probably an f state.

7.2. DEUTERON GROUPS

Deuteron groups leading to O^{18} levels at 0 and 1.982 MeV have been observed. The angular distribution of the ground state group agrees with a previous report [3]).

The authors acknowledge the technical help given by Mr. M. R. Hiranandani in developing the nuclear emulsions.

References

1) E. Kondaiah, K. V. K. Iyengar and C. Badrinathan, Nuclear Physics **5** (1958) 346
2) N. Austern, S. T. Butler and H. McManus, Phy. Rev. **92** (1953) 350
3) F. L. Ribe, Phy. Rev. **106** (1957) 767
4) D. L. Allan, Nuclear Physics, **6** (1958) 464
5) M. G. Mayer and J. H. D. Jensen, Elementary theory of nuclear shell structure (John Wiley and Sons Inc., New York 1955) p. 75
6) F. Ajzenberg-Selove and T. Lauritsen, Nuclear Physics **11** (1959) 1

NORTH-HOLLAND BOOKS

Proceedings of the VIIth International Conference

on

LOW TEMPERATURE PHYSICS

Toronto
August 29 - September 3, 1960

editors | G. M. GRAHAM and
A. C. HOLLIS HALLETT
University of Toronto

1. Second Fritz London Award
2. The Mössbauer Effect
3. Magnetic Relaxation
4. Liquid and Gaseous H_2
5. Magnetism below 1°K
6. Further Communications on Magnetism
7. Polarization of Protons
8. Nuclear Orientation
9. Fermi Surface
10. Ultrasonic Attenuation
11. Resistance Minima
12. Further Communication on Transport Properties in Solids
13. Theory of Superconductivity
14. Electrical Properties of Superconductors
15. Superconductivity of Hg and Ta
16. Specific Heat of Alloys
17. Intermediate State
18. Further Communications on Superconductivity
19. Flow Properties of Liquid Helium-4
20. Kapitza Boundary Layer
21. Ions in Liquid Helium
22. Helium Film
23. Further Communications on the Properties of He^4
24. Liquid and Solid He^3
25. Thermodynamic Properties of He^3-He^4 Mixtures
26. Further Communications on He^3-He^4 Mixtures
27. Equation of State and Thermodynamic Properties
28. Thermodynamic Properties of Argon
29. Further Communications on Thermodynamic Properties
30. Proposal for a He^3 Temperature Scale

745 pp. Gld. 57.00 (114s.)

Sole distributors outside U.S.A. and Canada:

NORTH-HOLLAND PUBLISHING COMPANY — AMSTERDAM

NORTH-HOLLAND BOOKS

Just out
Second, revised edition

PLASMA Physics

by **J. G. LINHART**
CERN, Geneva

From reviews of the first edition

The author has the three rare qualifications of experience, mathematical facility and inventive imagination. He also possesses didactic ability, but this will be appreciated only by those readers who share with him the advantages of mathematical ability and of an active mind. It is not a book which can be imbibed passively, or uncritically.

The arrangement is so clear, with full description of the experimental methods and with all the relevant theory required to explain the data, that the book can be equally recommended to the student and to the expert research worker.

Nature

The whole book provides an admirable, if laconic, summary to a vast and important field of work of great topical interest.

Journal of the Royal Institute of Chemistry

6 x 9" 290 pp. 125 figs. Gld. 25.00 (50s.)

NORTH-HOLLAND PUBLISHING COMPANY-AMSTERDAM

Sole distributor U.S.A.: Interscience Publishers Inc. New York